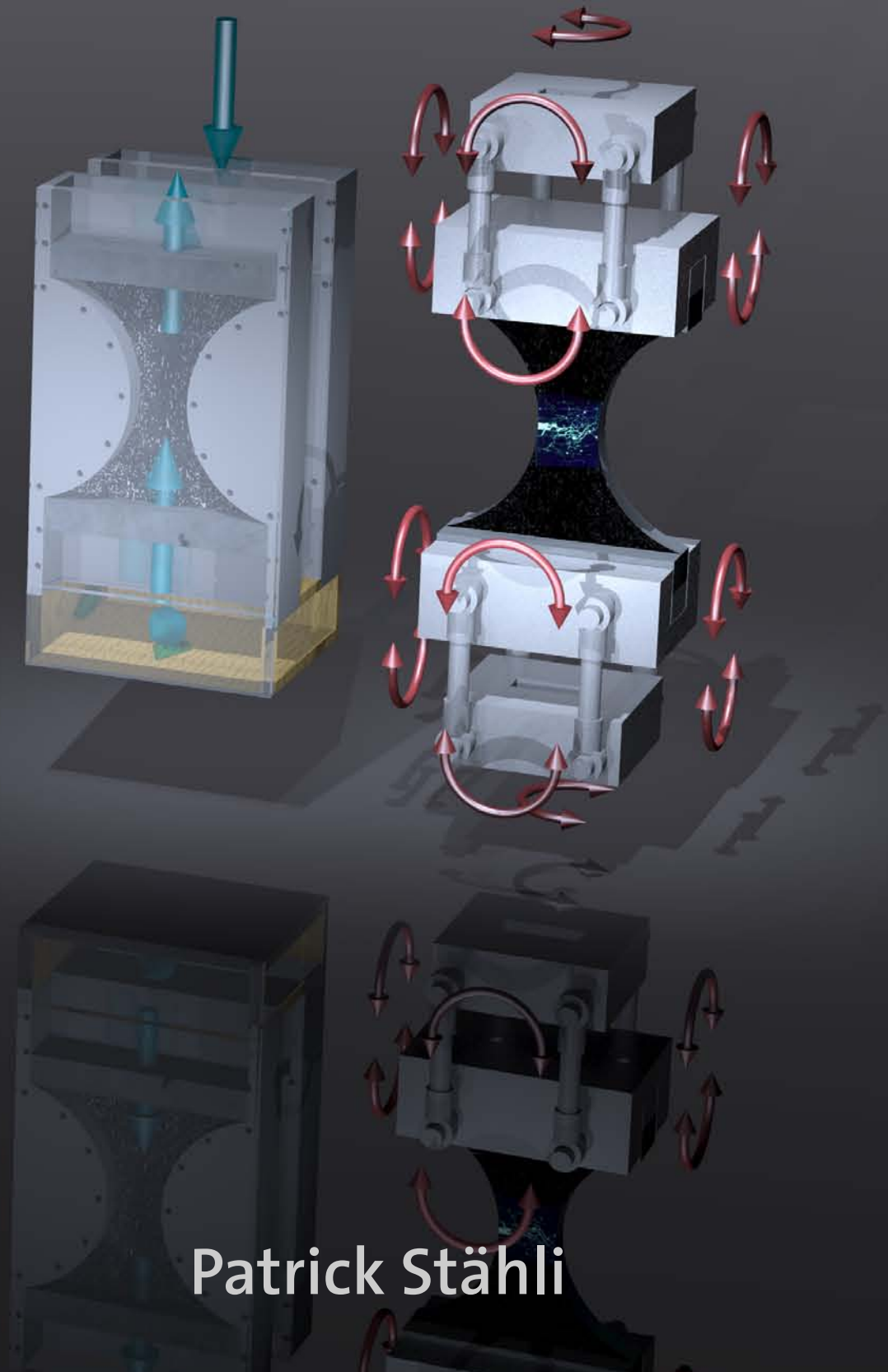


# Ultra-Fluid, Oriented Hybrid-Fibre-Concrete



Patrick Stähli

# Ultra-Fluid, Oriented Hybrid-Fibre-Concrete



Diss. ETH No. 17996

# Ultra-Fluid, Oriented Hybrid-Fibre-Concrete

A dissertation submitted to

ETH ZURICH

for the degree of

Doctor of Sciences ETH Zurich

presented by

PATRICK STÄHLI

Dipl.-Bauing, ETH Zurich

born 22.01.1975

citizen of

Oberhofen am Thunersee, Bern

accepted on the recommendation of

Prof. Dr. Jan G.M. van Mier, examiner  
Prof. Dr. Marco Di Prisco, co-examiner  
Prof. Dr. Viktor Mechtcherine, co-examiner

2008

Institute for Building Materials ETH Zürich

ISBN 978-3-9523454-0-5

©by Patrick Stähli

All rights reserved.

No part of this volume may be produced, stored in retrieval system or transmitted in any form or by any means, electronic, mechanical, photocopying, recording or otherwise, without the prior written permission of the publishers.

Printed by Repro-Zentrale, ETH Zürich, Switzerland

# Contents

<b>Summary</b>	<b>1</b>
<b>Zusammenfassung</b>	<b>3</b>
<b>List of symbols and notations</b>	<b>6</b>
<b>1 Introduction</b>	<b>9</b>
1.1 Aim of the research . . . . .	9
1.2 Research in the past 15 years . . . . .	10
1.3 Testing methods . . . . .	16
1.3.1 Tensile strength . . . . .	16
1.3.2 Tensile testing . . . . .	16
1.4 Outline of this PhD-Thesis . . . . .	19
<b>2 Mix Design</b>	<b>23</b>
2.1 Introduction . . . . .	23
2.2 Mixtures . . . . .	23
2.2.1 Components . . . . .	23
2.2.1.1 Cement . . . . .	23
2.2.1.2 Fly-ash . . . . .	24
2.2.1.3 Microsilica . . . . .	25
2.2.1.4 Aggregates . . . . .	27
2.2.1.5 Super-plasticizer . . . . .	29
2.2.1.6 Fibres . . . . .	29
2.3 Matrix design . . . . .	32
2.3.1 Content of the different components . . . . .	32
2.3.2 Mixing procedure . . . . .	33
2.4 Conclusions . . . . .	39

<b>3</b>	<b>Rheological and flow properties</b>	<b>41</b>
3.1	Introduction . . . . .	41
3.2	Rheological Tests . . . . .	42
3.2.1	SegBox . . . . .	42
3.2.1.1	Self-leveling degree of different HFC mixtures	44
3.2.2	Standard fresh concrete tests . . . . .	45
3.2.2.1	Slump flow tests . . . . .	45
3.2.2.2	Air void content test . . . . .	46
3.3	Results . . . . .	46
3.3.1	Influence of fibre-to-fibre ratio . . . . .	47
3.3.2	Influence of flowability . . . . .	50
3.4	Conclusions . . . . .	53
<b>4</b>	<b>Fibre distribution and alignment</b>	<b>55</b>
4.1	Introduction . . . . .	55
4.2	Manual counting . . . . .	56
4.2.1	Specimen preparation . . . . .	57
4.2.2	Fibre counting and orientation factor $\alpha$ . . . . .	57
4.2.3	Bending specimens . . . . .	59
4.2.3.1	'U-shaped' specimen . . . . .	59
4.2.3.2	Orientation-bar specimen . . . . .	61
4.2.4	Tensile test specimens . . . . .	61
4.3	Computer tomography (CT) . . . . .	62
4.3.1	Interpretation and data analysis . . . . .	65
4.4	Results . . . . .	65
4.4.1	Influence of the flowability . . . . .	66
4.4.2	Orientation-bar specimen . . . . .	66
4.4.3	Influence of the manufacturing method . . . . .	69
4.5	Conclusions . . . . .	76
<b>5</b>	<b>Mechanical testing</b>	<b>77</b>
5.1	Introduction . . . . .	77
5.2	Bending test . . . . .	77
5.2.1	Test set-up . . . . .	78
5.2.2	Specimen geometry . . . . .	78
5.2.3	Measurement . . . . .	81
5.2.4	Interpretation . . . . .	84
5.3	Tensile test . . . . .	88
5.3.1	Test set-up . . . . .	88
5.3.2	Specimen geometry and preparation . . . . .	88
5.3.3	Measurement . . . . .	94

5.3.4	Interpretation . . . . .	94
5.4	Impregnation technique . . . . .	94
5.4.1	Impregnation material - Epoxy resin . . . . .	94
5.4.2	Vacuum cylinder . . . . .	95
5.4.3	Impregnation procedure . . . . .	95
5.4.4	Interpretation . . . . .	96
5.5	Results . . . . .	99
5.5.1	Evaluation of the mixing system . . . . .	99
5.5.2	Properties development and curing conditions . . . . .	109
5.5.3	"Fibre-to-fibre" series - rheological and mechanical tests	112
5.5.4	Moulded or cut tensile specimens . . . . .	116
5.5.5	Crack pattern development and analysis . . . . .	119
5.6	Conclusions . . . . .	126
<b>6</b>	<b>Flow and mechanical properties</b>	<b>127</b>
6.1	Introduction . . . . .	127
6.2	Test series . . . . .	127
6.2.1	U-shaped specimen series . . . . .	127
6.2.1.1	Varying the w/b-ratio . . . . .	128
6.2.1.2	Varying the amount of super-plasticizer (SP)	130
6.2.2	Filling methods - tensile properties . . . . .	136
6.2.3	Influence of the filling method to the fibre distribution	143
6.3	Conclusions . . . . .	147
<b>7</b>	<b>Examples of applications</b>	<b>149</b>
7.1	Introduction . . . . .	149
7.2	Structural wall . . . . .	149
7.3	Sandwich-elements . . . . .	151
7.4	The perforated wall . . . . .	153
7.5	Architectural chairs and models . . . . .	158
7.6	Conclusion . . . . .	163
<b>8</b>	<b>Conclusions and outlook</b>	<b>165</b>
8.1	Conclusions . . . . .	165
8.2	Outlook . . . . .	168
<b>A</b>	<b>Appendix A</b>	<b>181</b>
A.1	Mix design programme . . . . .	181
A.2	Concrete mixers . . . . .	181
A.2.1	Hobart 1.5l . . . . .	181
A.2.2	Hobart 6.0l . . . . .	181



A.2.3	Wälti 30l . . . . .	183
A.2.4	Zyklos 65l . . . . .	183
A.2.5	Huggler 300l . . . . .	183
A.2.6	Huggler 500l . . . . .	185
A.2.7	Eirich 200l . . . . .	185
A.3	Standard mechanical test - Walter & Bai testing machine . . .	185
A.3.1	Compression tests . . . . .	187
A.3.2	Young's Modulus tests . . . . .	187
A.3.3	Bending test . . . . .	187
<b>B</b>	<b>Appendix B</b>	<b>189</b>
B.1	Crack pattern development . . . . .	189
	<b>Curriculum vitae</b>	<b>195</b>
	<b>Acknowledgement</b>	<b>201</b>

# Summary

## **Ultra fluid oriented hybrid fibre concrete**

In the research project presented in this PhD-Thesis, an ultra fluid hybrid fibre concrete (HFC) with three types of steel fibres was developed, with improved tensile strength and flow properties. Due to the ultra fluidity of the material the fibres aligned in the flow directions of the material and both, tensile strength and ductility could be increased. The fibres used were straight (small and middle fibres), notched or undulated (large fibres). All fibres are made of high strength steel ( $f_y=1100-2400$  MPa).

In this project many important aspects were considered. In more than 100 mixtures, which differed in the total amount and/or the amount of the single type of fibres, fresh concrete properties, alignment of the fibres and mechanical properties were determined. New testing methods to determine the orientation of the fibres, degree of self-leveling, bending and tensile strength were developed. Furthermore crack patterns for mixtures with different fibres and combinations of the fibres, loaded under different conditions were analyzed.

Bending test were performed using the newly developed pendulum-bar four-point bending test set-up. The rationale for using pendulum bars is based on the idea that during a four-point bending test the forces which act on the specimen should remain perpendicular to the specimen, the symmetry should be maintained throughout the whole test, there should be no friction between the supports and the specimen, and it should be possible to measure the forces at supports and load-points. Basically the same idea was used in order to develop a tensile test appropriate for the determination of the mechanical properties of HFC. The pendulum-bar tensile test set-up was developed and built. The reason for using pendulum-bars is based on the idea that during a tensile test the forces should remain centric and the supports should be able to rotate. This becomes important especially when a

material of increased ductility, such as HFC, is used. Van Mier et al. [1994b] showed that the boundary conditions in a uniaxial tensile test have a significant influence on the result of the test. The tensile strength and also the fracture energy obtained from uniaxial tensile tests between fixed boundaries are higher than the values received from tests with rotation supports.

The so called SegBox was developed in order to determine the segregation of the fibres and the degree of self-leveling of the fresh concrete. Later on the same test was used to determine the orientation of the fibres. Several filling methods and mould geometries were developed. The fibre orientation was determined and a flow-orientation model was elaborated. The orientation of the fibres was determined using cross-sections of hardened specimens or CT-scans from a medical CT-scanner. The fibres were counted manually and the orientation of the fibres could be determined. The advantage of the CT-scanner is apparent: the scanning is a non-destructive method and the mechanical properties can be determined after scanning a specimen. Relations between fibre orientation and mechanical properties were determined and are presented in this thesis.

Crack patterns were analyzed on specimens under load. The specimens were loaded in four-point bending. The deformations of the specimen were maintained by gluing two steel plates on the sides of the specimen while it was under load. Afterwards the specimens were impregnated using a fluorescent epoxy resin, cut and photographed under UV-light. The crack patterns were traced on the computer and analyzed using a self-developed MATLAB script. The results showed some interesting findings namely that the crack spacing is not dependent on the fibre type. A similar average crack spacing was observed for the non-elastic part of the load-displacement diagram for all types of fibres.

Finally in the last Chapter of this PhD-Thesis some samples of applications of the newly developed material are introduced. Most of these applications are architectural projects. Ultra-fluid fibre reinforced concrete was used in order to fill moulds with complicated geometrical details or to resist external forces such as demoulding forces or simple external loads.

**Patrick Stähli**  
8<sup>th</sup> October 2008

# Zusammenfassung

## **Ultra fluid oriented hybrid fibre concrete**

In der vorliegenden Doktorarbeit ist das Forschungsprojekt zusammengefasst, welches sich mit der Entwicklung von hybriden Faserbetonen (HFC) mit drei verschiedenen Fasertypen und verbesserter Zugfestigkeit und Fliessfähigkeit befasste. Durch die hohe Fliessfähigkeit richten sich die Fasern in der Fliessrichtung aus, wodurch sich die Zugfestigkeit und Verformbarkeit deutlich steigern lässt. Gerade (kleine und mittlere), gekerbte und gewellte (lange) Stahlfasern aus hochfestem Stahl ( $f_y=1100-2400$  MPa) wurden für die Betonmischungen verwendet.

Dieses Projekt deckt viele wichtige Aspekte der Faserbetonforschung ab. In mehr als 100 Mischungen, welche sich in Fasertypen und deren Kombination und/oder Fasermengen unterschieden, wurden die Frischbetoneigenschaften, die Faserausrichtung und die mechanischen Eigenschaften bestimmt und untersucht. Neue Testmethoden zur Bestimmung der Ausrichten der Fasern, des Selbstnivellieren des Frischbetons und das Bestimmen der Biegezug- und Zugfestigkeiten wurden entwickelt. Rissbilder von Betonmischungen mit verschiedenen Fasern und deren Kombinationen wurden an Probekörpern analysiert, welche unterschiedlich belastet wurden.

Mit der neuentwickelten Pendulum-Bar Vierpunkt Biegezugeinrichtungen wurden Biegezugprüfungen durchgeführt. Der Grund, weshalb Pendulum-Bars (Pendelstäbe) zum Einsatz kamen ist, dass die Kräfte während der ganzen Versuches senkrecht auf den Prüfkörper wirken, die Symmetrie während des ganzen Versuches erhalten bleibt, die Reibung zwischen Prüfkörper und Prüfeinrichtung minimiert wird und die Kräfte in den Kraftereinleitungspunkten und den Auflagern gemessen werden konnten. Die gleiche Ideen (Pendelstäbe) wurde verwendet um einen Zugversuch zu entwickeln, welcher geeignet ist, die mechanischen Eigenschaften von HFC zu bestimmen. Die Pendulum-Bar Zugversuchseinrichtung wurde entwickelt und gebaut. Pendelstäbe ka-

men hier zum Einsatz, dass die Kräfte während des ganzen Versuches zentrisch bleiben und sich die Lager frei drehen konnten. Diese Eigenschaften sind besonders wichtig, wenn Materialien mit erhöhter Duktilität (HFC) geprüft wird. Van Mier et al. [1994b] zeigten, dass die Randbedingungen in einem Direktzugversuch die Resultate beträchtlich beeinflussen. Die Werte der Zugfestigkeit, sowie diejenigen der Bruchenergie sind höher bei Versuchen mit fixierten Lagern als diejenigen bei Versuchen mit frei rotierenden Lagern.

Die sogenannte SegBox wurde entwickelt um die Segregation von Fasern und das Selbstnivellieren des Frischbetons zu bestimmen. Derselbe Versuch wurde später verwendet um die Faserausrichtung im Innern von Betonproben zu bestimmen. Verschiedenste Füllmethoden und Schalungsgeometrien wurden entwickelt um die Faserausrichtung zu kontrollieren. Anhand dieser Ergebnisse wurde ein Fluss-Orientierungs Modell erarbeitet. Um die Faserausrichtung zu bestimmen kann man Probekörper aufschneiden oder mittels Computertomographie virtuelle Schnitte durch die Probekörper legen und mittels Handzählung der Fasern die Faserverteilung bestimmt. Die Vorteile eines CT's liegen auf der Hand: Das scannen ist eine zerstörungsfreie Methode und die mechanischen Eigenschaften der gescannten Probekörper können zusätzlich bestimmt werden. Verschiedene Schnitte können an demselben Probekörper untersucht werden. Zusammenhänge zwischen Faserausrichtung und Festigkeit werden in dieser Doktorarbeit präsentiert.

Weiter wurden Untersuchungen an Rissbilder von Probekörpern unter Last durchgeführt. Die Proben wurden in Vierpunkt Biegung belastet. Die Verformungen/Durchbiegung für man mittels ankleben von Stahlplatten an die Seiten des Probekörpers ein. Danach imprägnierte man die Probekörper mit fluoreszierendem Epoxydharz, schnitt sie und fotografierte sie unter UV Licht. Am Computer konnte das Rissbild nachgezeichnet und mittels MATLAB analysiert werden. Die Resultate zeigten einige interessante Gesichtspunkte:

- die Rissabstände sind nicht vom Fasertyp abhängig
- es stellt sich ein ähnlicher durchschnittlicher Rissabstand für den nicht elastischen Bereich des Last-Verformungs-Diagramms für alle Fasertypen ein.

Schlussendlich werden im letzten Kapitel dieser Doktorarbeit Anwendungen vorgestellt, welche mit diesem neu entwickelten Material realisiert wurden, meistens Projekte von Architekturstudenten. Um die komplizierten Geometrien derer Modelle und Strukturen füllen zu können und den hohe Anforderung an Festigkeit während des Ausschalprozesses gerecht zu werden

wurde extrem flüssiger faserverstärkter Beton mit erhöhter Festigkeit und Duktilität verwendet.

**Patrick Stähli**  
8<sup>ter</sup> Oktober 2008

## List of symbols and notations

### Capital Roman letters

$F_{fib}$	= Fibre factor $F_{fib} = \sum(V_F \cdot \frac{l_f}{d_f})$	[-]
$F_{SL}$	= Self-leveling degree	[-]
$F_{SG}$	= Segregation degree	[-]
$V_F$	= total fibre volume	[%]
$V_f$	= fibre volume of each fibre	[%]
$SP$	= Amount of super-plasticizer	[%]
$N_c$	= average number of fibres in a cross section	[-]
$N$	= theoretical average number of fibres in a cross section	[-]
$A_{fib}$	= Area of the fibre cross section	[mm <sup>2</sup> ]
$A_{grid}$	= Area of a single mesh (100 mm <sup>2</sup> )	[mm <sup>2</sup> ]
$E$	= Young's Modulus	[GPa]
$W$	= section modulus $\frac{b \cdot h^2}{6}$	[mm <sup>3</sup> ]
$A_{real}$	= cross section of the cracked area	[mm <sup>2</sup> ]
$A_{nom}$	= minimum cross section of the dog bone specimen	[mm <sup>2</sup> ]
$W_f$	= specific work of fracture $W_f = \int F \cdot dw$	[kN·mm]
$W_{fpeak}$	= specific work of fracture $W_{fpeak} = \int_0^{w_{peak}} F \cdot dw$	[kN·mm]
$M_{max}$	= maximum bending moment	[kN·mm]

### Small Roman letters

$l_f$	= length of the fibre	[mm]
$d_f$	= diameter of the fibre	[mm]
$l_{sf}$	= large slump flow (Abrahams cone)	[cm]
$s_{sf}$	= small slump flow	[cm]
$f_b$	= flexural bending strength	[MPa]
$f_{b\ 3pt}$	= three point flexural bending strength	[MPa]
$f_{b\ 4pt}$	= four point flexural bending strength	[MPa]
$f_c$	= compressive strength (cylinder)	[MPa]
$f_{cc}$	= compressive strength (cube)	[MPa]
$f_t$	= tensile strength	[MPa]
$f_{t\ nom}$	= nominal tensile strength	[MPa]
$f_{t\ real}$	= real tensile strength	[MPa]
$f - t - f$	= fibre-to-fibre factor	[small to middle to large]

### Small Greek letters

$\alpha$	= Orientaton factor	[-]
$\sigma_{t \text{ nom}}$	= nominal tensile stress	[MPa]
$\sigma_{t \text{ real}}$	= tensile stress in the crack cross-section	[MPa]
$\eta$	= ratio between bending and tensile strength $\eta = \frac{f_t}{f_b}$	[-]
$\eta_{min}$	= minimum of $\eta$ , $\eta_{min} = \frac{f_t}{f_b \text{ min}}$	[-]
$\kappa$	= normalizing factor $\kappa = \frac{\eta}{\eta_{min}}$	[%]
$\beta$	$\beta = \frac{\text{numberofverticalcracks}}{\text{numberofhorizontalcracks}}$	[-]

### List of abbreviations

HFC	Hybrid Fibre Concrete
FRC	Fibre Reinforced Concrete
SFC	Single Fibre Concrete
SFRC	Single Fibre Reinforced Concrete
ECC	Engineered Cementitious Composites
SHCC	Strain Hardening Cementitious Composites
SIFCON	Slurry Infiltrated Fibre Concrete
UHPFRCC	Ultra High Performance Fibre Reinforced Cement Composite
MMFRC	Multi-Modal Fibre Reinforced Concrete
CMOD	Crack Mouth Opening Displacement
LVDT	Linear Variable Differential Transformer
SP	Super-Plasticizer
ESEM	Environmental Scanning Electron Microscope





# Chapter 1

## Introduction

Concrete has been the most utilized building material (in volume) for the last century. Because of the freedom of shape concrete is preferable for many applications. Concrete can be used for architectural applications as well as for structural elements. Concrete is mainly used where compressive stresses are present. The compressive strength of concrete varies from a low strength concrete with a compressive strength of less than 10 MPa to a high strength concrete with a compressive strength of more than 200 MPa. This large range of compressive strength makes concrete an adaptable building material. Unfortunately the tensile strength of plain concrete is almost negligible. Concrete cracks and fails under very low tensile loading. These cracks propagate very fast and thus the "ductility" of plain concrete is very low. Usually steel bar reinforcement is used to solve this problem. Nevertheless, the concrete is still not ductile and cracks are still present. Reinforced concrete structures are generally cracked, and the cracks reduce the durability of structures. The situation may likely be improved by using different types of fibres. Synthetic, steel, glass or even carbon fibres are mixed in the concrete. In the past, only low amounts of fibres were used and only the ductility could be increased while the tensile strength was still very low. In this research project the aim is to enhance the tensile properties of fibre-reinforced concrete, and thus both ductility and strength.

### 1.1 Aim of the research

The main aim of this research is to improve the tensile strength of concrete. Steel fibres and cocktails of different steel fibres (HFC) were used. In order to optimally embed the fibres into the concrete matrix the concrete had to be as

fluid as possible. Therefore the research was mainly restricted to produce self-compacting concretes. Unfortunately some exceptions were necessary. Next to self-compacting, self-leveling was important as well. The flowability had to be improved so that the concrete could flow even in complicated moulds or over a long distance. Unfortunately a test set-up where self-leveling could be measured was not yet established. Reason enough to develop such a test set-up. Later on the question about the alignment of the fibres has arisen. Obviously fibres had to be aligned in the direction of the tensile stresses in order to improve tensile strength as much as possible. However this field was relatively new and new tests and procedures had to be developed.

Mechanical tests to determine tensile and flexural properties had to be performed. The test set-ups had to satisfy demands such as improved tensile strength and improved ductility of the tested material. Therefore a further aim was to develop a bending and a tensile test set-ups, specially designed for such concretes with enhanced mechanical properties. The work reported in this thesis includes the needed needed steps necessary to achieve the mentioned aims.

This Chapter summarizes the development of fibre reinforced concrete over the last 15 years. Recent developments are described at the end of Section 1.2. In the second part of this chapter different mechanical tests and test set-ups are presented. Advantages and disadvantages of these tests and test set-ups are pointed out. Finally, the structure of this thesis is given at the end of this chapter.

## 1.2 Research in the past 15 years

The idea of adding fibres into concrete in order to increase strength and fracture energy goes back to a patent dated 1918 by H. Alfsen. He described a process how to improve the tensile strength by adding longitudinal bodies (fibres) of different material into the concrete. Afterwards several patents of different fibers and fiber geometries were proclaimed. A historical overview of the development of fibre reinforced concrete from the end of the 19th century to late 1980ies is given by Naaman [1985] and Reinhard & Naaman [2005]. With the development of super-plasticizer of the newest generation it was possible to add larger amounts of fibres and the mixtures became self-compacting.

Compaction may have a significant influence on the properties of fibre reinforced concrete. In particular fibre orientation and fibre distribution may be affected, especially when vibration needles are inserted in the fresh concrete, see Soroushian & Lee [1990]. With the development of self-compacting con-

crete, the use of vibrational energy for compaction has become obsolete, and with the current generation of super-plasticizers it is possible to develop self-compacting fibre concrete as well (Grünewald [2004], Lappa [2007], Markovic [2006], Rossi [1997], Stähli & van Mier [2004a, 2007a]). Increasing the amount of fibres may have a positive effect on the mechanical properties, but because not all fibres are necessarily aligned in the direction of stress, the effectiveness is debatable. To align fibres in the direction of stress might be a more efficient way to improve the performance of fibre reinforced concrete (FRC) and hybrid fibre concrete (HFC) in a structure, probably at lower cost. Not only strength should be considered, but also ductility. Aligning fibres has been tried in the past under a variety of circumstances. Recently a method based on magnetic fields was proposed by Linsel [2005]. For SIFCON, fibre alignment can be achieved by sprinkling fibres in a narrow space, or in very thin elements (van Mier [1996], van Mier & Timmers [1992]). Moreover, during extrusion of FRC, fibres align in the longitudinal direction as well (see for example Shao & Shah [1997]). The ensuing anisotropy is probably related to differences of properties in the various directions.

According to the concept suggested by Rossi [1997], fibres in cement composites can act at both the material and structural levels. On the material structural level, the fibres can enhance the ductility and strength of the cement composite, whereas on the structural level the fibres can improve the bearing capacity of the composite by transferring force across the large cracks in the cement composite. The idea of adding fibres with different lengths is obvious. The first who proposed adding different steel fibres in the same concrete mixture was Rossi [1997] and named it "multi-modal fibre reinforced concrete" (MMFRC). Small fibres act as reinforcement of the matrix (material level) and strength could be increased, whereas the larger fibres act on the structural level and the ductility could be increased. Orange et al. [1999] developed a concrete called DUCTAL®, a material which is based on the multi-modal fibre reinforced concrete proposed by Rossi [1997], Rossi et al. [1987]. Recently several on-going projects use DUCTAL® (see Behloul [2007]). In Switzerland the first application of UHPFRCC were crash barrier walls of a bridge (Oesterle et al. [2007]). The material was used because of its very low permeability and its height strength and deformability. The durability and mechanical performance of the structure could be improved significantly. In Cardiff, Karihaloo et al. [2002] developed a material using large amounts of small steel fibres with high tensile/flexural strength. The so called CARDIFRC™ has a high energy-absorption capacity and is suitable for repairing and upgrading existing concrete structures. Karihaloo et al. [2002] showed promising results of CARDIFRC™ used as retrofitting dam-

aged concrete structural members. Markovic [2006] picked up the idea of using different types of fibre in a single mixture and developed Hybrid Fibre Concrete (HFC) using two types of fibres. In the present thesis the developments proceed and three different types of steel fibres were used within one single mixture.

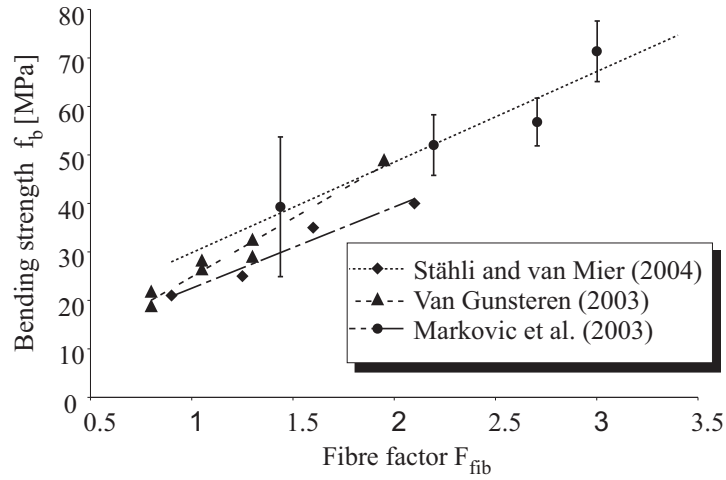


Figure 1.1: Comparison between three point bending tests, after Stähli & van Mier [2004a]

A comparison between different investigations on hybrid fibre concrete with similar matrix designs is given in Figure 1.1. The Figure compares the data by Stähli & van Mier [2004a] with the results of three-point bending tests made in Zürich by van Gunsteren [2003] and in Delft by Markovic et al. [2003]. This diagram shows that the strength increases, at constant fibre factor, from the tests by Markovic et al. [2003] to the experiments by Stähli & van Mier [2004a]. The strength increase is a little larger compared to tests done by van Gunsteren [2003]. In this diagram it can also be seen that the results of van Gunsteren [2003] and Markovic et al. [2003] are at a lower level than the results reported by Stähli & van Mier [2004a]. An explanation for this could be that Stähli & van Mier [2004a] were working with three types of fibres, whereas van Gunsteren [2003] and Markovic et al. [2003] used two types of fibres only. These results indicate that HFC with three types of fibres may be more efficient than mixtures with two or even one type of fibre.

Since the the beginning of the development of concretes with increased tensile strength, high-performance concretes (compressive strength of more than 100 MPa) moved to the background and so called high-performance

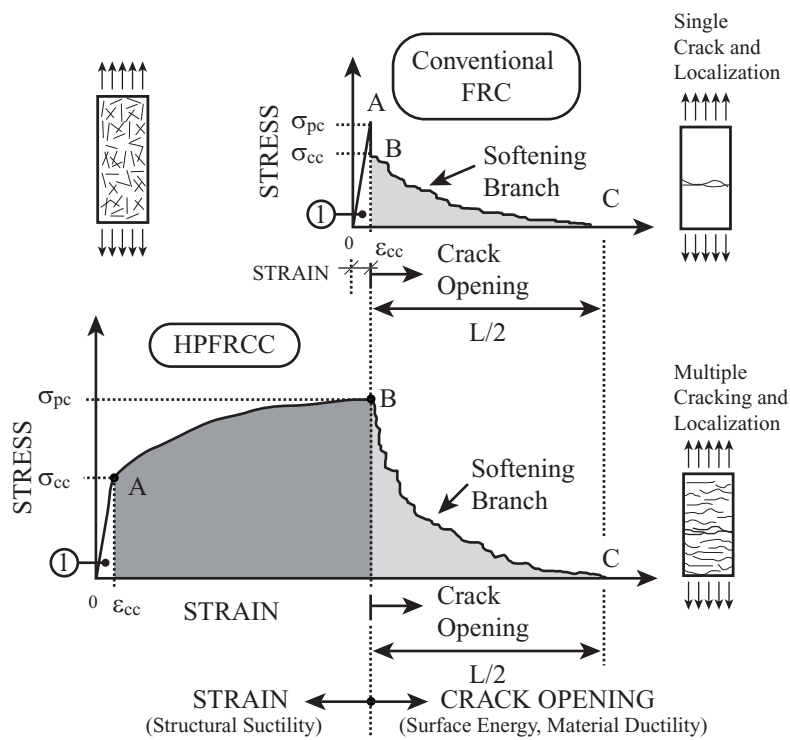


Figure 1.2: Definition of High Performance Fibre Reinforced Cement Composites, after Naaman & Reinhard [2003], opposed to 'softening' fibre reinforced concrete (FRC)

fibre-reinforced cement-composites (HPFRCC) received the main attention. From 1992 till present Naaman and Rheinhardt organized several workshops on the subject HPFRCC. HPFRCC was defined as a material with enhanced strain hardening. Figure 1.2 shows the definition of strain hardening of HPFRCC in contrast to ordinary FRC, which usually shows brittle behaviour.

Consequently, a key characteristic of fibre reinforced materials is whether strain hardening behaviour in tension is present. Naaman & Reinhard [2005] proposed a flow chart classifying the different fibre-reinforced materials by its ability to deform. Regarding these definitions it has to be mentioned that the behaviour is strongly dependent on the test set-up and the geometry of the specimen. Smaller and thinner specimens show a more pronounced strain/deflection hardening than larger and thicker specimens. Wall effects and aligned fibres are mainly responsible for such different behaviours. Therefore the flow chart was adjusted and the new flow chart is presented in Figure 1.3 and a definition of the different stages and the characteristic point in the stress-strain diagram is given in Figure 1.4. Van Mier [2004] was the first who proposed such a 'universal' four stage crack model. In van Mier [2004] and van Mier [2008] the development of these four stages has been describes in quite some detail, including (experimental) proof for the four stages. According to van Mier [2004] and Figure 1.4 each material shows strain hardening. The only difference is how pronounced the strain hardening is. Even a plain concrete shows strain hardening (see Evans & Marathe [1968], van Vliet [2000]).

Van Zijl [2005] showed that the production method and fabrication of fibre-reinforced concrete influences the mechanical properties. Investigations on spinned, cast and extruded specimens were carried out. Due to the different fabrication methods the fibre alignment and orientation was different and therefore the mechanical properties altered. Van Zijl [2005] determined the orientation of the fibres on cut cross-sections of the material. Peled & Mobasher [2007] compared two different manufacturing methods for fabric cement based composites using different fibres and fabrics. Mechanical properties were determined on pultruded and cast specimens. They found that the mechanical properties can be improved by using the pultrusion technique and that the production process should be adapted to the structure of the fabric to optimize the reinforcing efficiency. Earlier, Rosenbusch [2004] also determined the influence of fibre orientation on the mechanical properties. Wuest et al. [2007] introduced image analysis to analyze and determine fibre orientation on cut specimens. They showed that a complex sample preparation is necessary in order to get decent results. At least two perpendicular cross-sections were analyzed and the resulting fibre orientation was deter-

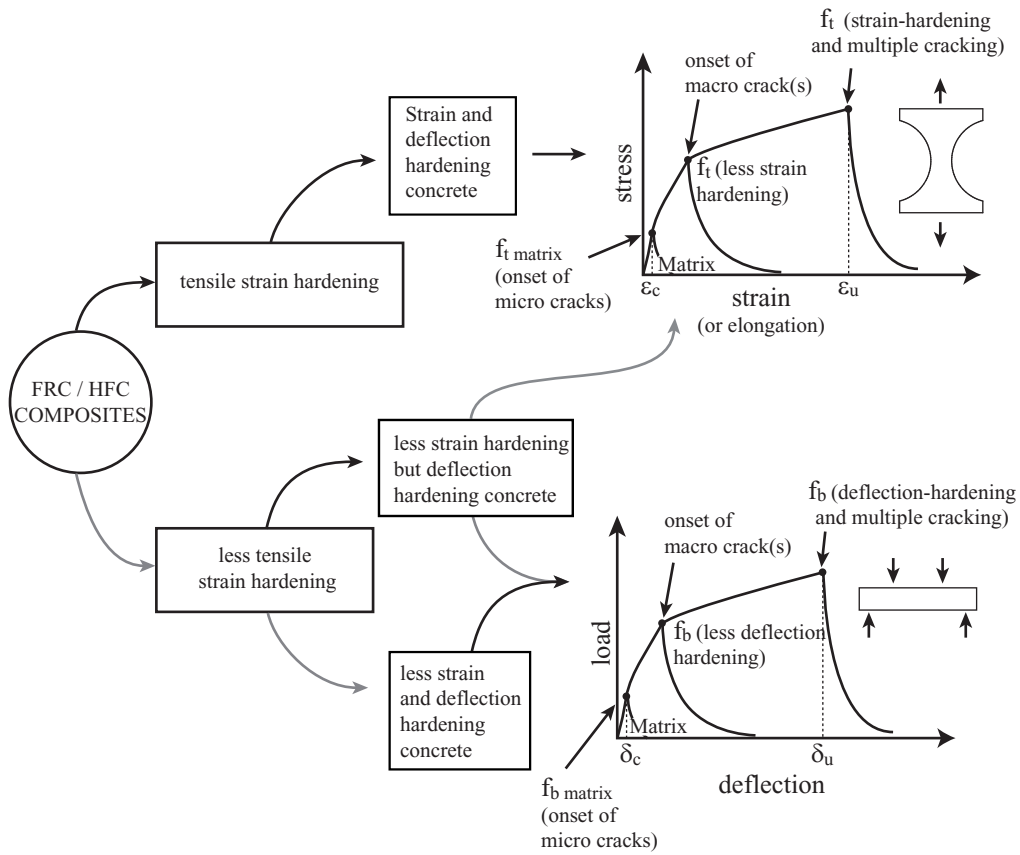


Figure 1.3: Classification of fibre reinforced composites (FRC/HFC) based on their tensile stress-strain response

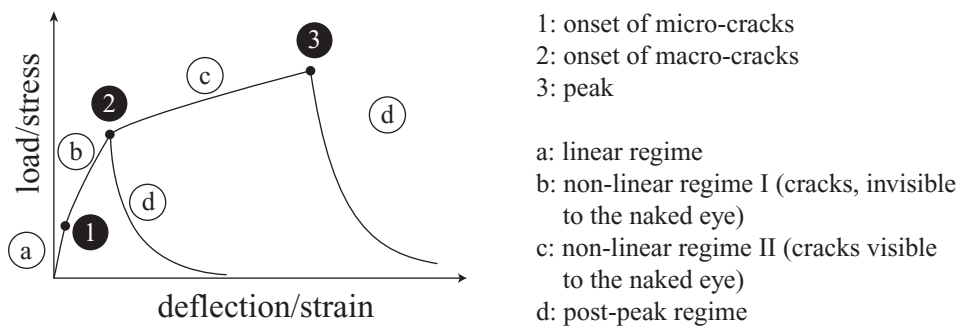


Figure 1.4: Definitions of the four stages and the three characteristic points in the stress-strain diagram



mined. Ozyurt et al. [2006a, 2007] investigated a non destructive method how to determine fibre orientation by use of AC-impedance. With such a none-destructive technique it is possible to monitor fibre clumping and fibre dispersion during the filling process and as well as in the hardened specimen. The results are promising. Kim et al. [2008] showed that the fibres also align in large scale tests. A large plate was cast and specimens were cut out of this plate. Afterwards fibre distribution, alignment and mechanical properties were determined. They showed that the fibres align in the direction of the flow and that the discrepancy between the lowest and highest ultimate strength was up to 50%. di Prisco et al. [2008] performed full size structural tests on thin plates which can be used for thin roof elements. The results showed that casting should be performed very carefully. Different bending behaviours in terms of either maximum bearing capacity or ductility were observed using the same concrete mixture. All these results indicate a dependency between filling/casting and mechanical properties of FRC.

## 1.3 Testing methods

### 1.3.1 Tensile strength

The tensile strength of plain concrete can be determined using different tests such as bending tests, Brazilian tests (split cylinder test), wedge splitting tests or uniaxial tension tests. The latter is the only one where the tensile behaviour is determined directly. Elasticity theory has to be used to calculate the tensile strength using the other above-mentioned tests. For these tests the advantage is the simplicity of the test set-up and the reduced demands on the testing machine. Uniaxial tension tests require a large expense of time and energy. Only few specimens can be tested because each specimen consumes a lot of time for preparing and testing. On the contrary, common bending tests can be carried out very quickly, and many tests can be performed on a single day.

### 1.3.2 Tensile testing

In a material like hybrid fibre concrete (HFC) the important properties to be improved are the tensile strength and ductility (hardening). These properties can be improved by adding different types of fibres (see Markovic [2006], Markovic et al. [2003], Rossi [1997], Stähli & van Mier [2007a]) or by aligning the fibres in the stress direction (see Linsel [2005], van Zijl [2005]). A uniaxial tension test is privileged and recommended to test such an improved material.

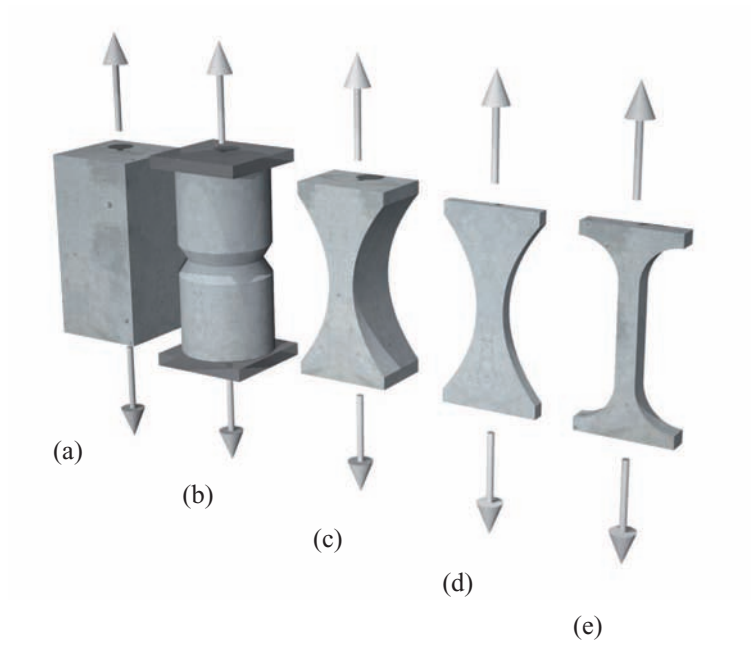


Figure 1.5: Different kinds of tensile specimens. (a) and (b): prisms and cylinders with or without notches; (c) and (d): thick and thin dog bone specimens; (e): dumbbell tensile specimen

However up till now there is no standard tensile test, there is not even a standard tensile test specimen. Figure 1.5 gives an overview of different specimen geometries which were and are still used. A uniaxial tension test allows determining the "real" tensile strength and ductility because the stress state is rather well defined in comparison to the stresses of indirect test methods and the stresses are more-or-less uniformly distributed over the whole cross-section up to peak stress. To be able to test the ductility the supports of the test set-up should have no restrained freedom of movement during the whole test. This has been achieved by means of an arrangement based on 'pendulum-bars' (see Stähli & van Mier [2007b]). Gjørv et al. [1977] showed the influence of fixed and rotating supports on the load-displacement-diagram in bending tests. Due to friction (fixed supports) or less friction (rotating supports) the effect is significant as shown in Figure 1.6. The values of the tensile/bending strength and the ductility are on a higher level using fixed supports.

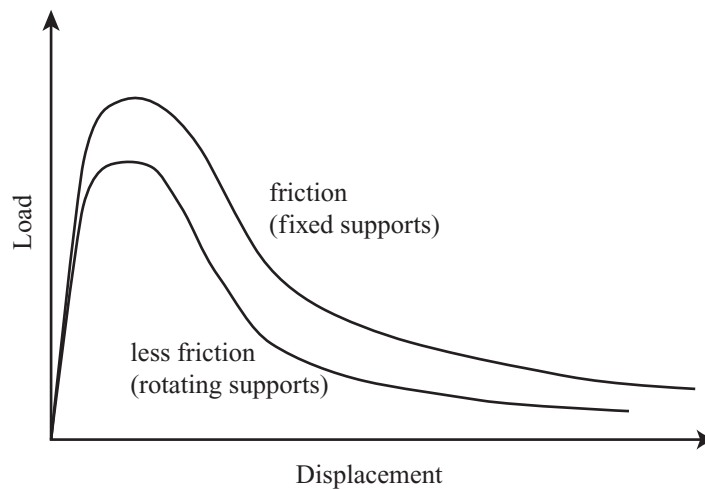


Figure 1.6: Influence of the supports on the load-displacement-diagram in bending after Gjørv et al. [1977].

The diameter of the smallest cross-section of the dog-bone shaped tensile test specimens should be at least three times the length of the largest fibre to reduce possible wall effects and to have a representative volume of the material which is needed for many continuum variables like stress and strain. Uniaxial tensile tests on plain cement and concrete were already performed from micro (Trtik et al. [2007]) to macro level (van Vliet [2000]). For fibre reinforced concrete similar test set-ups can be used even if the tensile strength is on a much higher level. The test does not necessarily have to be

deformation-controlled because of the enhanced ductility of FRC and HFC (see Mechtcherine [2007]). Naaman et al. [2007] give an overview of the different types of tensile test set-ups for thin specimens. Different support conditions such as fixed or rotating and specimen preparation (notched, un-notched) are well discussed. Further more, Naaman et al. [2007] recommends to use different boundary conditions for differently classified fibre reinforced concretes. For HFC with enhanced mechanical properties un-notched specimens are strongly recommended in order to determine strength and ductility. Additionally, the supports of the test set-ups should be free to rotate. Van Mier et al. [1995] already showed that with rotational supports the lowest value of fracture energy and tensile strength was found. Reason enough to use free-rotating supports only.

## 1.4 Outline of this PhD-Thesis

This PhD-thesis consists of eight chapters and its structure is given in Figure 1.7

In Chapter 2 the mixture design of HFC is given including a description of the main materials used. The sub-chapters describe the composition of the concrete matrix and an optimized mixing procedure including some results given at the end of this chapter.

Chapter 3 describes rheological tests such as slump flow tests and introduces a new flow test which is especially designed for HFC; the so called 'SegBox'. Results using the SegBox are presented at the end of the chapter.

In Chapter 4 different moulds and production methods are presented. Techniques for determining fibre distribution and orientation are presented. Finally results using the above mentioned production methods and techniques are presented.

Chapter 5 describes the developed pendulum-bar four-point bending and tensile test set-up. A sub-chapter gives a description of the impregnation technique and describes methods to analyze crack patterns. Results of mechanical tests and impregnation analysis are presented at the end of this chapter.

Chapter 6 combines all previous chapters. The influence of the filling method on the mechanical properties and fibre orientation was investigated. Flow properties were optimized in order to fill the different moulds in the

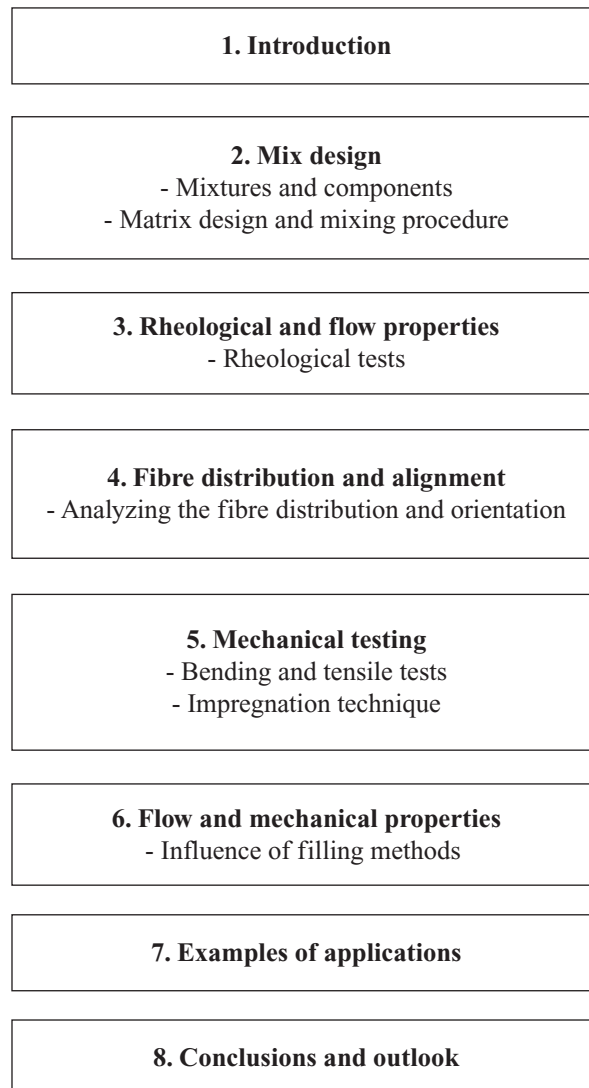


Figure 1.7: Structure of this PhD-Thesis

best possible way. Further more, due to an optimum flowing of the material, fibres were orientated in the direction of the flow. Results using bending or tensile specimens are presented.

Chapter 7 shows possible applications of hybrid fibre and ultra fluid concretes. Several projects which were carried out during this PhD project using such materials are presented.

In Chapter 8 the main conclusions are summarized. The development of hybrid fibre concrete with enhanced flow-ability appears to lead to much improved mechanical behaviour. Based on the results of this PhD-thesis, needs and recommendations for further investigations on high performance concrete are given at the end of Chapter 8.



# Chapter 2

## Mix Design

### 2.1 Introduction

Mechanical and rheological properties of fibre reinforced concrete are dependent on the mix design. Mechanical properties can in addition be influenced by the filling method (aligning of the fibres, see Chapter 6) and the storage of the specimens which will be discussed later. A mix design with an adjusted geometry of the aggregate grains anchors the fibres under optimum conditions and lets the concrete flow as demanded which may lead to higher strength (Ferrara et al. [2007b], Markovic [2006]).

To satisfy the rheological and mechanical demands of hybrid fibre concrete such as low viscosity and high tensile strength, an engineered mix design is central. The following Chapter describes the used components, such as cement, fly-ash, microsilica, sand, super-plasticizer and steel fibres. Furthermore, the matrix compositions, two mixing procedures and some results are described and discussed.

### 2.2 Mixtures

#### 2.2.1 Components

##### 2.2.1.1 Cement

The cement used was a CEM I 52.5R from Holcim AG, product name 'Normo 5R'. An ESEM image and a photograph are shown in Figure 2.1. This Type I cement contains 95% -100% portland-cement-clinker, therefore the early age strength is raised and the hydration is fast. The particle size distribution is given in Figure 2.2. The size distribution was determined us-



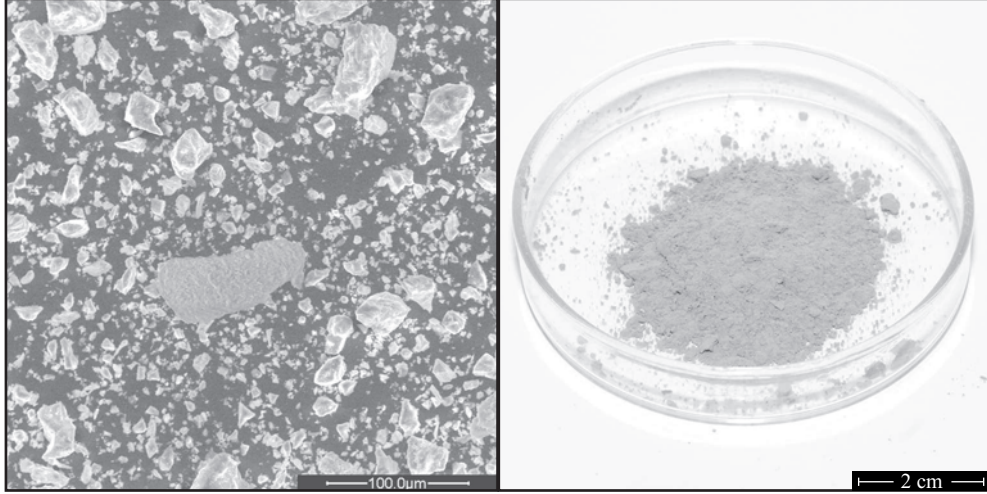


Figure 2.1: ESEM image and a photograph of the cement used

ing a laser scattering particle size distribution analyzer. Normo 5R has a density of  $3100 \text{ kg/m}^3$ . This cement was used because of its strength and fine milled grains.

### 2.2.1.2 Fly-ash

The used fly-ash was Hydrolent from Holcim AG. This pozzolanic coal fly-ash contains much silicic acid. An ESEM image and a photograph are shown in figure 2.3. The particle size distribution is given in Figure 2.2. The size distribution was determined using a laser scattering particle size distribution analyzer. The spheroidal shape and the smooth surface of the fly ash particles (see Figure 2.3) have a positive effect on the work-ability of the fresh concrete. These particles act like a "lubricatant" for fresh concrete. Using fly-ash, the fresh concrete becomes self-compacting and self-leveling at the same water to binder (w/b) ratio. The water to binder ratio was calculated taking the whole amount of fly-ash into account (see Equation 2.1).

$$w/b = \frac{\text{Water [kg]}}{\text{Cement [kg]} + \text{Fly-ash [kg]}} \quad (2.1)$$

Cement and fly-ash have the same grain size distribution. The hydration of the cement starts right after the water was poured into the mixture while the pozzolanic reaction starts after the hydration has started. These

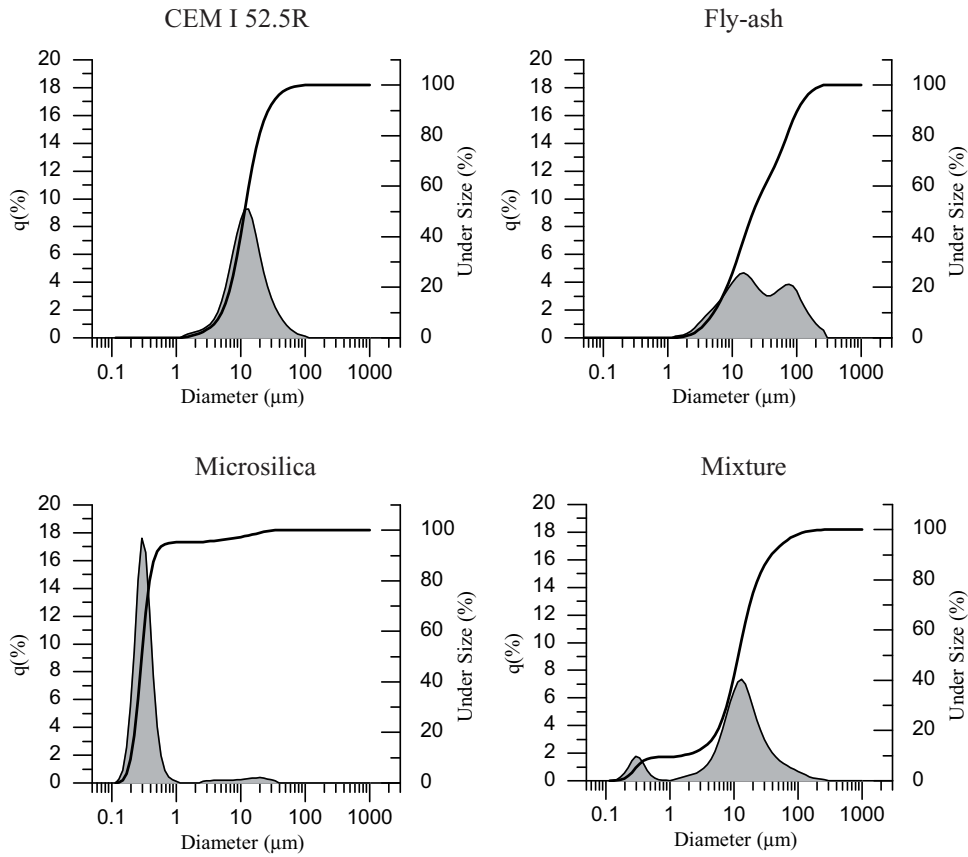


Figure 2.2: Particle size distribution ( $q\%$ : quantity) of the cement used, fly-ash, microsilica and the total binder

two reactions are deferred and the hydration temperature can be decreased. The final strength will be the same as cement only would have been used. Therefore fly-ash can also be used as a substitute of cement and as a fine aggregate. The specific surface is  $3000 \text{ cm}^2/\text{g}$  and the density is  $2600 \text{ kg}/\text{m}^3$ .

### 2.2.1.3 Microsilica

The used microsilica was a grade 940-U undensified microsilica from Elkem Materials. This microsilica contains up to 94% of  $\text{SiO}_2$ . 95.3% of the microsilica particles are smaller than  $2 \mu\text{m}$ . The particle size distribution is given in Figure 2.2. The size distribution was determined using a laser scattering particle size distribution analyzer. An ESEM image and a photograph

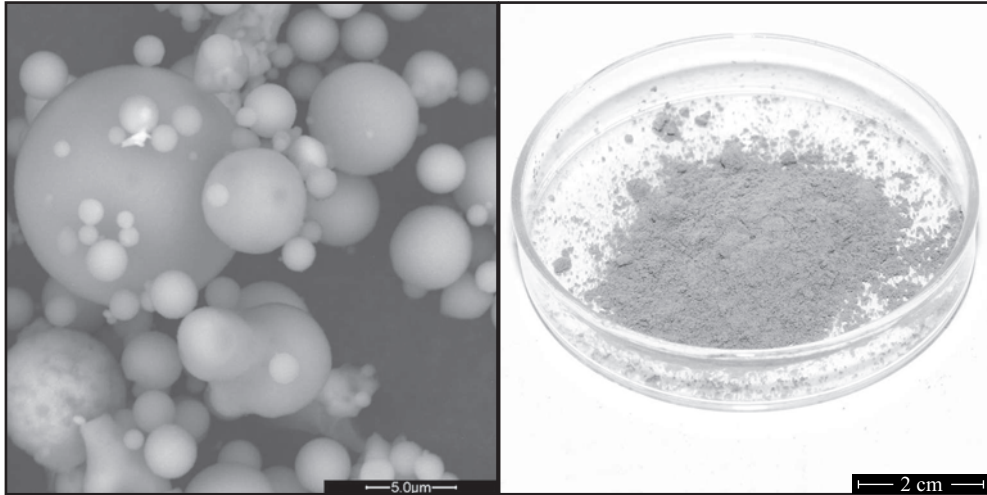
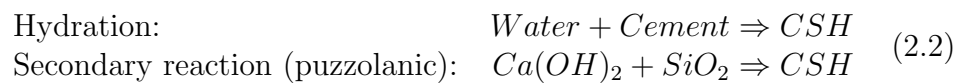


Figure 2.3: ESEM image and a photograph of the used fly-ash

are shown in Figure 2.4. Microsilica was used to complete the aggregate distribution and consequently the aggregate density could be increased and the bond between fibres and matrix could be optimized (see Figure 2.5). Additionally microsilica reacts as a pozzolanic and the final strength of the concrete can be increased. This secondary reaction closes the micro-pores and the matrix becomes denser. The reaction equation is given in Equation 2.2. The specific surface is  $3000 \text{ cm}^2/\text{g}$  and the density  $2200 \text{ kg/m}^3$ .



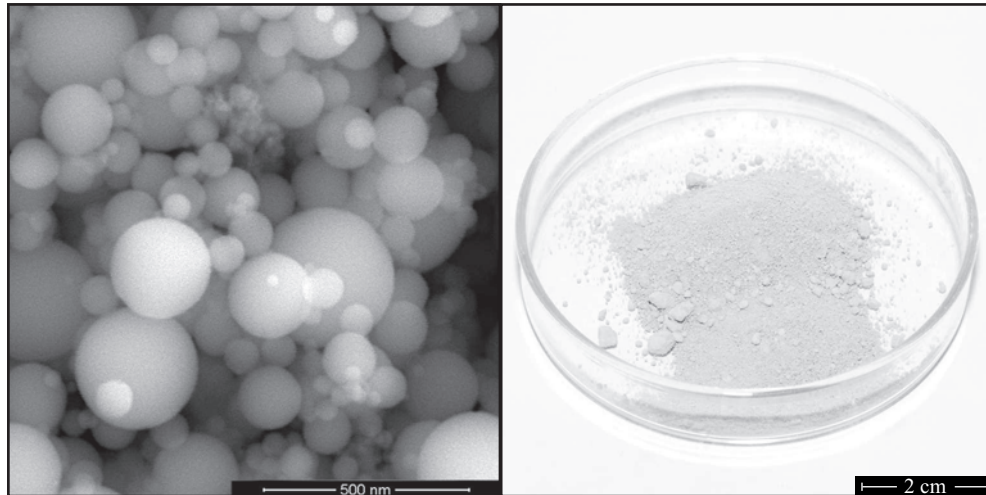


Figure 2.4: ESEM image and a photograph of the used microsilica

#### 2.2.1.4 Aggregates

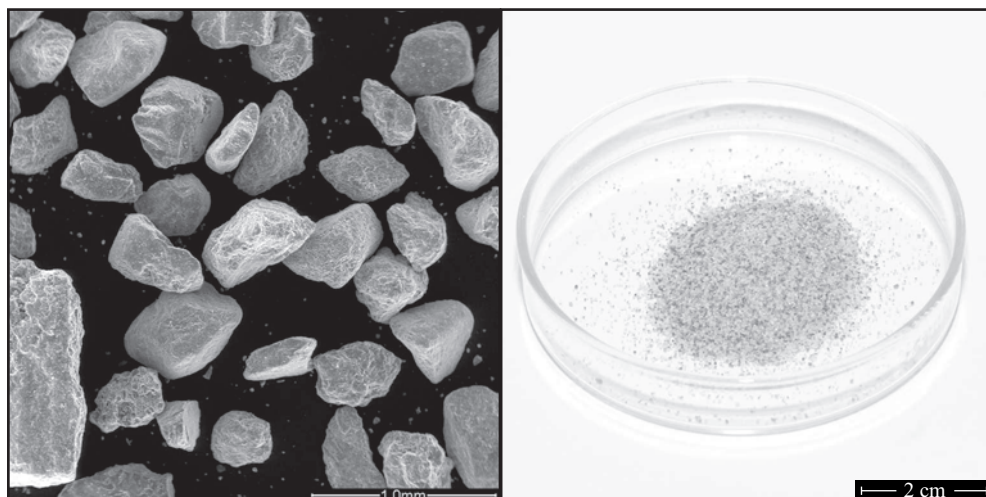


Figure 2.6: ESEM image and a photograph of the sand used 0-1mm

The sand used was a 0-1 mm ordinary river sand. Originally the sand was a 0-4 mm sand. This 0-4 mm sand was sieved at the EMPA Dübendorf and the 0-1 mm particles only were used. Table 2.1 gives the values of the grading curve of the sand used. The dry density is  $2630 \text{ kg/m}^3$ .

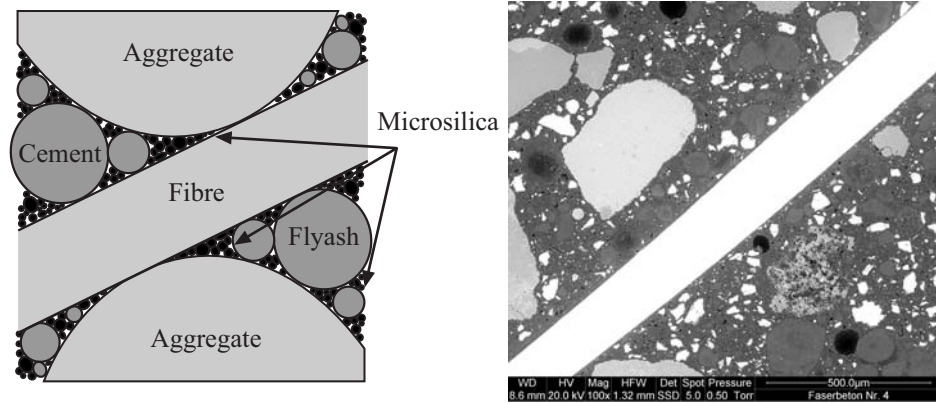


Figure 2.5: Particle packing (cement, sand, fly-ash, microsilica, etc.) around a fibre. Left: model of the particle packing. Right: ESEM image of an embedded fibre in the unhydrated matrix. The matrix was stabilized using epoxy resin.

Table 2.1: Grading curve of the 0-1 mm sand

Sieve size [mm]	0.125	0.250	0.500	1.000	2.000
Passing [%]	4.3%	22.8%	75.0%	90.6%	100.0%

### 2.2.1.5 Super-plasticizer

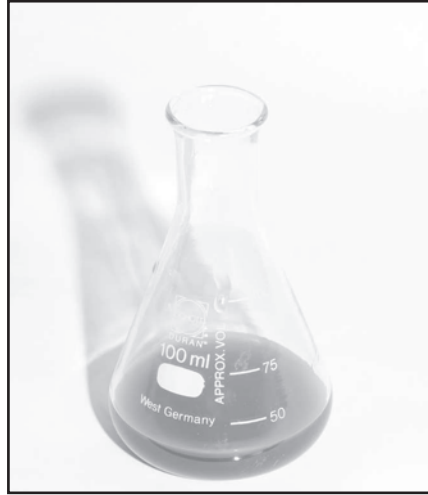


Figure 2.7: A photography of the super-plasticizer used

The super-plasticizer used was Glenium<sup>®</sup> ACE30 from B.A.S.F. Glenium<sup>®</sup> ACE30 is a second generation super-plasticizer of polycarboxylic ether polymers. The particular molecular configuration of Glenium<sup>®</sup> ACE30 accelerates the cement hydration. Rapid absorption of the molecule onto the surface of the cement particles thus causing a steric and electrostatic repulsion between the cement particles, combined with an efficient dispersion effect, exposes an increased surface of the cement grains to react with water (see product details of the manufacturer and Flatt et al. [2004]). The density is  $1100 \text{ kg/m}^3$ . The maximum amount which the producer suggests is 2% of the cement used weight.

### 2.2.1.6 Fibres

All the fibres used were Weidacon fibres from Stratec GmbH. Different geometries and shapes were used. The density was  $7800 \text{ kg/m}^3$ . Figures 2.8 to 2.11 show ESEM images and photographs of the fibres used. The mechanical properties and the geometry of each fibre are given in this subsection.

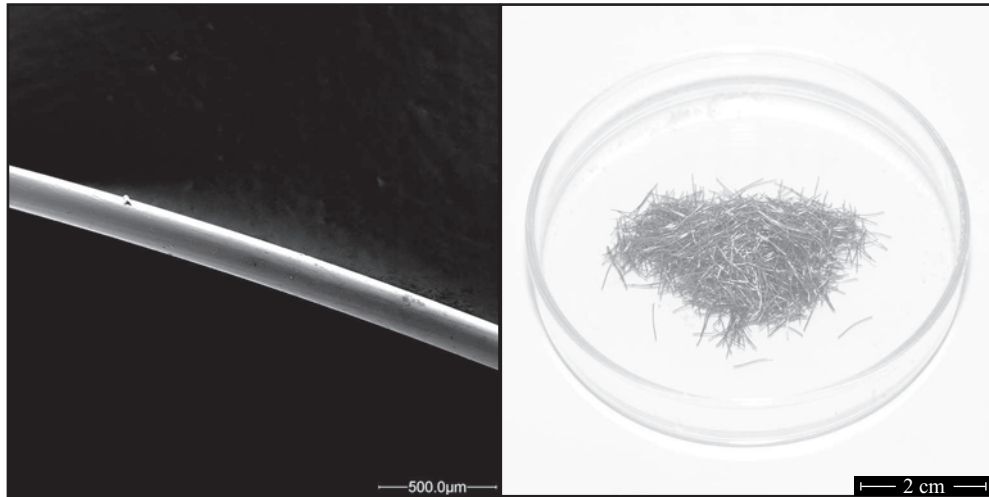


Figure 2.8: ESEM image and a photograph of the  $l/d = 6/0.15$  fibre

The smallest fibre was the  $l/d = 6/0.15$  steel fibre. This is a straight fibre with a diameter of  $150 \mu\text{m}$  and a length of 6 mm. The fibre has a brass coloured look. The yield stress is 1500 MPa and the maximum tensile strength is 2400 MPa.

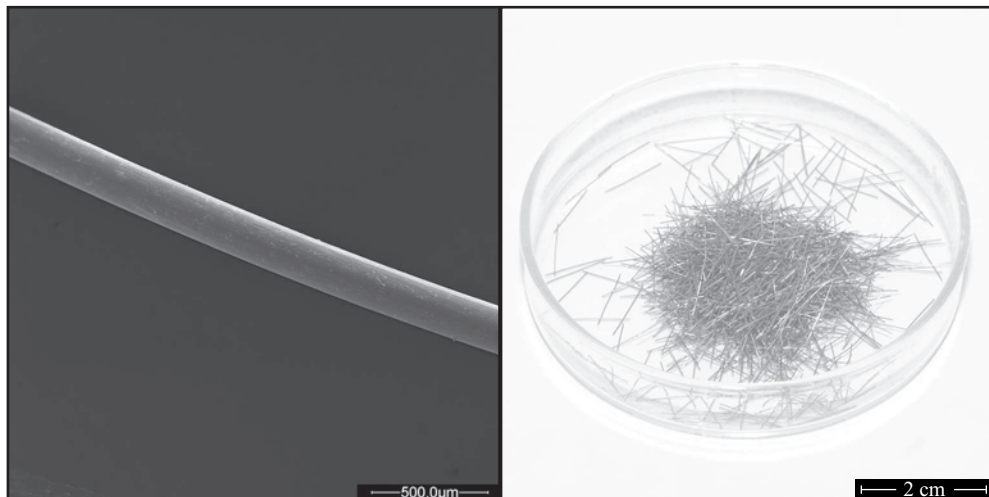


Figure 2.9: ESEM image and a photograph of the  $l/d = 12/0.2$  fibre

The  $l/d = 12/0.2$  steel fibre is a straight fibre with a diameter of  $200 \mu\text{m}$  and a length of 12 mm. The maximum tensile strength is in between 1980 and 2180 MPa.

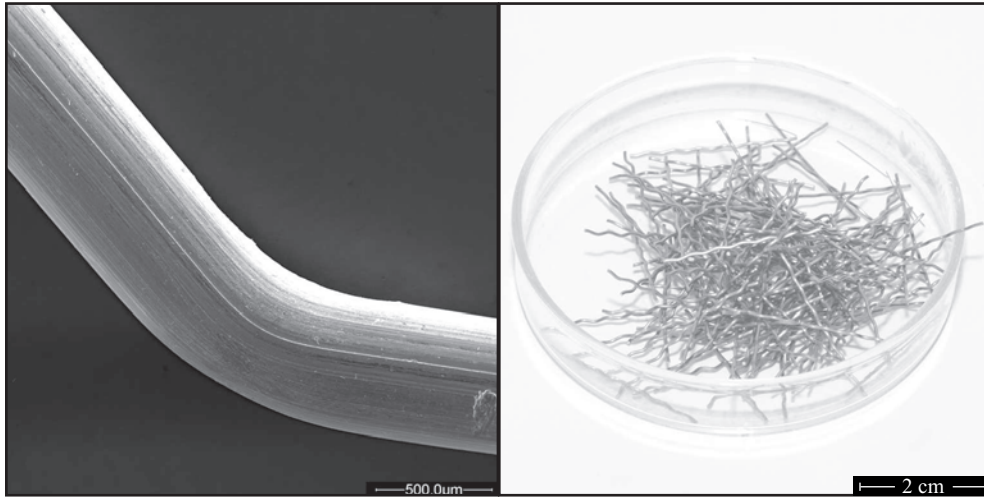


Figure 2.10: ESEM image and a photography of the  $l/d = 27/0.6$  corrugated fibre

The  $l/d = 27/0.6$  steel fibre is a corrugated fibre with a diameter of  $600 \mu\text{m}$  and a length of  $27 \text{ mm}$ . The elongated fibre would have a length of  $30 \text{ mm}$ . The maximum tensile strength is  $1100 \text{ MPa}$ .

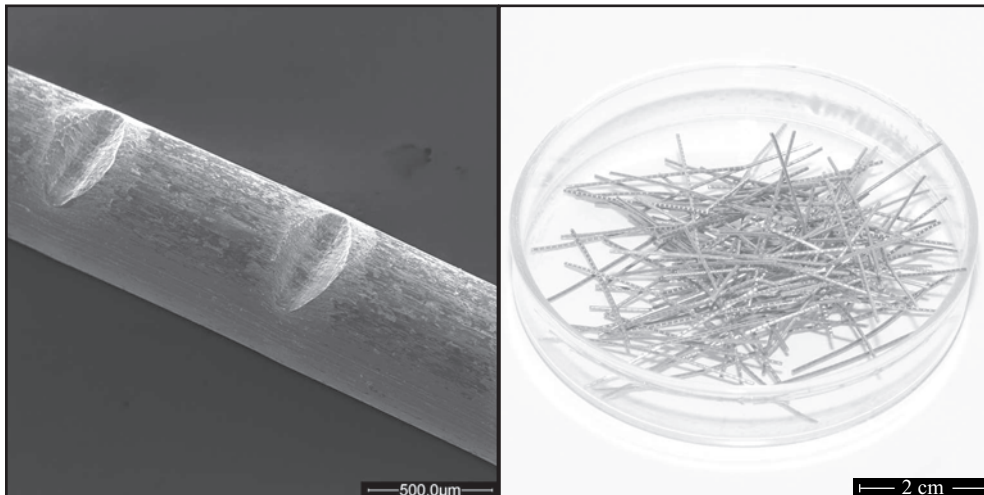


Figure 2.11: ESEM image and a photography of the  $l/d = 30/0.6$  notched fibre

Finally, the  $l/d = 30/0.6$  steel fibre is a notched fibre with a diameter of  $60 \mu\text{m}$  and a length of  $30 \text{ mm}$ . The notch spacing is  $1 \text{ mm}$  and the notch



depth about 150  $\mu\text{m}$ . The maximum tensile strength is 1100 *MPa*. This fibre was primarily used for fibre distribution tests. All the above mentioned numbers are given by the manufacturer.

## 2.3 Matrix design

The matrix was designed (i) to be as dense as possible and (ii) to be as flowable as possible. An effort was made to reduce the amount of cement because of shrinkage and thermal effects. Because the geometry of the particle structure only is responsible for almost all properties of HFC the particle size distribution was adjusted in such a way that the anchorage of the fibres was an optimum. The steel fibres could only float in the matrix by increasing the density or the viscosity of the matrix. Both could be achieved by reducing the w/b-ratio and raising the amount of fine aggregates. Super-plasticizer was added to control the flowability of the mixtures. A self-compacting material was desirable to enhance the mechanical Properties (see Markovic [2006]). For all mixtures the same matrix was used except for two parameters which were adjusted, namely the w/b-ratio and the amount of super-plasticizer in order to control the flowability of the fibre concrete. The w/b-ratio and the amount of super-plasticizer varied between 0.16 - 0.20 and 2.00% - 2.60% respectively for all mixtures.

### 2.3.1 Content of the different components

The binder was composed as follows: 75% cement, 15% fly-ash and the remaining 10% microsilica; all specifications are given in volume percentages. This composition was kept constant for all mixtures. Further on, an attempt was made to add as much fibre (strength) and sand (reduction of cement) as possible into the mixture while retaining a sufficient workability. The main object of the matrix design was to have a self-compacting concrete in order to maximize performance of the fibres. Markovic [2006] showed that the mechanical properties of self-compacting HFCs are much better than those of ordinary FRCs in particular the pull-out strength of the fibres and the bending strength of the material itself. The fact that the mixtures have to be self-compacting influenced the mix-design significantly. The matrix should also be suitable for all fibres and all possible fibre-combinations in the range between 0.2% of one type of fibre to 6% of three types of fibres.

Preliminary tests were performed with up to 6% of steel fibres where the amount and the maximum grain size varied. These experiments showed that a content of 40% of sand (0 - 1 mm) was the maximum amount that could be

added while retaining self-compacting properties. Therefore all the mixtures used contained 40% of the above mentioned sand (see Section 2.2.1.4). This composition ensured a skeleton which embedded the fibres most effectively because of the large amount of cement, fly-ash and microsilica. Results can be seen in Chapter 4 to 6. To be able to compare different mixtures with different amounts of fibres the fibre factor was introduced (Hughes & Fattuhi [1976]). The fibre factor  $F_{fib}$  describes the fibre composition for mixtures contains varying amounts of fibres of different length by the fibre aspect ratio  $l_f/d_f$  and the amount  $V_f$  of each type of fibre ( $V_{f_i}$ ). The fibre ratio is defined by the following equation.

$$F_{fib} = \sum_i V_{f_i} \cdot \frac{l_{f_i}}{d_{f_i}} \quad (2.3)$$

where:  $V_{f_i}$  is the amount of each type of fibre (by volume),  
 $l_{f_i}$  is the length of the fibre,  
 $d_{f_i}$  is the diameter of the fibre

The name of the hybrid fibre mixtures, i.e. the mixture code represents the amounts of the fibres used. The mixture code always contains three numbers. Each number represents the percentage of the amount of each fibre by volume. The first number represents the small  $l/d = 6/0.15$ , the second the middle  $l/d = 12/0.2$  and the third number the large  $l/d = 27/0.6$  fibres, e.g. mixture code 2.05 1.25 0.75 means 2.05 vol-% of the  $l/d = 6/0.15$  fibres, 1.25 vol-% of the  $l/d = 12/0.2$  fibres and 0.75 vol-% of the  $l/d = 27/0.6$  fibres. The  $l/d = 30/0.6$  notched fibre was only used to investigate fibre orientation and distribution (see Chapter 4). Therefore this fibre is not included in the mixture code.

All the weights of the different components for the mixtures were calculated using Excel. The input parameters were: the w/b-ratio, the amount of additives and the amount of the different fibres. The output was the complete mixture design including control factors for mixing; such as the weight of w/b = +0.1. For more information on the Excel mixture design program see Appendix A.

### 2.3.2 Mixing procedure

In order to have comparable results it is necessary to assure that the mixing procedure is optimized and kept uniform for all the mixtures. A first recommendation for HFC was given in Stähli & van Mier [2004a]. This recommendation reflects the main issues of a robust mixing procedure for HFC

such as being well prepared, visual testing while mixing, defined mixing times and defined order of adding the components into the mixer. A scheme of the mixing process is shown in Figure 2.12.

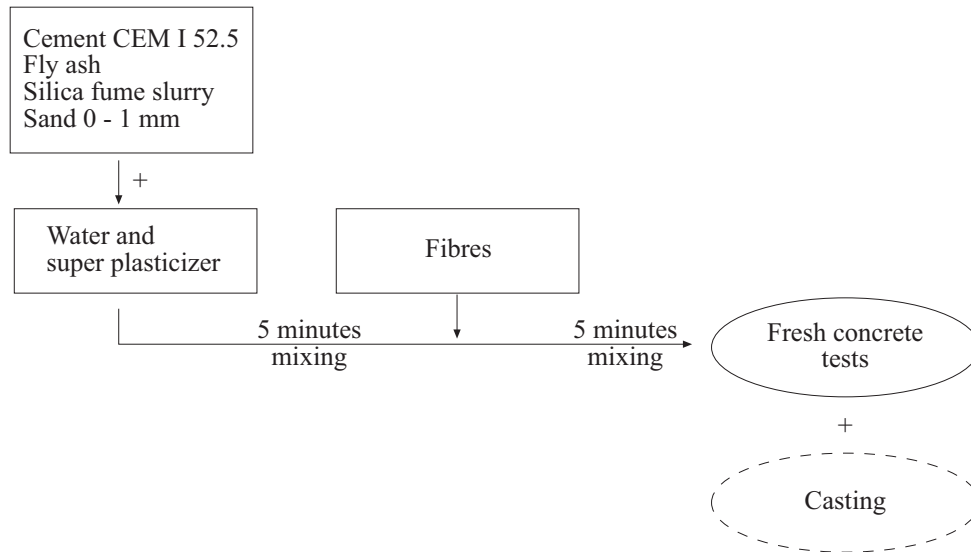


Figure 2.12: Scheme of the mixing procedure for HFC

Commonly the mixing and testing equipment had to be damp. Unfortunately damp conditions are not well defined and comparisons of the flowability of different mixtures can hardly be compared. Therefore it was recommended to use dry equipment only (Stähli & van Mier [2004b]), not only for the mixing tools but also for the fresh concrete test equipment. Consequently a series of experiments where the state of moisture of the test equipment varied was carried out. The series consisted of slump flow test on four different mixtures, using test equipment with three stages of moisture - dry, moist and wet.

- For the 'dry' slump flow test, all the equipment was properly dried with a paper tissue. New paper was used for each test.
- For the 'wet' slump flow test, the slump flow plate was treated with a water-soaked sponge. This treatment results in a fairly uniform layer of water on the plate which allows the slump cone to exhibit 'aquaplaning'. The cone was treated in the same way.

- For the 'moist' slump flow test, the equipment was treated with a damp sponge only. After treatment the surface was moist, but did not allow for 'aqua-planing'.

The influence of this parameter on the test results of the small slump flows is shown in Figure 2.13 and summarized in Table 2.2.

Table 2.2: Different moisture stages of the slump flow test equipment

	<b>Wet slump</b> [mm]	<b>Moist slump</b> [mm]	<b>Dry slump</b> [mm]
Mixture 1	25	22	21
Mixture 2	18.5	17	16.5
Mixture 3	19	18.5	17.5
Mixture 4	13	11	11

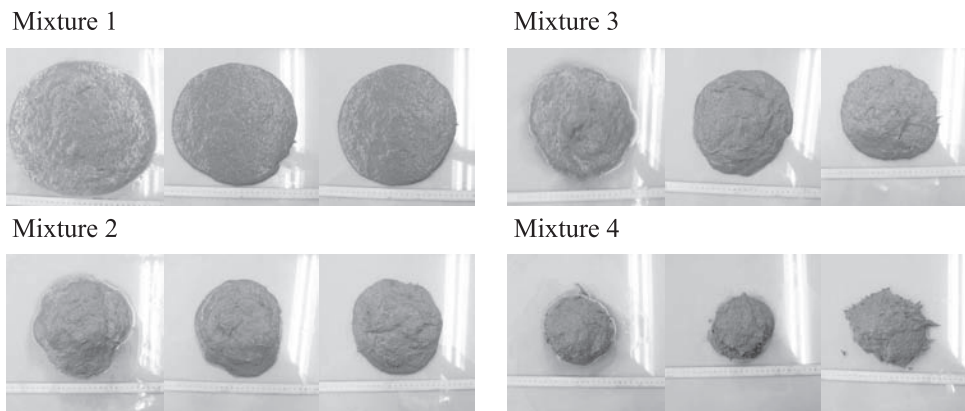


Figure 2.13: Influence of different state of moisture on slump flow results (Table 2.2) For each mixture from left to right the state 'wet', 'moist' and 'dry' are shown

Even though the results shown in Table 2.2 are based on one measurement only, an apparent trend can be observed: more moisture on the testing equipment leads to a larger slump flow. In the case of Mixture 4, there is no difference between 'moist' and 'dry' test results. The reason for that might be that the material was of high viscosity and therefore flowed more slowly than for the other tests. Because of that the water on the test plate was allowed to evaporate for a longer time. Based on these test results, it was

decided to carry out the slump flow test using dry tools only, in that way the moisture condition of the test equipment is well defined. In order to optimize the rheological properties and to minimize the amount of water and super-plasticizer a test series was carried out where the mixing sequence varied but the mix design was kept constant.

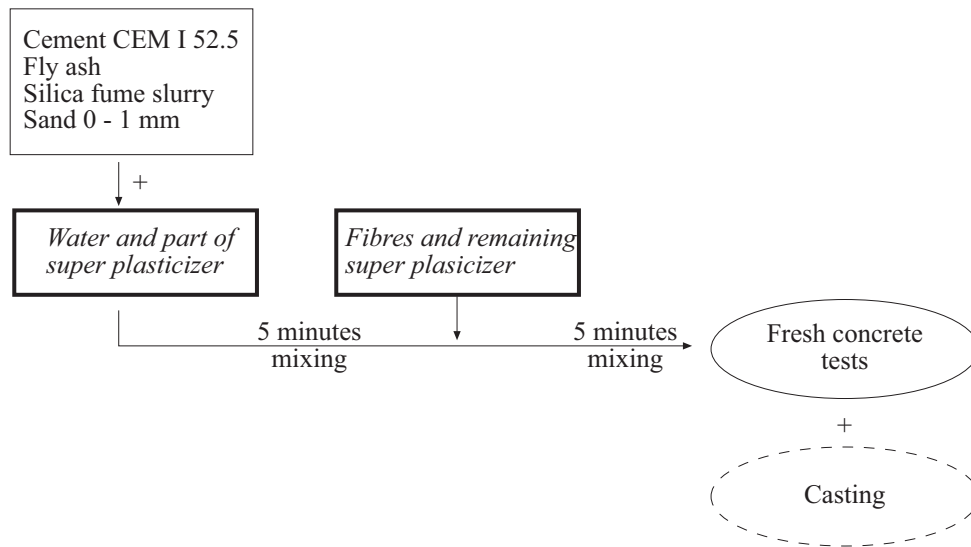


Figure 2.14: Scheme of the optimized mixing procedure for HFC

For each mixture the above mentioned mixing procedures and an optimized mixing procedure were performed. Small slump flow tests were carried out (see Chapter 3) and the diameter of the slump flow was measured. In an optimized procedure only a part of the super-plasticizer was added together with the water and mixed for 5 minutes (see Figure 2.14). The remaining super-plasticizer was added together with the fibres and mixed for the remaining 5 minutes. Table 2.3 gives an overview of the used fibre mixes and Figure 2.15 shows images of the respective small slump flows. This figure shows that in some cases the material mixed with the optimized procedure flowed twice as far (the diameter of the small slump flow cone is 10 cm) as the one mixed with the common procedure. These results show that the performance of the super-plasticizer can be increased by adding it in two steps. The majority of the super-plasticizer should be added with the water; the remainder with the fibres. This increase in the "flowability" can be caused by the fact that the aggregates and the cement were already saturated with the initial water and super-plasticizer mix, i.e. part of the firstly added super-plasticizer was absorbed by the aggregates and its performance could

not develop. The remaining super-plasticizer was not absorbed anymore and therefore the performance is much enhanced. For the common mixing procedure part of the whole super-plasticizer can be absorbed by the aggregates and less 'free' super-plasticizer can have an effect on the flowability. An optimum would be if the whole amount of super-plasticizer could be added together with the fibres. Unfortunately this is not possible because of the concrete mixer. A certain amount of super-plasticizer is needed in order to be able to mix mix-designs with low w/b-ratios with the available concrete mixers (see Appendix A). The power of the concrete mixers is not sufficient to mix such dry mixtures.

Table 2.3: Overview of the concrete mixtures used for the optimized mixing procedure

Mixture code <sup>1)</sup>	300	<i>300*</i>	030	<i>030</i>	003	<i>003</i>	111	<i>111</i>	311	<i>311</i>
Small fibre $l/d = 6/0.15$	3%	3%	-	-	-	-	1%	1%	3%	3%
Middle fibre $l/d = 12/0.2$	-	-	3%	3%	-	-	1%	1%	1%	1%
Large fibre $l/d = 30/0.6$	-	-	-	-	3%	3%	1%	1%	1%	1%
Super-plasticizer	2.3%	2.15%	2.6%	2.3%	2.5%	2%	2.45%	2.3%	2.6%	2.3%
Remaining super-plasticizer	-	0.15%	-	0.3%	-	0.5%	-	0.15%	-	0.3%

\* The mixtures where the optimized mixing procedure was applied are shown in italics

<sup>1)</sup> The mixture code shows the percentage of short, middle and large fibres respectively

The effect of the super-plasticizer on the flowability of a mixture is dependent on the mixing time. A series where small slump flow test were performed after a certain mixing time was carried out by Hafner & Brändli [2004]. Four slump flows from the same batch were performed in two minute intervals. The results can be seen in Table 2.4. It can be seen that a minimum mixing time of 8 minutes is needed in order to ensure that the flow-ability does not change with the mixing time any further.

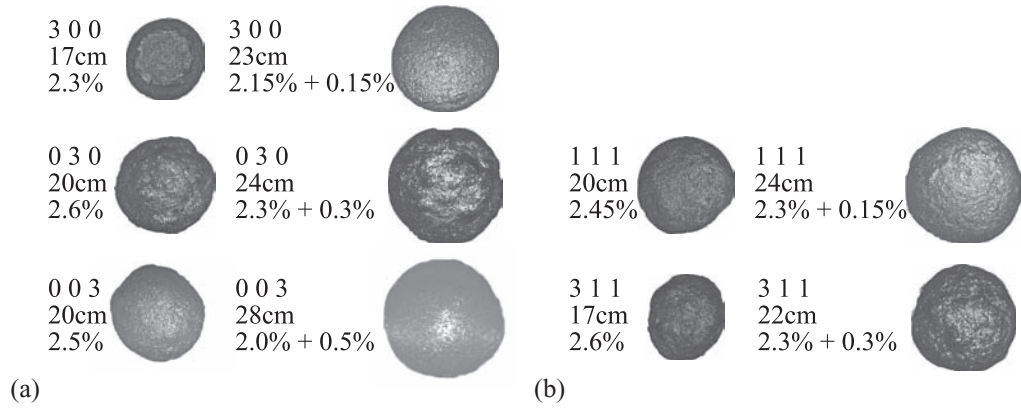


Figure 2.15: Images of slump flows for (a) FRC mixtures and for (b) HFC mixtures, showing the mixture code, the diameter of the slump flow test and the amount of super-plasticizer

Table 2.4: Time-dependency of the effect of the super-plasticizer

Mixing time	small fibres $l/d = 6/0.15$	$s_{sf}$ [cm]
2 min	7%	19
4 min	7%	23
6 min	7%	24.5
8 min	7%	24

## 2.4 Conclusions

From these results the following conclusions can be drawn:

- In order to get comparable results all rheological tests should be carried out using dry equipment, especially the slump flow cone and the slump flow plate must be dry.
- The performance of the super-plasticizer can be increased by adding it in two steps. The majority should be added with the water and the remainder together with the fibres (improved mixing procedure). Using such a two-step procedure the performance of the super-plasticizer can increase the small slump flow by more than 50%.
- The total mixing time should be in the order of 8 - 10 min to improve the effect of the super-plasticizer. This has been taken into account by the mixing procedure.





# Chapter 3

## Rheological and flow properties

### 3.1 Introduction

This Chapter gives an overview of the performed rheological tests for mixtures that differed in their w/b-ratio, the amount of super-plasticizer and the amount of the different fibres. The rheological properties determined are the flowability and flow properties only. Different fresh concrete and fresh mortar tests were performed to be able to compare different mixtures with each other. These tests can not be used to determine rheological properties such as viscosity or critical shear stress. Kuder et al. [2007] determined rheological properties, such as yield stress, for matrix only and fibre reinforced concrete using different types of rheometers. They found that it is possible to determine rheological properties of FRC using a parallel plate rheometer. However in this Thesis, common and newly developed tests were used in stead of rheometers. The so-called SegBox test was specially developed for 'wide' flowing materials such as HFC. This test was already introduced in Stähli & van Mier [2007a]. Slump flow tests with the inverted Abrahams cone, slump flow tests using the cone from the Hagman table and air void content tests were performed as well. All the slumps were photographed and the diameter was determined. Later on the images of the different slumps were compared.

## 3.2 Rheological Tests

### 3.2.1 SegBox

The so called SegBox (**Segregation Box**) was developed to analyze the flow properties, the fibre segregation and the fibre alignment of HFC. The dimension of the SegBox are  $300 \times 300 \times 100 \text{ mm}^3$  with a wedge ( $200 \times 20 \times 100 \text{ mm}^3$ ) inside which divides the box into a filling and a climbing branch (see Figure 3.1). The SegBox is made of PVC without any surface treatment. The wedge is slightly inclined so that the cross section of the climbing part is constant at  $100 \times 100 \text{ mm}^2$ . Therefore the flow of the material is constant and not influenced by an apparent conical or decreasing cross section which is apparent in the climbing branch. Later on the SegBox was cut and the fibre distribution, i.e. fibre segregation, fibre clumping and fibre alignment could be analyzed (see Chapter 4). Originally the SegBox was developed to analyze fibre segregation in the climbing branch. It turned out that only the large fibres tend to segregate and that the SegBox can also be used to observe self-leveling behaviour of the material itself.

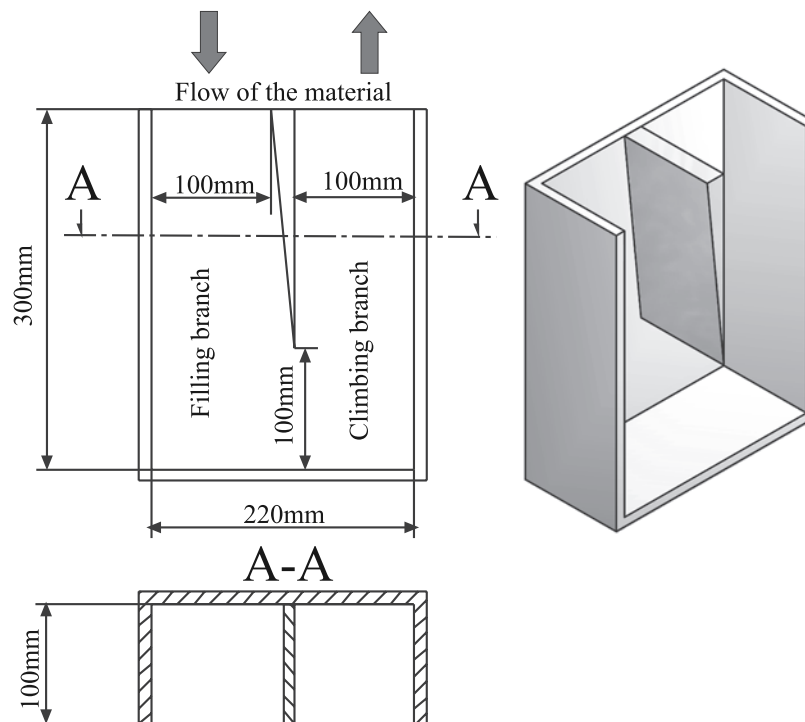


Figure 3.1: Sketch of the SegBox

The fresh concrete was filled from one side only until the filling branch was completely filled (approximately 6 liters of concrete). During filling the concrete would rise on the other side as well. The SegBox experiment was performed with 'dry' equipment only.

After one day the SegBox was demoulded and the length of the two branches of the hardened and cut concrete were measured and the self-leveling-degree was determined using Equation 3.1 and 3.2. Images of the filling process are shown in Figure 3.2. The images in Figure 3.2 were taken using a special SegBox with a plexiglass wall which was only used to be able to observe the filling process. The SegBox was filled with a small laboratory shovel. It can be seen that the material starts to level out from the beginning, although in the example complete leveling was never reached.

$$F_{SL} = 1 - \Delta l / l_{fill} \quad (3.1)$$

with

$$\Delta l = l_{fill} - l_{climb} \quad (3.2)$$

when  $l_{fill}$  and  $l_{climb}$  are defined in Figure 3.2d.

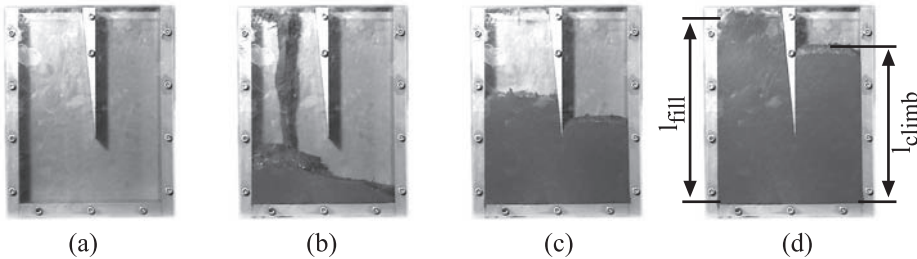


Figure 3.2: (a) to (d): Filling process of the SegBox. (d): Lengths of the different branches

At the end a difference of the lengths at the filling branch ( $l_{fill}$ ) and the climbing branch ( $l_{climb}$ ) can be observed.

### 3.2.1.1 Self-leveling degree of different HFC mixtures

SegBox experiments with material which only differed in the w/b ratio were performed to analyze the self-leveling behaviour of HFC mixtures. For each SegBox experiment 6 Liters of concrete were produced, and a small slump flow test and a SegBox test were carried out. The lengths of the filling and the climbing branch were measured. Figure 3.3 shows the image of the cut SegBox specimens and Table 3.1 gives an overview of the results.

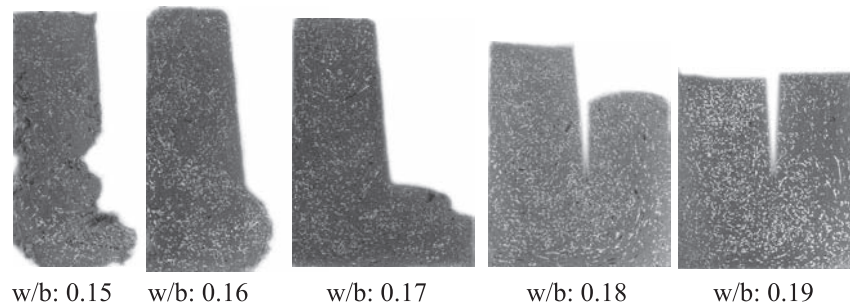


Figure 3.3: Images of SegBox specimens cast out of HFC with different w/b-ratios

Figure 3.3 clearly shows that both the self leveling behaviour and fibre alignment and segregation are very sensitive to the flow properties of the material such as slump flow diameter. For the w/b-ratio between 0.15 - 0.17 randomly distributed fibre can be observed while for w/b = 0.18 and 0.19 the fibres starts to align in the direction of the flow. w/b = 0.19 shows a slight segregation of the fibres in addition to flow-alignment (see Figure 3.3, w/b: 0.19, right branch = climbing branch); less fibres were observed in the upper part of the climbing branch than in its lower part. The fibre distribution and orientation was also analyzed. The results can be found in Chapter 4. An other interesting point is that the material is self-compacting even if it does not flow (w/b: 0.16, small slump flow: 10 cm). The matrix contains small particles only. These small particles are already 'compacted' on the macro level, no voids can be seen with the naked eye. The surface layer (cement skin) is closed and the concrete appears dense and compacted. For the lowest w/b = 0.15 the material does not appear to be self-compacting and would need some external energy like vibration to compact completely.

Table 3.1: Overview of the SegBox experiment results

w/b-ratio	$s_{sf}$	$l_{fill}$	$l_{climb}$	$F_{SL}$
0.15	10 cm	31.0 cm	0.0 cm	0.0%
0.16	10 cm	32.0 cm	0.0 cm	0.0%
0.17	11 cm	30.0 cm	9.5 cm	31.7%
0.18	17 cm	27.0 cm	21.5 cm	79.6%
0.19	27 cm	24.0 cm	24.5 cm	100.0%

### 3.2.2 Standard fresh concrete tests

The fresh concrete behavior and properties were determined using the above mentioned SegBox and standard tests such as small and large slump flow tests and air void content test. All these tests were carried out immediately after mixing. Depending on these results moulds were cast or the mixture was adjusted.

Fresh concrete test results were used to compare mixtures or to develop new mixtures with desired flow properties. Roussel et al. [2005] developed a method to link slump flow test results with rheological properties such as yield stress. The method is only valid for mortars with a minimum small slump flow of 20 cm. The latter criterion was not fulfilled for all the used mixtures. However while the mixtures contained fibres, the matrix material was a mortar and therefore this method could be applied to determine the properties of the mixtures. For the mixtures, during the mixing procedure and the casting of the moulds the material flows and the fibres start to align in the direction of the flow and the rheological properties change. Therefore the yield stress is dependent on the degree of fibre alignment in the fresh concrete and can not be determined as a single value. Fresh concrete tests were only performed to compare mixtures and to determine influences of fibre mixtures on the flow properties.

#### 3.2.2.1 Slump flow tests

The slump flow test using the Abrahams cone was carried out as the Swiss codes 162/1 [1989] recommended but inverted. Ramsburg [2003] showed that the results of upright or inverted slumps do not differ but it is much easier to carry out inverted slumps. Self leveling mixtures required an average diameter of 65 cm or larger (see DAfStb [2001], Markovic et al. [2003], MBT [2000]). The Abrahams cone was carried out for most of the mixtures at least for the main test series. For all concrete mixtures small slump flow

tests using the cone from the Hagermann table were carried out. The lower diameter of this cone is 10 cm. The criterion for self-leveling was a minimum average diameter of 23 cm, see Stähli & van Mier [2004a]. Sketches and images of the cones and their pertinent slumps are shown in Figure 3.4.

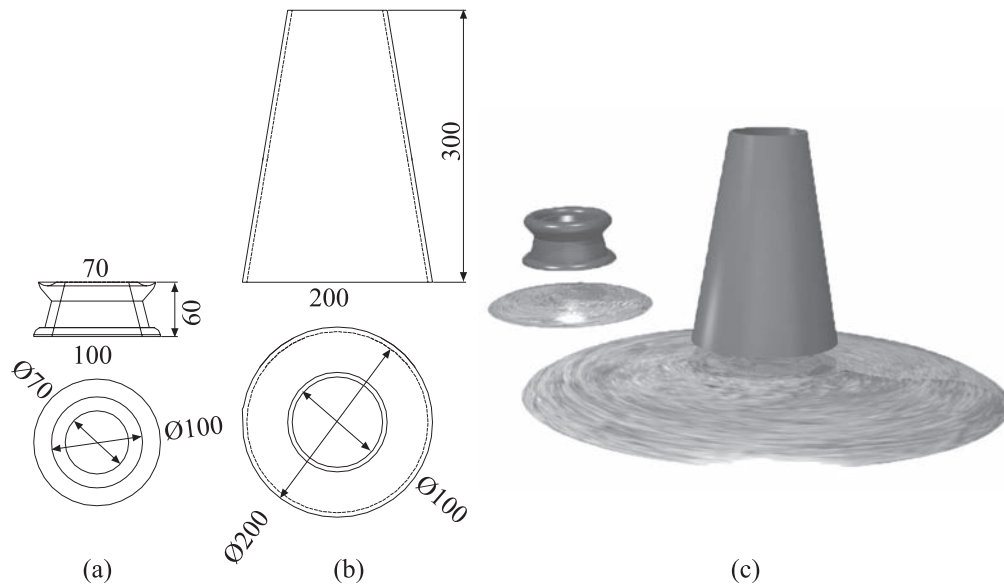


Figure 3.4: (a): Small slump flow cone (Hagermann table); (b): large slump flow cone (Abrahams cone); (c): 3D images of the cones with their pertinent slumps

### 3.2.2.2 Air void content test

The air void content test was carried out as the Swiss codes (162/1 [1989]) recommended. The fresh concrete density could also be determined. The air void content was dependent on the amount of fibres and the fresh concrete behavior.

## 3.3 Results

Several test series were carried out to determine the flow properties of fresh HFC. The amount of fibres, water and super-plasticizer varied but the matrix design and the materials used such as cement, fly-ash, micro silica and sand were the same. Hafner & Brändli [2004] tried to find limits for the maximum amounts of fibres and their combinations by performing small slump flow

tests with a variation of fibre mixtures. They found that these limits can hardly be found because of segregation effects. The fibres tended to build clusters in ultra fluid mixtures during mixing (see Nakamura et al. [2004]) and the small slump flow results are not representative. They also performed large slump flow tests with the same mixtures and the fibres did not segregate. Therefore they suggested to perform large slump flow tests with mixtures which tend to segregate.

### 3.3.1 Influence of fibre-to-fibre ratio on flow behavior

In order to determine the fibre-to-fibre ratio, i.e. the ratio between the different amounts of the different fibres (small:middle:large), on the flowability of HFC, slump flow tests using HFC with four different fibre-to-fibre ratios (f-t-f), e.g. 16:2:1, 5:3:1, 4:3:1, 1:1:1 and different fibre factors  $F_{fib}$  were carried out (see also Stähli & van Mier [2004b]). The mixtures contained 2% of super-plasticizer and the w/b ratio was 0.17. The test results are summarized in Figures 3.5 and 3.6. The diameter of the flow is given in centimeters in the upper right corner of the images in Figure 3.5. These slump flows all had approximately circular shape except in test series 1:1:1 ( $F_{fib} = 3$ ). Otherwise, the only difference in the slump flow tests was the diameter of the 'cakes' themselves. It can be seen that the diameter of the slump flows decreases with increasing fibre factor. It is apparent from Figure 3.6, that the diameter of the slump flow decreases when the fibre-to-fibre ratio approaches 1:1:1. This is likely due to the influence of the long fibres.

An important aspect of self-compacting concrete is its 'self-venting'. Self-venting leads to little air-bubbles being released from the fresh concrete directly after casting. When these bubbles appear on the surface, they burst and the air escapes. However in some cases, for example when a tight film caused by the super-plasticizer builds on the surface of fresh HFC (elephant skin), the bubbles cannot escape anymore. In such cases, when the specimen is cut after hardening, the bubbles can be observed right below the surface (Figure 3.7). This condition was observed when the slump flow exceeded 20 cm. If that happens, the concrete is still self-compacting, even though it does not seem to be self-venting.

In order to get a general idea of the influence of the fibre-to-fibre ratio and the fibre factor, a series with 24 different mixtures with 8 different fibre-to-fibre factors and three different fibre ratios was carried out. An overview of the different mixtures and their small slump flow diameter is given in Table 3.2. The w/b ratio was kept constant at 0.18 and the amount of super-plasticizer was 2.0%.

Images of the small slump flows of the different mixtures are shown in



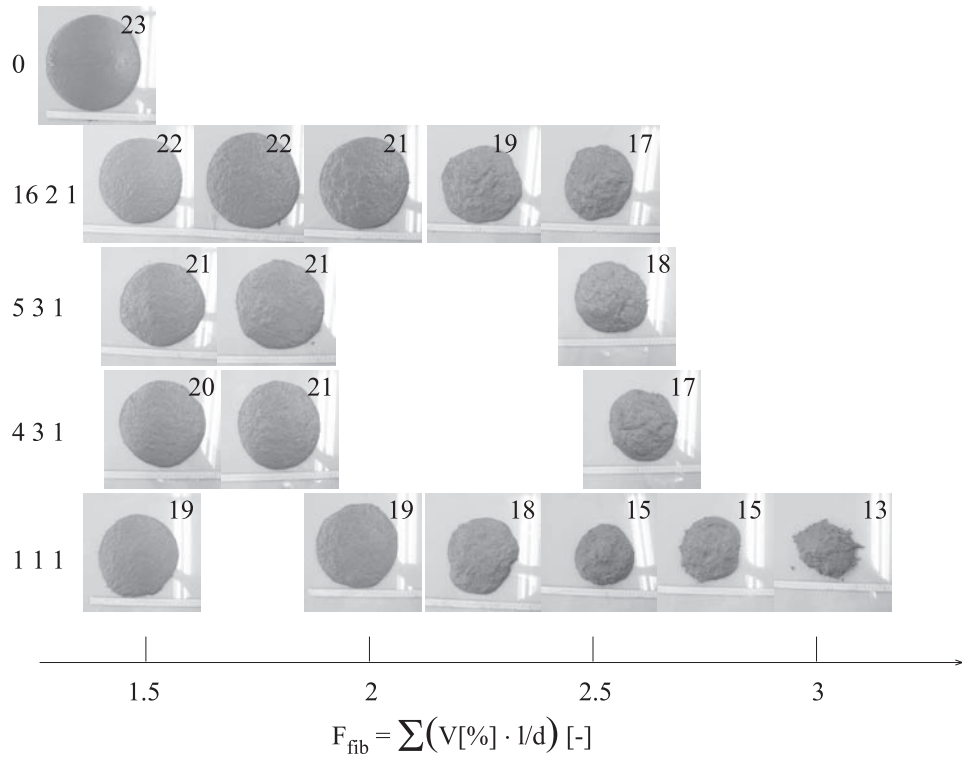


Figure 3.5: Flow-diagram of different mixtures with constant fibre-to-fibre ratios. '0' denotes plain concrete

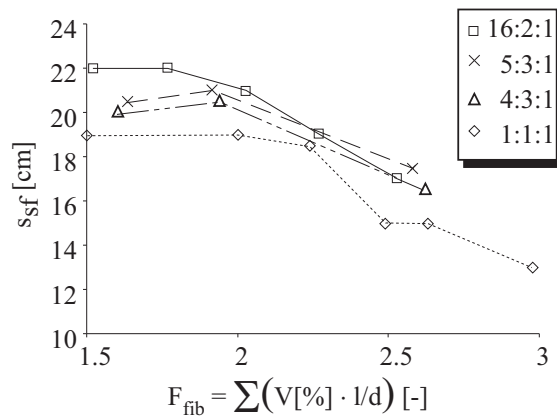


Figure 3.6: Slump flow vs. fibre factor diagram

Table 3.2: Overview of the Fibre-to-Fibre experiment mixtures

Fibre-to-Fibre* ratio	$F_{fib}$	$V_f$ (amount of the fibres)			$V_F$	$s_{sf}$ [cm]
1:1:1	1.5	1.00%	1.00%	1.00%	3.00%	29
	2.0	1.33%	1.33%	1.33%	4.00%	28
	2.5	1.66%	1.66%	1.66%	5.00%	22
4:2:1	1.5	1.80%	0.90%	0.45%	3.15%	25
	2.0	2.45%	1.23%	0.61%	4.29%	23
	2.5	3.05%	1.53%	0.76%	5.34%	19
7:2:1	1.5	2.35%	0.67%	0.34%	3.36%	22
	2.0	3.10%	0.89%	0.44%	4.40%	21
	2.5	3.90%	1.11%	0.56%	5.57%	20
10:2:1	1.5	2.65%	0.53%	0.27%	3.45%	26
	2.0	3.50%	0.70%	0.35%	4.55%	23
	2.5	4.40%	0.88%	0.44%	5.72%	20
6:2:1	1.5	2.20%	0.73%	0.37%	3.30%	20
	2.0	2.90%	0.97%	0.48%	4.35%	20
	2.5	3.65%	1.22%	0.61%	5.48%	19
6:3:1	1.5	1.90%	0.95%	0.32%	3.17%	27
	2.0	2.55%	1.28%	0.43%	4.26%	21
	2.5	3.20%	1.60%	0.53%	5.33%	19
6:4:1	1.5	1.70%	1.13%	0.28%	3.11%	28
	2.0	2.25%	1.50%	0.38%	4.13%	24
	2.5	2.85%	1.90%	0.48%	5.23%	21
6:5:1	1.5	1.55%	1.29%	0.26%	3.10%	26
	2.0	2.05%	1.71%	0.34%	4.10%	22
	2.5	2.55%	2.13%	0.43%	5.11%	20

\*) small-middle-large fibres

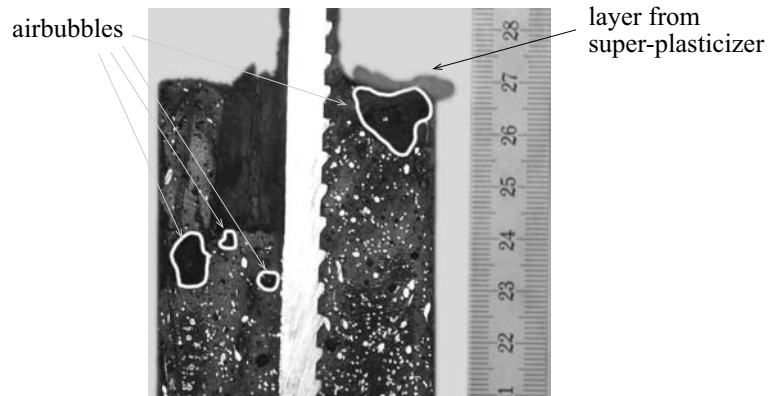


Figure 3.7: Enlarged view of the surface layer

Figure 3.8. It can be seen that most slumps are almost perfect circles and that the diameters of the slump flows decrease with an increase of the fibre factor. No fibre balling or segregation was observed. All the fibres were homogeneously distributed in the fresh concrete. Most of the concretes were self-leveling because their slump flow diameter was at least 23 cm. The self-leveling degree was in between 90% (mixture 3.05% 1.53% 0.76%) and 100%. At first sight Figure 3.9 does not show a clear trend; the flowability seems to decrease with higher content of small fibres, (left side of the diagram in Figure 3.9), and increase with the amount of the middle fibre, (right side of the diagram in Figure 3.9). With the increase of the volume of the middle fibres the content of the small fibres decreases. Therefore it might be concluded that the slump flow increases with a decrease of the small fibres and the middle and large fibres have no significant influence on the slump flow diameter for all the used fibre factors. This statement is valid for the whole diagram in Figure 3.9. On the other hand the large and the middle fibres are responsible for clumping and segregation effects; there the small fibres have no influence. The results concerning the mechanical properties of these mixtures are presented in Chapter 5.

### 3.3.2 Influence of flowability on fibre distribution and alignment

In order to investigate the influence of the flowability on the fibre distribution and alignment a series with five different w/b-ratios and constant fibre contents for three different fibres was carried out. The fibre content was adjusted in such a way that, theoretically, on a cross-section 10 fibres per square

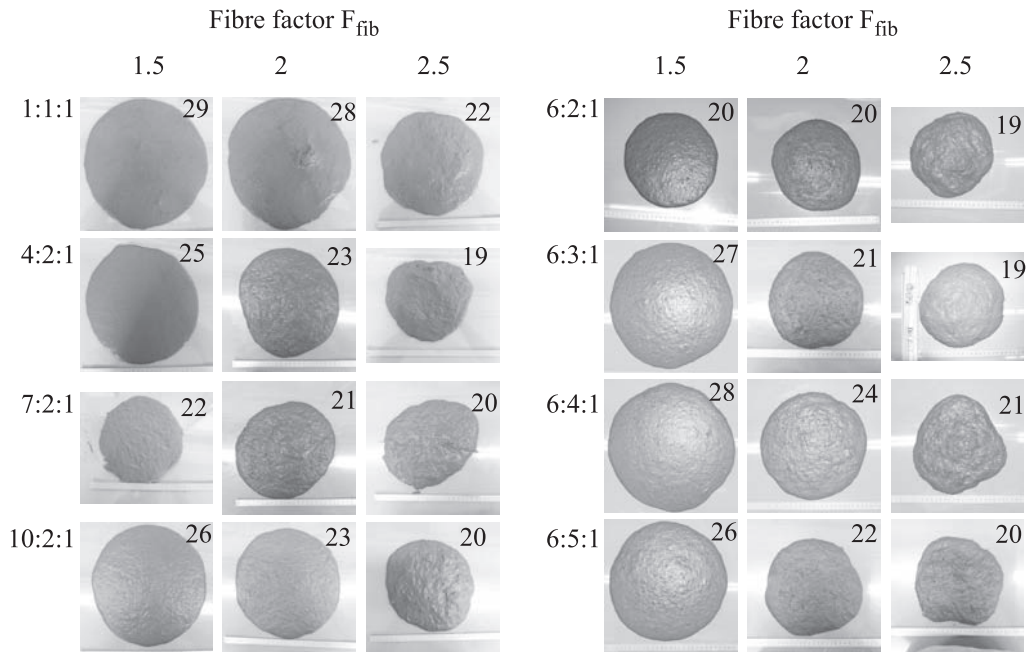
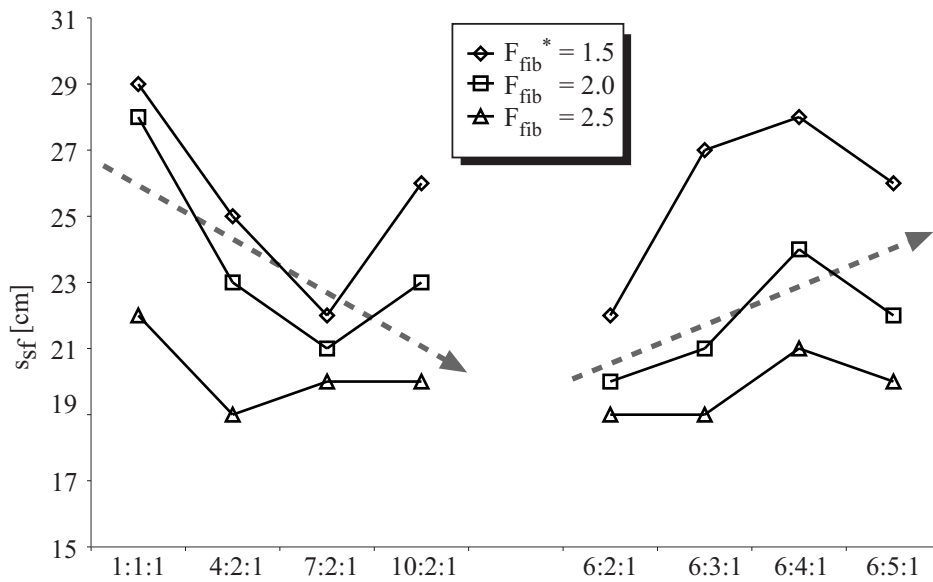


Figure 3.8: Images of the slump flows of the different mixtures with constant fibre-to-fibre ratios



\*Fibre factor  $F_{fib} = \sum(V_f[\%] \cdot l_f/d_f)$  [-]

Figure 3.9: Slump flow vs. fibre-to-fibre factor diagram

centimeter should be discerned. Therefore single fibre mixtures with 0.2% of the small  $l/d = 6/0.15$ , 0.4% of the middle  $l/d = 12/0.2$  and 3% of the large  $l/d = 27/0.6$  fibres were used. In this subsection only the results from the self-leveling experiments using the SegBox and the small slump flow are presented. Further results concerning the fibre distribution and fibre alignment are presented in Chapter 4. The segregation degree  $F_{SG}$  was determined using Equation 3.3. The numbers of fibres were counted at the bottom and the top part of the climbing branch of the SegBox. If the concrete did not flow sufficiently and the material did not climb, the  $F_{SG}$  was determined using the filling branch of the SegBox. Figures 3.10 and 3.11 show the cross sections of the specimens with the small and large fibres only. The segregation degree can be positive or negative. A negative value means that more fibres per  $1 \text{ cm}^2$  were counted at the top part of the climbing branch of the SegBox than at the bottom part of the climbing branch. In this case the fibres rise perfectly up to the top part of the SegBox and no segregation occurred.

$$F_{SG} = \frac{N_{bottom} - N_{top}}{N_{top}} \quad (3.3)$$

with

- $N_{bottom}$ : Average number of fibres per  $1 \text{ cm}^2$  in the bottom part  
 $N_{top}$ : Average number of fibres per  $1 \text{ cm}^2$  in the top part

The results in Table 3.3 show that with an increasing flowability the large fibres only tend to segregate. The small and the middle fibres are homogeneously distributed over the whole climbing branch. The orientation factor  $\alpha$  will be described and discussed in Chapter 4. The relatively high negative value for the sample 0.4%/0.18 can not be explained with segregation effects only. It is possible that this is just an exception due to the fact that only one specimen per w/b-ratio was analyzed. On the other hand it could also be an effect caused by fibre alignment. In Chapter 4, a model for fibre-alignment in the flowing concrete is described. This model indicates that fibre alignment increases with the traveling distance and with the flowability of the concrete. Therefore the fibres at the top part of the SegBox are better aligned than those at the bottom part, if the flow was constant over the whole distance. The more the fibres are aligned in the direction of the flow, the less fibres can be counted in a cross section parallel to the flow which was the orientation of the analyzed cross sections. The high negative value can now be explained as follows. The flow at the bottom of the SegBox was nearly laminar and

the fibres aligned perfectly. After the change of direction, swirls develop and cause the fibres not to be orientated anymore. Consequently more fibres were counted at the top of the SegBox and a relatively high negative value for the segregation degree  $F_{SG}$  was calculated.

Table 3.3: Overview of the segregation series experiment mixtures

Fibre type and content	w/b ratio	$s_{sf}$ [cm]	$F_{SL}$	$F_{SG}$	orientation factor $\alpha$	evaluated branch
small fibres 0.2%	0.15	10	22.6%	-	0.41	fill
	0.16	15	58.7%	-7%	0.34	climb
	0.17	15	42.8%	-7%	0.38	climb
	0.18	27	100%	9%	0.23	climb
	0.19	30	100%	9%	0.19	climb
middle fibres 0.4%	0.15	10	0.0%	11%	0.38	fill
	0.16	10	0.0%	8%	0.49	fill
	0.17	16	79.6%	3%	0.31	fill
	0.18	20	98.0%	<b>-29%</b>	0.29	climb
	0.19	25	100%	12%	0.36	climb
large fibres 3.0%	0.15	10	22.6%	7%	0.47	fill
	0.16	10	58.7%	19%	0.58	fill
	0.17	11	42.8%	2%	0.50	fill
	0.18	17	100%	3%	0.48	fill
	0.19	27	100%	<b>49%</b>	0.37	climb

### 3.4 Conclusions

From the results presented in this chapter the following conclusions can be drawn.

The self-leveling properties of HFC can be determined using the SegBox experiment. Further more, the alignment of the fibres in the hardened state can be observed and analyzed in the same test. In the tested mixtures only the large fibres tended to segregate. Small and middle fibres stick together to some extent. Segregation can be observed using the SegBox experiment. The sticking of fibres becomes apparent in the slump flow experiments. Thus, the combination of SegBox and slump flow tests helps to characterize the mixtures in their fresh state.

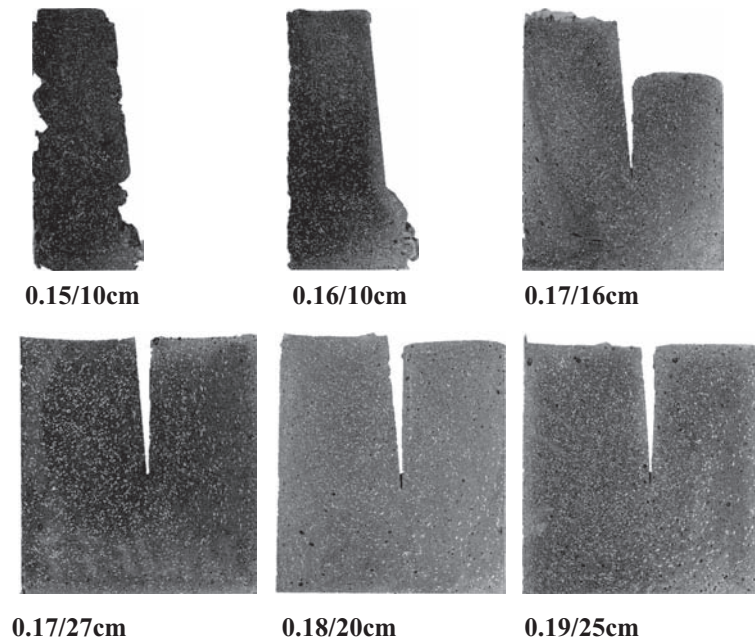


Figure 3.10: Cut SegBox specimens; small fibre series

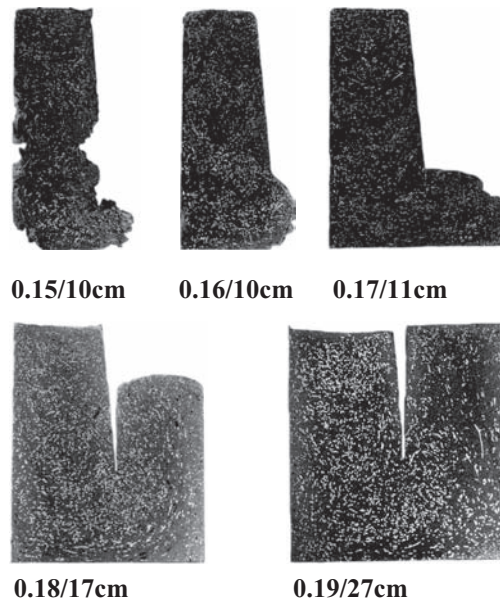


Figure 3.11: Cut SegBox specimens; large fibre series

# Chapter 4

## Fibre distribution and alignment

### 4.1 Introduction

To improve the mechanical properties of fibre reinforced concrete one can either increase the fibre content, use hybrid fibre systems, or one can attempt to align fibres in the direction of main stresses. Compaction may have a significant influence on the properties of fibre reinforced concrete. In particular fibre orientation and fibre distribution may be affected, especially when vibration needles are inserted in the fresh concrete. With the development of self-compacting concrete, the use of vibrational energy for compaction has become obsolete, and with current generation of super-plasticizers it is possible to develop self-compacting fibre concrete as well (Grünwald & Walraven [2001], Lappa [2007], Markovic [2006]). Increasing the amount of fibres may have a positive effect on the mechanical properties, but because fibres are not necessarily all aligned in the direction of stress, the effectivity is debatable. Better would be to align fibres in the direction of stress, which might lead to improved performance of FRC in a structure, probably against lower cost. Not only strength should be considered, but also ductility. Aligning fibres has been tried in the past under a variety of circumstances. Recently a method based on magnetic fields was proposed by Linsel [2005]. For SIFCON, fibre alignment can be achieved by sprinkling fibres in a narrow space, or in very thin elements (see van Mier & Timmers [1992, 1996]). Moreover, during extrusion of FRC, fibres align in the longitudinal direction (see for example Shao & Shah [1997]), leading to a notable anisotropy, probably leading to a corresponding anisotropy of the mechanical properties. As mentioned, the development of self-compacting concrete leads to easier placement of the fresh material, and the fibre distribution and orientation is not affected since compaction becomes obsolete. An interesting idea is to investigate to what



extent the flow properties of the fresh material can be used to affect the fibre distribution and orientation, and to see if a possible influence on the mechanical properties emerges. In Chapter 5 experiments are reported that confirm that the idea is basically correct, and that mechanical properties are improved when fibres are aligned. In this Chapter first the techniques used for determining the fibre distribution and the degree of the fibre alignment and for controlling the fibre distribution and alignment by the filling method are presented. Next, results from Computer Tomography experiments using the CT-scanner at the University Hospital Zurich are presented. They clearly reveal fibre orientation and alignment in FRC.

## 4.2 Manual counting

In order to determine the fibre distribution and the fibre alignment, cross sections of specimens were analyzed by overlaying a grid of 1 cm spacing over the cross section. Afterward the fibres in the single boxes were counted and recorded. Because of some smearing effects of the fibres while cutting the specimens and consequently not being able to separate the single fibres from each other (see Figure 4.1), only concretes with small amounts of fibres were used to analyze fibre distribution and alignment. While analyzing cross sections with some ordinary steel reinforcement, it could be seen that the fibres are also distributed between the ribs of the reinforcement (see Figure 4.2). This figure also shows some smearing effects caused by cutting.

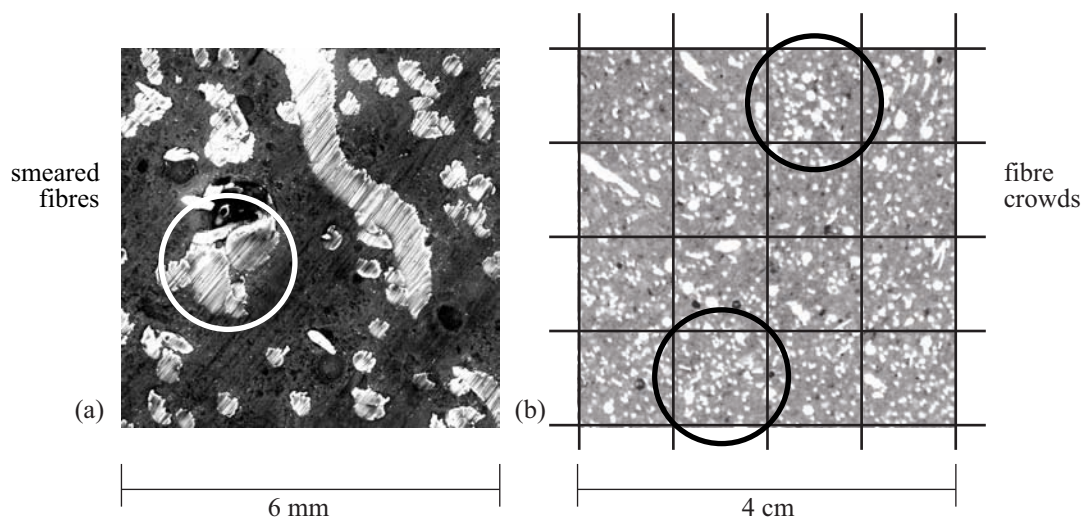


Figure 4.1: (a): ESEM image of smeared fibres; (b): Image of fibre clusters

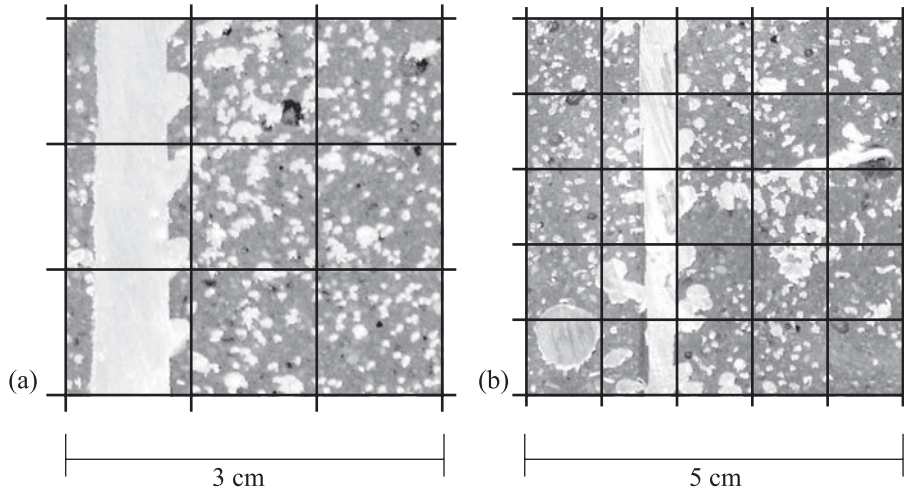


Figure 4.2: Images of fibres near steel reinforcement (a): detail of the ribs; (b): larger section of the fibre distribution including a perpendicular reinforcement

All the above mentioned effects led to the conclusion that a maximum of ten fibres per square centimeter should not be exceeded; otherwise the counting of the fibres would become quite tedious, and time consuming with debatable accuracy. Therefore only 0.2% of the small fibres, 0.4% of the middle fibres and 3% of the large fibres were used in the remaining mixtures.

#### 4.2.1 Specimen preparation

Before the fibres were counted the specimens had to be prepared as follows with Figure 4.3 showing the subsequent steps. First the specimen was cut at the cross section of interest with a common diamond wheel cutting machine. The maximum height which could be cut was 150-200 mm and the maximum length was about 2 m. Afterwards the specimens were cleaned and photographed. The photographs were taken under special light conditions. The light sources were placed in such a way that the fibres reflected the light and individual fibres could be counted easily without improving the pictures by using any post-processing software.

#### 4.2.2 Fibre counting and orientation factor $\alpha$

In order to analyze the fibre distribution in SegBoxe sections square charts of 10 by 10  $cm^2$  were created (see Figure 4.4) and analyzed. The average number of fibres for each grid-box (1  $cm^2$ ) in such a square (10 by 10  $cm^2$ ) was

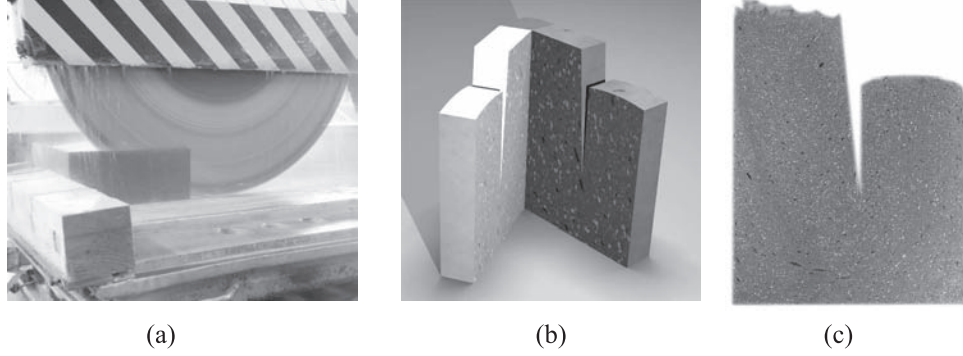


Figure 4.3: (a): cutting the SegBox; (b): cut SegBox; (c): image of a cut surface

calculated ( $N_c$ ). Dividing this number with the theoretical average of fibres perpendicular to the cross section ( $N$ ) the orientation factor  $\alpha$  can be determined using Equation 4.1. The orientation factor  $\alpha$  was introduced by Soroushian & Lee [1990] and used by several researchers (Dupond & Vandewalle [2005], Markovic [2006], Ozyurt et al. [2006b], Stähli & van Mier [2007c], Wuest et al. [2007])

$$\alpha = \frac{N_c}{N} \quad (4.1)$$

with

$$N = \sum \frac{V[\%]}{A_{fib}[mm^2]} \cdot A_{grid}[mm^2] \quad (4.2)$$

If no segregation occurs, an orientation factor of 1 means that all fibres are orientated perpendicular to the cross-section and therefore perfectly aligned. An orientation factor of 0 would mean that all fibres are orientated parallel to the cross-section whereas an orientation factor of around 0.5 would indicate a theoretical random distribution of the fibres and therefore of the fibre orientation. Anything in between would mean that the fibres are not perfectly aligned but have a tendency to do so. In real samples segregation can occur as well which will influence the number of fibres per unit cross section. Therefore at least two perpendicular cross-sections have to be analyzed in order to prevent misinterpretation.

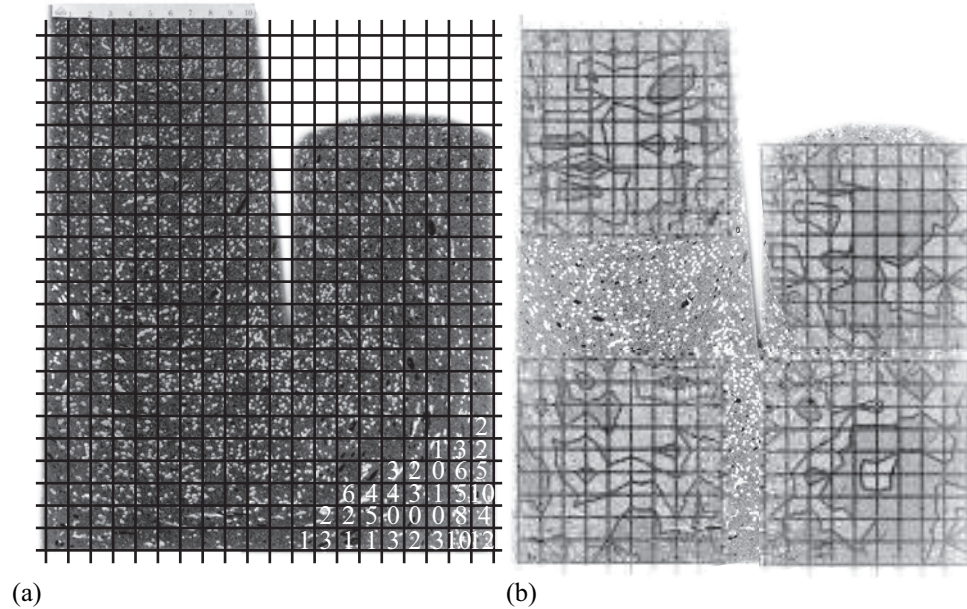


Figure 4.4: Manual counting of the fibres. (a): Mesh and numbers of counted fibres (lower right corner only); (b): Results overlaid on the original image

### 4.2.3 Bending specimens

Investigations on the influence of production methods on the mechanical properties of HFC and FRC such as bending strength were performed using the following moulds/specimens.

#### 4.2.3.1 'U-shaped' specimen

In order to determine the influence of the fresh concrete behaviour on the fibre distribution and orientation, and on the mechanical properties, a so-called 'U-shaped' mould was developed. This 'U-shaped' mould was designed in such a way that the concrete first "flows" down (Figure 4.5, branch "A"), then flows horizontally (Figure 4.5, branch "B"), and finally rises again (Figure 4.5, branch "C"). After demoulding the 3 specimens (prisms of size  $70 \times 70 \times 280 \text{ mm}^3$ ) were cut out, one from each branch of the 'U-specimen'. The prisms fitted in the pendulum-bar four-point bending test set-up which is described in Chapter 5.

To determine the fibre distribution and fibre orientation the specimens were tomographed in a medical CT-scanner (see section 4.3). From one 'U-specimen' three prisms, each from a different location, were analyzed (see

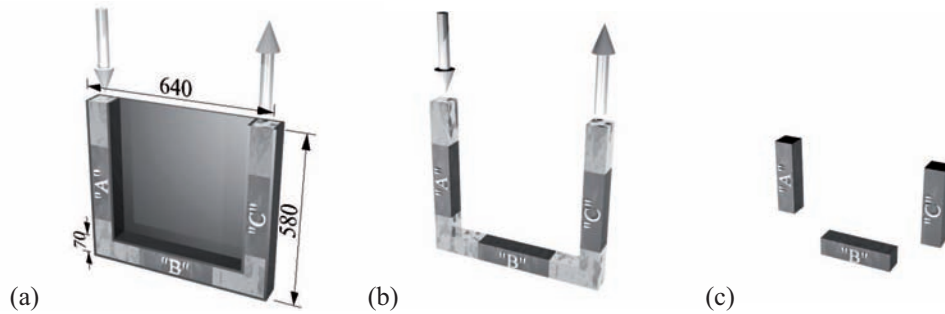


Figure 4.5: Preparation of the 'U-shaped' mould specimens: (a): U specimen in the mould with the specimens "A" (climbing branch), "B" (horizontal branch) and "C" (climbing branch); (b): Demoulded U specimen; (c): U specimen prisms

Figure 4.5, prisms marked "A", "B" and "C" for the 'falling' 'horizontal' and 'rising' parts of the 'U-shaped specimen', respectively). To avoid the material falling into the mould during the casting process and the fibres aligning, or even segregating, due to the "free fall" of the material, the U-mould was tilted and the material could flow (or slide) from the shovel into the mould. Images of the casting process are shown in Figure 4.6.



Figure 4.6: Casting of the 'U-shaped' specimen: the mould is given an inclination to prevent "free fall" of the concrete along the "A"-side

#### 4.2.3.2 Orientation-bar specimen

The orientation-bar is a further development of the 'U-mould'. Contrary to the 'U-mould' the material flows in a straight line without any change of direction. Figure 4.7 shows scheme and a sketch of the orientation-bar mould including the three specimens. The difference between the specimens "A", "B" and "C" is the flowing distance and/or the flowing time. The cross section of the mould is  $70 \times 70 \text{ mm}^2$ . For each mixture three bars were cast. While casting the material flowed continuously. The flowing time from the start of casting till the material reached the bottom (end of specimen "C") was measured.

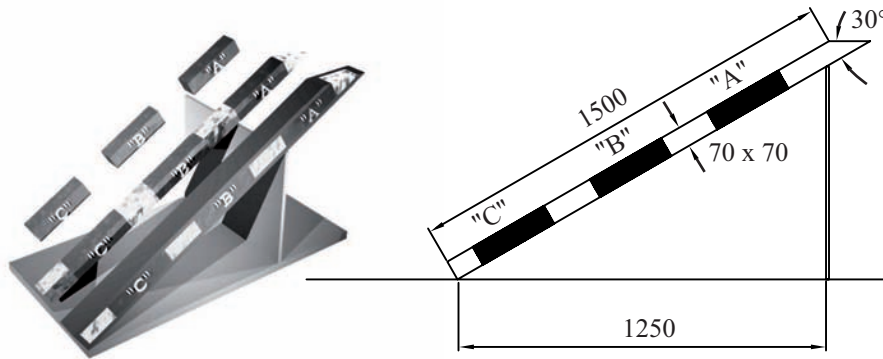


Figure 4.7: Orientation bar mould with the specimens "A", "B" and "C"

#### 4.2.4 Tensile test specimens

In order to optimize the filling process and the resulting fibre orientation and distribution in the tensile test specimens four different filling methods were used. A complication here is that the tensile experiments require dog-bone shaped specimens. The 'conventional' method (C), where the concrete was poured from the top and the material did not flow, but fell in the mould (Figures 4.8 and 4.9); the 'fill' method (F), where the concrete was filled in the mould in such a way that the material flowed a little (see Figures 4.8 the bold arrows in the corner of the mould and 4.10), the 'climb' method (CL), where the material was filled/pumped from the bottom to the top of the mould (Figures 4.8 and 4.10) and the 'lying' method where the mould was in a horizontal position and the concrete flowed horizontally into the mould (Figures 4.8 and 4.11).

Due to the unavailability of a concrete pump the 'climb' method was performed in such a way, that the material was first placed in the 'fill' method specimen and from there the material flowed through a connecting part up into the 'climb' method specimen (Figure 4.10). The difference between the conventional method and the 'fill' method is in the flow of the material. Figure 4.8b shows that for the 'conventional' method as soon as the material starts to fill the mould, swirls develop in the material flow due to the bottom wall of the moulds. The swirls persist until the mould is almost filled (Figure 4.8c). Figure 4.8f and g show that for the 'fill' method the more the mould is filled the more the material starts to flow downward. No swirls develop and the fibres can properly align in the direction of the material flow. The last method was the 'lying' method where the mould was lying on the ground while being filled with the material (Figure 4.11). On both sides of the mould additional parts were attached so that the material could really flow through the whole mould. The difference between the 'climb' and the 'lying' method is obviously the flowing angle of the material and the symmetry in the cross section in the middle part of the specimen. While the specimen with the 'climb' method is filled constantly over the whole cross section and duration of the filling process the 'lying' specimen is filled from the bottom (ground) of the specimen to the top even if the whole material was first filled into the box and the "slide valve" was removed at once, the material flowed first at the ground of the mould (Figure 4.11) before it rose up to fill the whole specimen.

### 4.3 Computer tomography (CT)

In order to visualize the fibre distribution and alignment in the interior of a specimen without cutting it, computed tomography scans were made at the University Hospital Zürich (see Figure 4.12). The tomograph was a Siemens SOMATOM Sensation 64. The scan parameters were 300mAs and 140kV. The specimens were scanned by the employees of the University Hospital and the data sets were reconstructed immediately after the scan. One scan took about 15 seconds and produced nearly 500 MB of data. The resolution (voxel size <sup>1</sup>) was 0.4 mm. Therefore only mixtures containing the large  $l/d = 30/0.6$  notched fibres could be analyzed.

---

<sup>1</sup>A voxel is a 3D pixel

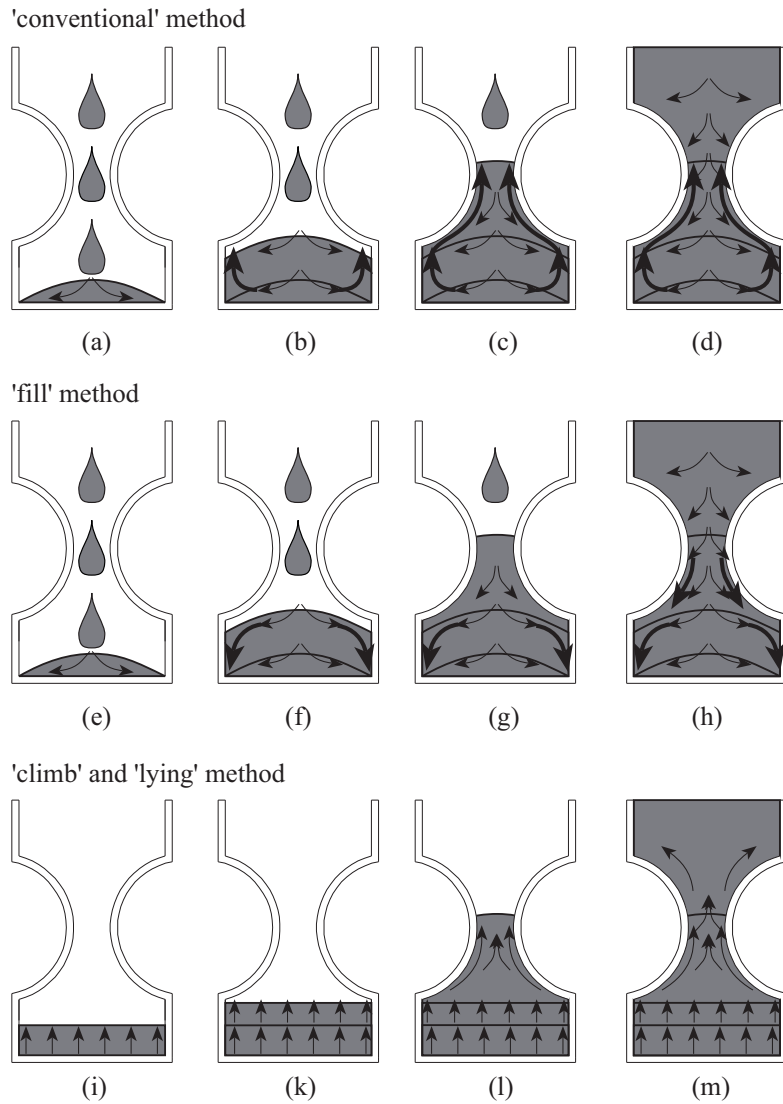


Figure 4.8: Schemes of the different filling methods: 'conventional' method (a to d), 'fill' method (e to f) and 'climb' and 'lying' method (i to m). The arrows show the direction of the flow of the material during the filling process



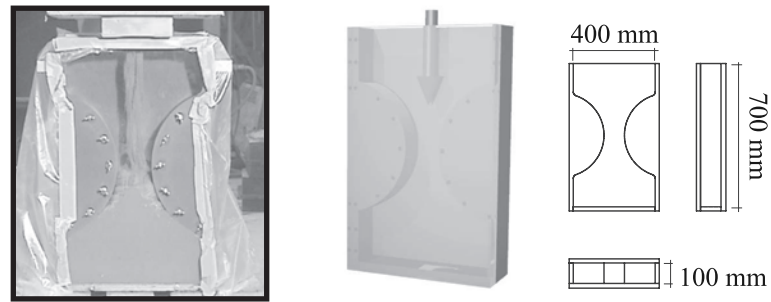


Figure 4.9: Conventional filling method

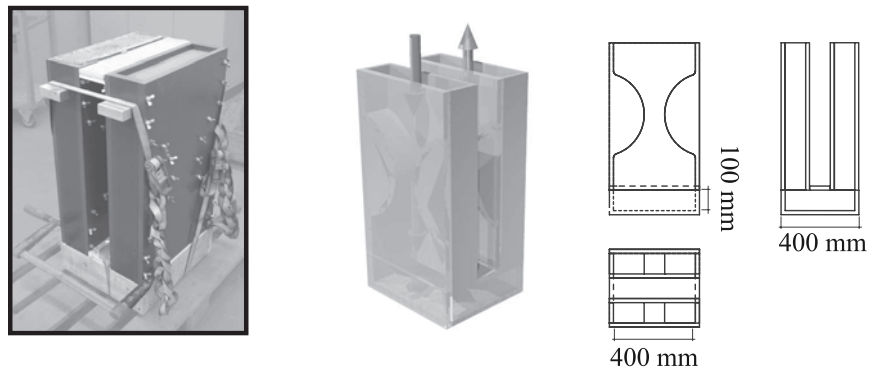


Figure 4.10: 'Fill' and 'climb' method

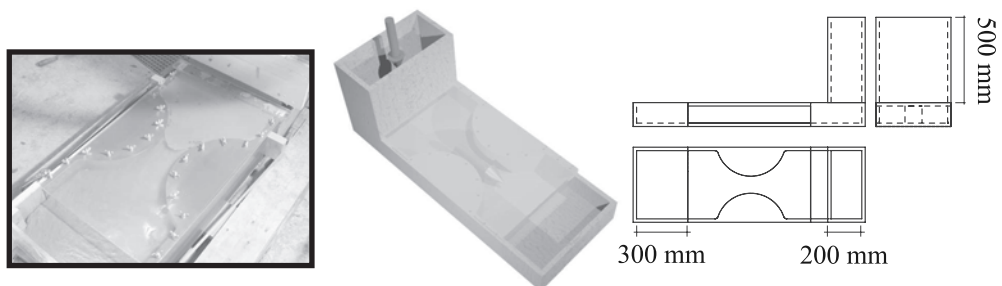


Figure 4.11: 'Lying' filling method

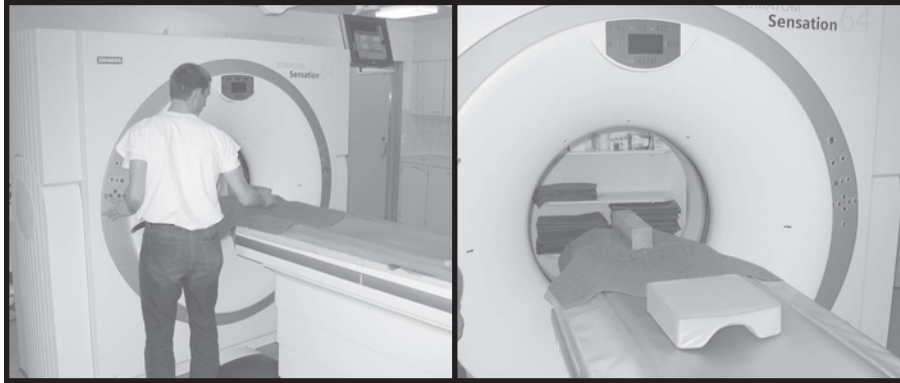


Figure 4.12: Fibre count specimen in the CT-scanner of the University Hospital Zurich

### 4.3.1 Interpretation and data analysis

The interpretation of the data presented a challenge. Figure 4.13 shows (a) a 3D reconstruction of the fibres only and (b) three different orthogonal slices through a reconstructed FRC specimen. Both images are from the same specimen which contained 3% of the large steel fibres. It is obvious that only the sliced specimen could be analyzed because the 3D reconstruction of the steel fibres is strongly dependent on the chosen threshold which separates the fibres from the matrix. Moreover the voxel size was almost equal to the diameter of the fibre. Therefore only virtual slices were analyzed. The analysis was the same as described in section 4.2.2. The fibres were counted for each section. The number of counted fibres indicated a certain fibre distribution. Perpendicular slices were analyzed to confirm the indication and to be able to determine the 3D fibre distribution and alignment. The advantage of this non-destructive method is that the mechanical tests could be performed after the fibre distribution and alignment were determined and correlations between fibre distribution and mechanical properties could be established.

## 4.4 Results

To analyze and optimize the fibre distribution and alignment of FRC and HFC several test series were performed. In Chapter 3 the flow properties were discussed and the influence of the flow properties on the fibre alignment will be discussed in this Chapter. In addition to the influence of the flowability,

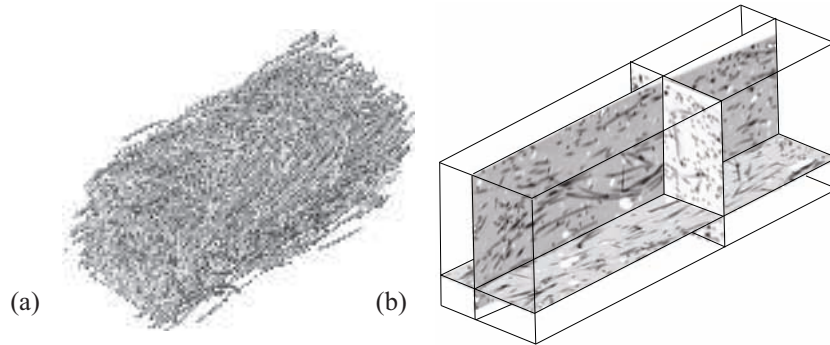


Figure 4.13: (a): 3D reconstruction of the steel fibres only (b): Three different orthogonal slices through a reconstructed FRC specimen from a CT-scan

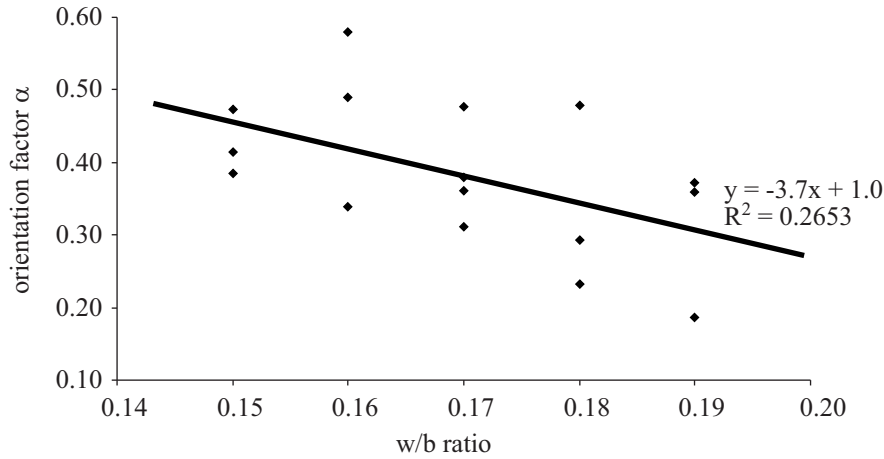
the influence of the specimen geometry and the manufacturing method on the fibre distribution and alignment will be presented.

#### 4.4.1 Influence of the flowability on the fibre distribution and fibre alignment

In Chapter 3, section 3.3.2 the flow properties were already discussed and the results were summarized in Table 3.3. The analyzed cross sections are parallel to the flowing material and therefore the lower  $\alpha$ , the more the fibres are aligned in the direction of the flow. Figure 4.14 confirms the assumption that the fibres align in the direction of the flow and that the alignment increases with an increase of the flowability of the material. The geometry of the fibres has no significant influence on this alignment; the small, the middle and the large fibres all appear to align equally well.

#### 4.4.2 Orientation-bar specimen

In order to investigate the influence of the flow time and the flow distance on the fibre distribution and alignment the same material as in the previous section was used to perform orientation bar experiments. The flow time was determined by measuring the time from the start of filling the orientation bar till the material was visible at the bottom/end of the mould. Table 4.1 shows an overview of the results. Mixture 1 ( $SP = 1.8\%$ ) with an  $s_{sf}$  of 14.5 cm shows a very long flowing time in comparison to Mixtures 2 ( $SP = 2.0\%$ ) and 3 ( $SP = 2.2\%$ ) with 47" and 42" flow time respectively. One day after casting the specimens were cut out of the orientation bars and a CT-scan

Figure 4.14: w/b-ratio vs orientation factor  $\alpha$ 

was made at the University hospital in Zurich. The specimens could now be cut virtually into slices and the fibre distribution could be analyzed. Furthermore the mechanical properties such as bending and compression strength were determined and will be presented in Chapter 5.

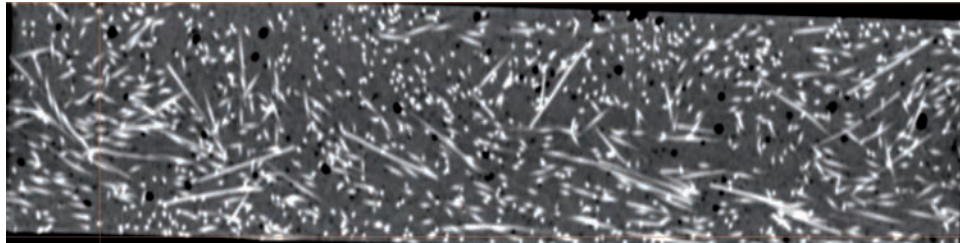
Table 4.1: Flow properties

	Mixture 1 ( $SP = 1.8\%$ )	Mixture 2 ( $SP = 2.0\%$ )	Mixture 3 ( $SP = 2.2\%$ )
Filling time	2'55"	47"	42"
$s_{sf}$ [cm]	14.5	20.0	22.0
$l_{sf}$ [cm]	50.0	59.0	63.0

Figure 4.15 shows longitudinal sections through "A" and "C" prisms of Mixture 3 (2.2%). The analyzed sections were sections of the center of the specimen. A slight segregation and a clear fibre alignment can be observed. The total number of fibres which were counted in the longitudinal cross section of the prisms "A" and "C" were 1044 and 791 respectively. This decrease in fibres per cross sections also indicates an alignment of the fibres. Schmid [2006] showed that the fibres align with the flow distance of the material especially for a material with a low viscosity. The fibres in the perpendicular cross sections were also counted and their correlation with the mechanical properties was observed.

Mixture 3 "A"

5	6	5	7	6	7	5	2	5	5	8	11	6	3	1	6	3	4	7	5	2	3	1	2	6	6	4	2
3	6	3	7	4	7	6	2	6	6	10	5	4	2	5	6	4	4	8	9	6	5	10	2	6	4	3	5
4	4	5	7	7	3	6	6	5	3	7	9	7	8	8	7	4	8	6	5	2	8	8	6	5	5	6	7
3	5	9	6	7	7	8	6	3	6	6	6	3	4	7	4	4	4	3	4	5	4	4	5	5	3	5	5
6	4	6	4	1	11	8	8	4	10	5	7	9	4	6	7	4	6	7	2	1	2	4	4	3	5	5	3
5	4	3	7	7	8	5	8	7	1	6	5	4	6	7	3	5	6	5	6	5	5	4	5	5	6	5	5
4	5	3	4	9	9	8	8	7	8	6	6	4	3	4	6	5	8	7	6	8	6	6	6	3	3	3	7



Mixture 3 "C"

6	4	6	3	5	2	6	3	3	4	5	2	2	5	3	4	3	3	3	0	3	1	2	2	1	4	1	1
2	3	3	3	5	3	4	5	4	5	2	4	5	2	4	3	3	5	3	2	3	2	4	6	6	6	2	5
7	3	7	3	2	4	2	5	3	8	5	4	6	1	1	3	3	6	1	5	4	3	3	2	2	4	5	5
2	4	5	6	7	1	1	6	2	2	3	2	5	4	2	6	5	4	3	3	1	4	1	2	3	1	6	2
4	8	6	6	6	2	4	3	4	4	4	5	6	4	2	1	4	6	3	8	4	2	2	6	4	6	3	4
7	4	4	5	5	7	2	4	5	5	5	7	5	5	7	4	6	4	6	9	9	7	6	7	5	8	4	8
4	2	3	3	4	4	4	4	5	3	5	1	2	5	5	8	5	5	7	7	4	3	3	2	7	1	5	8

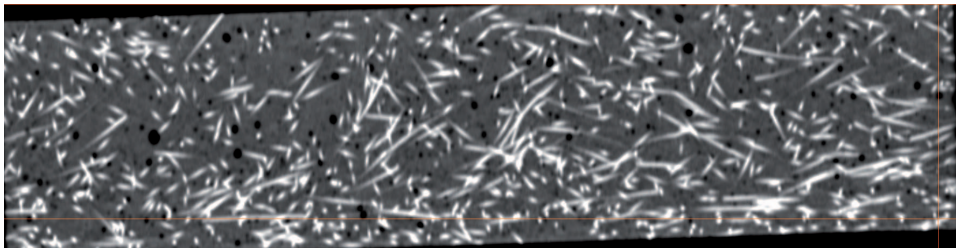


Figure 4.15: Scheme and Image of longitudinal sections of the prisms "A" and "C" of Mixture 3 (2.2%)

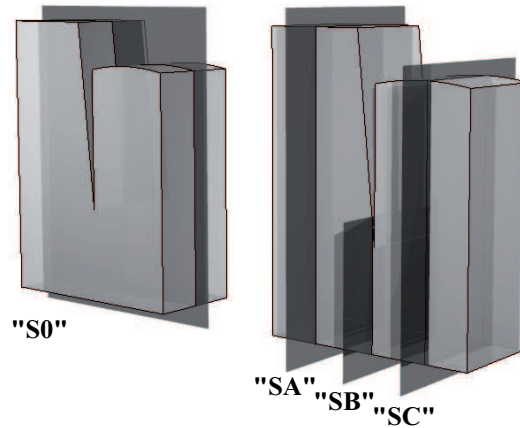


Figure 4.16: Schematic view of the cross sections

In order to analyze the fibre distribution in the SegBox the fibres were counted in sections that were perpendicular to each other. Two SegBoxes were cast and cut. The first SegBox ("S0") was cut as described in Section 4.2.1. Cross sections, perpendicular to the flow of the material, were analyzed in the second SegBox ("SA", "SB" and "SC"). Figure 4.16 and 4.17 shows a scheme and images of the section and the results. The results show that the less fibres can be counted in "S0" in a certain area, the more fibres can be counted in "SA", "SB" and "SC", e.g. the section "SB" shows an average value of 6.1 per  $cm^2$  of fibres in the region of interest (region of interest (ROI); 10 by 10  $cm^2$ ) while "S0" shows an average of only 2.9 per  $cm^2$  in a region of interest in the same area of the sample (width: 4 cm; height: 10 cm). This clearly indicates that the fibres are aligned parallel to the "S0" cross section in areas where less fibres can be seen in "S0". But nothing can be said about the alignment within the section itself. It can only be assumed, that the fibres align with the flow of the material. As seen before, the results derived by the CT scan gave more convincing results.

#### 4.4.3 Influence of the manufacturing method on the fibre alignment

Investigations on new filling methods are needed due to the fact that the fibres align with the flow of the fresh material (see Stähli et al. [2008]). Four different filling methods were investigated. First, the conventional method

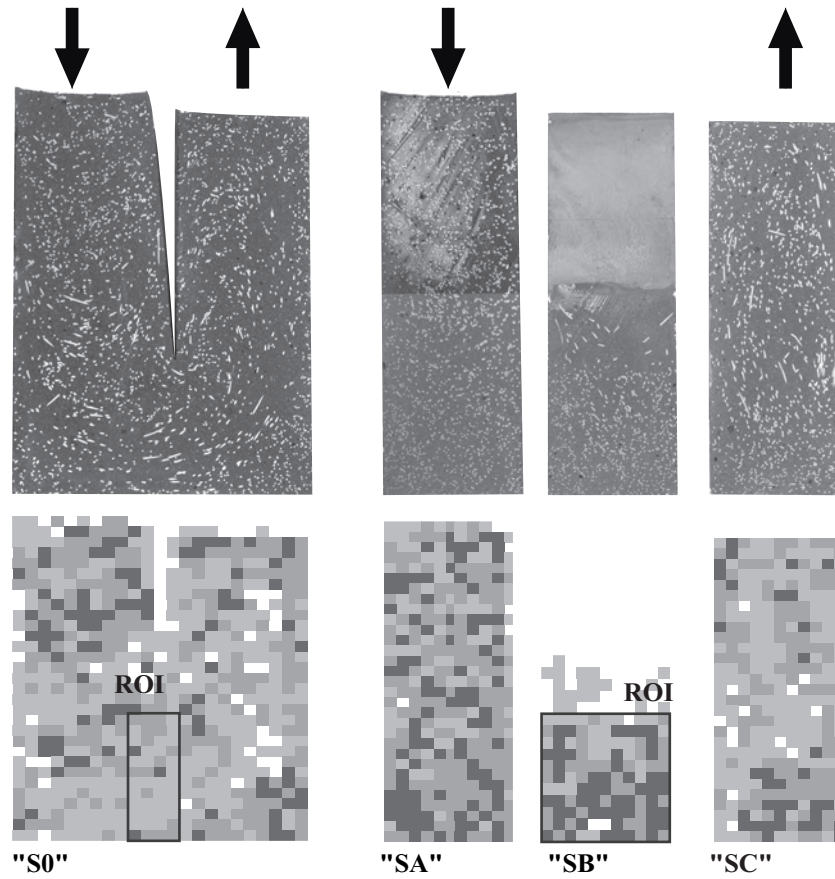


Figure 4.17: Images and schematic views of the fibre distribution in the SegBox for Mixture 3 (2.2%). Darker squares indicates a higher fibre-count. The arrows indicate the filling direction of the material.

Table 4.2: Results derived from the SegBox experiments

	Mixture 1 (1.8%)	Mixture 2 (2.0%)	Mixture 3 (2.2%)
Average fibre amount (ROI "S0")	4.9	4.0	3.7
Average fibre amount (ROI "SB")	5.3	4.4	4.7
increase [%]	6.3%	10.2%	26.1%

(Figure 4.9) where the concrete was filled from the top and the material could not flow through the mould. The second and third methods were the so called 'U-mould' methods (Figure 4.10) where the concrete used was poured into the first mould and then flowed through a connection part and could finally 'climb' into the second mould. The difference between the 'fill' and 'climb' method is the angle between the segregation and the flow direction and the flowing distance of the material. The last filling method was the 'lying' method where the mould was placed horizontally on the ground while filling the material in (Figure 4.11). On both sides of the mould additional mould parts were attached so that the material could really flow through the whole mould. For each filling method two different mixtures were produced, a mixture with increased ('low viscous') and a mixture with reduced ('high viscous') flow-ability. 3% of the large straight notched fibres were added which allowed the observation of the fibre alignment and distribution in the hardened state.

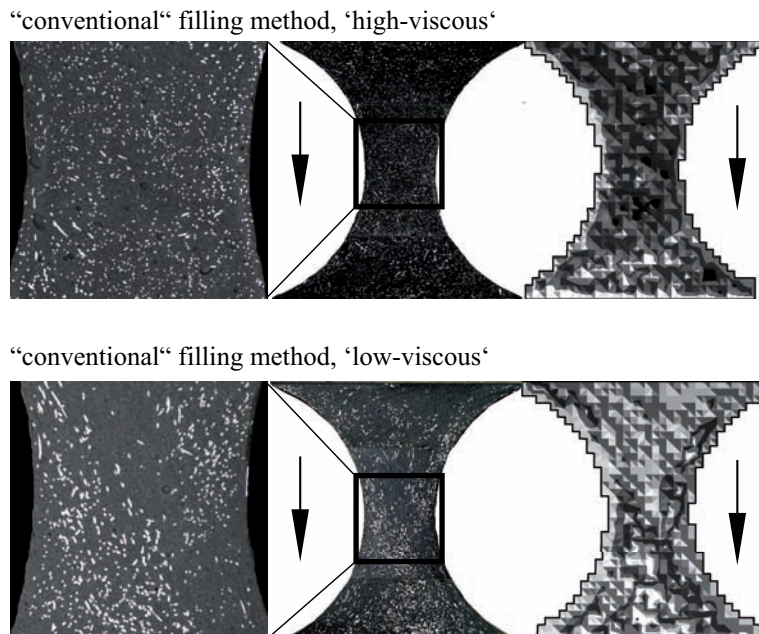


Figure 4.18: Cross-sections of two specimens filled with the 'conventional' method. The arrows indicate the filling direction.

One day after casting the specimens were demoulded and cut along the length of the specimen in such a way that the fibres in the middle of the specimen were visible. These sections were photographed, the individual



images were stitched together and filtered in such a way that the fibres are nicely visible. The final images are shown in Figures 4.18 to 4.21. The pixel size is 0.1 mm for all the images. Figure 4.18 clearly shows the different fibre distributions for the mixtures with different flow-ability (viscosity) using the conventional filling method. It can be seen that the 'low viscous' mix with an increased flow-ability tended to segregate and that the distribution is not uniform over the whole cross section. Some aligned fibres can be seen in the upper left part of the region of interest (marked with a square of 10 by 10  $cm^2$ ) of the cross section of the 'low viscous' specimen. These fibres probably aligned while sinking down. On the other hand, the 'highly viscous' mixture with reduced flow-ability shows uniformly distributed fibres and no visibly aligned fibres.

Figure 4.19 and 4.20 show images of the cross-section of four specimens filled using the 'U-mould'. For each 'U-mould' two filling methods were investigated, the 'fill' and the 'climb' method. For both viscosities the 'fill' specimens shows some fibre alignment in the centre part but the alignment in the 'climb' specimens is much stronger. The 'climb' specimen with the 'low viscous' mixture shows the strongest fibre alignment but the total number of visible fibres is not as large as the one from the mixture with the 'high viscosity'. It seems that the material could not transport the fibres all the way up into the 'climb' specimen. The reason why the 'fill' specimens also show some fibre alignment is that even there the material flowed during the casting process. When the material started to level out all the material flowed and the fibres could align in both specimens.

The results from the 'lying' method are shown in Figure 4.21. For both mixtures fibre alignment can be observed but the 'low viscous' mixture shows some segregation, therefore fewer fibres are present compared to the 'high viscous' mixture.

In summary it can be said that these methods differ significantly with respect to fibre distribution and alignment. Furthermore, it can be said that the filling method together with the flow-ability influences the alignment and distribution of the fibres. Figure 4.22 shows the results of the manual fibre counting. An average of fibres per  $cm^2$  of the whole section and of a section of 10 by 10 cm was determined. The less fibres that could be counted the more the fibres are aligned in the direction of the flow. For the conventional method the fibres in the region of interest are better aligned than outside this region. This is caused by the fact that in this part the velocity of the material during the filling process is faster, even if the flow-ability of the material is reduced. For the other methods the number of fibres per  $cm^2$  in the middle part is higher than for the whole specimen. A reason could be that the number of fibres per section perpendicular to the cross-section is

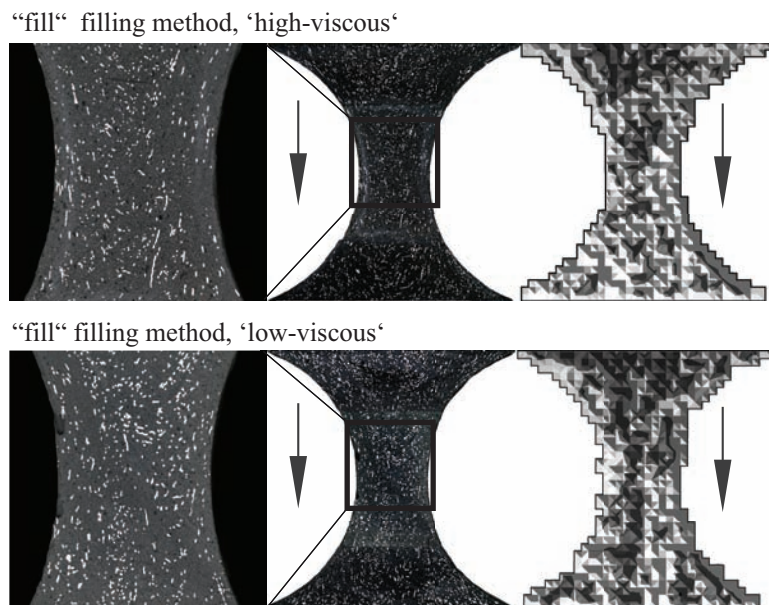


Figure 4.19: Cross-section of two specimens filled with the ‘fill’ method. The arrows indicate the filling direction.

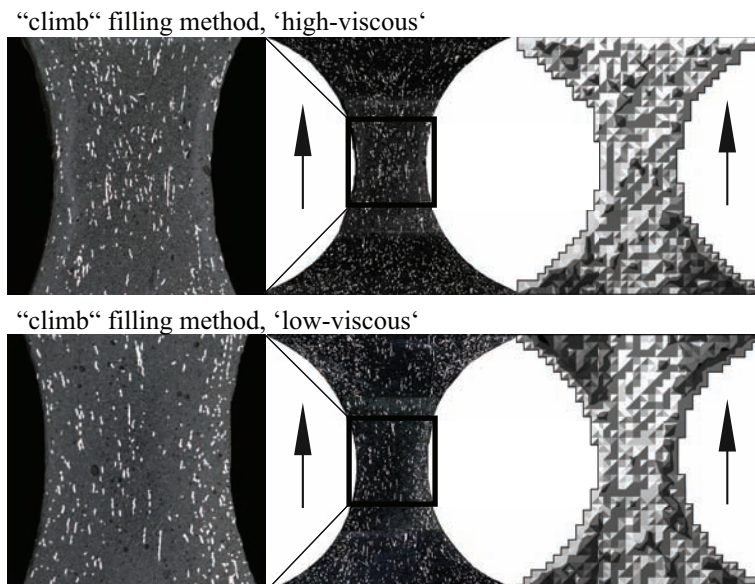


Figure 4.20: Cross-section of two specimens filled with the ‘climb’ method. The arrows indicate the filling direction.

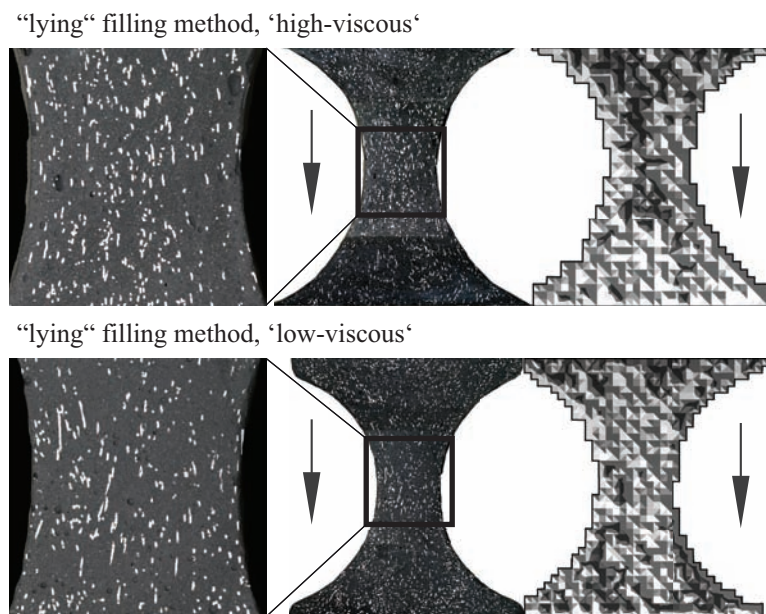


Figure 4.21: Cross-sections of two specimens filled with the ‘lying’ method: top ‘low viscous’ concrete; bottom row ‘low viscous’ concrete. The arrows indicate the filling direction.

constant. Because in the region of interests the width is 10 cm x 10 cm only, the fibre density is higher and more fibres can be counted, even if they are better aligned. A slight increase of the fibre alignment can also be observed from the 'fill' to the 'climb' method. This may be caused by the flow-distance of the concrete. The longer this distance, the better the fibres are aligned.

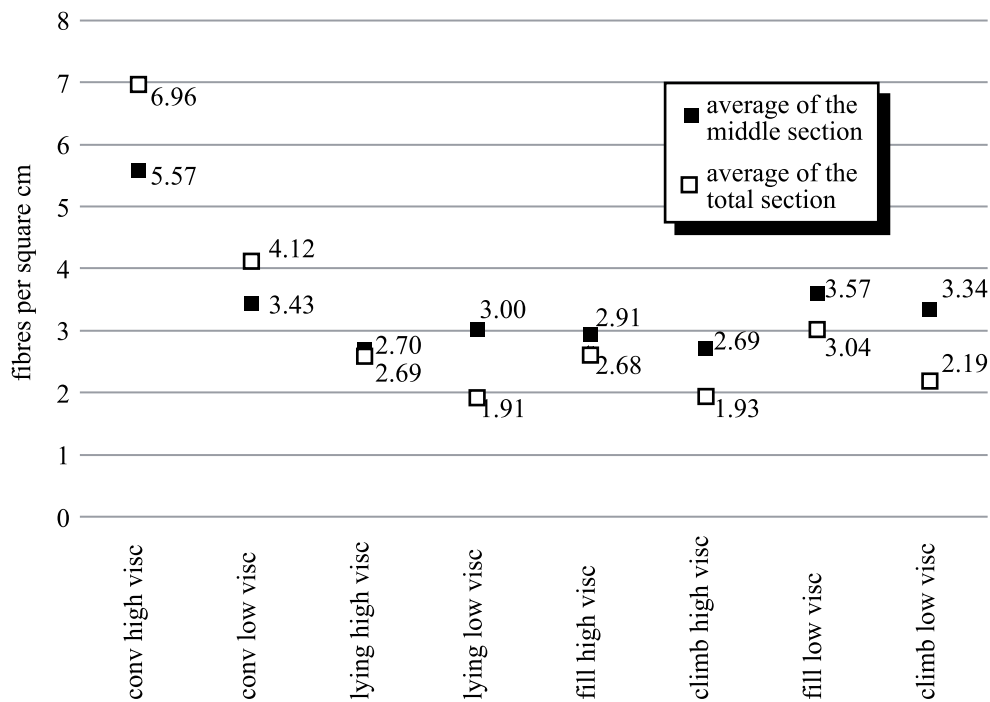


Figure 4.22: Results of the fibre counting for the different filling methods

## 4.5 Conclusions

From the relatively small number of experiments presented in this Chapter, the following conclusions can be drawn.

- Manual counting can be used to determine fibre alignment
- The filling method has a significant influence on the fibre alignment in a specimen. In order to be able to compare properties of different materials the filling method has to be exactly the same.
- The fibres align with the flow of the material. The alignment increases with the flow-distance. This fact was also shown by Ferrara et al. [2007b] and Kim et al. [2008].
- Material with increased flow-ability shows a stronger alignment of the fibres than a material with reduced flow-ability.

# Chapter 5

## Mechanical testing

### 5.1 Introduction

To determine the mechanical properties standard compression, three and four point bending and Young's modulus tests were performed using the Walter & Bai testing machine (see Appendix A). The more sophisticated all-round Zwick testing machine was used for the pendulum-bar four-point bending and the pendulum-bar tensile test, which will be described in this chapter. Both testing machines are located in the Institute of Building Material and the test set-ups were developed within the scope of this work. After Rossi et al. [1994] the load rate influences the test results significantly. Therefore only quasi static tests with very slow load rate were performed. Test results using the mentioned devices are presented at the end of this chapter. Most of the mechanical tests were performed using a Zwick 1484 servo-electro all-round testing machine with a maximum capacity of 200 kN. Tests can be carried out under force-, displacement- or strain-control. An integrated, so called multisens displacement sensor could also be used to measure and/or to control tests. The following section describes the newly developed test set-ups for bending and uniaxial tension.

### 5.2 Bending test

The rationale for using pendulum bars is based on the idea that during a four-point bending test the forces which act on the specimen should remain perpendicular to the specimen, the symmetry should be maintained throughout the whole test (thus also during fracture), there should be no friction between the supports and the specimen, and it should be possible

to measure the forces at supports and load-points. These issues become especially important when a material of increased ductility, such as HFC, is tested. Van Mier et al. [1995] showed that the lowest value for fracture energy and tensile strength was found using rotating supports which implies that the boundary influence was minimal using rotating supports instead of fixed supports (see also Schlangen [1993], van Vliet [2000]). Figure 5.1 shows the principal difference between the ordinary four-point bending test and the pendulum-bars four-point bending test. In order to achieve the above mentioned objectives, the forces are transferred onto the specimen by means of a set of long pendulum bars. During the test between pendulum bars the directions of the external forces continuously changes in the same way as the geometry of the specimen changes, so that they remain at right angles to the surface of the specimen. The symmetrical setup of the test arrangement is maintained during the test. This is also achieved by the fact that the pendulum bars and the whole test arrangement have many degrees of freedom of movement. Thus, the supports are free to move in lateral directions. Moreover the forces in the individual bars can easily be measured with strain gages. In the ordinary four-point bending test the forces remain vertical and the angle between force and surface of the specimen changes continuously as shown in Figure 5.1. By raising the angle, friction between the supports and the specimens grows and the symmetry changes (Gjørsv et al. [1977]).

### 5.2.1 Test set-up

The test set-up was manufactured in-house. After the production process, all the pieces were coated with an anti corrosion layer. The strain gages were applied on the pendulum-bars, cabled-up and finally covered by a plexiglass protection tube. The length of the pendulum-bars is 470 mm and the bearing width of the supports is 20 mm. Sketches of the test arrangement and a photograph of the whole test setup are shown in Figure 5.2. At the top and the bottom of the set-up two UNIBAL<sup>®</sup> hinges served as connector to the loading frame. Each of the eight pendulum-bars was connected to the set-up with two UNIBAL<sup>®</sup> hinges. This construction enabled all the above mentioned degrees of freedom. The dimensions of the set-up was driven by the geometry of the testing frame and the capacity of the Zwick loading machine.

### 5.2.2 Specimen geometry

Two geometries can be tested using the pendulum-bar four-point bending test; small  $70/70/280 \text{ mm}^3$  and larger  $150/150/600 \text{ mm}^3$  specimens. Sketches

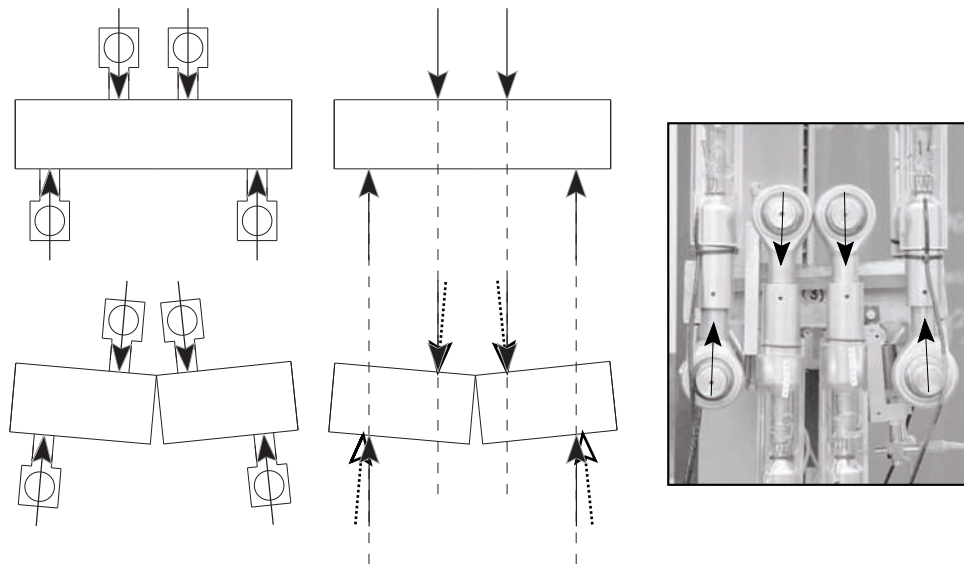


Figure 5.1: Comparison of load setups in ordinary and the pendulum-bars four-point-bending tests. At the left side the force directions in a pendulum bar test are shown and on the right side those in a conventional four-point bending test. On the Figure to the right the loading direction from the pendulum-bar test are shown by means of dashed-lines/arrows.



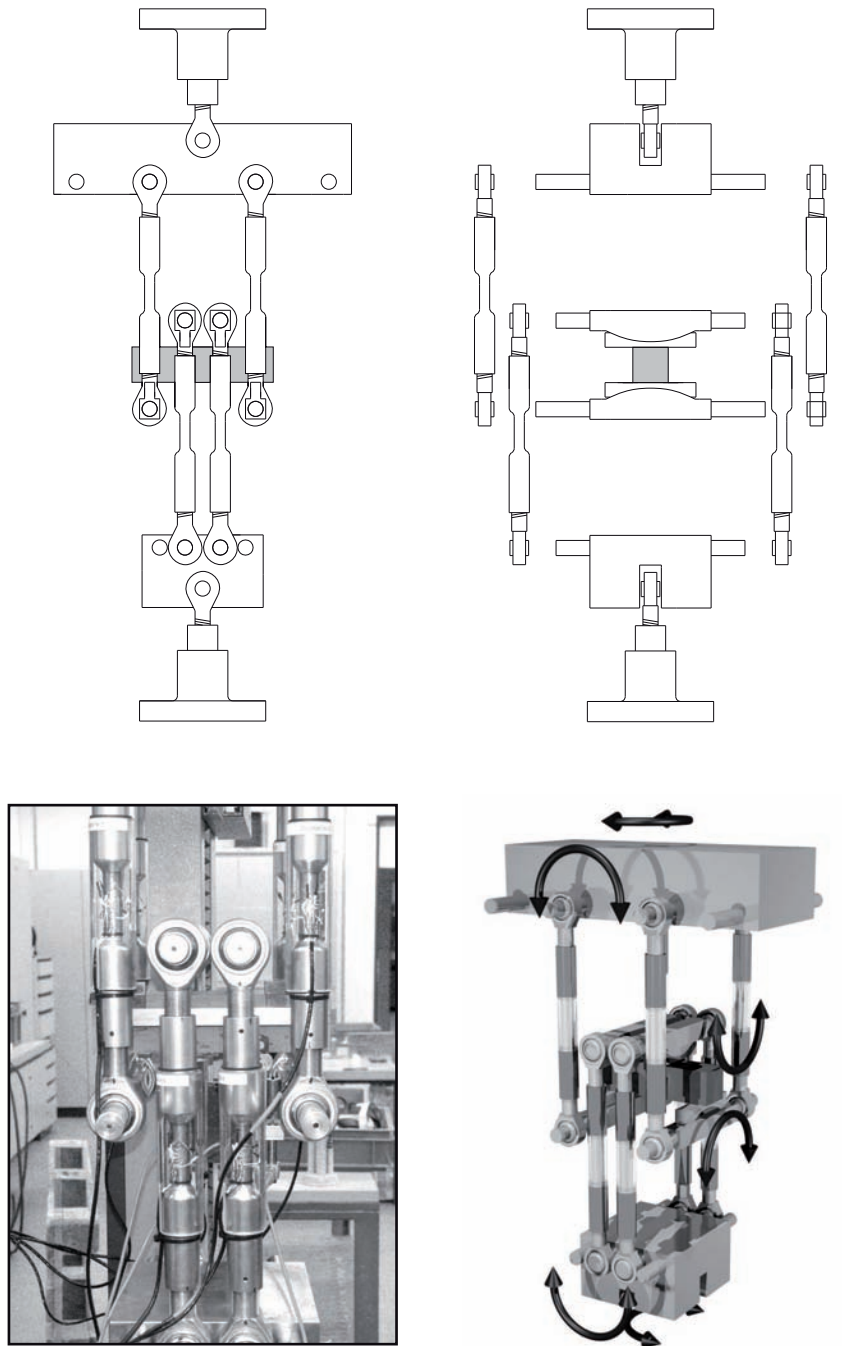


Figure 5.2: Image and sketches of the pendulum-bar four-point bending test

are shown in Figure 5.3. To adjust the test set-up for different specimen sizes only the pendulum-bars have to be rearranged from the inner to the outer position of the upper and the lower steel block (see Figure 5.2).

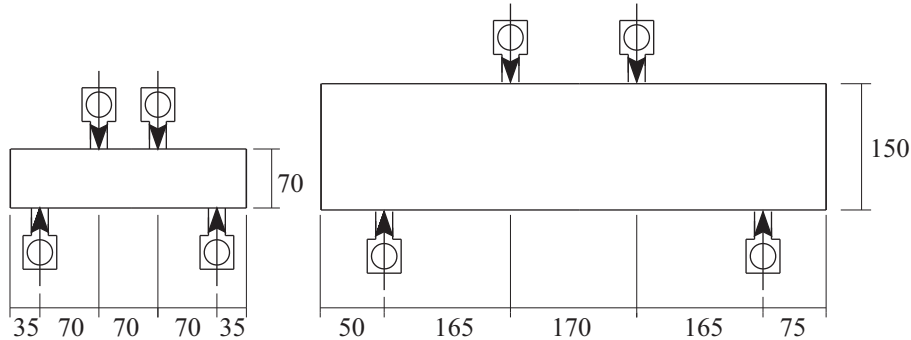


Figure 5.3: Geometry of the pendulum-bar four-point bending specimens

### 5.2.3 Measurement

Figures 5.4 to 5.6 show the arrangement for deformation measurement and data acquisition. The deflection of the beam is derived from readings of two pairs of linear variable differential transformers (LVDT), the arrangement of which is shown in Figure 5.4. The 'maximum' deflection of the beam has been calculated as the intersection of the two straight lines given by the displacement of the LVDT and the geometry of the setup. This method assures that no sensor is in the zone where cracks are expected. In most cases the derived deflection provides an upper boundary value. The crack mouth opening was measured using a steel wire that was fixed along the bottom side of the specimen. A sketch and a photograph of the crack mouth opening displacement (CMOD) sensor is shown in Figure 5.5. The reading of the CMOD includes all deformations and corrections were unnecessary.

Two computers were needed to carry out the test. As shown in Figure 5.6, one computer controlled the tests, whereas the other was used for logging the data.

The test was carried out in deformation-control. The control deformation was an internal displacement sensor of the Zwick loading machine, which sufficed to keep stability of crack propagation throughout the test. The deformation rate was kept constant at 0.002 mm/min.

As mentioned above the forces in the pendulum bars were also measured. Having the results of the loads in the bars, the symmetry of the load setup

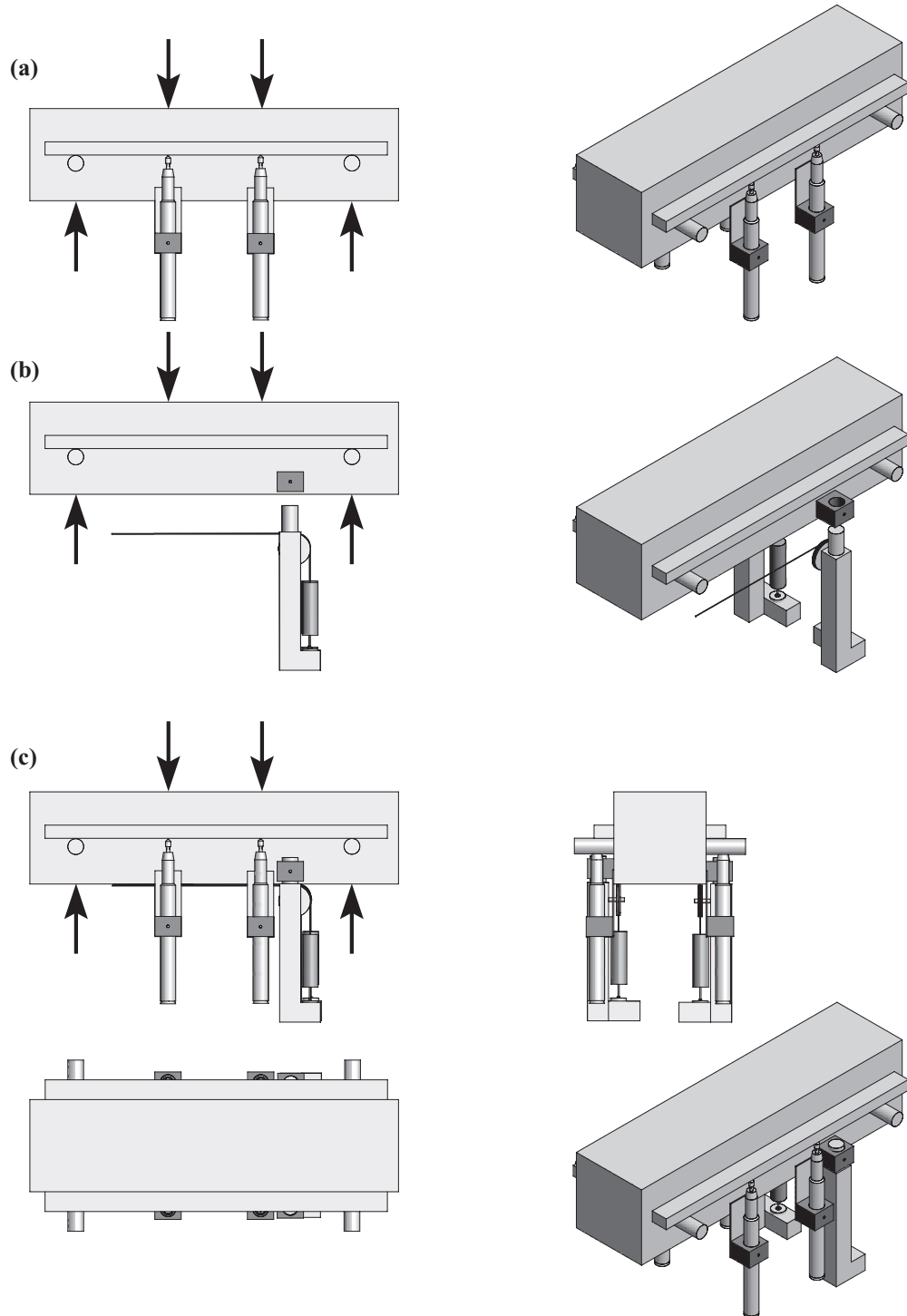


Figure 5.4: Arrangement of deformation measurement devices for the pendulum-bar four-point bending tests; (a) LVDT sensors at the loadpoints, (b) CMOD sensor, (c) Mutual positioning of all sensors.

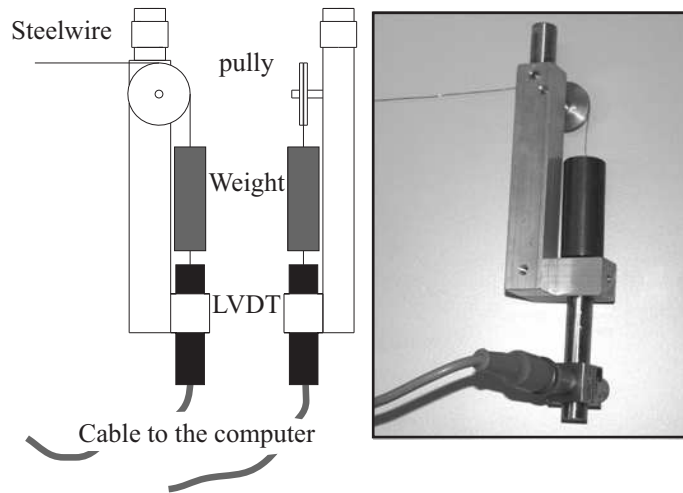


Figure 5.5: CMOD sensor

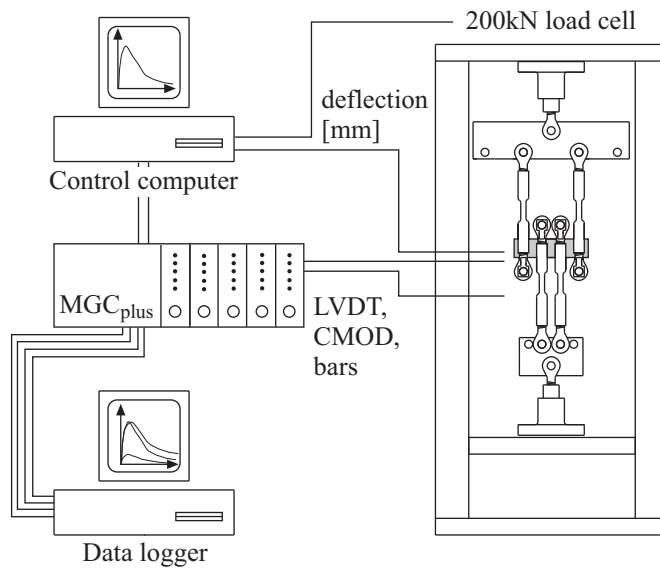


Figure 5.6: Data acquisition and test set-up for the  $70/70/280 \text{ mm}^3$  specimens

could be assessed as shown in Figure 5.7. In all tests the difference between the most loaded and the least loaded bar was less than 6%. This result corroborates the fact that with pendulum bars the test setup remains continuously symmetric.

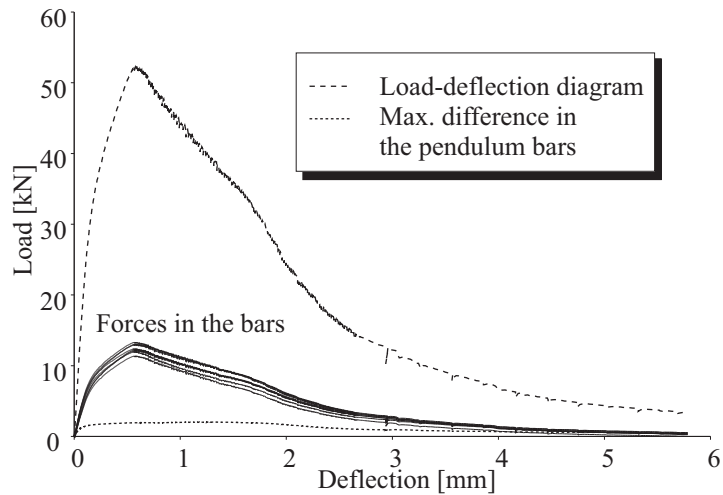


Figure 5.7: Load-deflection-diagram in the pendulum-bar four-point bending test set-up. The range of the force in the individual pendulum bars is shown as well as the maximum force differences between the pendulum bars.

### 5.2.4 Interpretation

Once the tests were performed all data had to be analyzed. The nominal stress is calculated assuming the beam to remain elastic throughout the loading process by dividing the bending moment  $M$  by the section modulus  $W$  ( $\sigma = \frac{M}{W}$ ). The nominal stress is plotted along the y-axis of the stress-displacement diagrams (Figure 5.8). On the x-axis the average of the displacements measured at the loading points is shown.

The middle deflection can be calculated as the intersection of the two straight lines given by the displacement at the loading points and the geometry of the setup (see Figure 5.9a and Equation 5.1). However, although this calculation is a good approximation for the maximum value of the middle displacement, it only holds for the post-peak stage. In the post-peak stage a macro crack opens and the elastic deformations can be neglected since they are comparatively small. In the pre-peak stage the deformation line is everything but a straight line (Figure 5.9b) and all the deformations are influenced

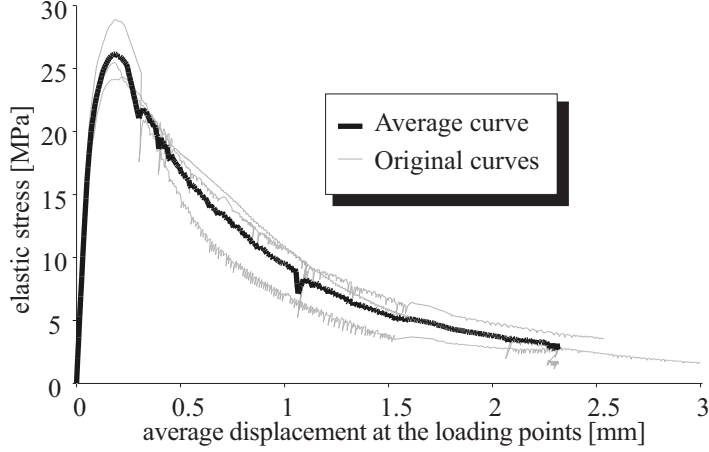


Figure 5.8: Deformation of stress-average displacement curves from four LVDT readings.

by non-linear elasticity. From elasticity theory, the deforming line can be calculated from the principle of virtual work (5.2). The calculation is given in Equations 5.1 to 5.7 and Figures 5.10 and 5.11 shows the principles on which the calculation is based. Equation 5.1 gives the middle displacement based on the intersection of the two straight lines.

$$\delta_m = \frac{(2a + b) \cdot \delta_1 \cdot \delta_2}{a \cdot (\delta_1 + \delta_2)}, \quad (5.1)$$

where  $a$  is the distance between support and loading point and  $b$  the distance between the loading points. In Figure 5.9a  $\delta_1$  and  $\delta_2$  are the displacements at the loading points.

$$\delta = \int_0^{a+b+a} \overline{M}_b(x) \cdot \frac{M_b(x)}{E \cdot I} \cdot dx \quad (5.2)$$

$M_b(x)$  is the moment caused by the load and  $\overline{M}_b(x)$  is the moment caused by the virtual loading.

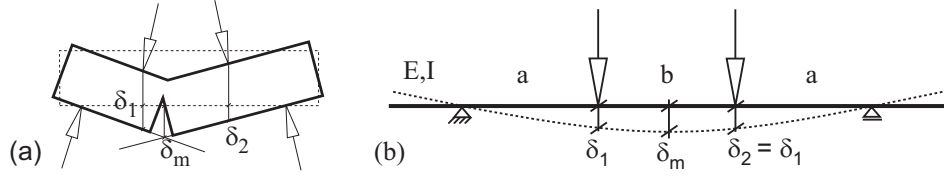


Figure 5.9: (a): Crack deformation; (b): elastic deformation

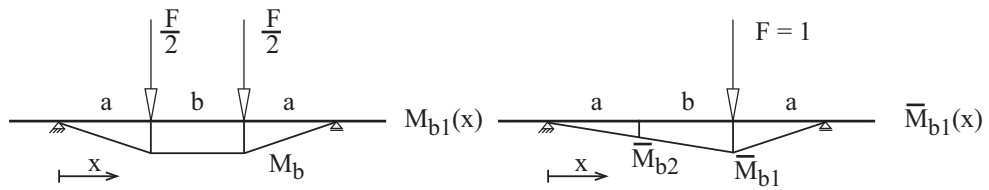


Figure 5.10: Sketch for calculation  $\delta_1$

$$\delta_1 = \frac{1}{E \cdot I} \left( \frac{1}{3} M_b \cdot \overline{M_{b2}} \cdot a + \frac{1}{2} M_b \cdot (\overline{M_{b1}} + \overline{M_{b2}}) \cdot b + \frac{1}{3} M_b \cdot \overline{M_{b1}} \cdot a \right) \quad (5.3)$$

$$\delta_1 = \frac{a^2(2a + 3b) \cdot F}{12 \cdot E \cdot I} \quad (5.4)$$

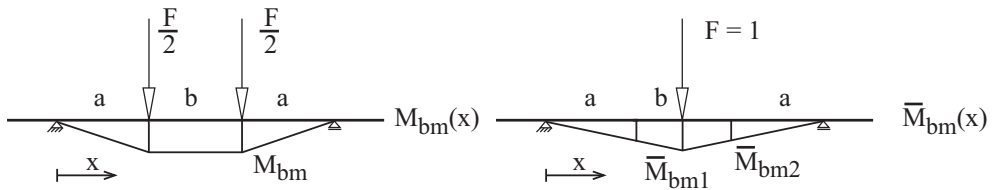


Figure 5.11: Sketch for calculation  $\delta_m$

$$\delta_m = \frac{2}{EI} \left( \frac{1}{3} M_b \cdot \overline{M_{bm2}} \cdot a + \frac{b}{2} M_b \cdot \overline{M_{bm2}} + \frac{b}{4} M_b \cdot (\overline{M_{bm1}} - \overline{M_{bm2}}) \right) \quad (5.5)$$

$$\delta_m = \frac{a \cdot (8a^2 + 12ab + 3b^2) \cdot F}{48E \cdot I} \quad (5.6)$$

Combining Equation 5.5 and Equation 5.6, the middle deflection can be calculated as

$$\delta_m = \frac{(8a^2 + 12ab + 3b^2) \cdot \delta_1}{4a(2a + 3b)} \quad (5.7)$$

In Equation 5.7,  $\delta_1$  is the average of the displacements at the loading points. Figure 5.12 shows the differences between the different methods of calculating  $\delta_m$ .

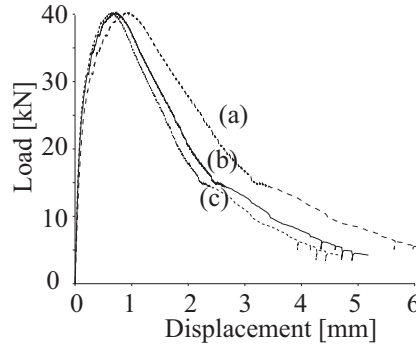


Figure 5.12: Differences between (a) calculation based on Equation 5.7, (b) calculation based on Equation 5.1, (c) average of the measured displacements at the loading points

In the pendulum-bar four-point bending test there are two methods for calculating  $\delta_m$  as seen before. The results of both methods are not valid for the whole stress-displacement diagram. The middle displacement based on Equation 5.7 is only valid for elastic displacements and the calculation based on the intersection of the two lines (Equation 5.1) only for the case where all deformations are associated with a propagation of one single crack. These two methods give an upper (Equation 5.1) and a lower (Equation 5.7) limit for the



real middle displacement. As the results of all calculations are similar (Figure 5.12) it can be concluded that the middle displacement in the pendulum-bar four-point bending test can be estimated from the displacement at the loading points only. Therefore, as a good approximation of the displacement the average displacement derived from the measurement of the four LVDT's was used in the pendulum-bar four-point test.

### 5.3 Tensile test

There is still an ongoing discussion about the best tensile test (van Mier & Mechtcherine [2007]). Mechtcherine [2007] and Naaman et al. [2007] propose a tensile test with fixed boundaries while Stähli et al. [2007] and van Mier et al. [1994b, 1995] propose one with rotating boundaries because rotating boundaries minimize the fracture energy as well as the influence of the supports. The reason for using pendulum-bars is based on the idea that during a tensile test the forces should remain centric and the supports should be able to rotate (Figure 5.13 and 5.15). This becomes important especially when a material of increased ductility, such as HFC, is used. Van Mier et al. [1994b] showed that the boundary conditions in a uniaxial tensile test have a significant influence on the result of the test. Not only the tensile strength but also the fracture energy obtained from uniaxial tensile tests between fixed boundaries are higher than the values received from tests with rotating supports.

#### 5.3.1 Test set-up

Figures 5.14 and 5.15 show the pendulum-bar tensile test set-up. The ability to rotate was achieved by the use of eight pendulum-bars. The same technique was used before by Schlangen [1993] and van Vliet [2000]. The bars connect two parts of each the upper and the lower supports. The length of the pendulum-bars is exactly 270 mm. The centre of rotation of the supports is positioned at the centre of the interface between the specimen and the glued aluminium plates.

#### 5.3.2 Specimen geometry and preparation

To determine the uniaxial tensile strength of concrete, dog-bone shaped specimens are well proven (Markovic [2006], van Vliet [2000], van Mier et al. [1994b], Carpinteri & Ferro [1994]). It is important to use curved bays and to avoid transitions from straight edges to curved edges in the specimen, see

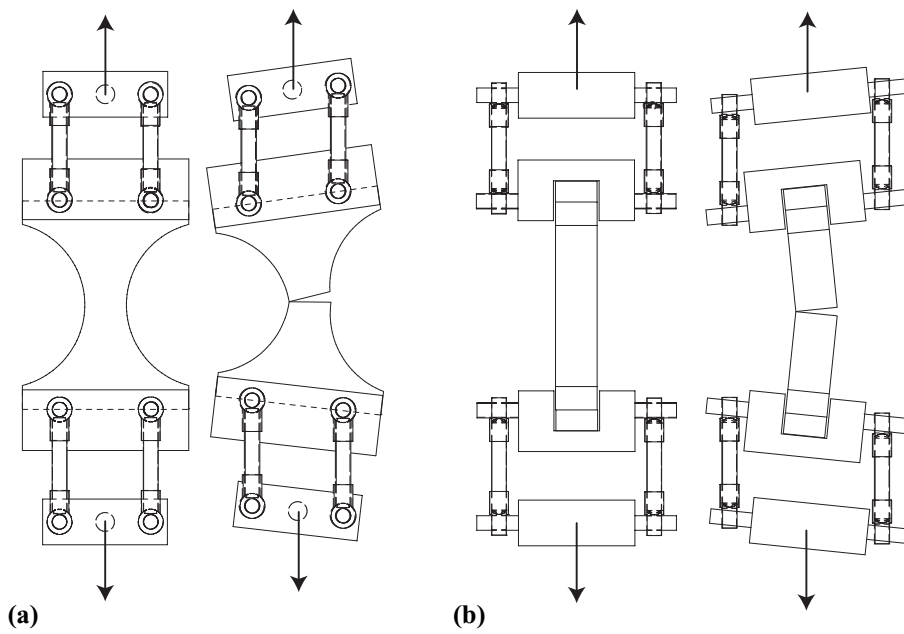


Figure 5.13: Principle of the pendulum-bars in the pendulum-bar tensile test in two orthogonal directions. (a): front view (in-plane direction); (b): side view (out-of-plane direction).

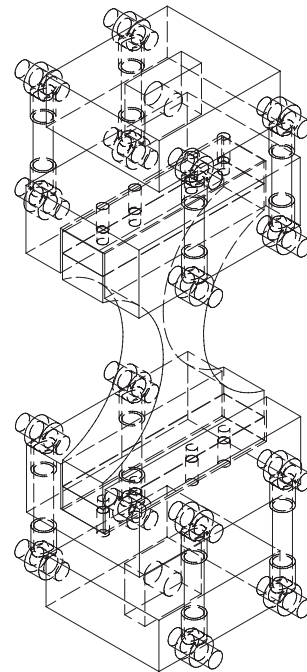
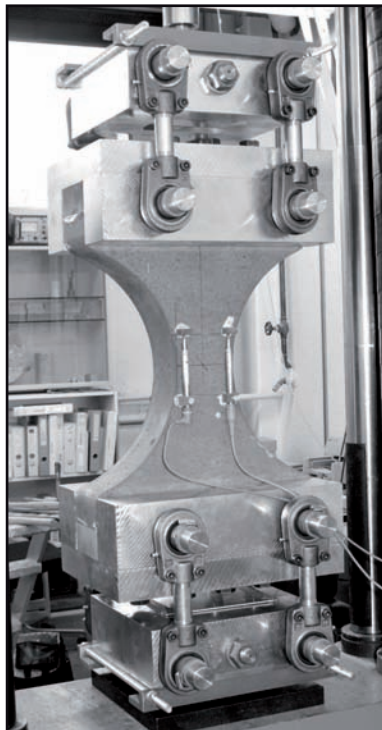
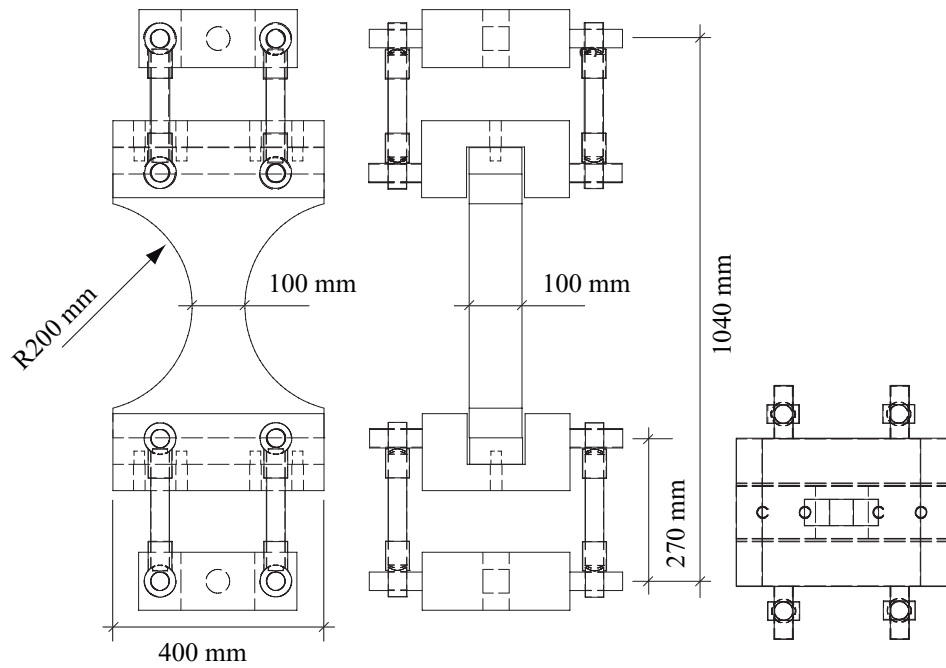


Figure 5.14: Sketches of the 'pendulum-bar' test set-up

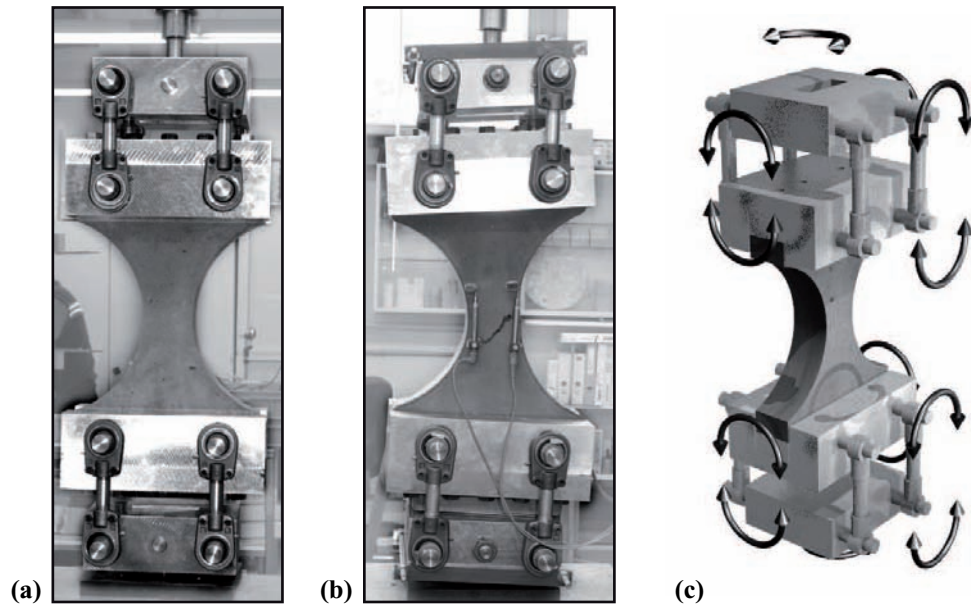


Figure 5.15: Images of the pendulum-bar tensile test. (a): un-cracked specimen, (b): cracked specimen, (c): scheme of pendulum-bar tensile test set-up; the arrows show the ability to rotate around the centre of rotation, e.g. around the interface between aluminium plate and specimen.

the analysis by van Vliet [2000]. In the present experiments, the geometry of the specimen was defined by the maximum fibre length, the glue and the testing machine. The minimum cross section was at least three times the length of the largest fibre (30 mm). This is in accord with Mechtcherine [2007] and 162/1 [1989]. Therefore the dimension of the smallest cross section of the specimen is  $100 \times 100 \text{ mm}^2$ . The height of the tensile test specimen is 500 mm. The maximum width is 400 mm and, as mentioned, the minimum width is 100 mm. The chosen depth of the specimen was 100 mm. The radius of the curved bays is 200 mm. The capacity of the load cell used in the testing machine is 200 kN and the tensile strength of the glue used was higher than 20 MPa.

One day after casting, the specimens were demoulded, cut to the final geometry (Figure 5.17) and stored for the next 24 days in a climate chamber with a humidity of 95% and a temperature of 20°C. Three days before testing the samples were prepared for gluing. Within two days, two aluminium plates with four M20 threads were glued to the top and the bottom of the specimen. Aluminium was used in order to smoothen the change of stiffness between the concrete and the test rig. The aluminium plates were used to fix the sample in the tensile test rig. The glue used was Araldite AW2101. Before gluing the surfaces of the aluminium plates and those of the specimen were cleaned and sand-blasted. The specimen was ground, the edges were smoothed (see Figure 5.16) using a carborundum stone and cleaned with pressurized air. The aluminium plates were cleaned using a methyl-butyl-ketone ( $C_4H_8O$ ) dissolver. It is of extreme importance that the whole surface of the aluminium plates is properly cleaned and no grease is left. Otherwise the joint would not resist the mechanical demand and the specimen would fail at the gluing line. Right after cleaning the two components of the glue were mixed and applied in furrows on the specimen. A single batch of glue was mixed for each aluminium plate. Afterwards the aluminium plates were pushed down till the glue was pressed out, the furrows closed and the plate could be positioned on the specimen. (Figure 5.16). The second side of the specimen was glued two hours after the first side. The gluing and preparation procedure is described in more detail in Looser & Tatti [2006] and in Sutter [2007].

After one day the adhesive was fully hardened and the holders for the LVDT's were glued to each side of the specimen, after which the sample was ready to be tested (Figure 5.17). The gluing of the holders is a rapid process and can be done right before testing. The glue used is X60 from HBM.

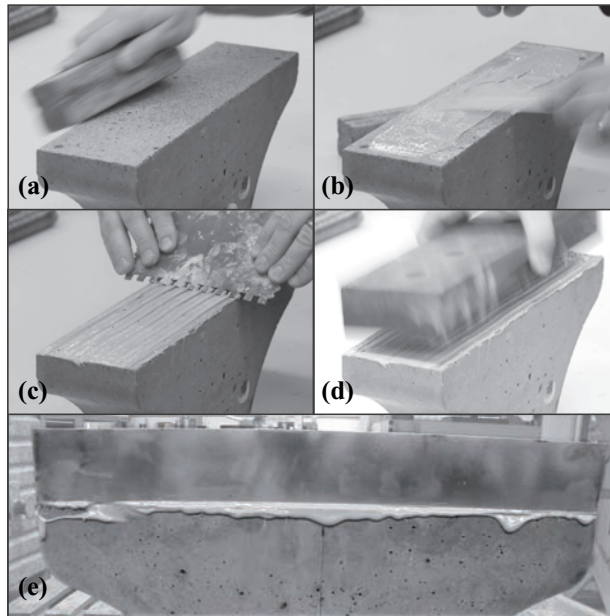


Figure 5.16: Gluing procedure, (a): smoothing of the edges, (b): applying the glue, (c): creating the furrows, (d): placing the aluminium plate (e): glue pressed out at the sides.

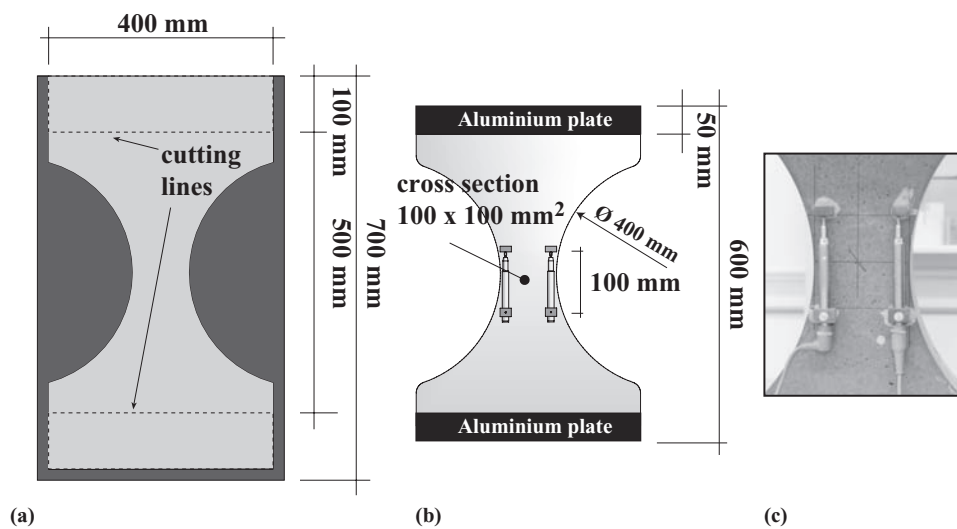


Figure 5.17: (a): A sketch of a tensile test specimen with its cutting lines. (b),(c): The same specimen after gluing the aluminium plates and the attaching the LVDT's.

### 5.3.3 Measurement

The deformation was measured using four LVDT's with a maximum range of 10 mm, two on each side of the specimen. The force was determined using a 200 kN load-cell at the top of the set-up. The test was carried out in displacement-control which is permissible for ductile materials (see Mechtcherine [2007]). The displacement rate was kept constant. The test was aborted when the first sensor reached its maximum range.

### 5.3.4 Interpretation

The cross-section where the crack propagated  $A_{real}$  and the minimum cross-section  $A_{nom}$  of the specimen were determined. The tensile strengths  $f_{tnom}$  and  $f_{treal}$  for the nominal tensile strength and the real (crack) tensile strength respectively were calculated. The strain at the first crack and at peak-load was also determined using the average deformations from the four LVDT's. The Young's Modulus and the specific work of fracture  $W_{fpeak}$  could now be calculated from the stress-strain diagram.

## 5.4 Impregnation technique

The crack pattern must be measured for describing fracture process. The following section describes the technique and the device which was used to impregnate fractured specimens and to visualize crack pattern. Information about the crack patterns was obtained using a vacuum impregnation technique that will be described in the former section.

### 5.4.1 Impregnation material - Epoxy resin

The epoxy resin used was EpoFix<sup>1</sup> with a pot life of 30 min, a hardening temperature of about 40°C and a hardening time of more than four hours. The product is ideal for vacuum impregnation due to its low viscosity and the negligible shrinkage. To visualize cracks, a fluorescent dye, EpoDye, was mixed into the resin and cracks can be easily identified in UV (ultra-violet) light.

---

<sup>1</sup><http://www.struers.com>

### 5.4.2 Vacuum cylinder

The impregnation device consists of a plexiglas cylinder fixed on a bottom plate. The cylinder can be closed with a steel lid on which a valve, a hopper, the vacuum hose and a pressure indicator are mounted (see Figure 5.18). The specimen is jacked up in the cylinder in such a way that the hose coming from the hopper is about one centimeter above the surface of the specimen to be impregnated so that the epoxy flows through the hose directly onto the surface of the specimen. The minimum air pressure that can be achieved is 200 mbar (20 kPa). The diameter and the height of the cylinder is 500 mm.

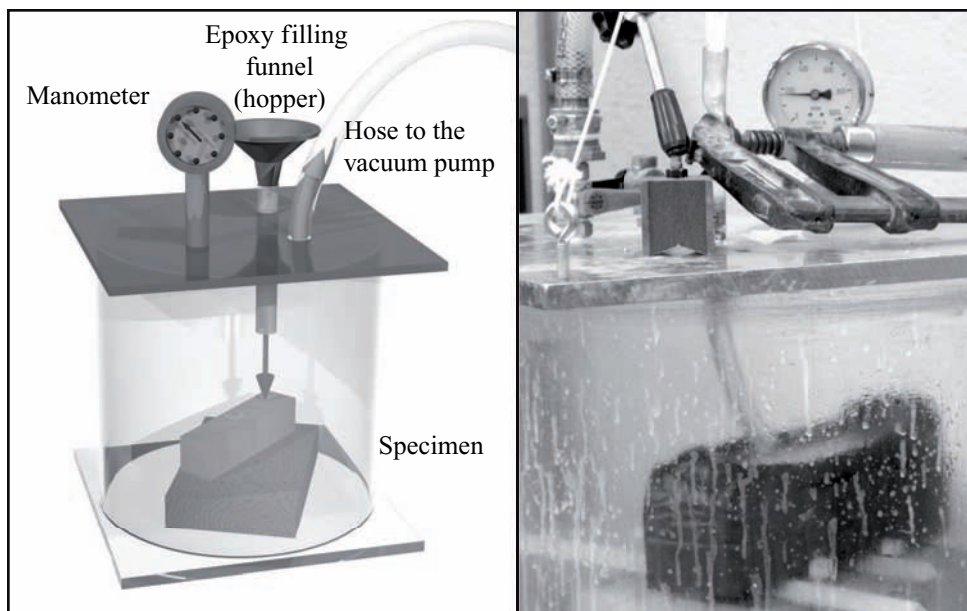


Figure 5.18: Sketch and image of the impregnation device with the attached installations

### 5.4.3 Impregnation procedure

The impregnation procedure is basically split into three parts (Figures 5.19 and 5.20). The first part is the mechanical testing. At least three specimens should be tested first in order to determine the load deformation curve. Afterwards the impregnation specimens can be loaded to a defined deformation (see Appendix B). In order to ensure that the cracks remain open, two steel plates were glued to the sides of the specimen while the specimen was still under load in the testing machine. One of the two steel plates had a pocket



which allowed the epoxy to penetrate into the crack from the side. The second part is the impregnation itself. The specimen was wrapped with tape so that the epoxy resin could not spill out and after the impregnation the air-pressure acted from one side only and the epoxy was pressed even further into the cracks. Only one side of the specimen was not wrapped; e.g. the bottom of bending specimens. It is important that the tape layer was completely closed otherwise the epoxy resin would spill out while flowing into the vacuum cylinder. The wrapped specimen could now be placed in the vacuum cylinder so that the filling hose was about one centimeter above the surface of the specimen. After all the valves were closed the vacuum was built and the specimen was impregnated. To improve the impregnation the pressure restoration had to be slowed down as much as possible. Usually it took about 40 to 50 min to restore atmospheric pressure in the cylinder. Next the specimen was placed into an oven (60°C) for one day in order to accelerate and improve the hardening process. The epoxy resin reaches high temperatures during the hardening process, especially when a large amount of epoxy resin is used. The heating in the oven guaranteed a well balanced temperature profile in the hole specimen and cracks in the epoxy, which appeared without heating up, were prevented. The last part was the cutting of the specimen. One day after impregnation, the specimen was cut. The cut was as close as possible to the surface where the plate with the pocket had been placed. This was the most obvious place/location since there the epoxy resin penetration into the specimen was best, and the cracks were nicely visible.

After the preparation of the specimen the cracks were photographed under UV-light (see Figure 5.21). One photo covered an area of  $25 \times 20 \text{ mm}^2$ . Several photos were needed to cover the entire crack pattern. All photos were subsequently stitched together using Adobe® Photoshop. Figure 5.22 shows an example of such a series of photos and the final result. The pixel size of the images equals 0.025 mm.

#### 5.4.4 Interpretation

The final image of the whole crack was converted (i) to a binary image and (ii) to a grey scale image where the crack, the matrix and the fibres were visible (for illustration purposes only). Using the grey-scale image the cracks were traced manually and analyzed. Additionally the relevant pores were traced and the resolution was reduced to 10 px/mm. Afterwards a threshold was set so that all traces were black. Crack-spacing, 'crack-density' and the number of vertical and horizontal cracks with different crack heights and width were

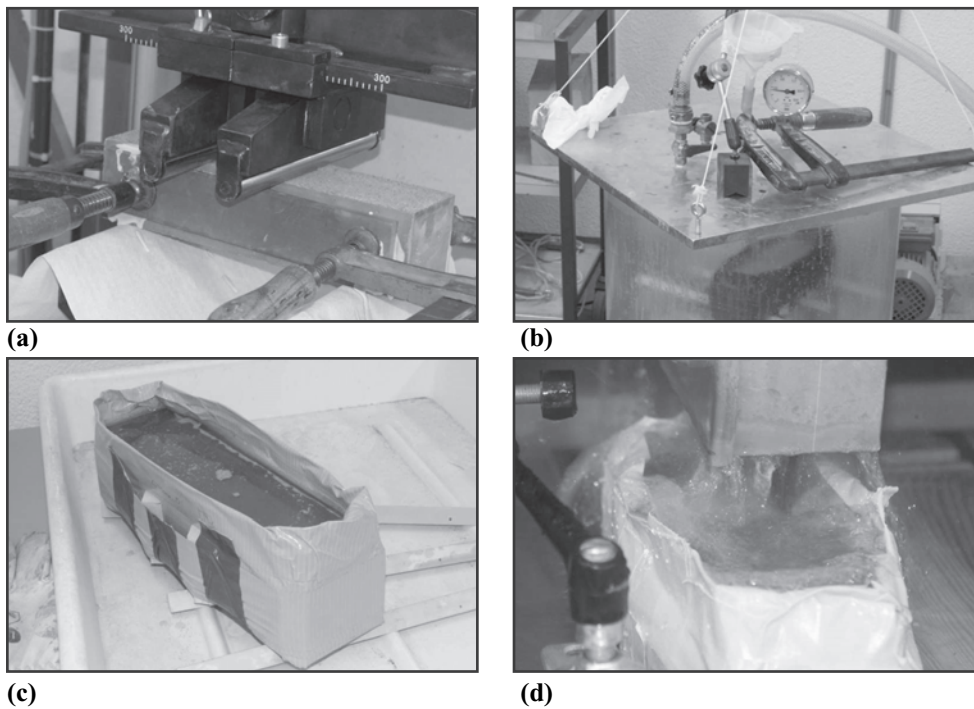


Figure 5.19: Work-flow of the impregnation process. (a): gluing two steel plates to the specimen under load. (b): impregnating the specimen. (c): the specimen right after impregnation. At this stage the epoxy was still liquid. (d): cutting the specimen.

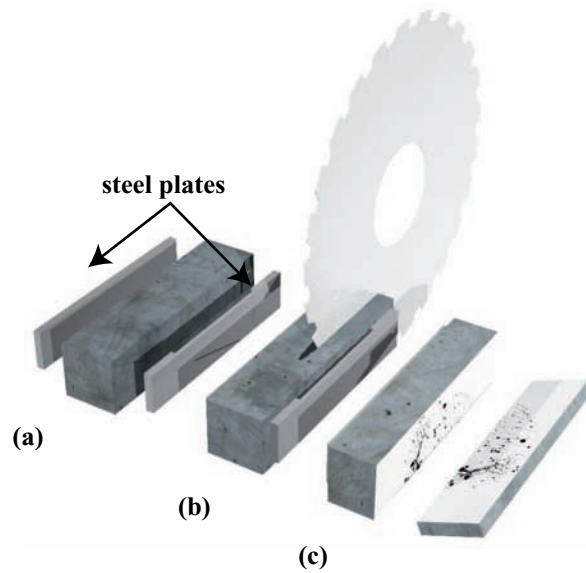


Figure 5.20: Scheme of the impregnation work-flow. (a): gluing the two steel plates to the sides of the specimen,(b): cutting the specimen,(c): analyzing the crack pattern

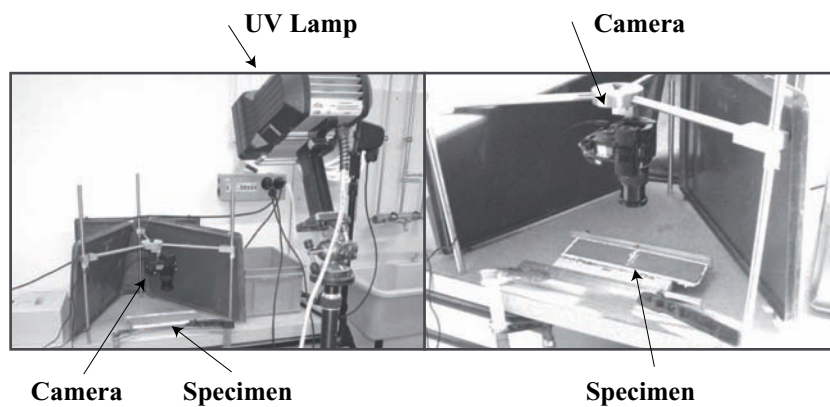


Figure 5.21: Images of the photo set-up. The dimensions of the area of one photo was  $25 \times 20 \text{ mm}^2$

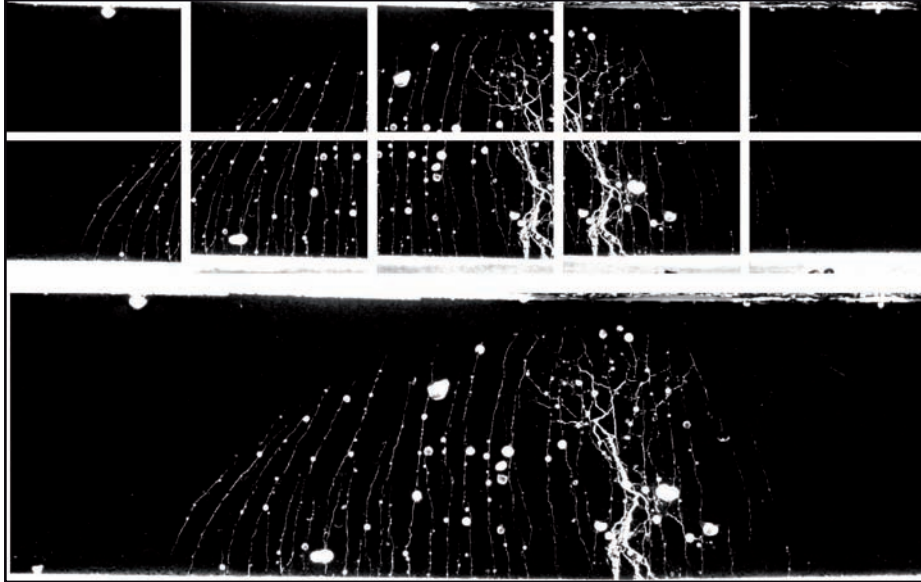


Figure 5.22: Creating the crack pattern by stitching ten individual images together.

determined. The crack-space was defined by the number of white pixels between two black pixels. The images were interpreted as a single matrix containing the values 0 for white pixels and 255 for black pixels (crack) and was analyzed using Mathworks MATLAB.

## 5.5 Results

In order to achieve the goal to increase the tensile strength of HFC several test-series were performed. The following section describes test-series where the mechanical properties of different fibre mixtures (HFCs) and single fibre mixtures (SFCs) in bending and tension were determined. Crack pattern and crack growth was analyzed in the last test series of this section.

### 5.5.1 Evaluation of the mixing system

Most of the work done on hybrid fibre concrete relates to small scale laboratory work where batches in the order of 50 liters have been prepared. With batches of that size parameter studies can effectively be carried out (e.g. the extensive work done by Markovic [2006]). However, for full-scale applications much larger batches are necessary (see also Di Prisco & Plizzari [2004]), and

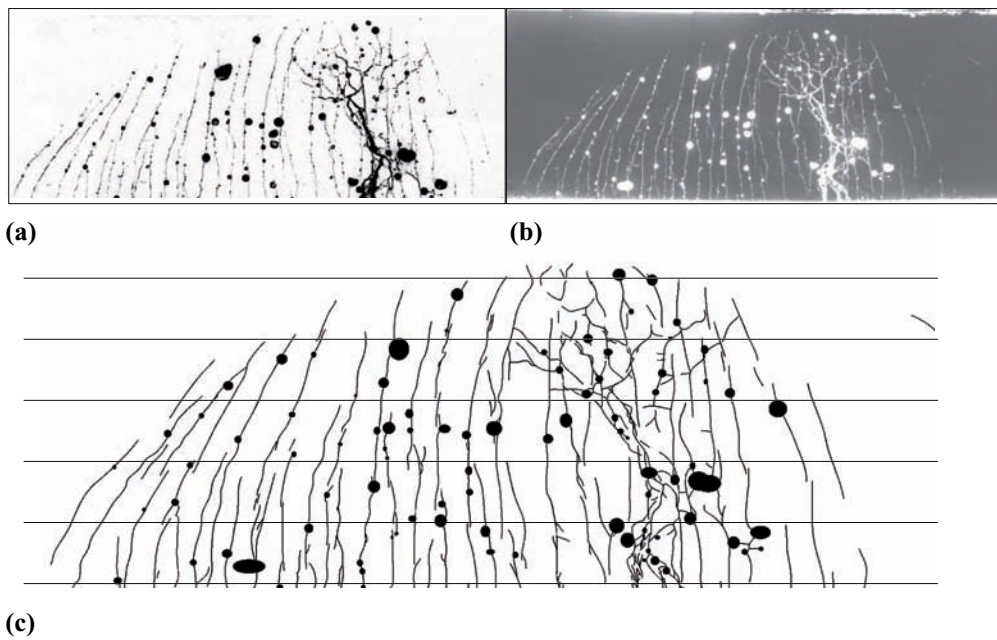


Figure 5.23: Image analysis of the cracks. (a): binary image after applying Adobe Photoshop filters, (b): grey-scale image which was ground for the manual tracing and (c): result after tracing including horizontal lines where the crack-spacing of vertical cracks was analyzed

consequently some experiments with batches between 200 and 400 liters were done, using two different mixing systems. In this section results from these 'larger scale' experiments are presented (see also Stähli & van Mier [2007a]). The 400 liter batch was produced in a planetary mixer (fabr. Huggler<sup>2</sup>), which was placed on an outside building site and the 200 liter batch was produced in an Eirich<sup>3</sup> mixer (which operates with a slightly different principle) at the EMPA<sup>4</sup>. Images and technical data can be found in Appendix A. Because of the relatively big effort of casting large batches, the study was concentrated on a single mix design, containing a total of 6% of steel fibres (4.5%, 1.0% and 0.5% for small, middle and large fibres respectively). When casting the material, fibres tend to align near the walls of the moulds, and anisotropic fibre distributions will result. The anisotropy has undoubtedly an influence on the fracture behaviour of hybrid fibre concrete (van Zijl [2005]), and because the large batches allowed the preparation of many laboratory specimens, it was possible to study the fracture behaviour under different conditions. For some of the specimens the sides, a 30 mm surface layer, was simply cut-off, thereby removing surface layers containing aligned fibres which were perhaps also areas with relatively high fibre volumes. In Figure 5.24 an overview is given of all the specimens that were produced.

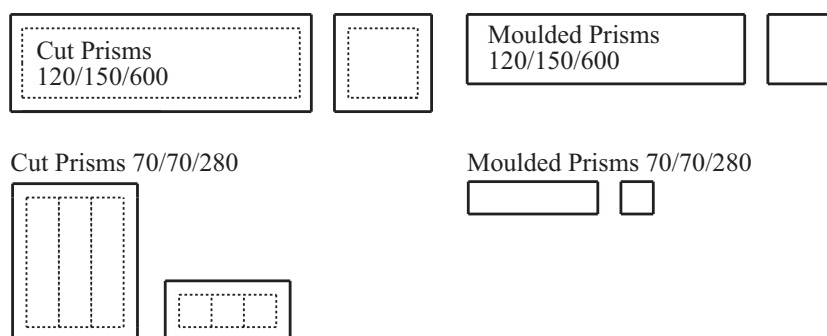


Figure 5.24: Overview of specimens used in different bending tests. Sizes of the specimens are given in [mm]. For the 'Huggler' and 'Eirich' batch the same specimens were tested, with the exception that no 'cut prisms' were produced from the 'Eirich' batch.

<sup>2</sup><http://www.huggler.ch>

<sup>3</sup><http://www.eirich.com>

<sup>4</sup>EMPA Materials Sciences & Technology in Dübendorf, Switzerland

As a result the 'cut prisms' (Figure 5.25) were sawn from larger concrete blocks. Blocks of size  $340 \times 280 \times 130 \text{ mm}^3$  were cut into three  $70 \times 70 \times 280 \text{ mm}^3$  prisms. Three prisms of size  $120 \times 150 \times 600 \text{ mm}^3$  were cut out of concrete block of size  $210 \times 210 \times 650 \text{ mm}^3$ .

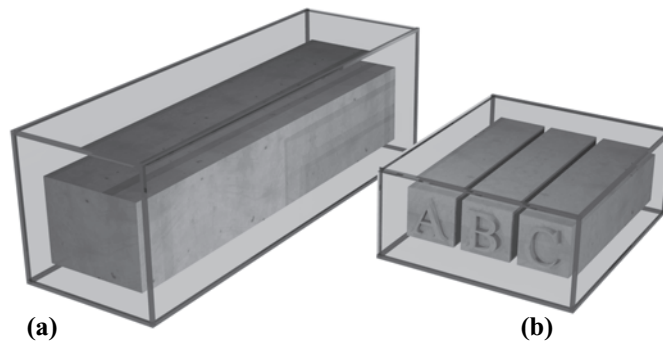


Figure 5.25: Scheme of the the 'cut prisms'. (a): large  $120 \times 150 \times 600 \text{ mm}^3$  and (b): small  $70 \times 70 \times 280 \text{ mm}^3$  prisms

The fracture response of the investigated hybrid fibre concrete is shown in the form of load-displacement diagrams from pendulum-bar four-point bending tests. In addition to the load-displacement behaviour, the progress of (multiple) crack growth in the hardening regime is shown in a series of impregnated specimens. Ultimate failure always happens through the development of a single localized macro-crack bridged by the largest fibres in the mixture.

In Figure 5.26 an overview of the mechanical properties from of the 'Huggler' batch is shown. It can be seen that the (elastic) flexural strength of the small  $70/70/280$  specimens was about double of the maximum strength of the larger  $120/150/600$  specimens. It can also be seen that the shape of the curves was not similar. In particular, the small specimens showed steeper post-peak behaviour than the larger beams. These figures clearly show that the curves for the cut specimens are lower than those for the moulded samples, although the various curves of cut and moulded samples remained more-or-less parallel throughout the test. Figure 5.26a ( $\sigma - CMOD$ ), also shows that at high CMOD the curves of the  $70/70/280$  and for the  $120/150/600$  specimens approach each other for both, the moulded and the cut specimens, the moulded at a higher stress level than the cut.

Figure 5.27 shows an overview of the results from tests of the 'Eirich' batch. This figure shows that the shapes of the curves are also different: the

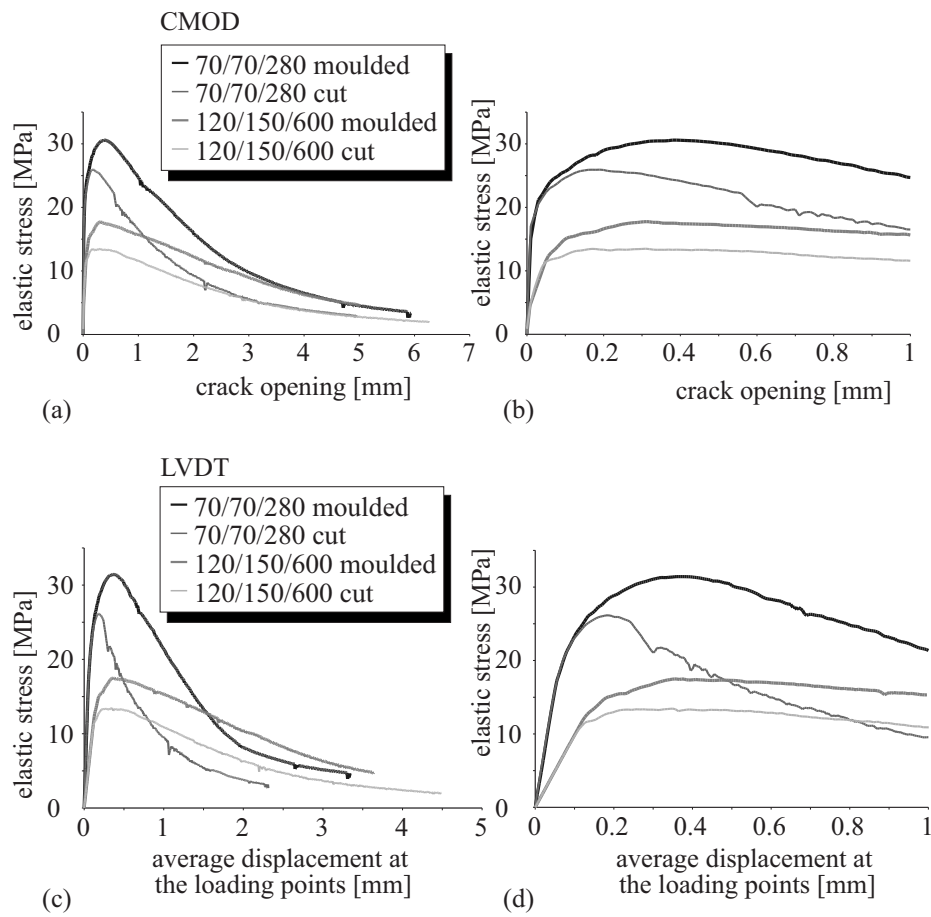


Figure 5.26: Flexural stress-CMOD (a, b) and flexural stress-displacement diagrams (c, d) for pendulum-bar four-point bending tests for the 'Huggler' batch. In (b) and (d) the first portion of the curves in (a) and (c) is shown enlarged



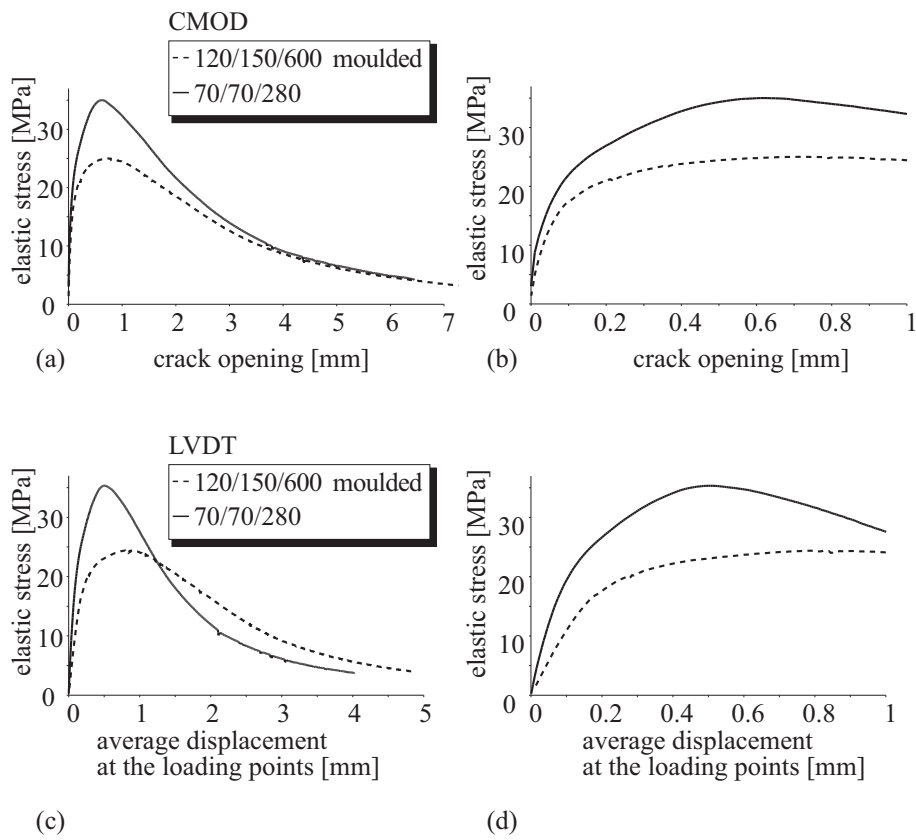


Figure 5.27: Flexural stress-CMOD (a, b) and flexural stress-displacement diagrams (c, d) for pendulum-bar four-point bending tests for the 'Eirich' batch. In (b) and (d) the first portion of the curves in (a) and (c) is shown enlarged

120/150/600 curve is just beyond peak not as steep as the curve from the 70/70/280 specimens, which is similar to the 'Huggler' series. From a global comparison of Figures 5.26 and 5.27 it can be concluded that no significant differences appear for HFC produced with two different mixers. For example, the characteristics of the moulded 70/70/280 and moulded 120/150/600 specimens were quite similar. Only the peak of the 'Eirich' 120/150/600 is somewhat smoother and at a slightly higher stress level than the one from the 'Huggler' batch.

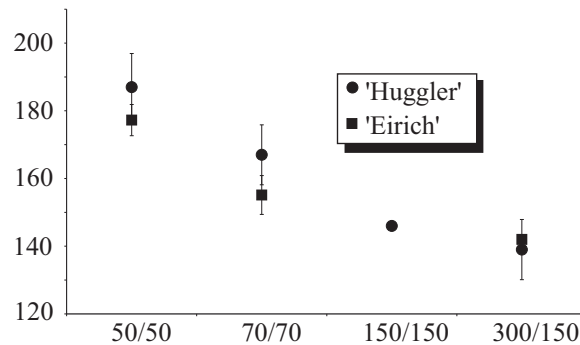


Figure 5.28: Compressive strength of the 6% HFC mixtures

In order to determine the compressive strength both 50 mm and 70 mm cubes were loaded to failure by cutting the cubes from the 'un-damaged' ends of the beams previously loaded in flexure. In total 30 specimens were tested in compression. In addition to these small cubes for each of the two batches, three 150 mm cubes and three 150/300 mm cylinders were cast and tested. The results from all compression tests are shown in Figure 5.28. They can be summarized as follows: for the 50 mm cubes, the average maximum compression strength was 187 MPa (coefficient of variation of 5.3%), for the 70 mm cubes, the average maximum compression strength was 167 MPa (coefficient of variation of 5.3%), for the 150 mm cubes, the average maximum compression strength was 146 MPa (coefficient of variation of 0.4%) and for the 150/300 mm cylinders the average compression strength was 139 MPa (coefficient of variation of 6.4%). The Young's modulus was determined from the three 150/300 mm cylinders and had an average value of 40.2 GPa with a coefficient of variation of 1.3%. The compression tests show that with the increase of the size of the specimen the value of the average compression strength decreases, which is a similar trend as observed in the testing of plain

Table 5.1: Influence of mixture type, beam size and boundary condition on flexural strength

Mixer	Beam size (# specimens)	Boundary condition	Flexural <sup>a</sup> strength [Mpa]	Coeff. of variation [%]
Eirich	70/70/280 (6)	moulded	35.5	13
Huggler	70/70/280 (3)	moulded	31.8	21
Huggler	70/70/280 (3)	cut	26.2	9
Eirich	120/150/600 (6)	moulded	25.9	28
Huggler	120/150/600 (3)	moulded	18.0	22
Huggler	120/150/600 (3)	cut	14.2	12

<sup>a</sup> Results from pendulum-bar four-point bending tests

concrete and corresponds to the different size effect laws.

The results derived from the 'Huggler' and the 'Eirich' batch show an increase of the maximum bending strength in favor of the 'Eirich' batch of 10% for the 70/70/280 and 30% for the 120/150/600 specimens. This increase is not necessarily due to the mixer. The increase can also be caused by the fact that the w/b-ratio was not the same in the two batches. The 'Huggler' batch was produced on a site when it was raining, and it was not possible to dry the mixer before filling with raw material. When the moulds were filled it still rained. Therefore, in the 'Huggler' batch the w/b-ratio is slightly higher than the one from the 'Eirich' batch, but the exact value cannot be given. Table 5.1 clearly shows that there is no difference in the coefficient of variation due to the mixer, which means that the fibres were regularly distributed by both mixers. Table 5.1 also shows that the scatter for the cut specimens is lower than for the moulded samples. That suggests that a large scatter in HFC is to a large extent caused by wall effects. On the other hand, the increase in bending strength with decreasing specimen size can also be explained by the fact that the small specimens have much more wall surface relative to the specimen volume than the larger specimens. Additionally to the commonly known size effect models (see Walsh [1972], Bažant [1984] and Carpinteri & Ferro [1994]), the strength difference can then be explained from the alignment of the fibres along the walls in the tensile direction and the resulting higher strength of the surface layers of the specimens. This alignment could also be the cause for the increased scatter because the fibre alignment cannot be controlled very well in different parts of the cross-section, and the fibre distribution is not homogeneous anymore.

The explanation for the smoother shape of the curves from the 120/150/600 from the 'Eirich' batch in comparison to the 'Huggler' batch can be a direct consequence of the w/b-ratio. A smooth peak indicates that the fibres are pulled out 'without' damaging the concrete matrix too much. With a higher w/b ratio, the concrete matrix loses strength and this loss of strength can cause the matrix to fail before the fibres are pulled out and this would lead to results as shown in Figure 5.26. Improved pull-out properties of the fibres and improved fresh concrete behaviour have a positive effect on the mechanical properties. This was already observed by Markovic [2006].

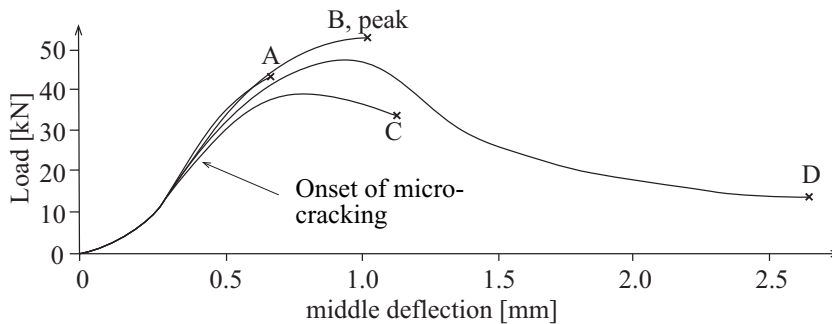


Figure 5.29: Load-deflection diagrams for four beams loaded in four-point bending, up to prescribed deflection: one pre-peak stage (0.6 mm), one at peak (1.0 mm), and two post-peak stages (1.1 and 2.6 mm, respectively)

In another series crack patterns at different stages of load were observed.  $70/70/280 \text{ mm}^3$  prisms were tested in four-point bending. In order to ensure that the cracks remain open, two steel plates were glued to the side of the specimen while the specimen was still under load in the testing machine. This was carried out at four different stages in the load-deflection diagram, namely in the pre-peak regime (Figure 5.29 A), peak (Figure 5.29 B) and two post-peak stages (Figure 5.29 C and D). Immediately after loading, the specimens were impregnated in vacuum with fluorescent epoxy resin and later cut into slices. After cutting, the complete area of each slice and details of the cracks were photographed under UV-light. To highlight the cracks, binary images were produced, see Figure 5.30. The pixel size of the detail images equals 0.025 mm. Figures 5.30a to c show that the cracks start developing at the bottom of the specimen in the area under the loading points. Figure 5.30a also shows that in the vicinity of relatively large pores (mm scale) a larger concentration of cracks develop, which seem to originate from the pore. At a deflection of more than 2.5 mm (Figure 5.30d), all deformations localize into a single macro-crack that is visible to the naked eye. The length of this

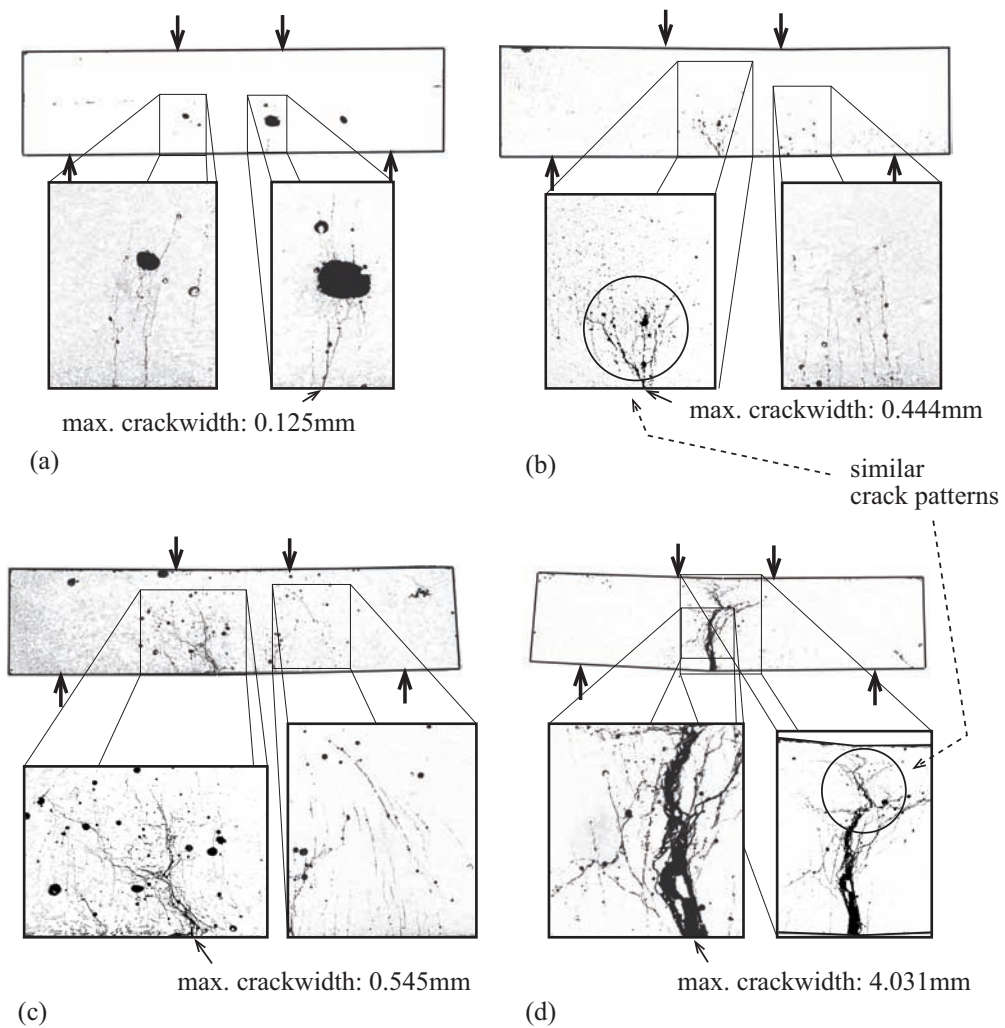


Figure 5.30: Crack evolution in hybrid fibre concretes shown through impregnation of partially cracked specimens of Figure 5.29. Multiple cracking is observed in the pre-peak regime (a), slowly transforming in a fully localized macrocrack bridged by fibres in (d). Images of crack bridging can be found in Appendix B.

crack is equal to almost the complete depth of the specimen. At the very top of this crack some horizontal branching and some small cracks can be observed. These small cracks are similar to those observed in Figure 5.30b. This image sequence clearly shows that the fracture zone moves with the crack and therefore with the neutral axis.

### 5.5.2 Properties development and curing conditions

In order to determine the influence of the curing conditions on the mechanical properties of HFC, three-point bending and uniaxial compression tests were carried out with specimens cured under different conditions, e.g. under water and room climate ( $T = 20\text{-}25^\circ\text{C}$  and  $\text{RH} = 50\text{-}60\%$ ) (see Stähli & van Mier [2007a]). One day after casting all but three of the 50/50/200 prisms were laid into a box filled with water for curing. At 1, 4 and 7 days before testing, three specimens were taken from the box and placed into the testing room. Finally after 28 days, standard 3 point bending tests and uniaxial compression tests were carried out on specimens that were cured under water for 28, 27, 24 and for 21 days and specimens that were cured in room climate only. This series gave insight in how to condition HFC samples before testing.

Figure 5.31 shows the results from the tests on specimens that were cured under different conditions, namely varying between 28 days under water storage until 0 days under water as described above. It can be seen that the flexural and compressive strength reach the lowest value when the specimens are taken out of the water 1 day before testing. The maximum values of flexural and compressive strength are reached when the specimens were taken out of the water 1 week before testing. Figure 5.31 also shows that there are no great differences between only water and only climate room curing. In those cases no important moisture gradient, and likely related to that, strain gradient developed within the specimens.

Figure 5.31 clearly shows that HFC is influenced by the curing conditions and the way specimens are stored before testing. The results also show that flexural and compressive strength are influenced by curing in the same manner. The obvious reason for the strength decrease after one or more days of exposure to laboratory conditions seems to be caused by differential drying shrinkage over the specimen cross-section. Shrinkage deformations are larger along the surface of the specimen than in the central parts where the material is still saturated. As a result, tensile eigen-stresses develop at the specimen surface and compressive stresses in the core. The net-effect is a decrease of strength, which is largest when the eigen-stress gradients are largest, i.e. after 1 day of drying. Similar behaviour is known for plain concrete, see

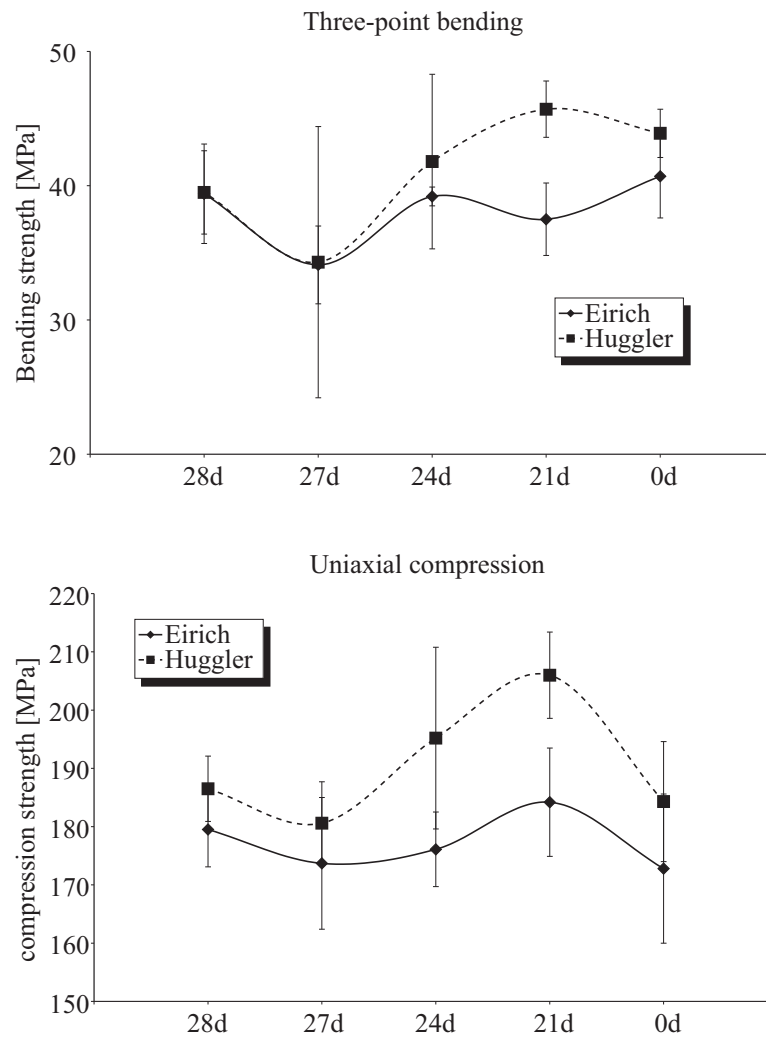


Figure 5.31: Flexural strength and compressive strength for specimens kept under water for different time intervals. After the indicated time of under water storage specimens were always placed in laboratory environment of  $\pm 50\%$  RH and  $T = 20^\circ\text{C}$ .

e.g. Bonzel & Kadlecek [1970]. Note that drying shrinkage can be the cause of substantial cracking in materials with high cement content, like the HFC used here. Drying shrinkage tests on model concrete by Bisschop & van Mier [2002] showed severe damage. These concretes contained up to  $1000 \text{ kg/m}^3$  cement as well.

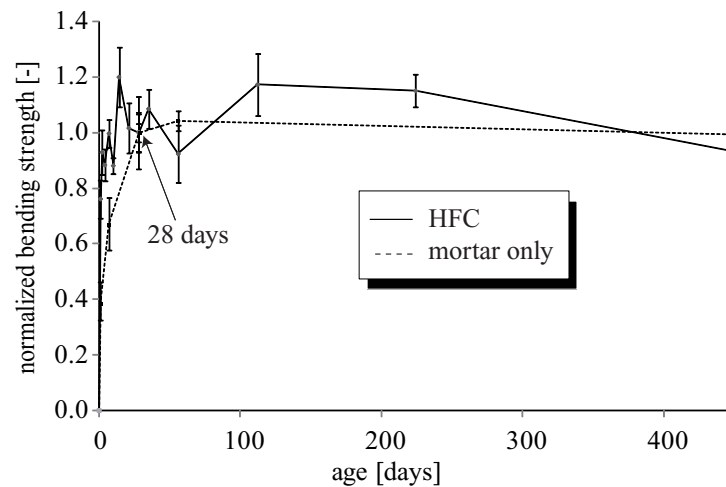


Figure 5.32: Development of bending strength in time (up to 448 days)

In order to analyze the strength development of HFC, experiments were performed over 448 days. Specimens out of three batches with fibres and one batch without any fibres were cast. After casting the specimens were stored in the climate chamber ( $T = 20^\circ\text{C}$  and  $\text{RH} = 95\%$ ) until they were tested. The mechanical properties of the HFC mixtures were determined after 1, 2, 4, 7, 10, 14, 21, 28, 35, 56, 112, 224 and 448 days and the mortar mixture after 1, 7, 28, 56 and 448 days. The results of the different time-series were normalized by the value of the bending strength after 28 days. Figure 5.32 shows the results for HFC and mortar. For each time-step 6 specimens were tested. The mortar shows a typical strength development in time. In contrast, the HFC mixture has a rapid strength increase in the first 14 days. After a loss of strength at 28 days the value increases to a maximum at 112 days and afterwards slightly decreases below the 28 days value. Such a decrease can be caused by corrosion effects of the fibres at the surface of the specimens. This suspicion arises as all the specimens were stored at a relative humidity of 95%. Such a huge relative humidity leads to corrosion of the steel fibre at the surface. Hence they lose bond capacity and the bending strength decreases.



### 5.5.3 "Fibre-to-fibre" series - rheological and mechanical tests

In Section 3.3.1 the rheological properties of the fibre-to-fibre (f-t-f) series were already introduced and discussed. In this section the mechanical properties will be presented and carefully analyzed. The mechanical properties were determined by performing bending tests, standard Young's modulus and standard compression tests (see Appendix A). Pendulum-bar four-point bending tests using small ( $70/70/280 \text{ mm}^3$ ) and large ( $120/150/600 \text{ mm}^3$ ) prisms were carried out. The bending test results showed that the more small fibres were used, the larger was the maximum bending strength. The results show that there is a significant size effect between the small  $70/70/280 \text{ mm}^3$  and the larger  $120/150/600 \text{ mm}^3$  HFC prisms similar to the previous discussed series in Section 5.5.1.

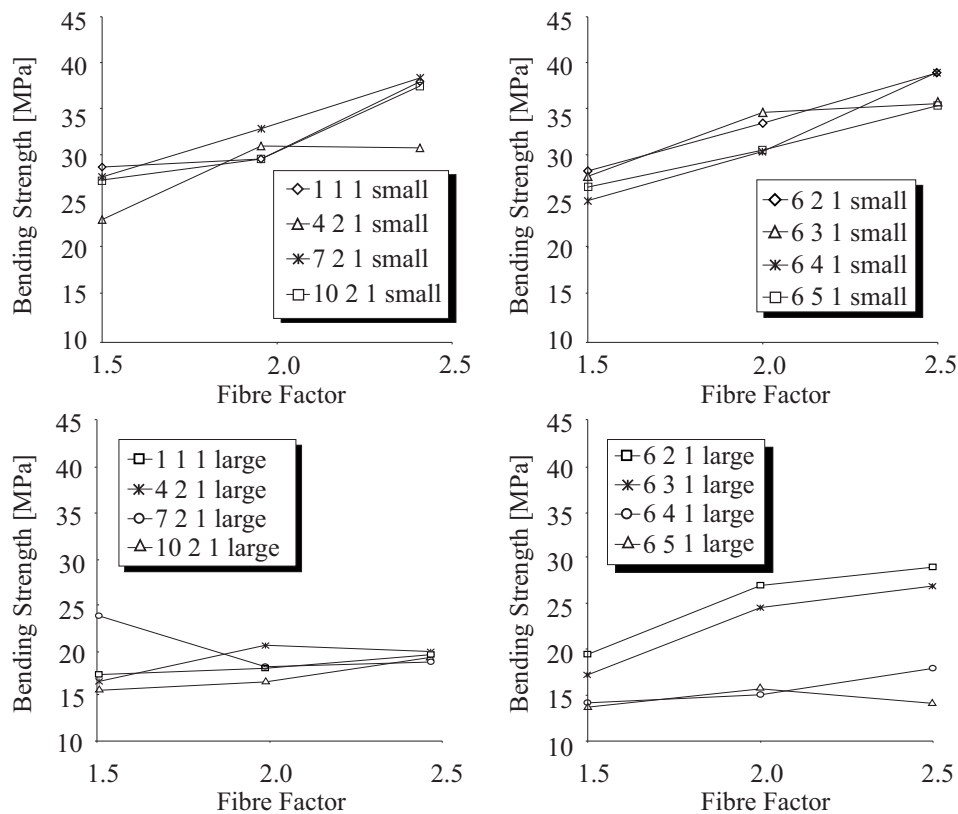
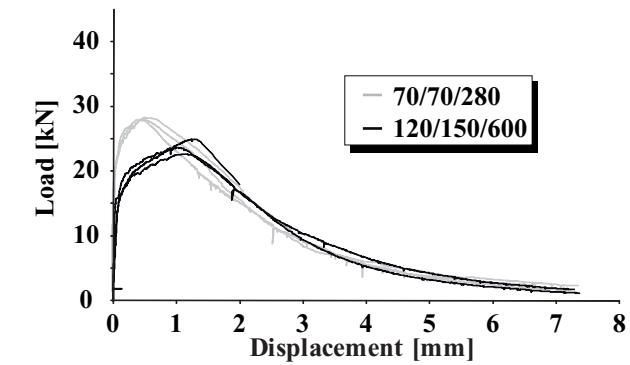


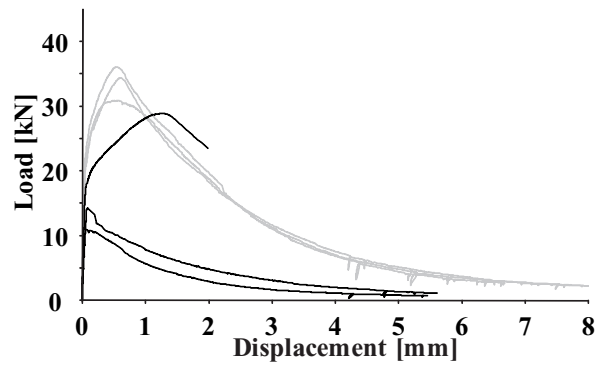
Figure 5.33: Overview of the bending results for the f-t-f series

Table 5.2: Overview of the mechanical properties of the f-t-f series

Fibre-to-Fibre	$F_{fib}$	$f_b$	$f_b$	$f_c$
		70/70/280 [MPa]	120/150/600 [MPa]	[MPa]
1:1:1	1.5	29.3	17.2	143
	2.0	30.3	17.9	150
	2.5	39.4	19.4	148
4:2:1	1.5	23.1	16.4	140
	2.0	31.8	20.5	135
	2.5	31.6	19.8	136
7:2:1	1.5	28.1	23.7	128
	2.0	33.9	18.1	139
	2.5	40.0	18.7	142
10:2:1	1.5	27.8	15.4	134
	2.0	30.3	16.4	142
	2.5	38.9	19.1	138
6:2:1	1.5	28.2	19.4	131
	2.0	33.4	26.9	140
	2.5	38.9	28.9	132
6:3:1	1.5	27.6	17.2	130
	2.0	34.6	24.5	121
	2.5	35.6	26.9	126
6:4:1	1.5	25.0	14.2	140
	2.0	30.4	15.0	125
	2.5	39.0	17.9	125
6:5:1	1.5	26.4	13.7	131
	2.0	30.5	15.7	129
	2.5	35.4	14.1	135



(a) 2.35% 0.67% 0.34%



(b) 3.1% 0.89% 0.44%

Figure 5.34: Comparison between strain hardening and softening. (a): mixture 2.35% 0.67% 0.4% where the large specimens showed strain hardening, (b) mixture 3.1% 0.89% 0.44% where only one large specimen showed strain hardening, the two others showed strain softening

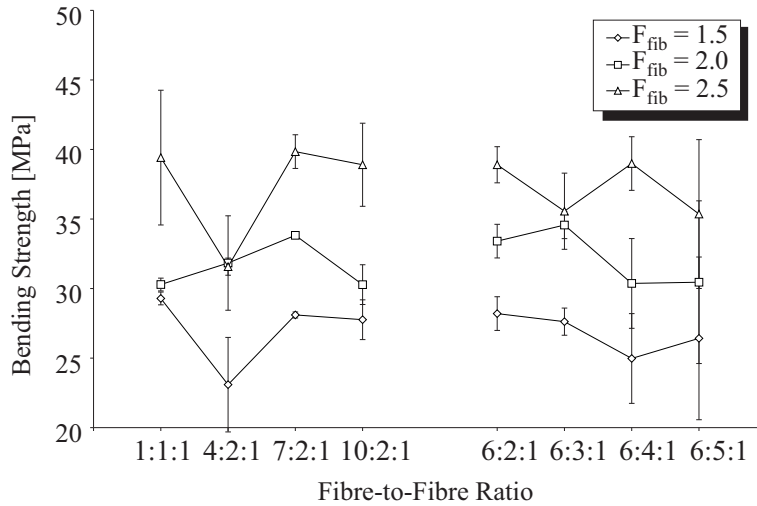


Figure 5.35: Fibre-to-Fibre ratio vs bending strength diagram

Table 5.2 shows an overview of the test results. Two series were examined. In a first series the ratio of the small fibres was increased while the ratio of the large ones was kept constant and the rate of the middle fibre was 2 except for the 1:1:1 series, there the rate was 1. In a second series the rate of the small and the large fibres was kept constant (6 and 1 respectively) and the rate of the middle fibre was increased. These two series covered the whole range of possible fibre mixtures with a minimum amount of 3% of fibres and a fibre-to-fibre ratio with a larger amount of small fibres than larger fibres. For all mixtures the Young's Modulus was about 40 GPa. Table 5.2 shows that the compressive strength did not vary with the different fibre mixtures; no significant trend is apparent. Figure 5.33 shows results derived from the pendulum-bar four-point bending test. A clear increase of the bending strength with an increase of the fibre factor was observed for small and large specimens and both 'ratio' series. Only the large specimen of the  $F_{fib} = 1.5$  and f-t-f = 7:2:1 behaves differently. This may be caused by the fact that the filling procedure of the large beams was tricky to hold constant for all specimens. Therefore, the alignment of the fibres and the fibre distribution could change in an un-controllable way and influence the results. In the outlier results, fibres were likely aligned at the bottom and the walls of the specimen due to the filling process. In comparison to the other results all beams of this series showed ductile strain hardening behaviour because the fibres were well aligned at the bottom of the specimens due to

segregation effects and/or wall effects. An example of two series, where the large specimens showed deflection hardening (2.35% 0.67% 0.4%) and where the large specimens showed deflection softening (3.1% 0.89% 0.44%) is given in Figure 5.34. The displacement is the average reading of the two CMOD sensors and the tests were stopped when one of the sensors lost its signal. The small 70/70/280 mm<sup>3</sup> prisms always showed deflection hardening. This can be explained from the higher wall to volume ratio leading to a higher influence of the aligned fibres along the walls and the bottom of the specimens.

Figure 5.35 shows a summary of the pendulum-bar four-point bending test-results of the small 70/70/280 mm<sup>3</sup> specimens. The range of the standard deviation is marked. It seems that this standard deviation decreases with the increase of the ratio of the small fibres and increases with the ratio of the middle fibres, which is the same. With the increase of the ratio of the middle fibres the amount of small fibres decreases relatively to the amount of the middle fibres. Therefore, it can be said that the standard deviation decreases with an increase of the ratio of the small fibres for the small 70/70/280 mm<sup>3</sup> specimens. With the increase of the small fibres the distribution is more homogenous and the fibre spacing is smaller. The probability of having a region with less fibres is smaller, hence the scatter is smaller as well. With the increase of the ratio of the small fibres the bending strength also increases slightly. On the right side of the diagram the bending strength decreases with the increase of the ratio of the middle fibre. Again, with a decrease of the ratio of the middle fibre the amount of small fibres increases and a conclusion can be drawn as follows: the bending strength increases with an increase of the amount of small fibres. The middle and the large fibres do not influence the maximum bending strength significantly. An important fact is that the number of small fibres is enormous. The number of fibres per liter were calculated in Stähli & van Mier [2007c]. One liter HFC with 1% of each fibre contains 94'314, 26'526 and 1'105 of the small, middle and large fibres respectively.

#### 5.5.4 Moulded or cut tensile specimens

In order to investigate wall effect Looser & Tatti [2006] performed tensile tests on moulded and cut specimens. Three 300 liter batches were produced. The mixture contained 3.5%, 1.5% and 1% of the small, middle and large fibres respectively. Besides cylinders, cubes and beams, six dog-bone shaped specimens and three blocks from which dog-bone shaped specimens were cut out (Figure 5.36 and 5.37), were cast. The specimens were cast under 45° so that the concrete could flow into the mould (Figure 5.36a). The values of the slump flows,  $s_{sf}$  were in the range of 14 to 19 cm and the compressive

strength,  $f_c$  was about 135 MPa.

One day after casting the bays in the neck region of the cut specimens were cut out using a large  $\phi 400$  mm core driller (see Figure 5.36b). Afterwards the final shape was cut out and the specimens were stored in the climate chamber ( $T = 20^\circ\text{C}$ ,  $\text{RH} = 95\%$ ). Two days before testing the aluminium plates were glued to the specimens and 28 days after casting the specimens were tested using the pendulum-bar tensile test set-up.

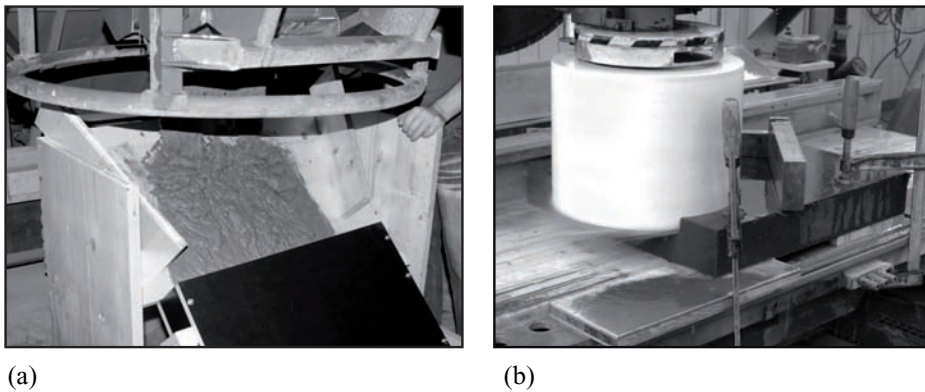


Figure 5.36: Images of the production process of the cut specimens: (a) casting under 45 degrees and (b) coring of the dog-bone shaped specimens

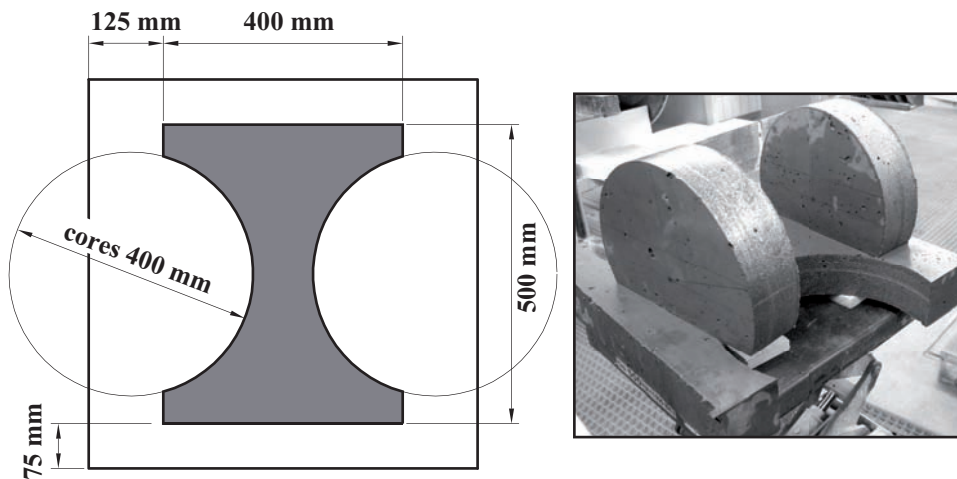


Figure 5.37: Scheme and image of the final cut specimen

Table 5.3 shows the results of this series of experiments. A clear difference between the tensile strength of moulded and cut specimens can be seen.

Table 5.3: Overview of the results from the moulded and cut tensile specimens including the location of the crack

Name	$f_{t \text{ nom}}$ [MPa]	$f_{t \text{ real}}$ [MPa]	crack location <sup>a</sup>
Batch 1 spec I <sup>a</sup>	15.23	6.12	outside
Batch 1 spec II	7.66	7.51	inside
Batch 1 spec III	12.50	8.16	outside
Batch 3 spec I	12.42	7.37	outside
Batch 3 spec II	10.70	10.24	inside
Batch 3 spec III	12.47	12.47	inside
<b>Average moulded</b>	<b>11.83</b>	<b>8.65</b>	
Batch 1 0°	4.00	4.05	inside
Batch 2 0°	5.36	5.36	inside
Batch 3 0°	3.60	3.40	inside
<b>Average cut</b>	<b>4.32</b>	<b>4.27</b>	

<sup>a</sup> inside or outside the LVDT's

<sup>b</sup> Batch 1, mould specimen I

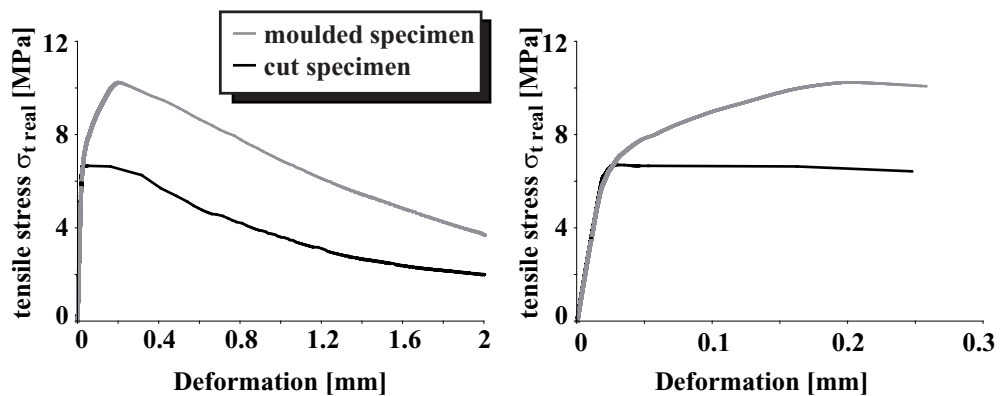


Figure 5.38: Deformation vs tensile stress curves for moulded and cut specimens

The difference (factor 2 to 3) can be explained as follows. First there is the wall effect which influences the fibre alignment significantly. Where the fibres align along the curved bays of the mould in the mould specimens, the fibres along the curvature in the cut specimens are less orientated. Furthermore, in the moulded specimen the flow of the material accelerates towards the neck of the dog-bone mould and the fibres align due to a large velocity gradient (Custer [2006]) while in the mould of the cut specimen the material has almost a constant velocity over the height and the width of the mould. This leads to the conclusion that the mould influences the fibre alignment not only because of wall effects, but also because of interactions between the mould shape and the viscosity of the material, which influences the flow of the material in the mould while casting.

An example of the resulting tensile stress-deformation curve of a moulded and a cut specimen is given in Figure 5.38. The characteristics of the the curves differ (i) in the maximum tensile strength and (ii) the pre-peak regime. The moulded specimen shows strain-hardening and the cut less strain-hardening ('strain-softening'). Note that the material was the same; only the preparation method of the specimens was different. Again, this shows that test results are dependent on the geometry of the mould and the manufacturing method. In Chapter 6 a third factor, the filling method, will be added which also influences the test results significantly.

### 5.5.5 Crack pattern development and analysis

In order to investigate the influence of the different fibres on the crack pattern a series of experiments with SFCs and HFC containing different fibres was performed. Crack patterns of different loading stages, using single and hybrid fibre concretes were analyzed. Table 5.4 gives an overview of the mixtures and the mechanical properties. The crack patterns were analyzed at four selected stages in the load-displacement diagram (see Figure 5.39), namely (A) right after the elastic stage, (B) in the non-linear regime before the peak, (C) at the peak and (D) in the post peak regime right after the peak (Figure 5.39). Figure 5.39(b) shows the average load displacement diagrams of the four mixtures. Clear differences in the characteristics of the different mixtures can be distinguished. The mixture with the small fibres only (3% 0% 0%) shows the least ductile behaviour while the mixture with the large fibres only (0% 0% 3%) shows the most ductile behaviour but the smallest bending strength. A strongly developed deflection hardening and a relatively high bending strength were observed for the 0% 3% 0% mixture. The evaluation of the crack pattern showed that mixture 0% 3% 0% has the smallest crack-spacings. This might be a reason for the strongly developed



strain hardening and the high bending strength.

The resulting load-displacement diagrams derived from the impregnated specimens and all the crack patterns are given in Appendix B.

Table 5.4: Overview of mechanical properties of the material used to determine the crack development

Mixture description	$f_b$ [MPa]	$f_{b\ 3pt}$ [MPa]	$f_c$ [MPa]	$f_{cc}$ [MPa]	E [GPa]
3% 0% 0%	23.3	26.8	122	160	36.6
0% 3% 0%	25.2	31.4	124	152	36.0
0% 0% 3%	19.8	21.4	120	145	38.3
1.5% 1.5% 1.5%	34.2	37.3	143	172	42.0

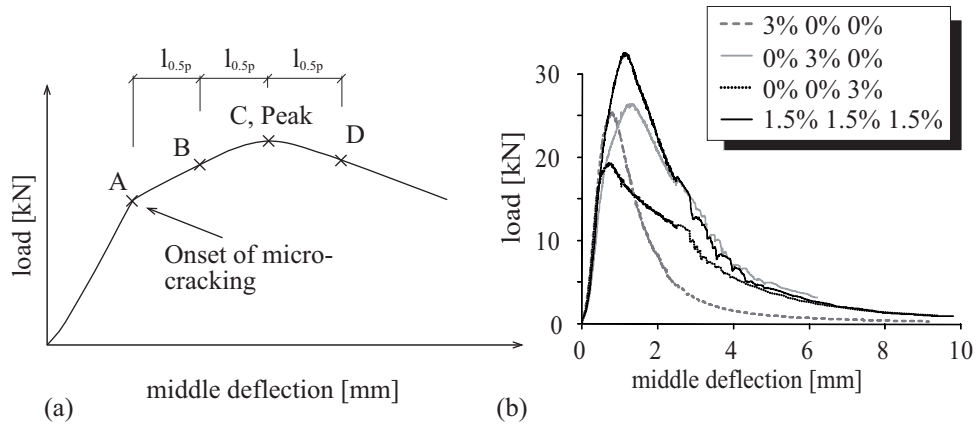


Figure 5.39: (a): Desired load stages on the load-deflection curve and (b) the measured load-displacement diagrams for the four tested mixtures. The curves are average curves out of four four-point bending tests on the Walter & Bai test machine.

Figure 5.40 shows an example of a crack pattern. The image is a binary image which was prepared using image filters. A threshold was set in such a way that the impregnated epoxy was black and the matrix, including the fibres were white. This pattern shows that the crack path is a connection between air pores. A detailed image of the influence of a fibre to the crack path is shown in Figure 5.41. Both images show that the crack direction is hardly influenced by the fibre but obviously the fibre bridges the crack.

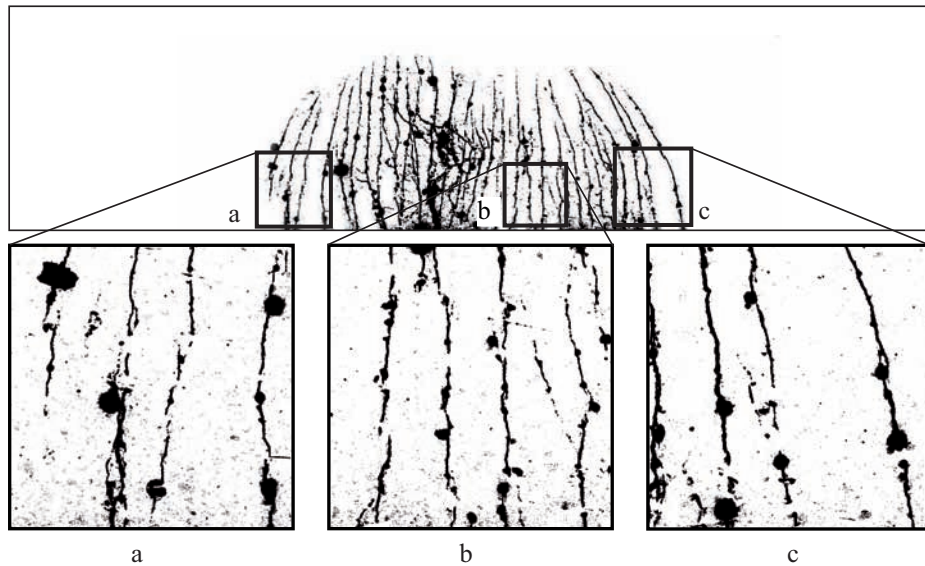


Figure 5.40: Example of a crack pattern. This pattern was observed at loading stage C on a 0% 3% 0% specimen. Detail images (a to c) shows an enlargement of the crack pattern at three different locations

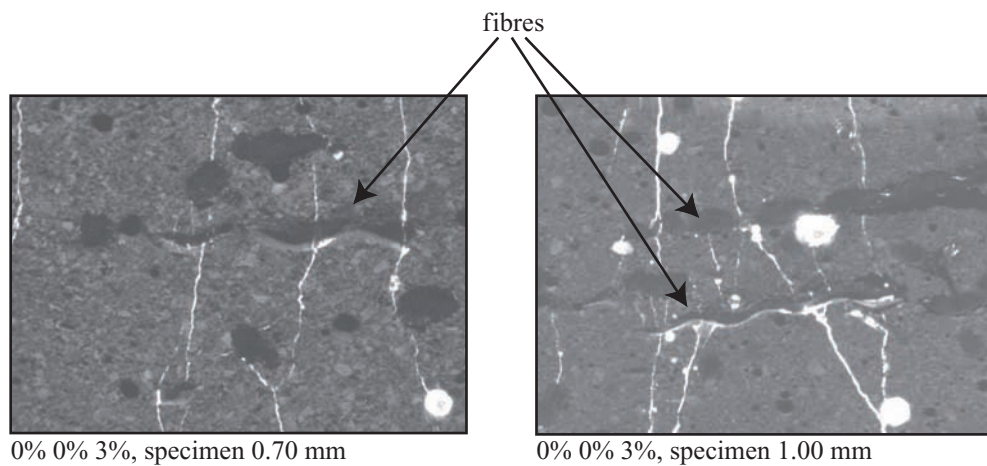


Figure 5.41: Examples of grey-scale images of the crack path close and along large fibres. The images are from (left) load stage C and (right) load stage D. The corrugated Stratec fibres can easily be recognized.

It can also be seen that on the left image of Figure 5.41 the fibre starts to debond while on the right image the pull out of the fibre has already started. This is indicated by the epoxy which flowed along the fibre. This is only possible if the bond between fibre and matrix is released and a hollow space exists.

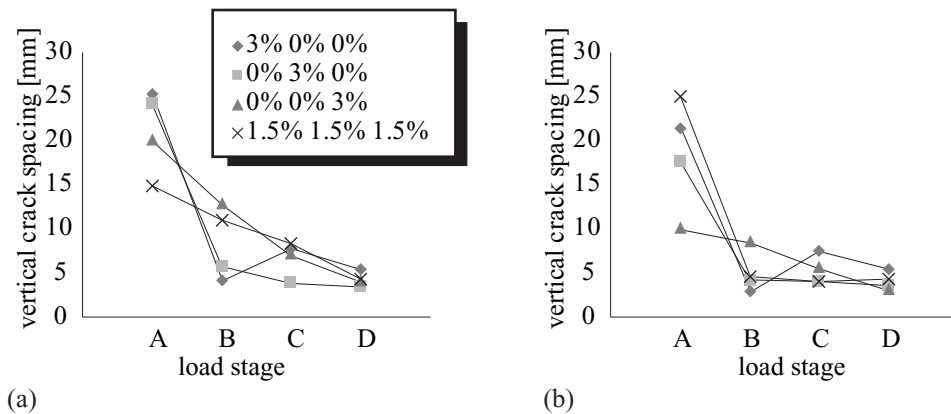


Figure 5.42: Load stage vs vertical crack-spacing diagrams. (a): average crack-spacing over the hole specimen, (b): crack-spacing at the bottom of the specimen

The final result is shown in Figure 5.42. The elements in the diagram represent the average crack spacing (a) over the whole specimen height and (b) at the bottom of the specimen. Each data point represents the average out of two specimens. The crack spacing clearly decreases from load stage A to D. It is also interesting that the average crack spacing for all fibres and even for HFC is not so different. It can be concluded that the crack spacing does not depend on the fibre type. Figure 5.42b shows the diagram of the average crack spacing at the bottom of the specimen for the different load stages and fibre mixtures. At stage A only few cracks were observed and the standard deviation of the crack spacing exceeded the value of the average crack spacing. However the results for the other load stages showed again that the crack spacing is not dependent on the fibres. The number of cracks at the bottom of the specimen increases with the increase of the load even if some of the cracks close after the peak (see Figure 5.44). In Figure 5.39 the load displacement curves are given. Comparing these curves with the results from the crack pattern analysis the following conclusions can be drawn: The more cracks develop the more ductile and cohesive a material is. On the other hand ductility and strength can be controlled individually by the fibre type, fibre mixture and the amount of fibres.

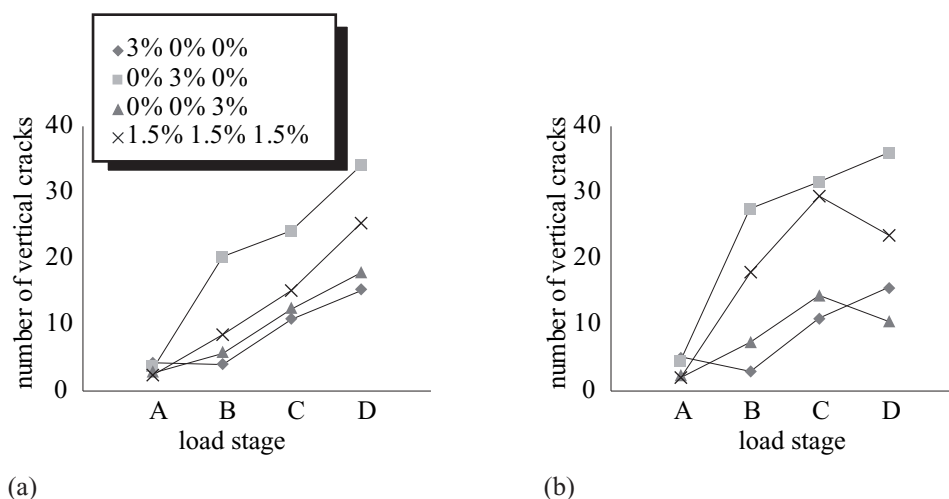


Figure 5.43: Load stage vs number of vertical cracks. (a): average number of cracks in the entire specimens, (b): number of cracks at the bottom of the specimens

Using the results from the crack spacing, the number of cracks can also be determined (the crack spacing is in between two cracks). Figure 5.43 shows the result for (a) the whole specimen and (b) for the bottom of the specimens. A clear increase of cracks with the loading stage can be observed for the average over the whole specimen for all load stages and at the bottom part of the specimen for load stage A to C. The increase is more pronounced for the average number of cracks over the whole specimen than for the bottom part only. However for the HFC mixture and less pronounced for the FRC mixtures a decrease in between load stage C (peak load) and load stage D can be observed. That means that the cracks at the bottom of the specimens disappear but looking at the whole specimens in total more cracks form. The crack patterns showed that after the peak a macro-crack formed. Due to this macro-crack, the load could not be transferred in the horizontal direction at the bottom of the specimen anymore. Consequently, micro-cracks close (through the elasticity of the fibres which restrained the crack) and could not be impregnated by the epoxy resin. As a result the micro-cracks disappear from the images, which does not mean that there are no cracks but they have become invisible for the used impregnation technique.

Horizontal cracks were also characterized by the same technique as the vertical cracks were determined. These horizontal cracks give information about branching and the deviation of the crack. The higher the number of such cracks, the more energy was necessary to fracture the specimen. The

ratio  $\beta$  between the number of vertical cracks and horizontal cracks was determined (see Equation 5.8). Table 5.5 and Figure 5.44 gives an overview of the results.

$$\beta = \frac{\text{number of vertical cracks}}{\text{number of horizontal cracks}} \quad (5.8)$$

Table 5.5: Number of vertical and horizontal cracks

Name	$f_b$	vertical crack at peak load	horizontal crack at peak load	$\beta$
3% 0% 0%	23.29	11.00	2.67	4.13
0% 3% 0%	25.17	24.08	4.56	5.28
0% 0% 3%	19.78	12.67	3.98	3.19
1.5% 1.5% 1.5%	34.24	15.17	3.41	4.44

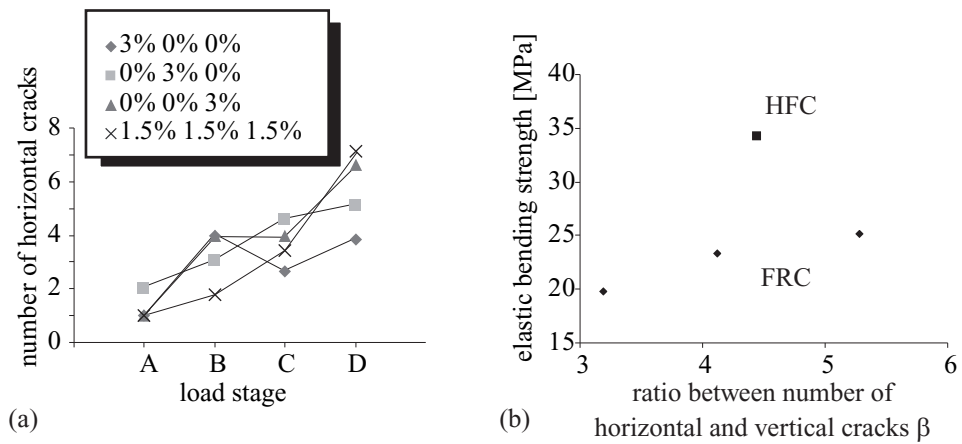


Figure 5.44: Load stage vs number of horizontal cracks. (a): Load stage vs number of horizontal cracks, (b): relation between bending strength and  $\beta$

Figure 5.44a clearly shows that the number of horizontal cracks increases with the loading stages for both HFC and FRC mixtures. Comparing these results with the mechanical properties of the materials the HFC mixtures stand out significantly in comparison to the FRC mixtures (Figure 5.44b). Again, the results represents only the impregnated cracks. Possibly the cracks

in the HFC specimens were thinner and therefore not visible. But it could also mean that the capacity of HFC mixtures to form cracks, is higher in comparison to FRC mixtures.

## 5.6 Conclusions

- Cutting part of a specimen close to the mould wall leads to a decrease in flexural strength. This decrease maybe caused by the fact, that at the walls the fibres are more or less perfectly aligned in the direction with the most tensile stress during a bending test.
- There is a large difference in the results of the bending test of small  $70/70/280 \text{ mm}^3$  and large  $120/150/600 \text{ mm}^3$  prisms. This size effect can possibly be explained by the fact that smaller specimens have a bigger specific surface and thus the surface regions where fibres are aligned have more influence.
- There is no significant difference in the results of the mechanical tests for the two mixers used, i.e. the influence of the mixing system does not significantly influence the mechanical properties of HFC.
- The storage conditions of specimens right before testing influences the test results significantly. The maximum drop in the maximum bending strength was found when the specimens were tested one day after taking them out of the climate chamber. Therefore the specimens should remain at the same curing conditions as long as possible. The optimum would be if the tests could be performed in the same climate as during the curing of the specimens. The same statement is valid for practical applications. The structures or structural elements should be cured as long as possible in a controlled environment, preferably in a climate chamber. This is only possible for relatively small elements which can/will be produced and stored in a prefabrication plant.
- The bending strength increases with an increase of the amount of small fibres. The middle and the large fibres do not influence the maximum bending strength significantly.
- Test results are dependent on the shape/geometry of the mould and the preparation (mould/cut) of the specimen.
- The crack spacing is not dependent on the fibre type. A similar average crack spacing was observed for the non-elastic part of the load displacement diagram for all tested mixtures.
- The images of the impregnated specimens showed that cracks in HFC are never straight. Branching and bridging were observed. It was also observed that HFC can show multiple cracking until, at peak, all the deformations localize into a single crack.

# Chapter 6

## Flow and mechanical properties

### 6.1 Introduction

The main topic of this work was to investigate the influence of the rheology on the fibre distribution and the resulting mechanical properties. Rosenbusch [2004], Ferrara et al. [2004] and Ozyurt et al. [2007] already investigated the fibre distribution, the fibre orientation and or their influence on the mechanical properties.

This Chapter combines the results of the previous chapters. Rheological properties, fibre orientations and the mechanical properties were determined on the same specimens (Custer [2006] series) or on material of the same concrete batch using different filling methods. SFC and HFC mixes were analyzed by means of CT-scanning, manual counting, pendulum-bar four-point/tensile tests and ordinary mechanical tests.

### 6.2 Test series

#### 6.2.1 U-shaped specimen series

An interesting idea is to investigate to what extent the flow properties of the fresh material can be used to affect the fibre distribution and orientation, and to see if a possible influence on the mechanical properties emerges.

With that goal in mind, two different series of experiments were performed using a U-shaped mould. The first series (see Hafner [2005]) contained mixtures which differed in the w/b ratio only. The mixtures were cast, the fibre distribution was analyzed and the mechanical properties were determined. The fibre content was 3% of small fibres and 1% of both, the middle and the



large fibres. The amount of super-plasticizer was kept constant at 2%. A second series where the  $w/b$ -ratio was kept constant and the amount of super-plasticizer varied from 1.8%, 2.0% to 2.2% was carried out (see Custer [2006], Stähli et al. [2008]). Because of available techniques to determine the fibre orientation and fibre distribution (namely CT-scan combined with manual counting), relatively large fibres were used (Figure 2.11). Such large fibres have the advantage that they can be detected by means of medical computer tomography with a resolution of 0.4 mm. Moreover, because of their size large fibres can also be easily counted manually. The three different mixtures contained 3% of these large straight notched fibres.

### 6.2.1.1 Varying the $w/b$ -ratio

The influence of the  $w/b$ -ratio on the fibre orientation and resulting mechanical properties were investigated by Hafner [2005]. U-shaped specimens with concretes of different  $w/b$ -ratios (0.17, 0.18 and 0.20) were cast and analyzed. The specimens were prepared as follows: One day after casting the bending prisms A to C were cut out of the U-shaped specimen and stored in the climate chamber waiting for further experiments. The fibre distribution was analyzed in the cut offs (top filling part, the edges and the top climbing part). Figure 6.1 shows an image of the cut offs and a graph of the fibre distribution. This example, where the  $w/b$ -ratio was 0.20, shows some segregation in the climbing branch (lower left corner of Figure 6.1b).

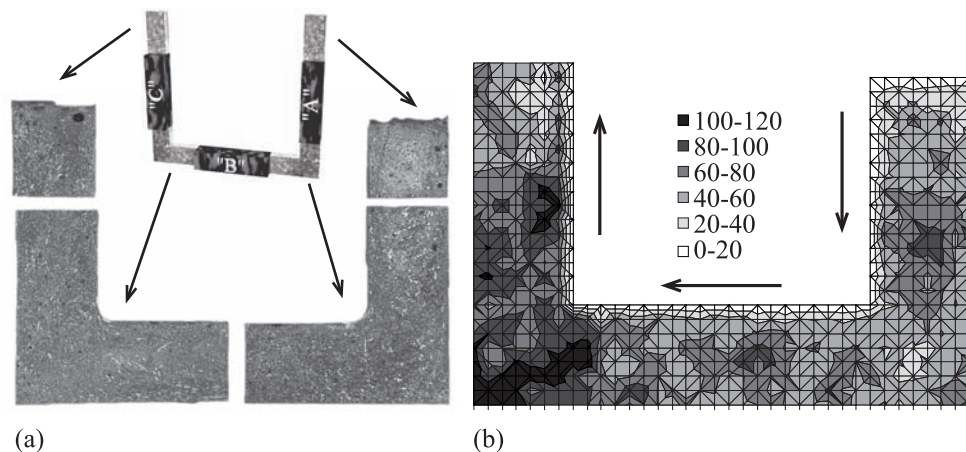


Figure 6.1: (a): image of the cut offs; (b): counted fibre distribution. The arrows in (b) show the flow direction of the concrete

An overview of the results is given in Table 6.1. It can be seen that the fibres align with the distance of the flow and with increasing w/b-ratio which corresponds the flowability of the material. The number of fibres of the top climb section for w/b = 0.20 is very low due to segregation of the fibres.

Table 6.1: Average number of counted fibres per  $1\text{cm}^2$

w/b-ratio	0.17	0.18	0.20
top fill ("A")	84.00	68.90	49.79
top climb ("C")	64.59	73.07	41.06

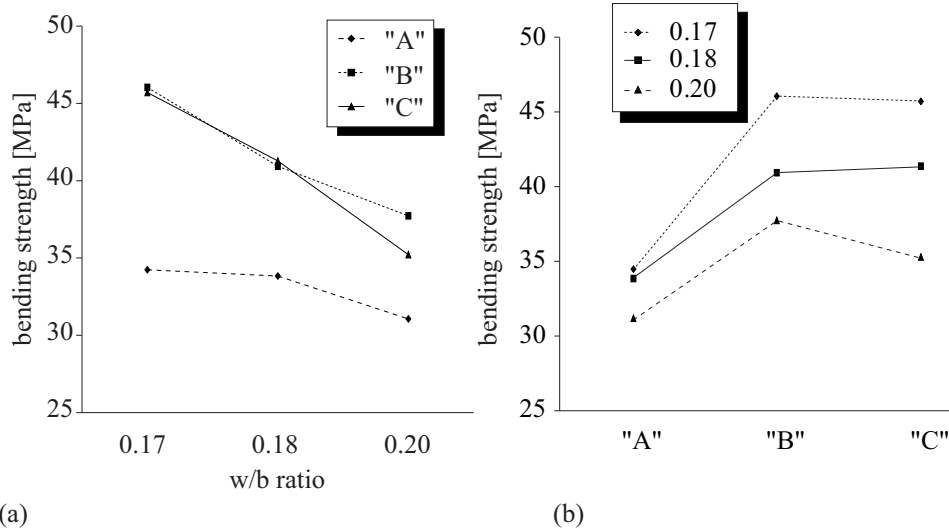


Figure 6.2: Results by Hafner [2005]. Each point represents an average value out of four tests.

Figure 6.2 shows the final result of the Hafner [2005] series. A clear trend of a decreasing bending strength with an increasing w/b-ratio can be observed, which was expected. The most important point concluding from Figure 6.2 is the relatively large increase of strength between the "A" and the "B" prisms while the bending strength was more or less constant between the "B" and the "C" prisms; note: the material was the same, the only difference was the flow distance and the direction of the flow and therefore the resulting fibre alignment. Hafner [2005] showed that only due to material flow and flow

direction the mechanical properties can be influenced significantly. The effect of segregation can nicely be seen in Figure 6.2b. The bending strength of the mixture with  $w/b = 0.20$  drops from prism "B" to "C" while the bending strength for the mixtures  $w/b = 0.17$  and  $w/b = 0.18$  remain constant or increase slightly.

### 6.2.1.2 Varying the amount of super-plasticizer (SP)

The influence of the flowability due to fibre orientation and the resulting mechanical properties were investigated in collaboration with Custer [2006]. Three different viscous concretes were produced using three different amounts of super-plasticizer (1.8%, 2.0% and 2.2%). U-shaped specimens were cast all containing 3% of large fibres. The specimens were prepared as follows: One day after casting the specimens "A" to "C" were cut out of the U-shaped specimen and scanned in the computer tomograph (Siemens SOMATOM Sensation 64) of the University hospital of Zürich. Detailed information about data acquisition and processing are described in Man & van Mier [2008]. In order to compare the fibre distribution in the specimens, two different sections were analyzed: a cross-section and a longitudinal section as shown in Figure 6.3. The images of the longitudinal section showed how the fibres were aligned in the specimen and the cross-section could be taken to confirm the results from the longitudinal section, i.e. the more the fibres are aligned with the flow the less fibres can be seen/counted in the longitudinal section and the more in the cross-section see Stähli & van Mier [2007a]. The longitudinal section also gave an idea about the flow profile of the fresh concrete.

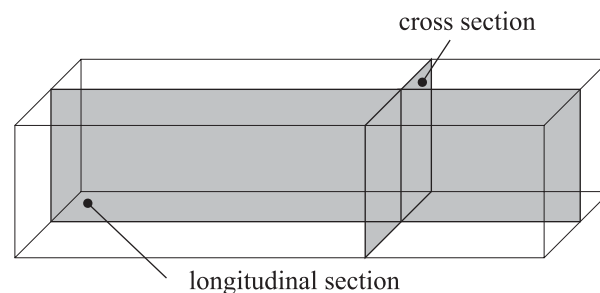


Figure 6.3: Nomenclature for the different cross-sections

Figure 6.4 shows two longitudinal sections of the "C" prism (rising branch) from mixture 2 (2.0%), one section of the centre of the prism (top image) and one of the areas near the wall (bottom image). This figure clearly shows that

fibres align with the flow of the concrete. It can also be seen that the faster the concrete flows (center part of Figure 6.4a) the better the fibres align. Moreover, it appears that the flow velocity is not constant over the whole cross-section because the fibres are not aligned over the whole area. In the centre the flow is faster than near the walls, which is typical for a material like fresh concrete (Tattersall & Banfill [1983]). What remains, however, is the question about the shape of the flow profile. A flow profile can be deduced from the image of the longitudinal section near the mould/wall (Figure 6.4b). A possible model is given later and will be discussed further-on. A comparison of the fibre distribution and alignment between the different mixtures can be made by comparing images of centre longitudinal sections of "B" prisms (horizontal branch). Figure 6.5 shows such an image of a centre longitudinal section for each mixture. The top of each image corresponds to the top surface of prism "B" during casting and hardening. In mixture 1 (1.8%) the fibre alignment and distribution is similar to the one from Figure 6.4 (i.e. wall longitudinal section), which leads to the assumption that flow profiles for both mixtures (1.8% and 2.0%) in longitudinal sections are equal.

Figure 6.5 also shows that the better the concrete flows the more the fibres align. In mixture 1 (1.8%), with a small slump flow of 16 cm, hardly any fibre alignment can be observed, while in mixtures 2 (2.0%) and 3 (2.2%) (with 20 and 22.5 cm slump flow diameter, respectively), the fibres were nicely aligned in the direction of concrete flow. Another phenomenon that can be observed is the fibre segregation in mixture 3 (2.2%). Segregation can have a negative effect in constructions where a constant tensile stress over the whole cross-section is expected. However, a positive effect could also emerge, for example, in a flexural beam with the majority of fibres aligned along the tensile stressed part of the beam.

The total number of fibres in four different cross-sections of each prism were counted and investigated. Figure 6.6 shows the location of the four analyzed cross-sections. Two cross-sections in the middle of the prism and one at each end of the prism (in-flow and out-flow) were analyzed and the results are presented in Figure 6.7. For quantitative assessment of the fibre alignment the total number of fibres in a cross-section was determined. The more fibres that can be counted in a cross-section the better the fibres are aligned, under the assumption that fibres are uniformly distributed. If the fibres are perpendicular to the cross-section, and uniformly distributed, most fibres can be counted; if the fibres are parallel to the cross-section, and uniformly distributed, least fibres can be counted (Stähli & van Mier [2007a]). The variation of the numbers of fibres per cross-section in the prisms is shown in Figure 6.7. It can be seen that the different cross sections have different

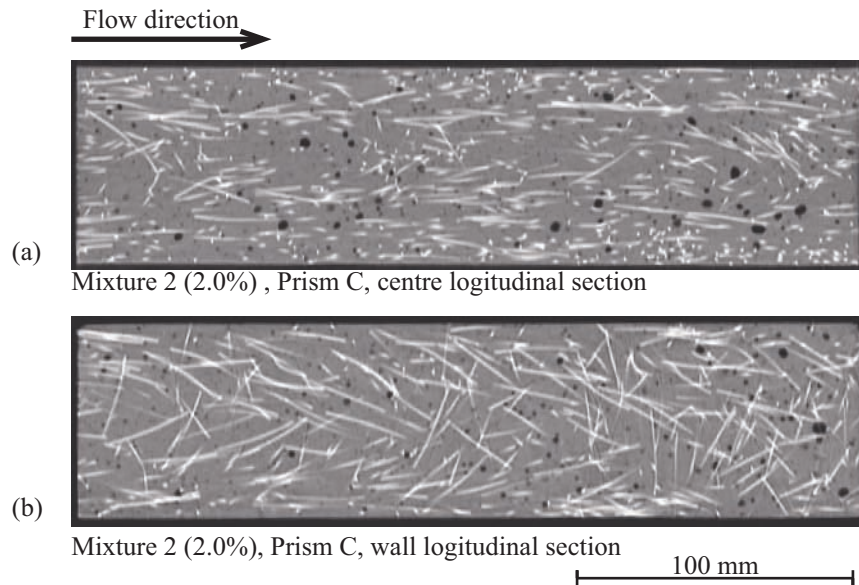


Figure 6.4: Longitudinal sections of the centre of a specimen (a) and a section close to the mould (b).

total numbers of fibres but the progress of the number of fibres in the prisms is more or less constant. Figure 6.7 shows that the progress of the counted fibres in the "A" prisms increases from the 'in-flow' to the 'out-flow', which means that the alignment of the fibres increases with the flow distance. The total fibres-count also increases with the flowability of the fresh concrete. By comparing the "A" prisms of the three mixtures, mixture 1 shows least fibres and mixture 3 (2.2%) has most fibres, or in different words less viscous concretes have an improved fibre alignment. The "B" and "C" columns show that the total fibres-count in mixture 3 (2.2%) decreases due to fibre segregation. Figure 6.7 also shows that for the "B" prisms the number of fibres per cross-section is well balanced while for the "A" and "C" prisms an increase or decrease, respectively can be observed. In the "B" prisms the flow was horizontal. During the filling process this branch was filled the way Markovic [2006] proposed how to cast HFC. He recommended to cast HFC layer wise to optimize the fibre orientation. Therefore the fibres are orientated equally over the hole length of the specimen. Figure 6.8 shows images of the casting sequence of a low viscous HFC. The concrete viscosity is thus an important parameter; if the material is not viscous enough, segregation may occur, but it will depend on the typical structural application whether this is beneficial or not. The discontinuity of the progress of mixture 1 in the

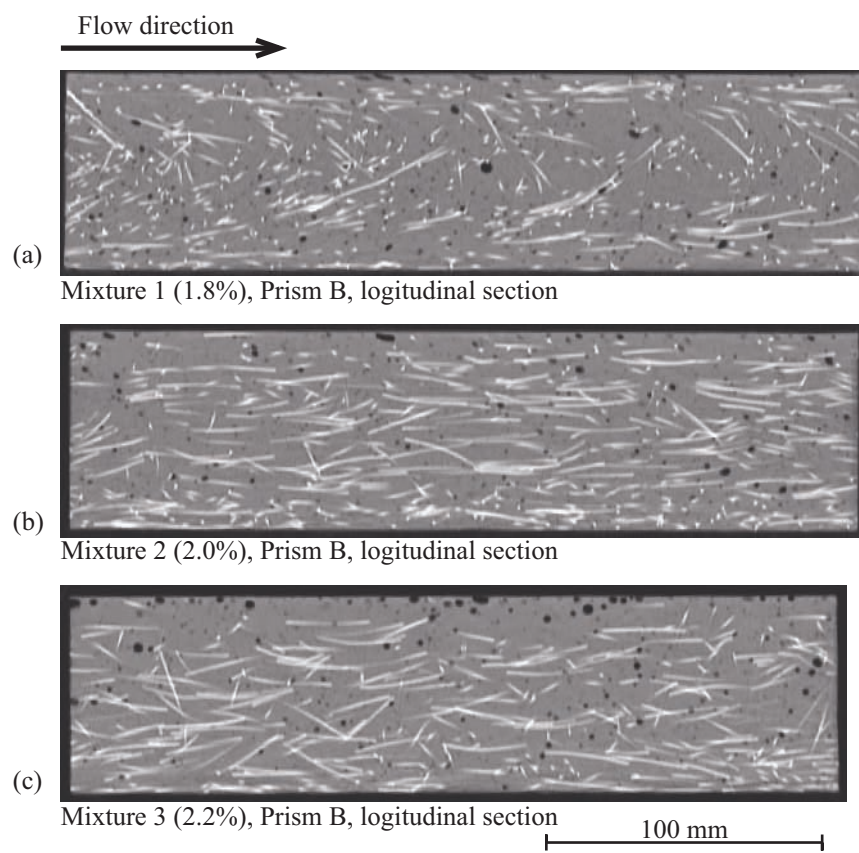


Figure 6.5: Longitudinal centre sections of the prisms "B" for each of the three tested mixtures

”C” prism is caused by the fact that the material did not ’level-out’ properly and the specimen was cut out only 2 cm from the end of the rising branch of the ’U-specimen’.

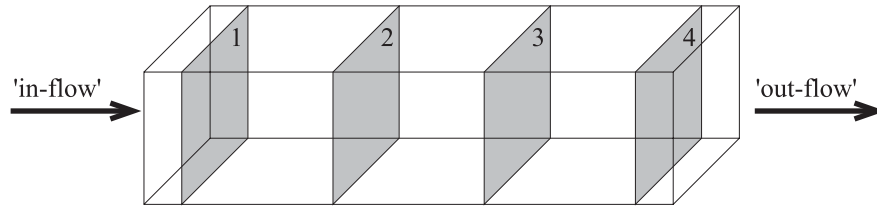


Figure 6.6: Analyzed cross-sections in a prism

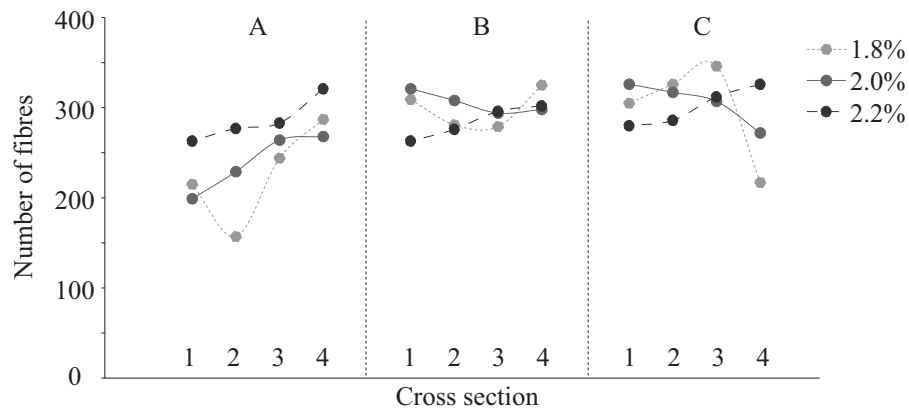


Figure 6.7: Results from the fibre counting of the various cross-sections for mixtures 1 to 3 and the prism positions ”A” to ”C”

In order to determine the mechanical properties pendulum-bar four-point bending tests were performed. The specimens were the same as used for the CT-scans. To normalize the results the nominal bending strength ( $f_{b \max} = M_{\max}/W$ ) was calculated and all the results are presented in Figure 6.9a. Figure 6.9a clearly shows that the bending strength increases with the increasing ’flow-ability’, except in the ”C” prisms, where the fibre segregation seems to have a negative influence on the bending strength. Nevertheless the bending strength is still on a relatively high level of 25 MPa. The fibre segregation is also the reason why the bending strength of the ”C” prism from mixture 3 (2.2%) is lower than the bending strength of the ”B” prism from mixture 3 (2.2%). The progress of the bending strength of the ”C” prisms in Figure 6.9a is constant: the bending strength does not increase with the

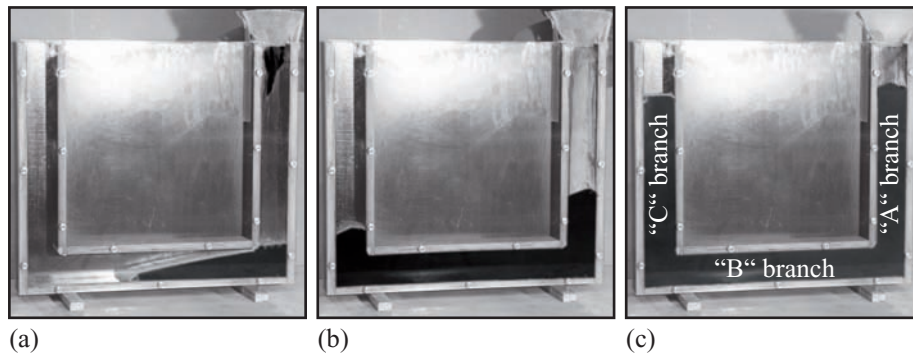


Figure 6.8: Filling sequence of the 'U-mould'. (a) the concrete flows layer-wise through branch "B", (b) the concrete levels out as soon as branch "B" was filled and (c) the complete filled 'U-mould'.

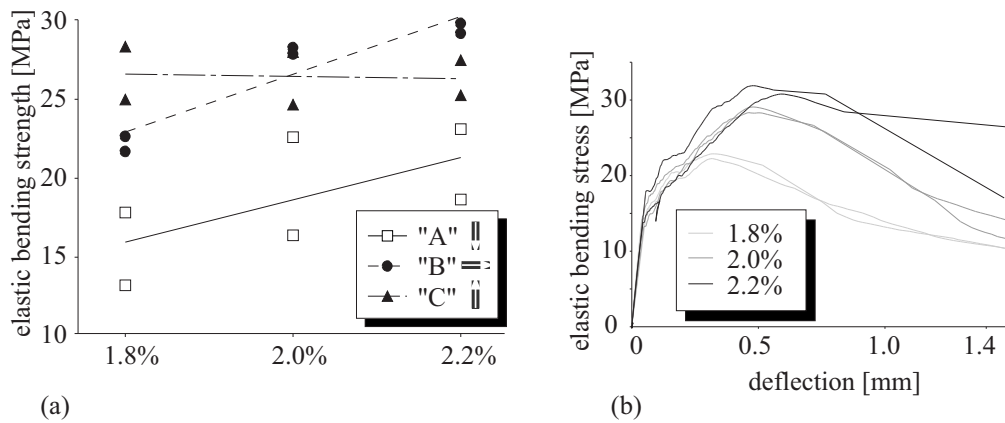


Figure 6.9: Results from the four-point bending test; (a): Nominal bending strength vs amount of super plasticizer for prisms A, B and C, (b): Nominal bending stress vs deflection diagram from "B" prisms



increase of the 'flow-ability' due to the fibre-segregation. The material was not able to transport the fibres all the way up to the "C" prisms but the fibres that travelled the whole distance were aligned. Thus, the increase of strength due to fibre alignment and the decrease due to segregation seem to compensate. For the "B" prisms where an increase of bending strength of 40% was measured, the effects of fibre alignment and fibre segregation amplify. Finally the "A" prisms are only influenced by the alignment of the fibres: an increase of the bending strength of 30% was observed.

In Figure 6.10 the prisms are arranged according to their bending strength; in 6.9b, examples of stress-deformation curves, derived from four-point bending tests are shown. It can be seen that with increasing fibre-count per cross-section the bending strength increases as well. This diagram shows that the alignment of the fibres improves the mechanical properties of fibre reinforced concrete. But why do fibres align? Most likely the fibres align because of the flow profile. A possible simplified model is shown in Figure 6.20. Different flow velocities affect the fibres and may cause the fibres to rotate in such a way that they align with the flow of the material. The effect is stronger at higher flow velocity, when the velocity can affect the fibre for a longer time (i.e. lower viscosity or longer flow duration); until finally a steady state is reached where the fibre alignment does not change anymore. These two behaviours contradict. The higher the flow velocity the less time the flow can affect on the fibre and vice versa. Further investigation on how strong the above mentioned effects (velocity or time) influences the orientation of the fibres and an optimum ratio between flow velocity and time, e.g. minimum flow distance, should be found. In this series large fibres only were investigated due to the resolution of the CT scanner. Suggestions of different flow velocities can be derived from Figure 6.4b and to a lesser extent from Figure 6.5a. In Section 3.3.2 the orientation of the small, middle and large fibres was investigated. These experiments showed that not only the large fibres orientate with the flow of the material but also the small and middle fibres. Therefore this model of how the fibres orientate is valid for all the used fibres. Because of the time consuming technique, manual counting of the fibres, even more experiments and numerical simulations must be carried out to validate the above mentioned model. Test series with other types of fibres, e.g. smaller and larger steel fibres, carbon, PVA, glass or PP fibres should be carried out.

### 6.2.2 Filling methods - tensile properties

As mentioned, the development of self-compacting concrete leads to easier placement of the fresh material, and the fibre distribution and orientation

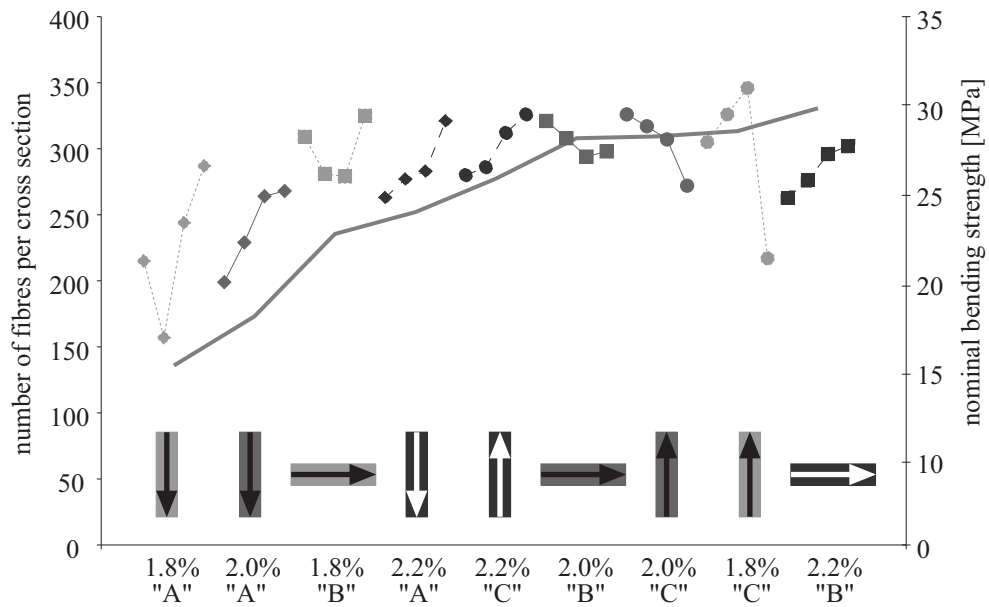


Figure 6.10: Comparison between the counted fibres per cross-section (left Y-Axis) and the bending strength (right Y-Axis). The solid line shows the results from the four-point bending test; dots, squares and diamonds are results from fibre counting

is not affected since compaction becomes obsolete (see Soroushian & Lee [1990]). An interesting idea is to investigate to what extent the filling method of the fresh material can be used to affect the fibre distribution and orientation, and to see if a possible influence on the mechanical properties emerges. In this section a test series is reported that confirms that the filling method has an influence on the mechanical properties of fibre reinforced materials. These and earlier experiments (see Stähli & van Mier [2007a]) also show that material properties for fibre reinforced materials are dependent on the geometry of the tested specimen. Therefore, parameters, such as the tensile strength, are not constant for the whole specimen. They change with the flow of the concrete in the specimen and the geometry of the specimen itself. This means that structures cannot be conventionally designed. Moreover, the whole filling process has to be taken into account in the structural design process. However, this also presents an entirely new chance for optimizing a structure by controlling the flow of the material so that fibres are orientated most favourably and perhaps fewer fibres need to be used.

'Conventional', 'fill' and 'climb' filling methods were investigated. The mixtures used can be found in Table 2.3. The tensile strength was determined using the pendulum-bar tensile test.

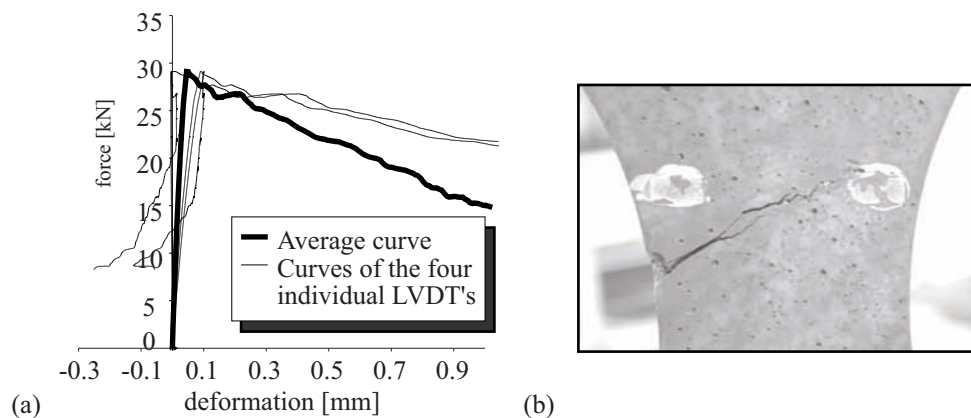


Figure 6.11: (a): Curves from the pendulum-bar tensile test with the specimen 003 'conventional'. (b): Crack pattern observed in the specimen.

Figures 6.11, 6.12 and 6.13 show results from the tensile tests. It can be seen that the characteristics of the load-displacement curves and the crack patterns are related. The figures show that the curves from the four LVDT's can have completely different shapes. In Figure 6.11 the peak is very sharp. The same 'sharpness' can be seen in the crack pattern of this specimen. This

crack propagated from the left to the right. After the peak, the deformations on the right side of the specimen decreases as expected. This behaviour is typical for a test set-up with freely rotating supports, see also the test on plain concrete by van Mier et al. [1994a], van Mier [1996], van Mier et al. [1995].

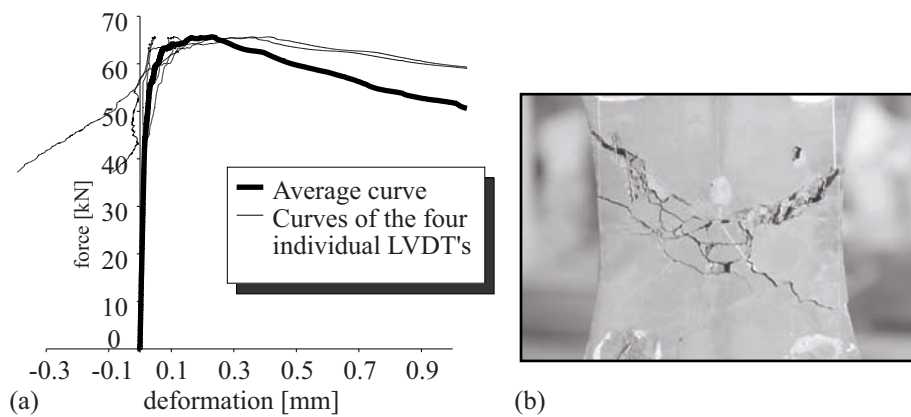


Figure 6.12: (a): Curves from the pendulum-bar tensile test with the specimen 003 'fill' (specimen I). (b): Crack pattern observed in the specimen.

Figure 6.12 shows similar characteristics, but where the deformation on the backside decreases the peak is very smooth. The crack propagated from the front to the back side of the specimen and its pattern is completely different. On the image of the crack pattern in Figure 10, it can be seen that there is not one single crack, but there is, typical for fibre reinforced materials, a crack zone with multiple cracking.

Figure 6.13 shows a third type of behaviour. The deformations of all sensors always increase during the tensile test. Here the whole cross-section is pulled symmetrically. The crack propagated from the left to the right and showed two branches. After cutting the aluminium plates from the sample with a water-cooled diamond saw, white lines appeared on the surface of the specimen in the cracking zone. It seems that these white lines are microcracks which can not be detected with the naked eye. Such phenomena also appeared on other specimens which are not reported in this Thesis. The influence of the filling method for mixtures with one fibre only is significant.

Figure 6.14 gives an overview of the results for the mixtures 300, 030 and 003. It can be seen that difference in the tensile strength for the conventional filling method is negligible. The tensile strengths are within the

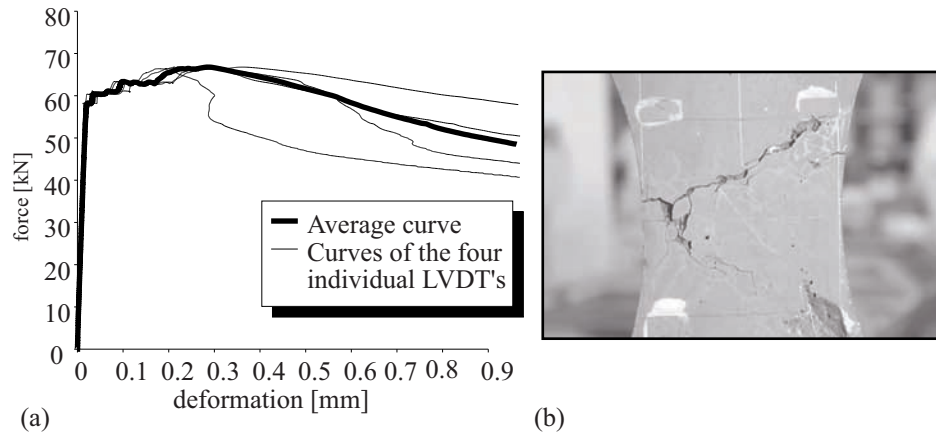


Figure 6.13: (a): Curves from the pendulum-bar tensile test with the specimen 003 'fill' (specimen II). (b): Crack pattern observed in the specimen.

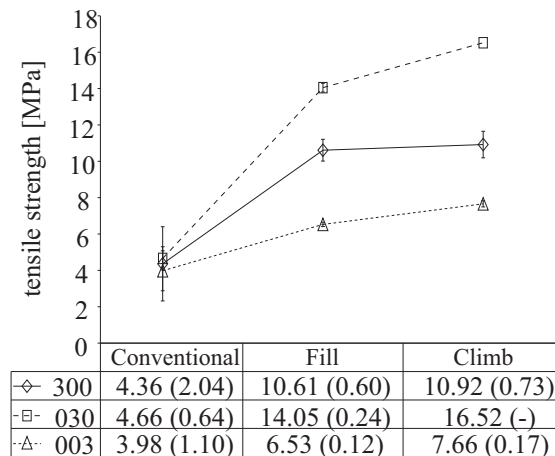


Figure 6.14: Summary of the results in [MPa] derived from tensile test from the mixtures with only one type of fibre. The standard deviation is given in brackets.

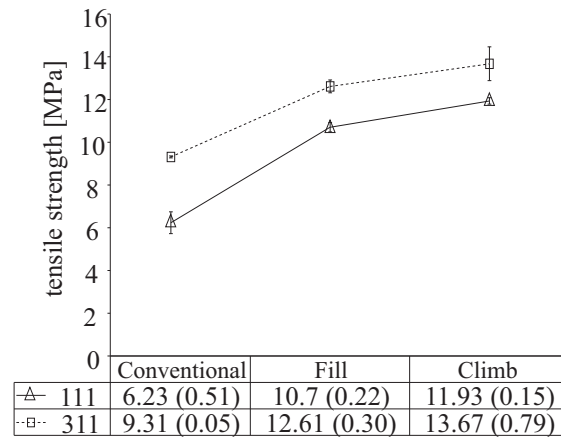


Figure 6.15: Summary of the results in [MPa] derived from tensile test from the mixtures with HFC. The standard deviation is given in brackets.

standard deviations. These standard deviations are relatively large in comparison to the ones from the two other filling methods. The fibre amount of these three mixtures was constant at 3%. The diagram also shows that the tensile strength for the 'fill' and the 'climb' method is higher than for the 'conventional' method. This leads to the assumption that the tensile strength increases with the ability of the fresh concrete to flow and with that the alignment of the fibres to the tensile direction. The longer the fresh concrete can flow, the higher the tensile strength. This can be seen for all types of fibres, even for the small 0.15/6 mm fibres. But why does the tensile strength increase? Again, as in the results presented in Section 6.2.1.2, the tensile strength increases because the fibres align with the flow of the material. This fact would explain the results from the tensile tests. As seen before, when casting a specimen with the 'fill' method, the flow distance of the material is less than with the 'climb' method, but the jump in tensile strength between 'fill' and 'climb' method is not that large. It seems that the material does not need to flow that long; only a short, but controlled flow can increase the tensile strength significantly. Figure 6.15 shows the summary of the results for the experiments with mixture 111 and 311. These two mixtures were both hybrid fibre concretes with three types of steel fibres. The fibre amounts were 3% and 5% for the mixtures 111 and 311 respectively. Both mixtures show that the tensile strength is dependent on the filling method. As seen before, the influence of concrete flowing results in an increasing tensile strength. Figure 6.15 also shows that the tensile strength for the mixture with 5% of fibres is higher than the one with 3% only. This

means that, by increasing the amount of fibres, the tensile strength increases as well. This was seen before in several studies, e.g. Markovic [2006].

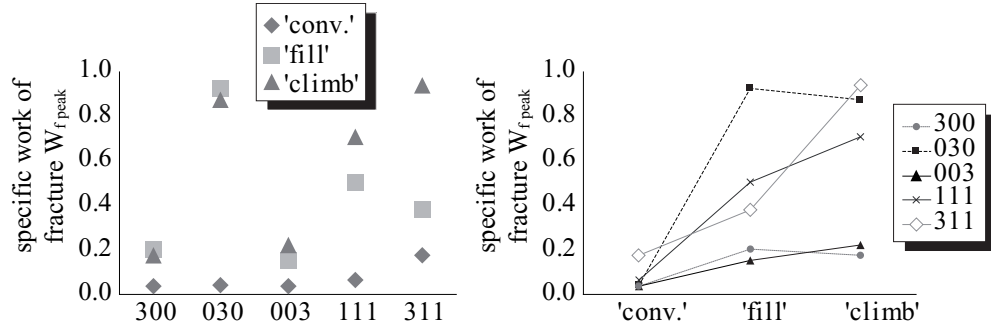


Figure 6.16: Specific work of fracture till the peak for SFC and HFC and different filling methods

Figure 6.16 shows the specific work of fracture till the peak for the above mentioned mixtures and filling methods. The values are strongly dependent on whether a material has a strain hardening behaviour or not. However the different filling methods influences the specific work of fracture dramatically. For the 'conventional' filled specimens the specific work of fracture is barely influenced by the different fibres while for the 'climb' and 'fill' specimens a dramatic increase of  $W_{f, peak}$  can be observed. Figure 6.16 also shows that the filling method has the largest influence on the middle fibres, as well as on the HFC mixtures in terms of  $W_{f, peak}$ . This increase of  $W_{f, peak}$  can be explained by the fact that the material shows strain hardening behaviour with the optimization of the filling method.

The values for the first cracking strength, the peak strength for the different mixtures are summarized in Table 6.2 and Figure 6.18. The values were determined using the force displacement diagrams derived from the tensile tests. The results clearly indicate that the specimens cast with the 'conventional' method do not show strain hardening behaviour. The values of  $\sigma_{1st crack}$  and  $\sigma_{max}$  are equal except for 311, which shows an increase of 3%. For the 'climb' and 'fill' method all the specimens showed an increase in stress from  $\sigma_{1st crack}$  to  $\sigma_{max}$ . The value of  $\sigma_{1st crack}$  was not constant for the different filling methods as expected. Table 6.2 shows that the value of  $\sigma_{1st crack}$  for the 'conventional' method is clearly lower than for the 'fill' and 'climb' method while there the values are equal. To sum it up it can be said that on the assumption that the concrete batch was the same,  $\sigma_{1st crack}$

increase with the flow of the material. In some cases this increase is nearly a factor of two.

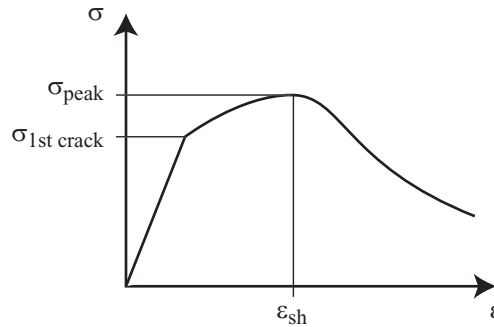


Figure 6.17: Definition of the stresses and strains

Table 6.2: First crack ( $\sigma_{1st\ crack}$ ) and peak ( $\sigma_{max}$ ) strength

	'conv.'	'fill'	'climb'	'conv.'	'fill'	'climb'
	$\sigma_{1st\ crack}$			$\sigma_{max}$		
300	4.36	10.5	10.5	4.36	10.61	10.92
030	4.66	11.0	11.0	4.66	14.05	16.52
003	3.98	6.0	7.0	3.98	6.53	7.66
111	6.23	9.0	9.0	6.23	10.7	11.93
311	9.00	11.0	11.0	9.31	12.61	13.67

The filling methods also influenced the strain hardening behaviour. From no strain hardening ('conv.' method) to a peak strain of 0.5% ('climb' method). Again, strain hardening behaviour was only achieved by letting the concrete flow. Without flowing the fibres were randomly distributed and orientated and the material had a brittle behaviour. Even worse, it appeared that the fibres acted like a defect in the material and  $\sigma_{1st\ crack}$  was much lower than for specimens where the material flowed into the mould.

### 6.2.3 Influence of the filling method to the fibre distribution

Four different filling methods were investigated. First, the 'conventional' method, second and third the 'fill' and 'climb' method and fourth, the 'lying'



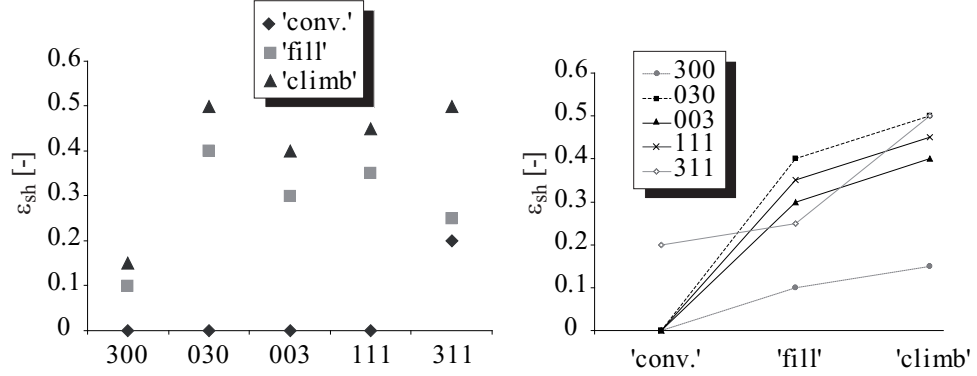


Figure 6.18: Peak strain for SFC and HFC using different filling methods

method. The results of the flow properties and the mixtures can be found in Section 4.4.3. The fibre distribution was analyzed by manual counting. To confirm the influence of the filling method on the mechanical properties uniaxial tensile tests using the 'pendulum-bar' test set-up were performed.

Table 6.3: Mechanical and rheological properties

	311	211
Small slump flow $s_{sf}$ [cm]	27	26
Slump flow $l_{sf}$ [cm]	84	n.a.
Young's Modulus $E$ [GPa]	34.4	39.5
Compression strength $f_c$ [MPa]	133.7	126.4
Elastic bending strength $f_b$ [MPa]	31.0	21.1

Two mixtures were analyzed. 311 and 211 which contained a total amount of 5 and 4% of fibres respectively. The mechanical (compression strength and Young's Modulus) and rheological properties of both mixtures were more or less identical (see Table 6.3) except for the bending strength: the nominal bending strength of the 211 was only 70% of the one from the 311 mixture. This is because the 311 mixture contains 1% more of the small 0.15/6 mm fibres. The values of the uniaxial tensile strength results were adjusted according to their bending strength to allow for comparison of the results (Table 6.4). The bending strength derived from four-point bending test using 70 mm x 70 mm x 280 mm prisms was taken to adjust the results because the fibre distribution and alignment in 'dog-bone' shaped specimens is dependent on the viscosity.

Table 6.4: Tensile properties

	Tensile strength $f_t$ [MPa]	$\eta = \frac{f_t}{f_b}$ [-]	$\kappa = \frac{\eta}{\eta_{min}}$ [%]
311 'conv.'	9.31	0.30	130
311 'fill'	12.61	0.41	178
311 'climb'	13.67	0.44	191
211 'conv.'	4.74	0.23	100
211 'lying'	11.49	0.54	235

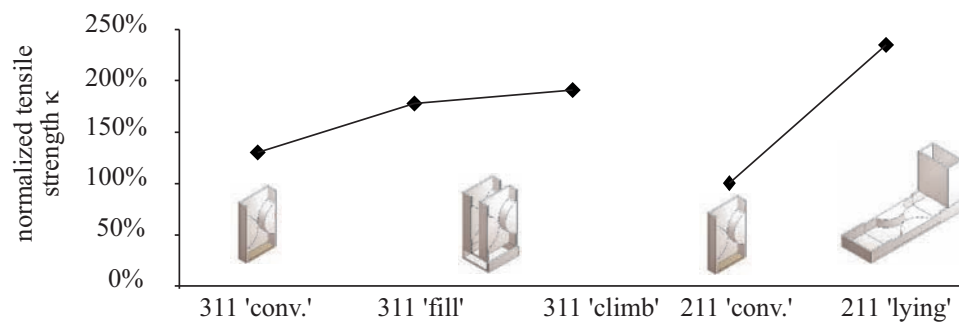


Figure 6.19: Normalized results derived from the 'pendulum-bar' tensile test

Figure 6.19 shows that the influences of the filling methods are significant. It can be seen that the 'lying' method has the largest increase in tensile strength. The increase of the tensile strength between the 211 'conventional' and 211 'lying' was much higher than for the 311 mixtures. It appears that the large fibres segregated and for the 'lying' specimens they settled at the bottom of the mould, i.e. at one of the specimens sides, but for the 'conventional' and the 'climb' specimens the fibres settled as well but at the bottom of the specimen. As already mentioned this bottom was cut in the preparation procedure. Therefore the performance of the fibres in the 'lying' specimens might have been over-estimated and underestimated for the 'conventional' and 'climb' specimens. Thus the increase of the normalized tensile strength between the 211 'conventional' and the 211 'lying' specimens might be over-estimated.

## 6.3 Conclusions

- If "material properties" should be determined, it is necessary to produce specimens with a minimum cross-section of three times the length of the largest fibre to avoid significant wall effects because of the flow profile in the cross-sections and its influence on the fibre aligning.
- The filling method has a significant influence on the tensile strength. The presented results clearly show that the maximum tensile strength is dependent on how the material flows into the mould. The best results were obtained by filling the mould from the bottom to the top.
- The fibres align with the flow of the material. A simple model is given in Figure 6.20. Different flow velocities affect the fibres and may cause the fibres to rotate in such a way that they align with the flow of the material. The effect is stronger at higher flow velocity (see Figure 6.21) or when the velocity can affect the fibre for longer time, (i.e. lower viscosity or longer flow duration). Due to this model the shape and geometry of the mould, the filling method and the viscosity influences the fibre alignment significantly.

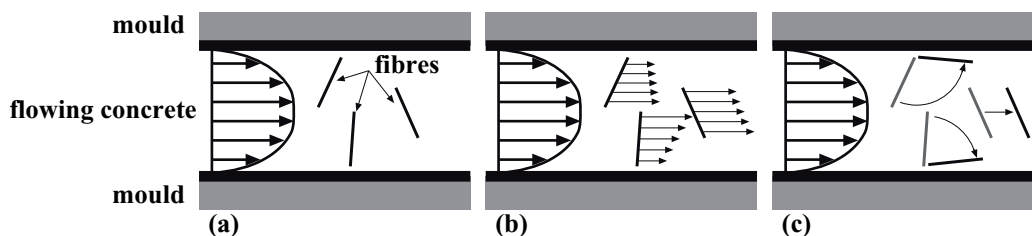


Figure 6.20: 2D model of flowing concrete. The fibres align in the direction of the flow caused by the velocity gradient of the flow profile.

- Therefore, each element/structure has its own characteristic and a standard test can not be performed for HFC or for (probably most) ordinary fibre reinforced concrete (FRC). That means that such materials should preferably be used in a prefabrication plant, where the material flow during the casting process can be well controlled, and with that the fibre alignment. Similar elements can be produced with one mould and the same material flow i.e. the same fibre alignment can be guaranteed. Di Prisco & Plizzari [2004] showed some examples of R/C slabs reinforced with steel fibres.

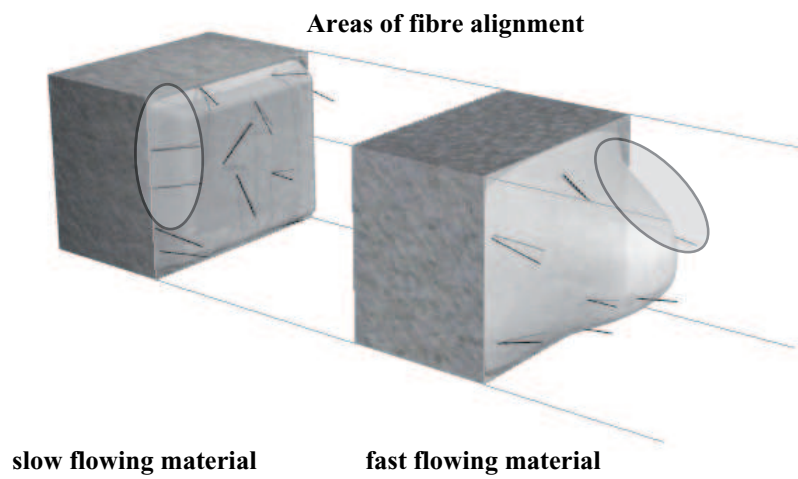


Figure 6.21: 3D model of flowing concrete. Different steepness of the flow profile caused by different flow velocities.

## Examples of applications

### 7.1 Introduction

Parallel to the research project ultra fluid concrete was used for different applications in collaboration with civil engineering or architectural students. Structural and perforated walls, inventory and several architectural models were produced. The demands of the fresh and the hardened concretes had to be adjusted for each individual project.

### 7.2 Structural wall

Buzzini et al. [2006] describes a project where HFC was used as a material to prevent buckling of the main steel reinforcement in structural wall element under cyclic loading. Different geometries and reinforcements were tested in large scale experiments.

The demand on the material was a strongly developed deflection hardening or even a strain hardening. But at this moment only the four-point pendulum-bar test was available and the tensile properties could not be determined within the given time schedule. The final mixture for the first wall contained 1.5% of the short fibres, 0.5% of the middle fibres and 1.5% of the large fibres. This mixture provided the demanded mechanical properties which were estimated in computer simulations. The test results of the wall showed that the tensile strength of the material was still too low. The reinforcement buckled and the concrete cover spalled. This was not only because of the load capacity of the material but also because of the very thin concrete cover which was only 20 mm. As a result of the first wall experiment the concrete cover was increased from 20 mm to 40 mm and the mixture was also adjusted



Figure 7.1: Images of the production of the structural walls: Production, transport and testing

to 3.0%, 1.5% and 1.5% of the small, middle and large fibres respectively. The flow-ability was not extraordinary but sufficient to fill the mould completely. The results and conclusions of the experiment can be found in Buzzini et al. [2006]. Figure 7.1 shows images of the production, the transportation and the testing of the wall. The results showed that HFC has several advantages. First of all, no shear reinforcement was needed, even if the cross section was very thin. The buckling of the reinforcement bars could be hindered using HFC and a large enough (3 cm) concrete cover. Nevertheless the production of the wall was rather labour-intensive in comparison with the result.

### 7.3 Sandwich-elements

Gartmann [2006] investigated a very interesting application of HFC combined with a light weight foam concrete. The sandwich element was built as follows: two thin HFC walls with or without ribs served as mould and as main carry element of the structure. Between the two HFC walls, foam concrete served as thermal insulation and increased the buckle resistance of the HFC walls.

The demands on the material to fill the mould were extremely delicate. The flowability had to be adjusted so that the material could flow into the thin moulds with its ribs without segregating. The final mixture contained 6% of fibres (3.5%, 1.5% and 1.0%). The problem of clogging on the casting side was solved by bringing in the material with a trowel very slowly so that the material could flow down before clogging the casting side of the mould. This was a very slow process which should be improved for further experiments.

Figure 7.2 shows images of the HFC walls and two examples of specimens under load. The results showed that the load was transferred through the HFC walls and the foam concrete did not carry any load but increased the stability of the thin walls. First the walls delaminated and with increasing load the walls buckled and were very brittle. By adding ribs in the HFC walls, the compression strength could even be increased (the cross-section area of the HFC walls was kept constant, only the geometry changed) and the sandwich specimens became more ductile. Gartmann [2006] showed that it is possible to build sandwich-elements using these two completely different concretes. Finally the compression strength and the thermal conductivity reaches values which are in the range of common wall structures such as masonry combined with thermal insulation.



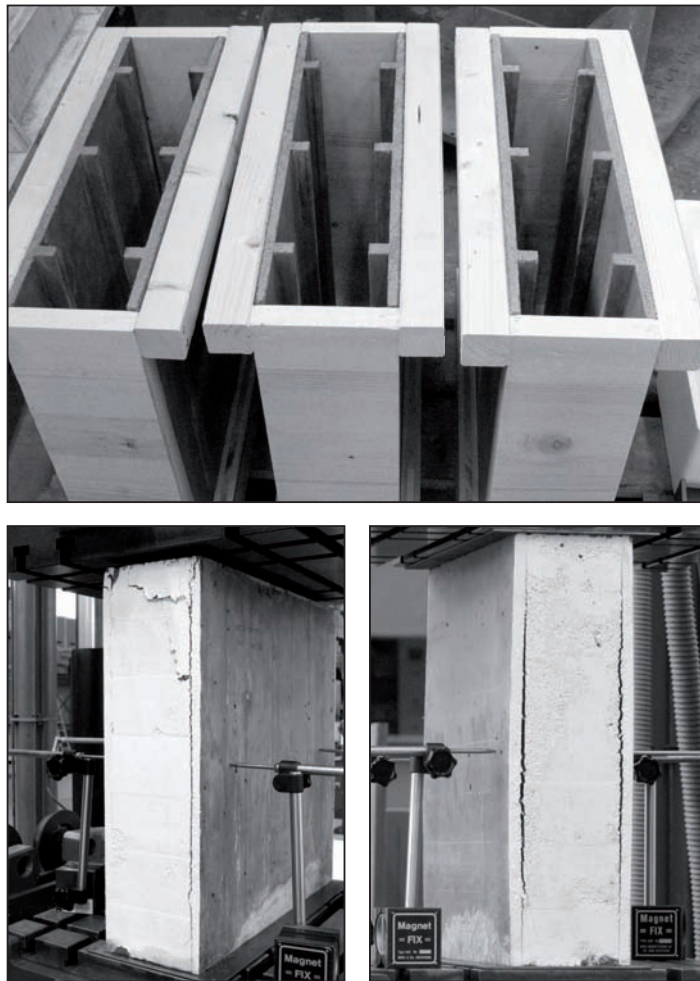


Figure 7.2: Images of the sandwich elements: HFC walls and two specimens under load

## 7.4 The perforated wall

Within a project of Gramazio & Kohler (Esslinger et al. [2006]) large scale perforated concrete walls ( $300 \times 150 \times 15 \text{ cm}^3$ ) were designed and produced. The whole process had several challenges such as drilling the holes into the mould, rheological properties of the concrete, mechanical properties of the structure and demoulding the perforated wall. Two walls with different concretes were produced. The first wall was produced out of HFC with 6% steel fibres. Because of the sharp edges and the leaking of the concrete around the plastic tubes (mould for the holes) and the resulting danger of injuring oneself, steel fibres were unsuitable, but there was no doubt about the need for reinforcement in such a high perforated concrete wall. Never the less the second wall was cast without any reinforcement and surprisingly it worked except for some pop offs while demoulding and hammering out the plastic pipes which served as moulds for the holes.

Two mould release agents were used, a common formwork oil and a silicon spray. Even though two agents were used, the demoulding of the plastic pipes took a lot of mechanical energy. Figure 7.3 shows images of the manufacturing process and the final walls. The framework had to be excessively strengthened as can be seen in Figure 7.3.

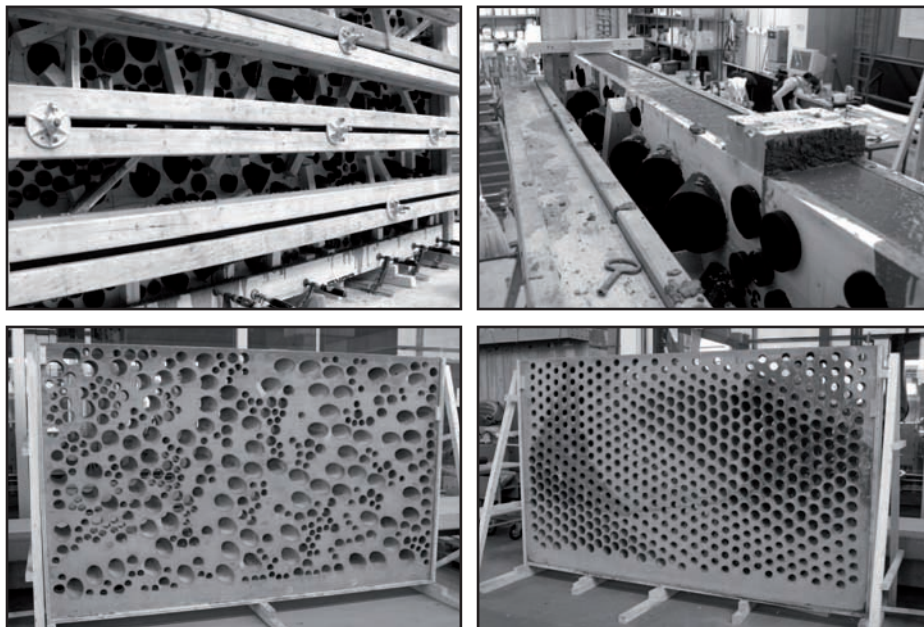


Figure 7.3: Images of the production and the final results of the perforated wall

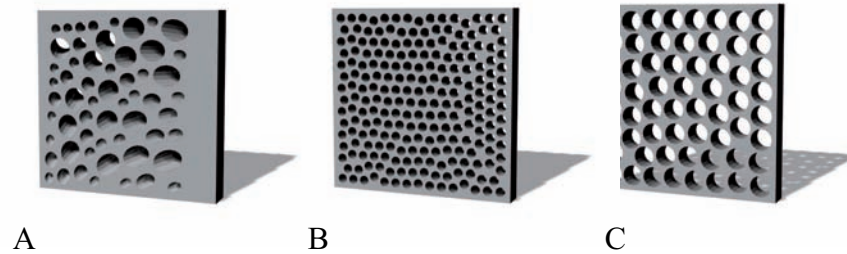


Figure 7.4: Schemes of the  $100 \times 100 \text{ mm}^2$  perforated wall specimens. A: 17 x  $\text{Ø}50 \text{ mm}$ , 9 x  $\text{Ø}56 \text{ mm}$ , 17 x  $\text{Ø}75 \text{ mm}$  and 14 x  $\text{Ø}110 \text{ mm}$  with a maximum orientation angle of  $50^\circ$ , B: 219 holes with a diameter of 50 mm and C: 59 holes with a diameter of 110 mm,

The question about the bearing capacity was still unanswered. A test series where the load capacity was determined with three specimens which differed in hole diameter, orientation of the holes and combinations of hole diameters (see Figure 7.4) was carried out at the EMPA<sup>1</sup>. The concrete used contained 1.5% of short PVA fibres (RF350x15 mm). The material was extremely fluid. The value of the small slump flow was in between 27 to 32 cm. Details about the mixture can be found in Table 7.1 and 7.2. Four-point bending tests were performed on  $70/70/280 \text{ mm}^3$  prisms after 1, 7 and 28 days. Figures of the production of the wall specimens and the crack pattern after testing them can be found in Figure 7.5.

Figure 7.6 shows curves derived from the bending tests after 1, 7 and 28 days. A clear increase of the bending strength can be observed but the age did not influence the ductility of the material. Because of the increase of the bending strength the material properties changed from deflection hardening to deflection softening or from a relatively low strength matrix to a high strength matrix. For the used application such a development of the mechanical properties left some room for improvement. Fortunately the increasing brittleness of the material did not influence the ductile behaviour of the perforated wall. This is commonly known for concrete where the matrix is also brittle but the whole system is somehow more ductile.

Figure 7.7 and Table 7.3 gives an overview of the results. Two specimens per configuration of holes were tested. The results show that the compression strength increases with the increasing density and the deflection of the holes have a negative influence on the strength as well. Therefore the value of the compression strength does not increase for the specimens "A" which are

<sup>1</sup>EMPA Materials Sciences & Technology in Dübendorf, Switzerland

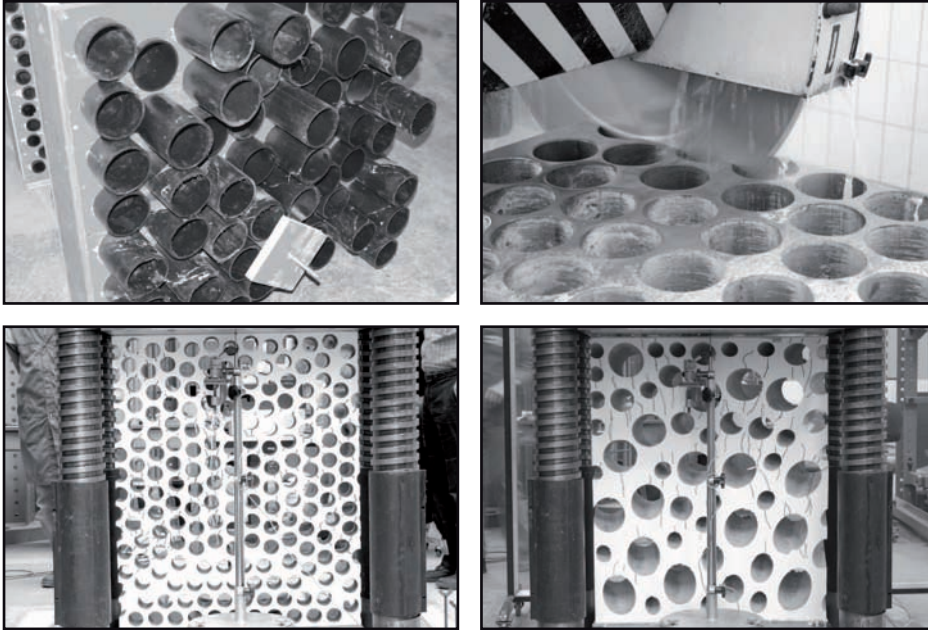


Figure 7.5: Images of the preparation and the final perforated wall specimens

Table 7.1: Mix-design for the perforated walls

		$[kg/m^3]$
Cement	CEM I 42.5	950
Fly-ash	Holcim Hydrolent	160
Microsilica	Elkem (BASF)	90
Sand	0-4 mm	710
Water	w/b = 0.22	260
Super-plasticizer	Glenium ACE 30 (2.6%)	25
Stabilizer	Glenium Stream 2 (0.5%)	4.7
PVA Fibres	RF350 x 12 mm	19.5

Table 7.2: Mechanical properties of the material used for the perforated walls

		1 day	7 days	28 days
$f_{cc}$ [MPa]	cube (150 x 150 x 150 mm <sup>3</sup> )	30	60	80
$f_c$ [MPa]	cylinder (ø150/300 mm <sup>2</sup> )	58	79	83
$E$ [GPa]	cylinder	28	30	30
$f_{b\ 4pt}$ [MPa]	70/70/280 mm <sup>3</sup>	6	12	17

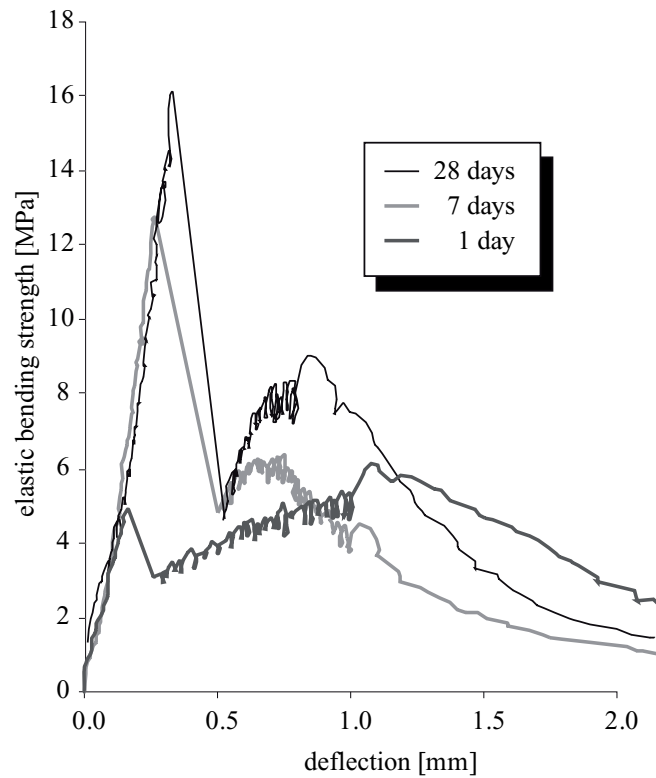


Figure 7.6: Bending test results

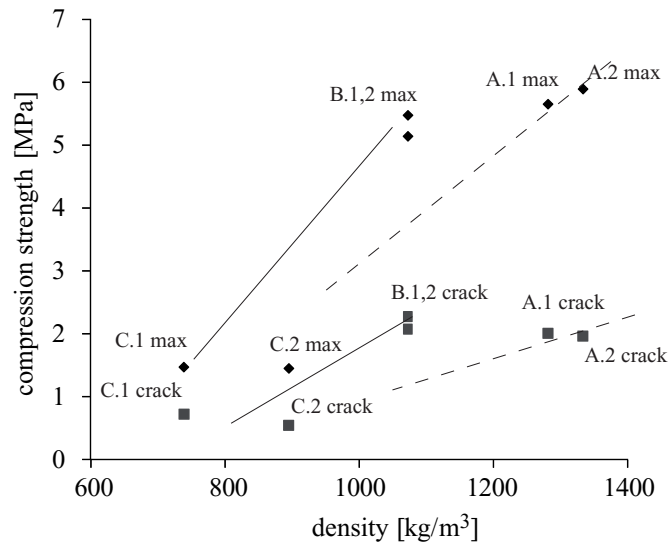


Figure 7.7: Overview of the perforated wall results

Table 7.3: Mechanical properties of the perforated walls

Specimen	density [ $kg/m^3$ ]	first crack strength [MPa]	ultimate strength [MPa]
A.1	1281	2.0	5.7
A.2	1333	2.0	5.9
B.1	1073	2.1	5.2
B.2	1073	2.3	5.5
C.1	896	0.6	1.5
C.2	740	0.7	1.5

more dense than the two others. This effect has to be investigated further to prove the results presented above.

## 7.5 Architectural chairs and models

Over the past fifteen years, computer-aided design has dramatically changed the development and fabrication cycle in most design industries. In the large design based professions outside of architecture, computer aided manufacturing (CAM) has evolved alongside CAD as the principal method of transferring a design from the digital world into a physical reality or a mould for a component out of concrete.

Recent changes in affordability and availability of computing power, complex modeling software, and facilities for CAM have made this technology available to architects and the greater design industry. This changes the current typical production cycle, from the distinction between design and fabrication, to a process where the designer is also involved in the manufacturing of the components for the assembly of the whole.

There are two different basic processes of 3D fabrication, additive and reductive. First, additive processes, are sometimes referred to as construct a model by building-up its geometry based on sectional layering of the material, the smaller the layer thickness - the greater the precision of the model. Contrarily, the reduction method where material is subtracted from a large block of material. Inner and outer boundaries of the final model can be produced. Such a pair of machined materials can be used as a mould. With this technique very thin structures can be cast. Figure 7.8 shows some examples of such structures. The fruit bowl and the chairs were produced within the Master of advanced studies in Architecture, Specialization in Computer Aided Architectural Design 2007.

The moulds were produced by milling them out of so called Styrodur<sup>®</sup> foam blocks. The concrete used contained 2% - 3% of either steel or PVA fibres. It had to be super-fluid to ensure that the moulds were filled completely. Venting holes were drilled into the moulds where necessary. Unfortunately the mould had to be destroyed in order to demould the concrete object. Even with special release agents the Styrodur<sup>®</sup> formwork stuck to the concrete surface and it was impossible to remove the mould without damaging it.



Figure 7.8: Clockwise: fruit bowl by Georg Munkel, Lounge chair by Alexandra Stamou, Conc chair by Seong Ki LEE and concrete table by Moritz Schwarz



In architecture the importance of having a model built out of the final material becomes more and more important. Therefore most of the architectural models were made out of concrete. The formworks were produced with a high degree of detail using CAD and CAM techniques. Thin walls and floors had to be cast within one cast of concrete and the concrete alone had to resist the demould and the static or dynamic (during transportation) forces of the whole structure. In order to avoid accidents, PVA fibres instead of steel fibres were used. In some cases where the forces exceed a certain level steel fibres had to be used. All the mixtures used were super fluid and contained sand of a maximum diameter of 1 mm.

Carol Egger went to the limit with his so called stairs tower. Everything was cast in one cast of concrete. The formwork enclosed stairs, walls with windows and doors and ceilings. Different surfaces were included in the formwork, such as plastic foil plywood and MDF<sup>2</sup>. The concrete used did not contain any aggregates and only 1% of small 3 mm PVA fibres. Problems arose while filling the concrete into the formwork. The formwork leaked and the leaks were sealed using plasticine and screw-clamps. The result was amazing. The concrete filled nearly every detail. Figure 7.9 shows an image of the model.

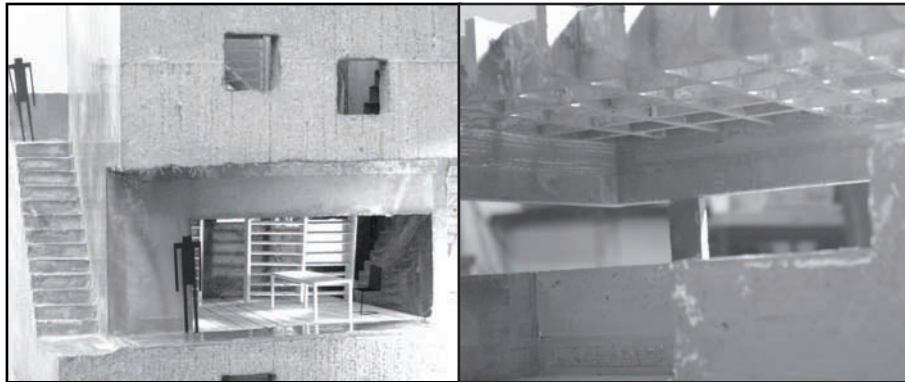


Figure 7.9: Architectural models from Carol Egger and Christine Hotz

The box ceiling of an indoor pool of Christine Hotz's model was a challenge because of its size. The width of the ligament was 2 - 4 mm. In a first attempt the ceiling was not filled completely. The concrete was not fluid enough. The mixture and the release agent were adjusted and the result can

---

<sup>2</sup>middle density fibre panel

be found in Figure 7.9. Using the model the play with the light in the interior of the indoor pool could be nicely traced.



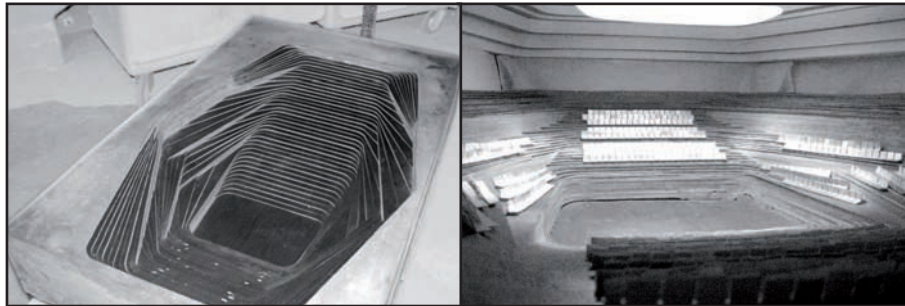
Figure 7.10: Architectural model by Pascal Flammer

Pascal Flammer<sup>3</sup> created a very filigree model of his design of the Centro Comunitario Julio Otoni in Rio de Janeiro, Brazil. The concrete which was used for the model was a FRC with small fibres only. The struts were cast into closed moulds. The concrete had to flow from the top to the bottom of each strut. The ceilings were cast upside down so that the mould surfaces pointed upwards in the direction of the viewer. Details about the project and the prizes which it won can be found in Flammer [2007].

Figure 7.11 shows large concrete models from a symphony hall. Each model was cast with one batch. The upper model (Ladina and Philippe) was reinforced with PVA fibres and the lower (Luca and Matthias) with small steel fibres because of its overhanging large elements. Because of the large dimensions of the model and the FRC used it was possible to sit or stand on the ceiling of Luca's and Matthias' model. In order to create such a line pattern at the interior of the walls, thin wooden stripes were glued into the mould. The paint on these wooden stripes remained on the concrete which was not planned but the students liked it, also because of the roughness and the changeability of the surface.

---

<sup>3</sup><http://www.pascalflammer.com>



Model by Ladina and Philippe



Model by Luca and Matthias

Figure 7.11: Large architectural models by Ladina, Philippe, Luca and Matthias of a symphony hall

## 7.6 Conclusion

The introduced material can be used for several applications such as structural walls, inventory or architectural models. The material is highly suitable for filigree structures with a high demand on the surface. Because of its ultra-fluid behaviour complicated moulds can be filled within one cast.



## Conclusions and outlook

The results presented in this Thesis show that not only tensile properties of Fibre Reinforced Concrete can be adjusted by adding different types of fibres (instead of just one single type as is common in FRC), but also by aligning the fibres in the direction of the stress. The fibres were successfully aligned by adjusting the filling method and the flowability of the material thereby further improving the tensile strength. Basically the better the material flows the more the fibres align. The alignment of the fibres can be investigated by the use of medical CT-scanners or by cutting the specimens and counting the fibres manually. The results clearly showed a significant increase in strength when the fibres are aligned in the direction of the stress. The results also showed that it is extremely important to adjust the flowability of the fresh concrete in such a way that (i) the moulds will be filled completely and (ii) the fibres float within the flow without segregating or clumping. Therefore such a material should be mainly used in prefab plants where the conditions of the mould and the material can be controlled. Furthermore it is important to examine the demands of such a structure by mechanical testing of the structure itself and by checking the fibre distribution and alignment in the structural element.

### 8.1 Conclusions

The following conclusions can be drawn from this PhD-Thesis:

- In order to get comparable results all rheological tests should be carried out using dry equipment, especially the slump flow cone and the slump flow plate.

- The performance of the super-plasticizer can be increased by adding it in two steps. The majority should be added with the water and the residual together with the fibres (improved mixing procedure). Using such a two-step procedure the performance of the super-plasticizer can increase the small slump flow by more than 50%.
- The self-leveling properties can be determined using the SegBox experiment. Furthermore, the alignment of the fibres in the hardened state can also be observed and analyzed from this experiment.
- Only the large fibres tend to segregate. For increasing fibre volume small and middle fibres stick together and clump. Segregation can be determined using the SegBox experiment and clumping can be determined in the slump flow experiments, where the clumps of the fibres appear.
- Manual counting can be used to determine fibre alignment
- The filling method has a significant influence on the fibre alignment in a specimen. In order to compare properties of different materials the filling method has to be exactly the same.
- The fibres align with the flow of the material. The alignment increases with the flow-distance. This fact was also shown by Ferrara et al. [2007a].
- Low viscous material shows a stronger alignment of the fibres than a high viscous material.
- Cutting part of a specimen close to the mould wall leads to a decrease in flexural strength. This decrease may be caused by the fact, that at the walls the fibres are quite perfectly aligned in the direction with the most tensile stress during a bending test.
- There is a large difference in the results of the bending test of small  $70/70/280 \text{ mm}^3$  and large  $120/150/600 \text{ mm}^3$  prisms. This size effect can be possibly explained by the fact that the surface area (where fibre alignment is high) per volume is much higher for of the  $70/70/280 \text{ mm}^3$  specimen.
- There is no significant difference in the results of the mechanical tests for the used larger scale mixers (Eirich and Huggler), i.e. the influence of the mixing system on the mechanical properties of HFC is not significant.

- The way the specimens were stored right before testing influences the test results significantly. A maximum loss of maximum bending strength was found, when the specimens were tested one day after taking them out of the climate chamber. Therefore the specimens should remain at the same curing conditions as long as possible. The optimum would be if the tests could be performed in the same climate as the specimens were cured in.
- The bending strength increases with an increase of the amount of small fibres. The middle and the large fibres do not influence the maximum bending strength significantly. This is in agreement with findings of Markovic [2006].
- The crack spacing is not dependent on the fibre type. A similar average crack spacing was observed for the non-elastic part of the load-displacement diagram for all types of fibres.
- The images of the impregnated specimens showed that cracks in HFC are never straight. Branching and bridging was observed. It was also observed that HFC can show multiple cracking until, at peak, all the deformations seem to localize into a single crack.
- If "material properties" should be determined, it is necessary to produce specimens with a minimum cross-section of three times the length of the largest fibre to avoid significant wall effects because of the flow profile in the cross-sections and its influence on the fibre alignment.
- The filling method has a significant influence on the tensile strength. The presented results clearly show that the maximum tensile strength is dependent on how the material flows into the mould. The best results were obtained by filling the mould from bottom to top.
- The fibres align with the flow of the material. A simple model is given in Figure 8.1a. Different flow velocities affect the fibres and may cause the fibres to rotate in such a way that they align with the flow of the material. The effect is stronger at higher flow velocity (see Figure 8.1b) or when the velocity can affect the fibre for a longer time, (i.e. lower viscosity or longer flow duration). Due to this model the shape and geometry of the mould, the filling method and the viscosity influences the fibres alignment significantly.

Therefore, each element/structure has its own characteristic and a standard test can not be performed for HFC or for (probably most) ordinary



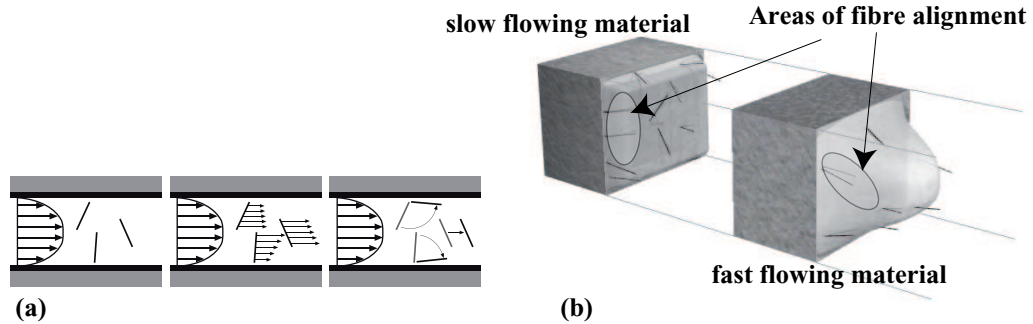


Figure 8.1: (a): 2D model of flowing concrete. The fibres align in the direction of the flow caused by the velocity gradient of the flow profile; (b): 3D model of flowing concrete. Different steepness of the flow profile caused by different flow velocities

fibre reinforced concrete (FRC). That means that such materials should preferably be used in a prefabrication plant, where the material flow during the casting process can be well controlled, and with that the fibre alignment. Similar elements can be produced with one mould and the same material flow i.e. the same fibre alignment can be guaranteed. Di Prisco & Plizzari [2004] showed some examples of R/C slabs reinforced with steel fibres and their resulting behaviours. The possibility of controlling the fibre distribution and orientation according to the prevalent stress inside a structural element in service would be the desirable aim.

## 8.2 Outlook

There is still a need for improving and understanding high performance fibre reinforced concrete. Further projects include the possibility of adding even more types of fibre into the mixture. Smaller fibers can help to increase the tensile strength significantly. First results of adding small fibres into concrete can be found in Schmid [2007] and there is an ongoing project about micro steel-fibres in concrete at the Institute of Building Materials.

The importance of aligning the fibres was shown as a major result of this thesis. How to control and predict the alignment and distribution should be investigated in further projects. Destructive and non-destructive testing methods have to be developed and established. Especially the walls of specimens and the resulting wall effect should be analyzed further.

Large scale tests should be performed on structural elements, cast with

different filling methods and/or material with different flow behaviours in order to determine the influence of aligned fibres on the mechanical resistance of large structural elements.

In the near future structures using hybrid fibre concrete may or will be possible. Using the results, methods and recommendations in this thesis, structures and elements can be produced economically. In order to minimize the amount of HFC material structures should be built using HFC with aligned fibres. Only thin panels of HFC should be used to carry the load; the spacing in between the panels can be filled with light material such as lightweight concrete introduced by e.g. Meyer & van Mier [2007], Meyer et al. [2005] or Gartmann [2006]. Such sandwich elements can be used as a replacement for masonry or reinforced concrete walls in buildings. The construction method is very fast and has the capability of carrying load immediately. Further more it is a good solution for thermal insulation.



# Bibliography

162/1, S. Betonbauten Materialprüfung (Concrete buildings and material testing). In , 1989.

Bažant, Z. P. Size effect in blunt fracture: concrete, rock, metal. In *Journal of engineering mechanics*, volume 110 (4): pp. 518 – 535, 1984.

Behloul, M. HPFRCC field of applications: DUCTAL ® recent experience. In Reinhardt, H. W. & Naaman, A. E., eds., *Proceedings 5th international conference on 'High Performance Fiber Reinforced Cement Composites' (HPFRCC 5)*, pp. 213 – 222. RILEM Publications S.A.R.L., Bagneux, France, Mainz, Germany, 2007. ISBN 978-2-35158-046-2.

Bisschop, J. & van Mier, J. G. Effect of aggregates on drying shrinkage microcracking in cement-based composites. In *Materials and Structure*, volume 35 (8): pp. 453 – 461, 2002.

Bonzel, J. & Kadlecěk, V. Einfluss der Nachbehandlung und des Feuchtigkeitsszustands auf die Zugfestigkeit des Betons (Influence of the curing and moisture condition on the tensile strength of concrete). In *Betontechnische Berichte*, 1970.

Buzzini, D., Dazio, A. & Trüb, M. Quasi-static cyclic tests on three hybrid fibre concrete structural walls. Report 297, IBK ETH Zurich, 2006.

Carpinteri, A. & Ferro, G. Size effects on tensile fracture properties: a unified explanation based on disorder and fractality of concrete microstructure. In *Materials and Structure*, volume 10 (2): pp. 563 – 571, 1994.

Custer, R. Fließverhalten von faserverstärktem Hochleistungsbeton (Flow behaviour of fibre reinforced high performance concrete). Semesterwork, Institute for building material (IfB), ETH Zurich, 2006.

- DAfStb. DAfSTb-Richtlinie - Selbstverdichtender Beton, Ergänzung zu DIN 1045: 1988-07 (DAfSTb guidelines - SCC, addition to DIN 1045: 1988-07). Technical Report DIN 1045:1988-07, Deutscher Ausschuss für Stahlbeton - DAfStb, Burggrafstrasse 6, 10787 Berlin-Tiergarten, Deutschland, 2001.
- Dupond, D. & Vandewalle, L. Distribution of steel fibres in rectangular sections. In *Cement & Concrete Composites*, volume 27 (3): pp. 391 – 398, 2005.
- Esslinger, L., Keller, C., Stähelin, W., Weingart, L., Kobel, D., Bärtsch, R., Lyrenmann, M., Gramazio, F. & Kohler, M. Die perforierte Wand (The perforated wall). Technical report, Architektur und Digitale Fabrikation, 2006.
- Evans, R. & Marathe, M. Microcracking and stress-strain curves for concrete in tension. In *Materials and Structures*, volume 1 (1): pp. 61 – 64, 1968.
- Ferrara, L., Meda, A., Lamperti, T. & Pasini, F. Connecting fibre distribution, workability and mechanical properties of SFRC: an industrial application to precast elements. In di Prisco, M., Felicetti, R. & Plizzari, G., eds., *Proceedings 6th RILEM symposium on fibre-reinforced concrete (BEFIB 2004)*, pp. 493 – 504. RILEM, RILEM Publications S.A.R.L., Bagnaux, France, Varenna, Italy, 2004.
- Ferrara, L., Dozio, D. & di Prisco, M. On the connection between fresh state behavior, fibre dispersion and toughness properties of steel fibre reinforced concrete. In Reinhardt, H. W. & Naaman, A. E., eds., *Proceedings 5th international conference on 'High Performance Fiber Reinforced Cement Composites' (HPFRCC 5)*, pp. 249 – 258. RILEM Publications S.A.R.L., Bagnaux, France, Mainz, Germany, 2007a. ISBN 978-2-35158-046-2.
- Ferrara, L., Park, Y.-D. & Shah, S. A method for mix-design of fibre-reinforced self-compacting concrete. In *Cement and Concrete Research*, volume 37 (6): pp. 957 – 971, 2007b.
- Flammer, P. Centro Comunitario Julio Otoni. In *Archplus*, volume 183, 2007.
- Flatt, R. J., Martys, N. & Bergström, L. The rheology of cementitious materials. In *MRS Bulletin*, volume 29 (5): pp. 314 – 318, 2004.
- Gartmann, J. Sandwichelemente aus Stahlfaser- und Schaumbeton (Sandwich elements out of steel fibre and foam concrete). Bachelor thesis, Institute for building material (IfB), ETH Zurich, 2006.

- Gjørsv, O. E., Sørensen, S. & Arnesen, A. Notch sensitive and fracture toughness of concrete. In *Cement and Concrete Research*, volume 7: pp. 333 – 344, 1977.
- Grünewald, S. *Performance-based design on self-compacting fibre reinforced concrete*. Thesis, 2004.
- Grünewald, S. & Walraven, J. C. Parameter-study on the influence of steel fibres and coarse aggregate content on the fresh properties of self-compacting concrete. In *Cement and concrete research*, volume 31 (12): pp. 1793 – 1798, 2001.
- van Gunsteren, E. Entwicklung eines hochwertigen selbstverdichtenden hybriden Faserbeton mit Bezug zum Versagen unter Zug und Schub (Development of a high performed self-compacting hybrid fire concrete with reference to fracture under tension and shear). Master thesis, Institute for building material (IfB), ETH Zurich), 2003.
- Hafner, C. HFC (Hybrid Fibre Concrete) Festigkeit und Fließverhalten (HFC strength and flow behaviour). Diploma thesis, Institute for building material (IfB), ETH Zurich), 2005.
- Hafner, C. & Brändli, H. Rheologie von hybridem Stahlfaserbeton (Rheology of hybrid fibre concrete). Semester thesis, Institute for building material (IfB), ETH Zurich), 2004.
- Hughes, B. & Fattuhi, N. Workability of steel-fibre-reinforced concrete. In *Magazine of concrete research*, volume 28 (96): pp. 157 – 161, 1976.
- Karihaloo, B., Alaei, F. & Benson, S. A new technique for retrofitting damaged concrete structures. In *Proceedings of the institution of civil engineers-structures and buildings*, volume 152 of 4, pp. 309 – 318. Thomas Telford Services Ltd, London, England, 2002.
- Kim, S. W., Kang, S. T., Park, J. J. & Ryu, G. S. Effect of Filling Method in Fibre Orientation & Dispersion and Mechanical Properties of UHPC. In Fehling, E., Schmidt, M. & Stürwald, S., eds., *Proceedings of the Second International Symposium on Ultra High Performance Concrete Kassel, March 05-07, 2008*, pp. 185 – 192. University Press Kassel, 2008.
- Kuder, K. G., Ozyurt, N., Mu, E. B. & Shah, S. P. Rheology of fibre-reinforced cementitious materials. In *Cement and Concrete Research*, volume 37 (2): pp. 191 – 199, 2007.

- Lappa, E. *High Strength Fibre Reinforced Concrete - Static and fatigue behaviour in bending*. Thesis, 2007.
- Linsel, S. Magnetische Positionierung von Stahlfasern in zementösen Medien (Magnetic positioning of steel fibres in cementitious medias). In *Thesis*, volume Technische Universität Berlin, 2005.
- Looser, L. & Tatti, N. Zugversuche an Stahlfaserbetonproben - Einfluss der Faserausrichtung auf die Zugfestigkeit (Tensile testing on steel fibre reinforced concrete - influence of the fibre orientation on the tensile strength). Bachelor thesis, Institute for building material (IfB), ETH Zurich, 2006.
- Man, H.-K. & van Mier, J. G. Size effect on strength and fracture energy for numerical concrete with realistic aggregate shapes. In *International Journal of Fracture (submitted)*, 2008.
- Markovic, I. *High-Performance Hybrid-Fibre Concrete - Development and utilisation*. Thesis, 2006.
- Markovic, I., Walraven, J. C. & van Mier, J. G. M. Development of high performance hybrid fibre. In Reinhardt, H. W. & Naaman, A. E., eds., *Proceedings 4th international conference on 'High Performance Fiber Reinforced Cement Composites' (HPFRCC 4)*, pp. 277 – 300. RILEM Publications S.A.R.L., Bagneux, France, Mainz, Germany, 2003. ISBN 2-912143-38-1.
- MBT. Werden Sie rheodynamisch - selbstverdichtender Beton machts möglich! (Become rheo-dynamic, self-compacting concrete makes it possible!). brochure, BASF Switzerland, 2000.
- Mechtcherine, V. Testing behaviour of strain hardening cement-based composites in tension - summary of recent research. In Reinhardt, H. W. & Naaman, A. E., eds., *Proceedings 5th international conference on 'High Performance Fiber Reinforced Cement Composites' (HPFRCC 5)*, pp. 3 – 12. RILEM Publications S.A.R.L., Bagneux, France, Mainz, Germany, 2007. ISBN 978-2-35158-046-2.
- Meyer, D. & van Mier, J. G. M. Influence of different PVA fibres on the crack behaviour of foamed cement past. In Carpinteri, A., Gambarova, P. G., Ferro, G. & Plizzari, G. A., eds., *Proceedings 6th international conference on 'fracture of concrete and concrete structures' (FraMCoS-6)*, pp. 1359 – 1365. Taylor & Francis Group, London, UK, Catagna, Italy, 2007. ISBN 978-0-415-44066-0.

- Meyer, D., Tritik, P., Rindlisbacher, M. & van Mier, J. G. Preliminary study on the properties of protein foam and hardened foamed cement paste. In N. Banthia, A. B., T. Uomoto & Shah, S., eds., *Proceedings 3rd international Conference on Construction materials: Performance, Innovations and Structural Implications (ConMat '05) and Mindess Symposium*. University of British Columbia, Vancouver, Canada, Vancouver, Canada, 2005.
- van Mier, J. G. Reality Behind Fictitious Cracks? In Li, V. C., Leung, C. K., Willam, K. & Billington, S., eds., *In Proceedings 5<sup>th</sup> International Conference on 'Fracture of Concrete and Concrete Structures' (FraMCoS-V)*, pp. 11 – 30. IA-FraMCoS, Evanston, IL, USA, 2004.
- van Mier, J. G. & Mechtcherine, V. Minimum Demands for Deformation-Controlled Uniaxial Tensile Tests. In Planas, J., ed., *RILEM TC 187-SOC "Experimental Determination of the Stress-Crack Opening Curve for Concrete in Tension", Report 39*, pp. 5 – 12. RILEM Publications S.A.R.L., Bagneux, France, 2007.
- van Mier, J. G., Vervuurt, A. & Schlangen, E. Boundary and size effects in uniaxial tensile tests: a numerical and experimental study. In Bažant, Z. P., Bittnar, Z., Jiràsek, M. & Mazars, J., eds., *Fracture and Damage of Quasibrittle Structures*, pp. 289 – 302. E&FN Spon, London/New York, 1994a.
- van Mier, J. G. M. *Fracture Processes of Concrete (New Directions in Civil Engineering Series)*. CRC, 1996. ISBN 0-8493-9123-7, 464 pp.
- van Mier, J. G. M. Framework for a generalized four-stage fracture model of cement-based materials. In *Engineering fracture mechanics*, volume 75 (18): pp. 5072 – 5086, 2008.
- van Mier, J. G. M. & Timmers, G. Shear fracture in slurry infiltrated fibre concrete (SIFCON). In Reinhardt, H. W. & Naaman, A. E., eds., *Proceedings RILEM/ACI workshop on high performance fibre reinforced cement composites*, pp. 348 – 360. E&FN Spon/Chapman & Hall, London/New York,, Mainz, Germany, 1992.
- van Mier, J. G. M. & Timmers, G. Werkwijze en inrichting voor de vervaardiging van een gewapend constructie-element en een dergelijk constructiedeel (device for manufacturing a reinforced construction element). Dutch patent No. 1000285, TU Delft, 1996.



- van Mier, J. G. M., Vernuurt, A. & Schlangen, E. Analysis of anchor pull-out in concrete. In *Materials and Structure*, volume 27 (5): pp. 251 – 259, 1994b.
- van Mier, J. G. M., Schlangen, E. & Vervuurt, A. Lattice type fracture models for concrete. In Mühlhaus, H., ed., *Continuum models for Materials with Microstructure*, pp. 341 – 377. John Wiley & Sons Ltd, 1995.
- Naaman, A. E. Fibre reinforced concrete. In *Concrete International*, volume 7 (3): pp. 21 – 25, 1985.
- Naaman, A. E. & Reinhardt, H. W. High performance fibre reinforced cement composites. In Reinhardt, H. W. & Naaman, A. E., eds., *Proceedings 4th international conference on 'High Performance Fiber Reinforced Cement Composites' (HPFRCC 4)*. RILEM Publications S.A.R.L., Bagneux, France, Mainz, Germany, 2003. ISBN 2-912143-38-1.
- Naaman, A. E. & Reinhardt, H. W. Proposed classification of HPFRC composites based on their tensile response. In N. Banthia, A. B., T. Uomoto & Shah, S., eds., *Proceedings 3rd international Conference on Construction materials: Performance, Inocations and Structural Implications (ConMat '05) and Mindess Symposium*, p. 458. University of British Columbia, Vancouver, Canada, Vancouver, Canada, 2005.
- Naaman, A. E., Fischer, G. & Krstulovic-Opara, N. Measurement of tensile properties of fibre reinforced concrete: Draft submitted to aci committee 544. In Reinhardt, H. W. & Naaman, A. E., eds., *Proceedings 5th international conference on 'High Performance Fiber Reinforced Cement Composites' (HPFRCC 5)*, pp. 3 – 12. RILEM Publications S.A.R.L., Bagneux, France, Mainz, Germany, 2007. ISBN 978-2-35158-046-2.
- Nakamura, S., van Mier, J. G. M. & Masuda, Y. Self compactability of hybrid fibre concrete containing PVA fibres. In di Prisco, M., Felicetti, R. & Plizzari, G., eds., *Proceedings 6th RILEM symposium on fibre-reinforced concrete (BEFIB 2004)*, pp. 525 – 535. RILEM, RILEM Publications S.A.R.L., Bagneux, France, Varenna, Italy, 2004.
- Oesterle, C., Denarie, E. & Brühwiler, E. UHPFRC protection layer on the crash barrier walls of a bridge. In Grosse, C. U., ed., *Advanced in construction materials 2007*, pp. 203 – 210. Springer-Verlag Berlin, Germany, 2007.
- Orange, G., Acker, P. & Vernet, C. A new generation of UHP concrete: DUCTAL(R) damage resistance and micromechanical analysis. In Reinhardt,

- H. W. & Naaman, A. E., eds., *Proceedings 4th international conference on 'High Performance Fiber Reinforced Cement Composites' (HPFRCC 3)*, pp. 101 – 111. RILEM Publications S.A.R.L., Bagneux, France, Mainz, Germany, 1999. ISBN 2-912143-06-3.
- Ozyurt, N., Mason, T. O. & Shah, S. R. Non-destructive monitoring of fiber orientation using AC-IS: An industrial-scale application. In *Cement and Concrete Research*, volume 36 (9): pp. 1653 – 1660, 2006a.
- Ozyurt, N., Woo, L. Y., Mason, T. O. & Shah, S. R. Monitoring fiber dispersion in fiber-reinforced cementitious materials: Comparison of AC-impedance spectroscopy and image analysis. In *ACI Materials Journal*, volume 103 (5): pp. 340 – 347, 2006b.
- Ozyurt, N., Woo, L. Y., Mason, T. O. & Shah, S. P. Fibre dispersion monitoring using AC-impedance spectroscopy and a conventional method. In Reinhardt, H. W. & Naaman, A. E., eds., *Proceedings 5th international conference on 'High Performance Fiber Reinforced Cement Composites' (HPFRCC 5)*, pp. 267 – 273. RILEM Publications S.A.R.L., Bagneux, France, Mainz, Germany, 2007. ISBN 978-2-35158-046-2.
- Peled, A. & Mobasher, B. Tensile behavior of fabric cement-based composites: Pultruded and cast. In *Journal of Materials in civil engineering*, volume 19 (4): pp. 340 – 348, 2007.
- di Prisco, M. & Plizzari, G. A. Precast SFRC elements: From material properties to structural applications. In di Prisco, M., Felicetti, R. & Plizzari, G., eds., *Proceedings 6th RILEM symposium on fibre-reinforced concrete (BEFIB 2004)*, pp. 81 – 100. RILEM, RILEM Publications S.A.R.L., Bagneux, France, Varenna, Italy, 2004.
- di Prisco, M., Lamperti, M., Lapolla, S. & Khurana, R. S. HPFRCC thin plates for precast roofing. In Fehling, E., Schmidt, M. & Stürwald, S., eds., *Proceedings of the Second International Symposium on Ultra High Performance Concrete Kassel, March 05-07, 2008*, pp. 675 – 682. University Press Kassel, 2008.
- Ramsburg, P. The SCC Test: inverted or upright. In *The concrete producer*, volume July: pp. 1 – 5, 2003.
- Reinhard, H.-W. & Naaman, A. E. History of the development of highly ductile concrete with fibre reinforcement. In *Ultra-ductile concrete with short fibres. Development. Testing. Applications*, pp. 1 – 9. TU Kaiserslautern, Ibidem-Verlag, Stuttgart, Germany, 2005.

- Rosenbusch, J. Einfluss der Faserorientierung auf die Beanspruchung von Bauteilen aus Stahlfaserbeton (Influence of the fibre orientation on the stress strain of a fibre reinforced element). In *Beton- und Stahlbetonbau*, volume 99 (5): pp. 372 – 377, 2004.
- Rossi, P. High performance multi-modal fiber reinforced cement composite (HPMFRCC): the LCPC experience. In *ACI Materials Journal*, volume 94 (6): pp. 478 – 483, 1997.
- Rossi, P. & Parant, E. Damage mechanisms analysis of a multi-scale fibre reinforced cement-based composite subjected to impact and fatigue loading conditions. In *Cement and Concrete Research*, volume 38 (3): pp. 413 – 421, 2008.
- Rossi, P., Acker, P. & Malier, Y. Effect of steel fibres at two different stages: The material and the structure. In *Materials and Structures*, volume 20 (6): pp. 436 – 439, 1987.
- Rossi, P., van Mier, J. G. M., Toutlemonde, F., le Maou, F. & Boulay, C. Effect of loading rate on the strength of concrete subjected to uniaxial tension. In *Materials and Structure*, volume 27 (5): pp. 260 – 264, 1994.
- Roussel, N., Stefani, C. & Leroy, R. From mini-cone test to Abrams cone test: measurement of cement-based materials yield stress using slump tests. In *Cement and concrete research*, volume 35 (5): pp. 817 – 822, 2005.
- Schlangen, E. *Experimental ad numerical analysis of fracture process in concrete*. Thesis, 1993.
- Schmid, S. Fibre-Reinforced-Concrete - Einfluss von Fließverhalten und Fließdistanz auf Faserausrichtung und Biegezugfestigkeit (Influence of the flow behaviour on the fibre alignment and bending strength). Semesterwork, Institute for building material (IfB), ETH Zurich), 2006.
- Schmid, S. Rentabilität von Mikrostaahlfasern in einer Zementmatrix (Profitability of micro-steel fibers in a cement matrix). Diploma thesis, Institute for building material (IfB), ETH Zurich), 2007.
- Shao, Y. & Shah, S. P. Mechanical properties of PVA reinforced cement composites fabricated by extrusion processing. In *ACI Materials Journal*, volume 6 (94): pp. 555 – 564, 1997.
- Soroushian, P. & Lee, C.-D. Distribution and orientation of fibres in steel fibre reinforced concrete. In *ACI Materials Journal*, volume 87 (5): pp. 433 – 439, 1990.

- Stähli, P. & van Mier, J. G. M. Three-fibre-type hybrid fibre concrete. In Li, V., Leung, C., Willam, K. & Billington, S., eds., *Proceedings 5th international conference on 'fracture of concrete and concrete structures' (FraMCosS-5)*, pp. 1105 – 1112. Evanston, IL: IA-FraMCos, Vail, Colorado USA, 2004a.
- Stähli, P. & van Mier, J. G. M. Rheological properties and fracture processes of HFC. In di Prisco, M., Felicetti, R. & Plizzari, G., eds., *Proceedings 6th RILEM symposium on fibre-reinforced concrete (BEFIB 2004)*, pp. 299 – 308. RILEM, RILEM Publications S.A.R.L., Bagneux, France, Varenna, Italy, 2004b.
- Stähli, P. & van Mier, J. G. M. Manufacturing, fibre anisotropy and fracture of hybrid fibre concrete. In *Engineering Fracture Mechanics*, volume 74: pp. 223 – 242, 2007a.
- Stähli, P. & van Mier, J. G. M. Effect of manufacturing methods on tensile properties of fibre concrete. In Carpinteri, A., Gambarova, P. G. & G. Ferro, G. A. P., eds., *Proceedings 6th international conference on 'fracture of concrete and concrete structures' (FraMCosS-6)*, pp. 1351 – 1357. Taylor & Francis Group, London, UK, Catagna, Italy, 2007b. ISBN 978-0-415-44066-0.
- Stähli, P. & van Mier, J. G. M. Stahlfaserverstärkte Betone (Steel fibre reinforced concrete). In *Schweizer Baujournal*, volume 3: pp. 43 – 45, 2007c.
- Stähli, P., Sutter, M. & van Mier, J. G. M. Improving the mechanical properties of HFC by adjusting the filling method. In Reinhardt, H. W. & Naaman, A. E., eds., *Proceedings 5th international conference on 'High Performance Fiber Reinforced Cement Composites' (HPFRCC 5)*, pp. 23 – 30. RILEM Publications S.A.R.L., Bagneux, France, Mainz, Germany, 2007. ISBN 978-2-35158-046-2.
- Stähli, P., Custer, R. & van Mier, J. G. M. On flow properties, fibre distribution, fibre orientation and flexural behaviour of FRC. In *Materials and Structures*, volume 41: pp. 189 – 196, 2008.
- Sutter, M. Optimierung der Zugfestigkeit von hybriden Stahlfaserbetonen (Optimization of the tensile strength of steel fibre concrete). Diploma thesis, Institute for building material (IfB), ETH Zurich, 2007.
- Tattersall, G. & Banfill, P. *The Rheology of fresh concrete*. Pitman Books Limited, 1983. ISBN 0-273-08558-1.

- Trtik, P., Stähli, P., Landis, E. N., Stampanoni, M. & van Mier, J. G. M. Microtensile testing and 3D imaging of hydrated Portland Cement. In Carpinteri, A., Gambarova, P. G. & G. Ferro, G. A. P., eds., *Proceedings 6th international conference on 'fracture of concrete and concrete structures' (FraMCoS-6)*, pp. 1277 – 1282. Taylor & Francis Group, London, UK, Catagna, Italy, 2007. ISBN 978-0-415-44066-0.
- van Vliet, M. R. *Size Effect in Tensile Fracture of Concrete & Rock*. Thesis, 2000.
- Walsh, P. F. Fracture of plain concrete. In *Indian concrete journal*, volume 46 (11): pp. 469 – 476, 1972.
- Wuest, J., Denarié, E. & Brühwiler, E. Measurement and modeling of fibre distribution and orientation in UHPFRC. In Reinhardt, H. W. & Naaman, A. E., eds., *Proceedings 5th international conference on 'High Performance Fiber Reinforced Cement Composites' (HPRCC 5)*, pp. 259 – 266. RILEM Publications S.A.R.L., Bagnoux, France, Mainz, Germany, 2007. ISBN 978-2-35158-046-2.
- van Zijl, G. Optimisation of the composition and fabrication methods; application for precast concrete members. In *Ultra-ductile concrete with short fibres. Development. Testing. Applications*, pp. 37 – 54. TU Kaiserslautern, Ibidem-Verlag, Stuttgart, Germany, 2005.

# Appendix **A**

## Appendix A

### **A.1 Mix design programme**

The mix design programme was programmed in Excel. The input parameters were basically the volume percentages of binder and aggregates. The binder itself was divided into the different components. W/b-ratio, amount of admixtures, the amounts of fibres and the total amount of the material used were input parameters as well. The outputs were the exact amounts of each component including correction amounts. Using the same sheet two correction steps, where the w/b-ratio, amount of admixture or the amount of fibres could be changed was implemented. The programme was designed by the author.

### **A.2 Concrete mixers**

#### **A.2.1 Hobart 1.5l**

The maximum amount which can be mixed (see Figure A.1) is 1.5 liter. Only mortars with a maximum aggregate size of 4 mm can be mixed. Using fibres the mixture should be very flow-able and the large fibres should not clump otherwise mixing is not possible. The mixer is basically a planetary mixer with one mixing tool.

#### **A.2.2 Hobart 6.0l**

The maximum amount which can be mixed (see Figure A.2) is 6 liter. The maximum aggregate size is 8 mm. There is no limitation in fibres or flow-ability. The mixer is capable of mixing even very viscous mixtures with a

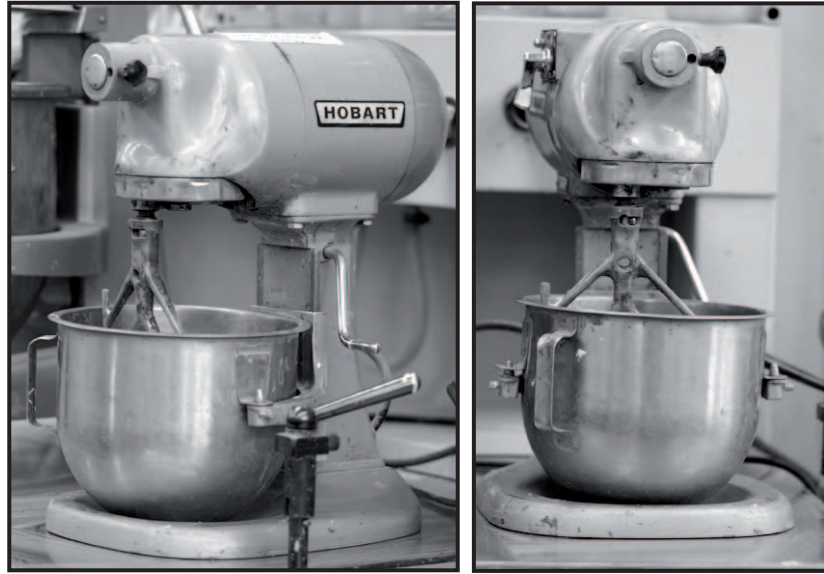


Figure A.1: Hobart 1.5l 'mortar' mixer

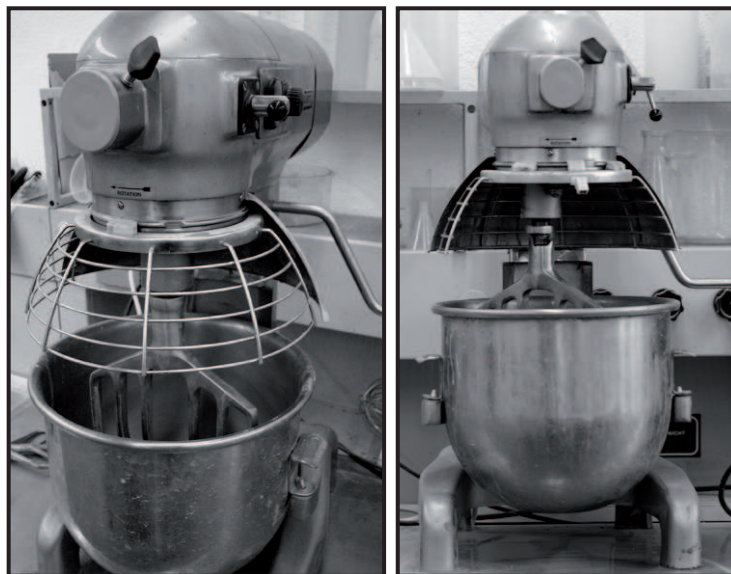


Figure A.2: Hobart 6l 'concrete' mixer

large amount of fibres. Two vessels for mixing 3 or 6 liters are available. The mixer is basically a planetary mixer with a single mixing tool.

### A.2.3 Wälti 30l

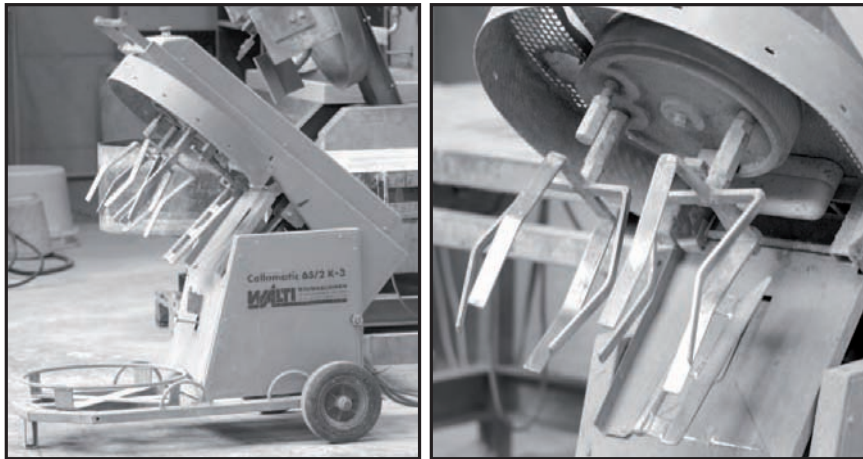


Figure A.3: Wälti 30l concrete mixer

The maximum amount which can be mixed (see Figure A.3) is 30 liters. A minimum of 10 liters is recommended in order to guarantee an optimal mixture. The maximum aggregate size is 8 mm. There are no limitations regarding fibres or flow-ability of the mixture. The mixer is a planetary mixer with two inverse rotating mixing tools.

### A.2.4 Zyklus 65l

The maximum amount which can be mixed with the Zyklus 65l (see Figure A.4) is 65 liters. A minimum of 20 liters is recommended in order to guarantee an optimum mixture. There is no limitation in fibres, flow-ability or aggregate size of the mixture. The mixer is an ordinary mixer.

### A.2.5 Huggler 300l

The maximum amount which can be mixed with the Huggler 300l (see Figure A.5) is 300 liters. A minimum of 150 liters is recommended in order to guarantee an optimal mixture. There are no limitations regarding fibres, flow-ability or aggregate size of the mixture. The mixer is an ordinary mixer.



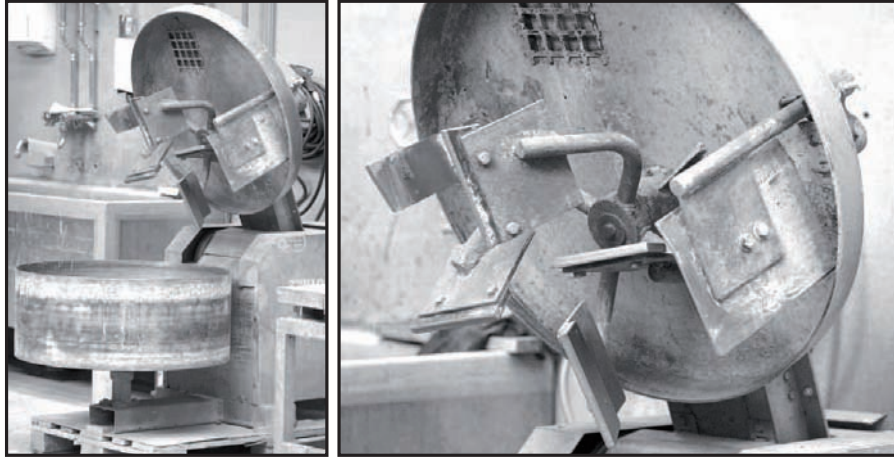


Figure A.4: Zyklos 65 concrete mixer

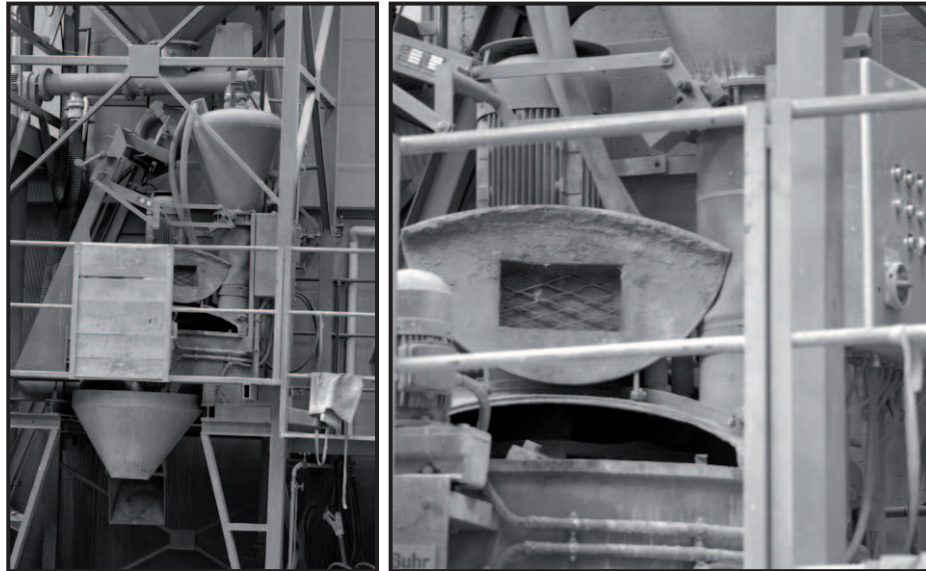


Figure A.5: Huggler 300l concrete mixer

### A.2.6 Huggler 500l

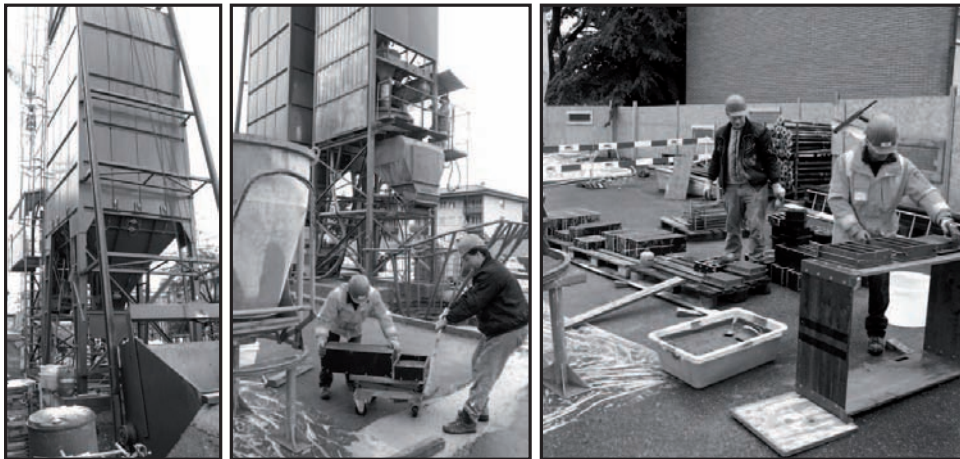


Figure A.6: Huggler 500l concrete mixer

The maximum amount which can be mixed with the Huggler 500l (see Figure A.6) is 500 liters. There are no limitations in fibres, flow-ability or aggregate size of the mixture. The mixer is a planetary mixer with two inverse rotating mixing tools.

### A.2.7 Eirich 200l

The maximum amount which can be mixed with the Eirich 200l (see Figure A.7) is 200 liters. The Eirich mixing system is based on a fast rotation vessel and an inverse rotating mixing tool. Therefore the material is whirled very fast and a decent mixture is guaranteed.

## A.3 Standard mechanical test - Walter & Bai testing machine

The Walter & Bai testing machine (see Figure A.8) is a standard testing machine for bending, compression and Young's modulus tests. Two testing machines were combined into one. A small one with a capacity of 100 kN where bending tests were carried out and a large one with a capacity of 4000 kN where the compression and Young's Modulus test were carried out. The elevation is limited to 100 mm.

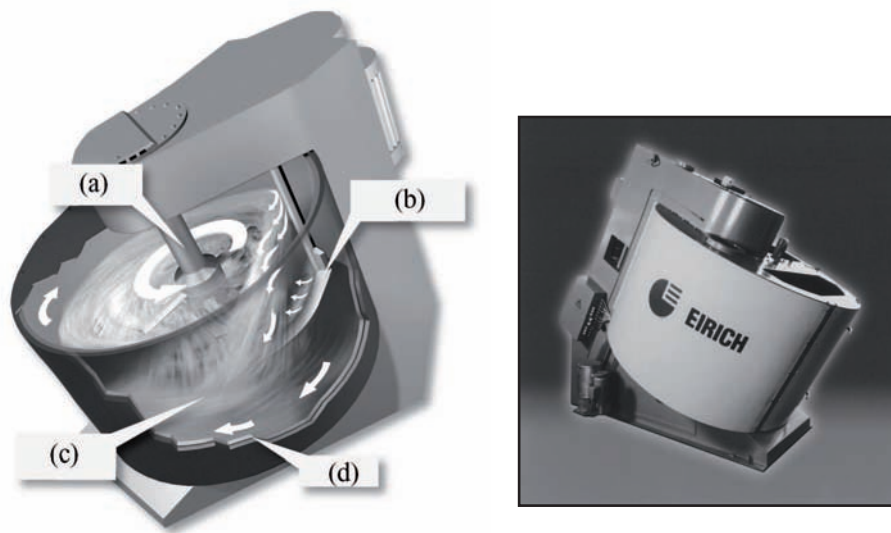


Figure A.7: Erich mixing system. (a): robust, maintenance friendly tools; (b): static combination tool functions as bottom-wall-stripper; (c): large velocity differences in the mixture; (d): turnable mixing vessel

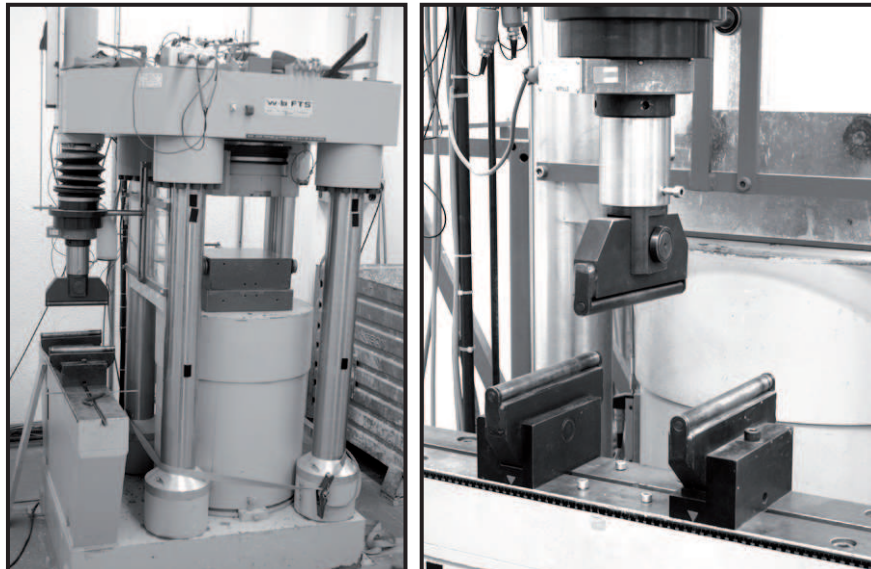


Figure A.8: Walter & Bai testing machine. Overview of the hole testing machine and a detailed image.

### **A.3.1 Compression tests**

Compression tests on different geometries of cubes (40/40/40, 50/50/50, 70/70/70 and 150/150/150) and cylinders (150/300) were performed on the large testing machine. The tests carried out were deformation controlled. In order to optimize the time per test, the testing velocity was divided into three phases. A slow, a middle and a fast phase. The slow phase ended shortly after the peak and was followed by the middle and the fast phase.

### **A.3.2 Young's Modulus tests**

The Young's Modulus tests were carried out as the model code SIA 162/1 [1989] recommends. After three cycles the load was held for 5 seconds before unloading. The Young's Modulus was determined in the last unloading branch. The maximum load was approximately a third of the compression strength.

### **A.3.3 Bending test**

Three or four-point bending tests on prisms with different geometries (40/40/160, 50/50/200 and 70/70/280) were performed on the small testing machine. The tests carried out were deformation controlled. In order to optimize the time per test, the testing velocity was divided into three phases. A slow, a middle and a fast phase. The slow phase ended shortly after the peak and was followed by the middle and the fast phase.



# Appendix **B**

## Appendix B

### **B.1 Crack pattern development**

The following figures are results in addition to Section 5.5.4. The diagrams in Figure B.1 are results from the bending specimens for the impregnation tests. Each curve represents one specimen. After impregnation the specimens were cut as close to the surface as possible and the cracks in the interior of the specimen were photographed under UV light. Afterwards the cracks were traced and the results are shown in Figures B.2 to B.5. These Figures show the individual crack patterns. Each image represents one specimen at a certain displacement stage. Two specimens per displacement stage are shown. In Figure B.2 crack pattern 0.65 mm is missing because there the cutting of the specimen failed and therefore no crack pattern was available. In Figure B.4 crack pattern 1.00 mm is missing because there the mechanical testing failed and therefore no crack pattern was available.

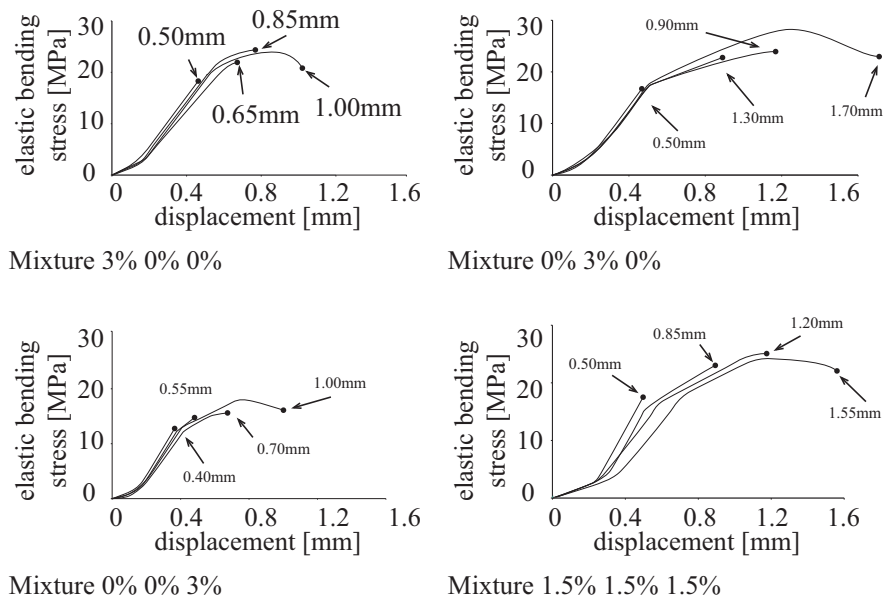


Figure B.1: Resulting load-displacement diagrams derived from the impregnated specimens

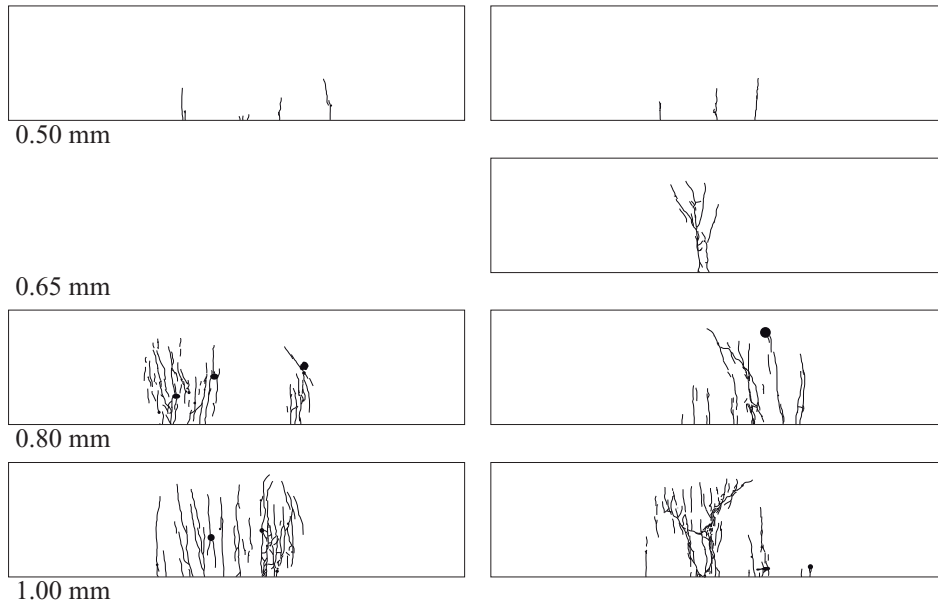


Figure B.2: Crack pattern of the 3% 0% 0% series for the different deformation stages

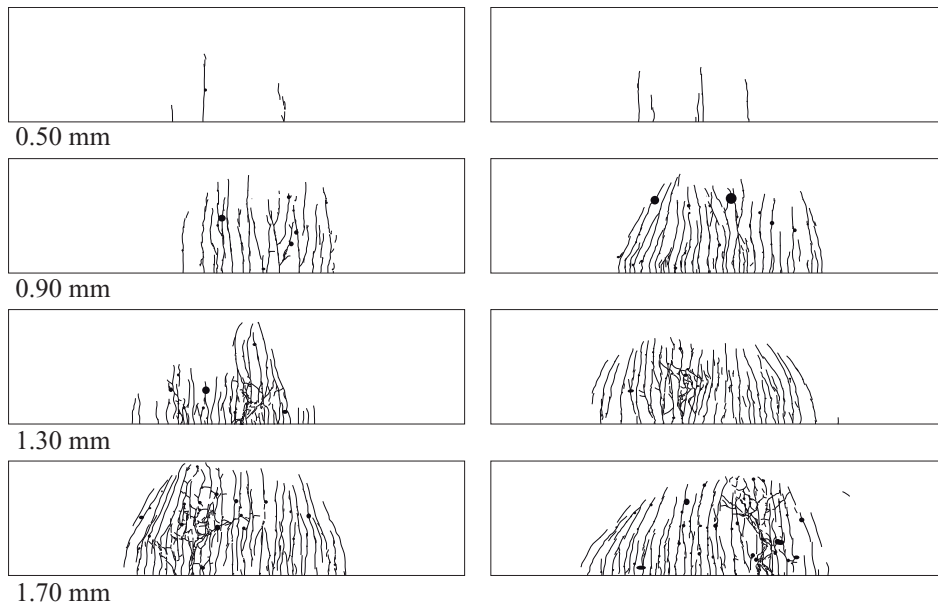


Figure B.3: Crack pattern of the 0% 3% 0% series for the different deformation stages



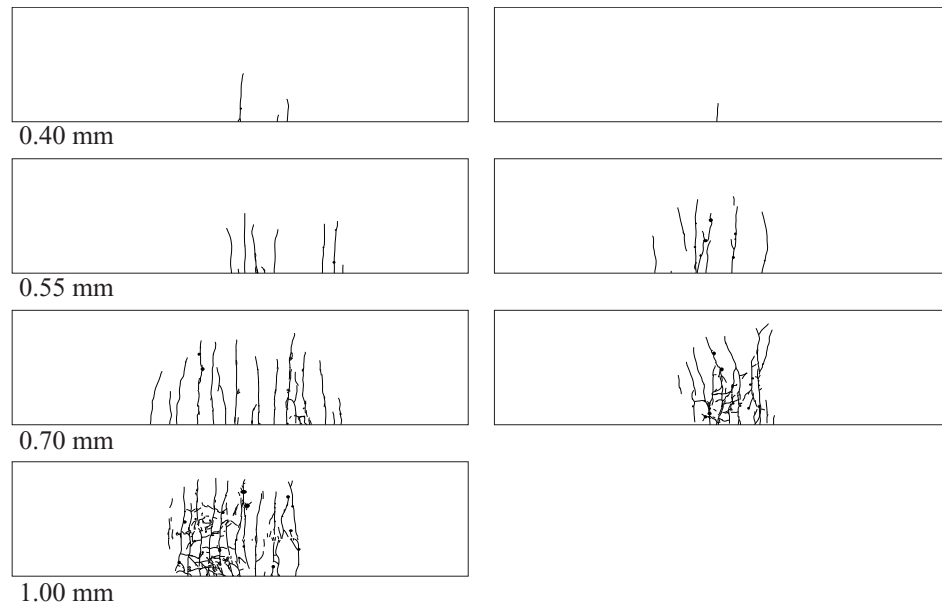


Figure B.4: Crack pattern of the 0% 0% 3% series for the different deformation stages

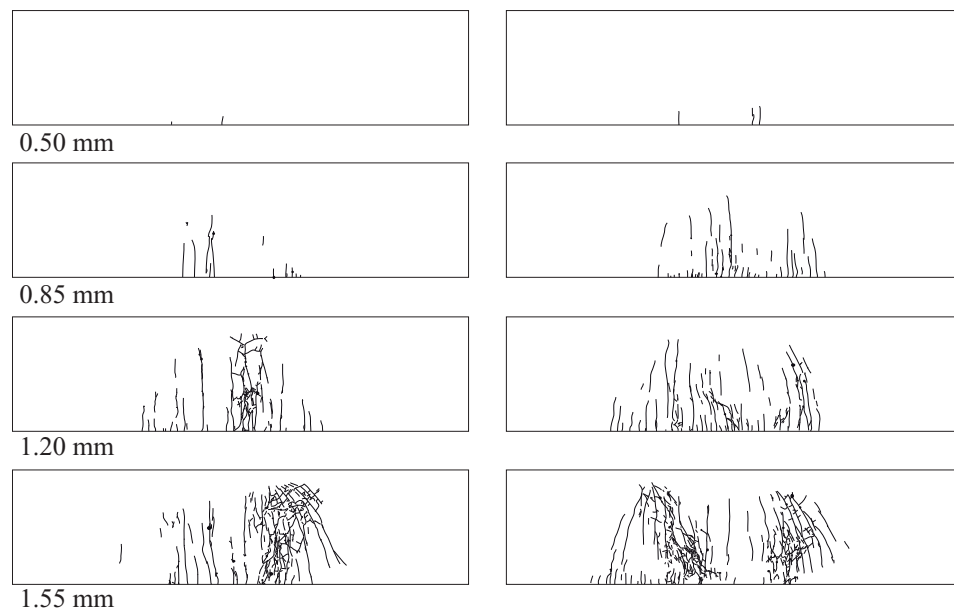


Figure B.5: Crack pattern of the 1.5% 1.5% 1.5% series for the different deformation stages

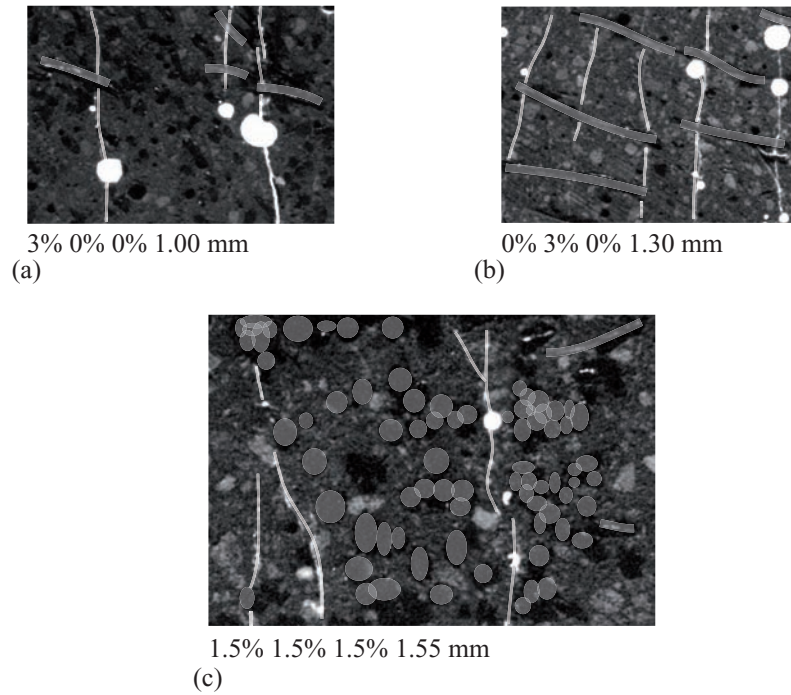


Figure B.6: Images of crack patterns of the different mixtures (a): small fibres only, (b): middle fibres only and (c): HFC mixture. See also Rossi & Parant [2008]

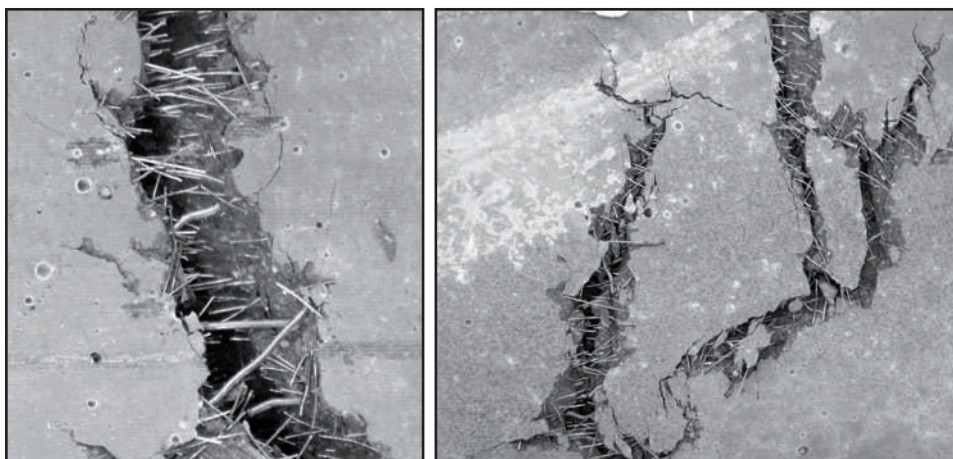


Figure B.7: Images of fibre bridging in a cracked specimen



# Curriculum vitae

Name	Patrick Stähli
Date of birth	22 January 1975 in Schlieren (Switzerland)
Nationality	Swiss

## Education

elementary school	1982 - 1991 in Bonstetten
high school	1991 - 1995 in Zurich

## Academic education

ETH Zurich Department of civil engineering	1997 - 2002
---	-------------

## Military education

Military training school	1996 - 1997 in Bremgarten
Office candidate school	1997 in Birmensdorf

## Employment

ETH Zurich, Institute for building materials	2002 - 2008
Concretum Construction Science AG	2008



## Peer reviewed articles

Patrick Stähli and Jan G. M. van Mier. Manufacturing, fibre anisotropy and fracture of hybrid fibre concrete. *Engineering Fracture Mechanics*, 74:223 – 242, 2007.

Patrick Stähli, Rocco Custer, and Jan G. M. van Mier. On flow properties, fibre distribution, fibre orientation and flexural behaviour of FRC. *Materials and Structures*, 41:189 – 196, 2008.

Pavel Trtik, Jürg Dual, Daniel Keunecke, David Mannes, Peter Niemz, Patrick Stähli, Andreas Kästner, Amela Groso, and Marco Stampanoni. 3d imaging of microstructure of spruce wood. *Journal of Structural Biology*, 159(1):46 – 55, 2007.



## Conference proceedings and other publications

Patrick Stähli and Jan G. M. van Mier. Three-fibre-type hybrid fibre concrete. In V.C. Li, C.K.Y. Leung, K.J. Willam, and S.L. Billington, editors, *Proceedings 5th international conference on 'fracture of concrete and concrete structures' (FraMCoS-5)*, pages 1105 – 1112, Vail, Colorado USA, 2004a. Evanston, IL: IA-FraMCoS.

Patrick Stähli and Jan G. M. van Mier. Rheological properties and fracture processes of HFC. In M. di Prisco, R. Felicetti, and G. Plizzari, editors, *Proceedings 6th RILEM symposium on fibre-reinforced concrete (BEFIB 2004)*, pages 299 – 308, Varenna, Italy, 2004b. RILEM, RILEM Publications S.A.R.L., Bagneux, France.

Patrick Stähli and Jan G. M. van Mier. Fracture testing of hybrid fibre concrete. In *Proceedings ICF-11*, pages CD–Rom, Torino, Italy, 2005.

Patrick Stähli and Jan G. M. van Mier. Effect of manufacturing methods on tensile properties of fibre concrete. In A. Carpinteri, P. G. Gambarova, and G. A. Plizzari G. Ferro, editors, *Proceedings 6th international conference on 'fracture of concrete and concrete structures' (FraMCoS-6)*, pages 1351 – 1357, Catagna, Italy, 2007a. Taylor & Francis Group, London, UK. ISBN 978-0-415-44066-0.

Patrick Stähli and Jan G. M. van Mier. Stahlfaserverstärkte Betone (Steel fibre reinforced concrete). *Schweizer Baujournal*, 3:43 – 45, 2007b.

Patrick Stähli, Martin Sutter, and Jan G. M. van Mier. Improving the mechanical properties of HFC by adjusting the filling method. In Hans W. Reinhardt and Antoine. E. Naaman, editors, *Proceedings 5th international*



*conference on 'High Performance Fiber Reinforced Cement Composites' (HPFRCC 5)*, pages 23 – 30, Mainz, Germany, 2007. RILEM Publications S.A.R.L., Bagneux, France. ISBN 978-2-35158-046-2.

Pavel Trtik, Patrick Stähli, Eric N. Landis, Marco Stampanoni, and Jan G. M. van Mier. Microtensile testing and 3D imaging of hydrated Portland Cement. In A. Carpinteri, P. G. Gambarova, and G. A. Plizzari G. Ferro, editors, *Proceedings 6th international conference on 'fracture of concrete and concrete structures' (FraMCoS-6)*, pages 1277 – 1282, Catagna, Italy, 2007. Taylor & Francis Group, London, UK. ISBN 978-0-415-44066-0.

Jan G. M. van Mier and Patrick Stähli. Development of Hybrid Fibre Concrete: Manufacturing, Material Structure and Mechanical Properties. In Victor Mechtcherin, editor, *Proceedings of symposium 'Hochduktile Betone mit Kurzfaserbewehrung', TU Kaiserslautern*, pages 55 – 68. Ibidem Verlag, Stuttgart, 2005.

# Acknowledgement

This Thesis is the result of the research topic Hybrid Fibre Concrete carried out from September 2002 to September 2007 at the Department of civil engineering at the Institute of Building Materials of the Swiss Federal Institute of Technology Zurich.

First of all I want to thank my supervisor Jan van Mier for giving me the opportunity to work on this research project. His support, advice, critical standings and detailed comments contributed very much to the quality of the performed research.

An essential part of this research project has been carrying out the experiments. This work would not have been possible without the help of my colleagues at the institute. Heinz Richner deserves a great compliment for his help with building moulds, casting, preparing and testing the specimens. His critical comments helped to find solutions for a variety of problems. Jürg Inhelder deserves a special thanks for his hard work on manufacturing the moulds and the pendulum-bar test set-ups. After manufacturing the pendulum-bar tensile test set-up he told me that this was the most sophisticated work that he had ever done. Also a special thanks to Tomi Jaggi who helped me with producing and preparing the specimens, on the site and in the laboratory. He was responsible for repairing and the service of the technical equipment of the Institute of Building Materials. Gabriele Peschke for taking all the ESEM images. Fruitful discussions with Pavel Trtik, Carsten Rieger, Dominik Meyer, Hau-Kit Man, Jan Bisschop, Silke Ruffing, Burcu Akcay Aldanmaz, Martin Bäuml, Stefan Meier, Giovanni Martinola, Markus Künstner, Norbert Stoop and Sandra Galmarini also contributed to the quality of this thesis. I also want to thank all the colleagues I met at conferences, workshops, courses and symposia for their many interesting discussions.

Thanks to Concretum, Holcim, B.A.S.F. and Sika for supporting me with cement, fly-ash, aggregates and admixtures.

Special thank to the employees of the University Hospital of Zurich who performed the CT.

At the end I have to specially thank my wife Barbara and my children Levia and Ben, my parents Gabriella and Hanspeter and my brother Dominique who supported me during the whole PhD and encouraged and motivated me especially during the final phase of the Thesis.

**Patrick Stähli**  
**8<sup>th</sup> October 2008**

**ETH**

Eidgenössische Technische Hochschule Zürich  
Swiss Federal Institute of Technology Zurich

**IfB**

Institut für Baustoffe  
Institute for Building Materials